

SHEAR STRENGTHENING OF PRESTRESSED CONCRETE I-GIRDERS

Using Externally Bonded Carbon-Fibre
Reinforced Polymers

J.C. Verhage



Shear Strengthening of Prestressed Concrete I-Girders

Using Externally Bonded Carbon-Fibre Reinforced Polymers

by

J.C. Verhage

November 2020

In partial fulfilment of the requirements for the degree of

Master of Science
in Building Engineering

at the Delft University of Technology,

to be defended publicly on Wednesday November 25, 2020 at 16.00 PM.

Delft University of Technology
Faculty of Civil Engineering and Geosciences
Applied Mechanics
Building Engineering (Structural Design)
Stevinweg 1, 2628CN Delft, the Netherlands

Master thesis committee

dr. ir. M.A.N. Hendriks (chair)
ir. S. Pasterkamp
dr. ir. Y. Yang
ir. R.N. ter Maten

Applied Mechanics
Applied Mechanics
Concrete Structures
Vogel B.V. & Mourik Infra



PREFACE

I have written this thesis as conclusion of the master Civil Engineering at the Delft University of Technology. The last year I have been working on my thesis, which was a challenging but also exciting period.

This thesis is strongly related to an ongoing research about the feasibility of CFRP reinforcement to strengthen I- and T-girders in shear.

I am thankful to the people of Vogel B.V. and Mourik B.V. for suggesting the research topic for my thesis and giving me the opportunity to be part of the research team. Many thanks go to my supervisor at Vogel B.V. ir. Richard ter Maten for the support and guidance. The discussions about my research were very helpful.

I would like to thank my graduation committee from the Delft University of Technology. First of all, I would like to thank dr. ir. Max Hendriks for the valuable advices on nonlinear finite element analyses and the feedback on my report. Further I would like to thank ir. Sander Pasterkamp for the critical comments on my research. I would like to thank dr. ir. Yuguang Yang for the advice on shear failure of prestressed concrete members.

J.C. Verhage
Zwijndrecht, November 2020

ABSTRACT

A considerable number of the concrete bridges built in the period before 1975 are reaching their intended service life. The structural safety of the concrete bridges built in the period before 1975 has been assessed by Rijkswaterstaat. It was concluded that bridges built with prestressed concrete I-girders potentially have insufficient shear capacity because of the combination of thin webs and insufficient shear reinforcement. Shear failure of these girders should be prevented because they do not warn before the element fails in shear.

Measures to guarantee the structural safety of these bridges are replacement and renovation. Replacement of all bridges with insufficient shear capacity is not possible because of insufficient economical resources and hindrance. Shear strengthening of prestressed concrete I-girders is the desired choice in a significant number of cases. However, the existing shear strengthening methods have some drawbacks. The innovative shear strengthening method using externally bonded CFRP reinforcement seems promising because of low installation costs, negligible increase in weight, no decrease of clear height underneath the bridge and minimising the hinderance.

The aim of this thesis is to investigate the feasibility of shear strengthening prestressed concrete I-girders using externally bonded CFRP reinforcement. The shear behaviour of prestressed concrete I-girders strengthened using externally bonded CFRP reinforcement has been investigated with the nonlinear finite element analysis (NLFEA) software DIANA. NLFEA is able to predict the crack pattern and failure mode of a concrete element. A three-dimensional finite element model of a 1.0 m high prestressed concrete I-girder with a kinked tendon profile and no shear reinforcement has been made to investigate several design parameters and aspects of the CFRP reinforcement. The CFRP sheets were modelled in vertical direction around the circumference of the I-girder. The parameters that have been investigated are the anchoring using horizontal CFRP sheets or anchoring using CFRP anchors, the CFRP width-to-spacing ratio and the number of CFRP layers. These parameters resulted in multiple research specimens with externally bonded CFRP reinforcement and one reference specimen without CFRP reinforcement. These specimens have been analysed for a shear span of 3.0, 4.0 and 5.0 m to investigate the effect of the shear span-to-depth ratio and the type of shear failure.

The finite element models of the reference specimens and the strengthened specimens were not validated because of the lack of good experimental data. A solution strategy validated in literature for quite similar concrete beams, but without CFRP reinforcement, have been used as a starting point. This solution strategy has been extended for the finite element model with CFRP reinforcement by evaluating the suitability of multiple finite element modelling options proposed in literature.

The reference specimen with a shear span of 3.0 m failed in shear tension failure while the specimens with a shear span of 4.0 and 5.0 m failed in flexural shear failure according to the NLFEAs of the reference specimens. The increase in shear capacity and ductility of the I-girder

strengthened with vertical CFRP sheets was limited due to the debonding of the CFRP in the re-entrant corners.

Shear strengthening of prestressed concrete I-girders with vertical CFRP sheets and CFRP anchors is a feasible strengthening method because of the demonstrated potential increase in shear capacity. The externally bonded CFRP reinforcement was especially effective to increase the flexural shear capacity of prestressed concrete I-girders. The numerical analysis showed a promising increase in flexural shear capacity between 40-55% and an increase in ductility of more than 80% compared to the I-girder without CFRP reinforcement

Keywords: CFRP, CFRP anchor, DIANA, Flexural shear failure, NLFEA, Prestressed concrete I-girders, Shear strengthening, Shear tension failure

TABLE OF CONTENTS

LIST OF FIGURES	XI
LIST OF TABLES	XV
LIST OF SYMBOLS	XVII
1. INTRODUCTION	1
1.1. Problem definition	2
1.2. Research objective	4
1.3. Outline	5
2. SHEAR STRENGTH ASSESSMENT IN LITERATURE	7
2.1. Shear behaviour of prestressed girders	8
2.2. Shear strength verification Eurocode	9
2.3. Shear strength verification ACI	11
2.4. Structural safety assessment concrete bridges	12
3. EXTERNALLY BONDED CFRP SHEAR STRENGTHENING IN LITERATURE	15
3.1. Introduction	16
3.2. Material characteristics CFRP	16
3.3. CFRP reinforcement applications	19
3.4. Failure mechanisms of CFRP	21
3.5. Existing analytical models	22
3.6. Design guidelines externally bonded CFRP strengthening	26
3.7. Previous studies on CFRP shear strengthening of I-girders	32
3.8. Parameters affecting the performance of CFRP	35
4. RESEARCH METHODOLOGY	39
4.1. Research outline	40
4.2. Finite element method	40
4.3. Parametric study	41
4.4. Research setup	42
5. SHEAR BEHAVIOUR OF I-GIRDERS STRENGTHENED WITH CFRP REINFORCEMENT	49
5.1. Finite element modelling	50
5.2. Shear behaviour reference specimen I-C	58
5.3. Shear behaviour specimen I-V	61
5.4. Shear behaviour specimen I-VH	68
5.5. Shear behaviour specimen I-VA	71
5.6. Discussion results of finite element analysis	83

6. ADDITIONAL DESIGN CONSIDERATIONS	89
6.1. Execution.....	90
6.2. Environmental conditions	91
6.3. Fire protection.....	92
6.4. Long-term behaviour	93
6.5. Management and maintenance.....	93
7. COMPARISON SHEAR STRENGTHENING METHODS	95
7.1. Alternative shear strengthening methods	96
7.2. Comparison shear strengthening methods	99
8. CONCLUSIONS AND RECOMMENDATIONS	103
8.1. Conclusions	104
8.2. Recommendations.....	106
REFERENCES	109
APPENDICES.....	113
A. Drawings I-girders Nijkerker Bridge	114
B. Geometry research specimens	115
C. Analytical analysis reference specimen I-C	118
D. Finite element model specimens.....	124
E. Nonlinear finite element analyses results	127
F. Nonlinear finite element analysis I-girder Ary and Kang	141

LIST OF FIGURES

Figure 1.1: History of concrete bridge construction in Dutch highways (Gaal, 2004)	2
Figure 1.2: Cross-sections I-girder, T-girder and box-girder	3
Figure 1.3: Nijkerker Bridge	3
Figure 1.4: Existing shear strengthening methods	4
Figure 2.1: Flexural shear failure	8
Figure 2.2: Shear tension failure	8
Figure 2.3: Shear compression failure	9
Figure 2.4: Shear failure (Walraven & Braam, 2019)	10
Figure 2.5: Truss model	10
Figure 2.6: Types of shear cracks in prestressed girder (ACI Committee 318, 2011)	11
Figure 2.7: Assessment procedure structural safety (Rijkswaterstaat, 2013)	12
Figure 3.1: Stress-strain curve carbon fibre and construction steel	16
Figure 3.2: CFRP lamellas (left) and CFRP sheet (right) (S&P Clever Reinforcement Company, 2017a)	17
Figure 3.3: Configurations of externally bonded CFRP sheets (Khalifa et al., 1998)	19
Figure 3.4: Distribution of externally bonded reinforcement (Khalifa et al., 1998)	19
Figure 3.5: Anchoring	20
Figure 3.6: CFRP anchor	20
Figure 3.7: Mechanical anchor	20
Figure 3.8: Multi-linear elastic CFRP model (Woo et al., 2013)	21
Figure 3.9: Local debonding of CFRP reinforcement (Kim et al, 2012)	22
Figure 3.10: CFRP anchor failure mechanisms (Ozbakkaloglu & Saatcioglu, 2009)	22
Figure 3.11: Bilinear bond-slip model (Teng, Yuan & Chen, 2006)	25
Figure 3.12: CFRP shear strengthening with CFRP sheets and CFRP lamellas	27
Figure 3.13: Configurations CFRP shear strengthening CUR 91 (CURNET, 2007)	27
Figure 3.14: Configurations CFRP shear strengthening DAfStb (DAfStb, 2012)	30
Figure 3.15: Schematic illustration U-wrap strips (DAfStb, 2012)	31
Figure 3.16: Extended bilinear bond stress-slip relationship (DAfStb, 2012)	32
Figure 3.17: I-girders in experimental programs	33
Figure 3.18: CFRP tension forces resisted by CFRP anchor (Garcia et al., 2018)	33
Figure 3.19: Inclined CFRP anchor re-entrant corner	34
Figure 3.20: CFRP wrapping configurations	36
Figure 3.21: Detail CFRP anchor re-entrant corner	37
Figure 4.1: Side view I-girder	43
Figure 4.2: Cross-sections I-girder	43
Figure 4.3: Test-setup I-girder	43
Figure 4.4: Specimens I-V and I-V-L2	45
Figure 4.5: Specimen I-V-S0	45
Figure 4.6: Specimen I-VH	45
Figure 4.7: Specimen I-VA	45
Figure 4.8: Specimen I-VA-S0	45
Figure 5.1: Finite element model prestressed concrete I-girder	51
Figure 5.2: Overview finite element model concrete	51
Figure 5.3: Stress-strain diagrams prestress strands and reinforcement bars	52
Figure 5.4: Overview finite element model CFRP	53
Figure 5.5: Finite element model	54
Figure 5.6: Bond-slip diagram	54
Figure 5.7: Finite element model CFRP anchor with three-dimensional elements	56
Figure 5.8: Finite element modelling approaches for CFRP anchors	56
Figure 5.9: Boundary conditions	57
Figure 5.10: Finite element model specimen I-C-SP4	58

Figure 5.11: Load-deformation curves reference specimens I-C-SP3, I-C-SP4 and I-C-SP5.....	60
Figure 5.12: Crack pattern and principal strain plot specimen I-C-SP3 at load step 25.....	60
Figure 5.13: Crack pattern and principal strain plot specimen I-C-SP4 at load step 40.....	60
Figure 5.14: Crack pattern and principal strain plot specimen I-C-SP5 at load step 42.....	61
Figure 5.15: Finite element model specimen I-V-SP4.....	61
Figure 5.16: Load-deformation curves specimens I-V-SP3, I-V-SP4 and I-V-SP5.....	63
Figure 5.17: Debonding CFRP sheets specimen I-V-SP3 at load step 27.....	64
Figure 5.18: Debonding CFRP sheets specimen I-V-SP4 at load step 50.....	64
Figure 5.19: Debonding CFRP sheets specimen I-V-SP5 at load step 51.....	64
Figure 5.20: Axial stress values specimens I-V-SP3, I-V-SP4 and I-V-SP5.....	64
Figure 5.21: Debonding propagation CFRP sheets.....	65
Figure 5.22: Load-deformation curves specimens I-V-S0-SP3, I-V-S0-SP4 and I-V-S0-SP5.....	66
Figure 5.23: Load-deformation curves specimens I-V-L2-SP3, I-V-L2-SP4 and I-V-L2-SP5.....	67
Figure 5.24: Finite element model specimen I-VH-SP4.....	68
Figure 5.25: Load-deformation curves specimens I-VH-SP3, I-VH-SP4 and I-VH-SP5.....	70
Figure 5.26: Debonding CFRP sheets specimen I-VH-SP3 at load step 25.....	70
Figure 5.27: Debonding CFRP sheets specimen I-VH-SP4 at load step 60.....	71
Figure 5.28: Debonding CFRP sheets specimen I-VH-SP5 at load step 74.....	71
Figure 5.29: Axial stress values specimens I-VH-SP3, I-VH-SP4 and I-VH-SP5.....	71
Figure 5.30: Finite element model specimen I-VA-ERS-SP3.....	72
Figure 5.31: Crack strain values specimen I-VA-ERL-SP3.....	74
Figure 5.32: Axial stress values specimen I-VA-ERS-SP3.....	74
Figure 5.33: Axial stress values specimen I-VA-LES-SP3.....	74
Figure 5.34: Axial stress values specimen I-VA-LEL-SP3.....	74
Figure 5.35: Load-deformation curves specimens I-VA-SP3, I-VA-SP4 and I-VA-SP5.....	77
Figure 5.36: Components of shear force specimens I-VA-SP3, I-VA-SP4 and I-VA-SP5.....	77
Figure 5.37: Crack pattern and CFRP debonding specimen I-VA-SP3 at load step 29.....	78
Figure 5.38: Crack pattern and CFRP debonding specimen I-VA-SP4 at load step 72.....	78
Figure 5.39: Crack pattern and CFRP debonding specimen I-VA-SP5 at load step 158.....	78
Figure 5.40: Axial stress values specimens I-VA-SP3, I-VA-SP4 and I-VA-SP5.....	78
Figure 5.41: Load-deformation curves specimens I-VA-S0-SP3, I-VA-S0-SP4 and I-VA-S0-SP5.....	81
Figure 5.42: Components of shear force specimens I-VA-S0-SP3, I-VA-S0-SP4 and I-VA-S0-SP5.....	81
Figure 5.43: Crack pattern and CFRP debonding specimen I-VA-S0-SP3 at load step 59.....	82
Figure 5.44: Crack pattern and CFRP debonding specimen I-VA-S0-SP4 at load step 147.....	82
Figure 5.45: Crack pattern and CFRP debonding specimen I-VA-S0-SP5 at load step 199.....	82
Figure 5.46: Axial stress values specimens I-VA-S0-SP3, I-VA-S0-SP4 and I-VA-S0-SP5.....	82
Figure 6.1: CFRP sheet in re-entrant corner (S&P clever reinforcement company).....	91
Figure 7.1: Shear strengthening with stirrups.....	96
Figure 7.2: Conventional shear reinforcement and concrete cover Nijkerker Bridge.....	96
Figure 7.3: Shear strengthening with vertical external prestressing brace.....	97
Figure 7.4: Prestressed shear reinforcement Kurtheater baden (Re-fer AG, 2019).....	97
Figure 7.5: Shear strengthening with horizontal external prestressing.....	98
Figure 7.6: External support structure.....	98
Figure 7.7: External steel support structure A4 Ringvaartviaduct (Mourik, 2019).....	98
Figure A.1: Side view I-girder Nijkerker Bridge.....	114
Figure A.2: Cross-sections I-girder Nijkerker Bridge.....	114
Figure B.1: Specimen I-V-SP3 and specimen I-V-L2-SP3.....	115
Figure B.2: Specimen I-V-S0-SP3.....	115
Figure B.3: Specimen I-VH-SP3.....	115
Figure B.4: Specimen I-VA-SP3.....	115
Figure B.5: Specimen I-VA-S0-SP3.....	115
Figure B.6: Specimen I-V-SP4 and I-V-L2-SP4.....	116
Figure B.7: Specimen I-V-S0-SP4.....	116
Figure B.8: Specimen I-VH-SP4.....	116
Figure B.9: Specimen I-VA-SP4.....	116
Figure B.10: Specimen I-VA-S0-SP4.....	116
Figure B.11: Specimen I-V-SP5 and I-V-L2-SP5.....	117
Figure B.12: Specimen I-V-S0-SP5.....	117
Figure B.13: Specimen I-VH-SP5.....	117
Figure B.14: Specimen I-VA-SP5.....	117
Figure B.15: Specimen I-VA-S0-SP5.....	117
Figure C.1: Cross-section specimen I-C.....	118

Figure C.2: Geometry specimen I-C	118
Figure C.3: Prestressing	119
Figure C.4: Self-weight.....	120
Figure C.5: Point load.....	120
Figure C.6: Stress distribution.....	121
Figure C.7: Shear resistance specimen I-C	123
Figure D.1: Finite element model reference specimen I-C-SP3	124
Figure D.2: Finite element model reference specimen I-C-SP5	124
Figure D.3: Finite element model specimen I-V-SP3.....	124
Figure D.4: Finite element model specimen I-V-SP5.....	125
Figure D.5: Finite element model specimen I-V-S0-SP3.....	125
Figure D.6: Finite element model specimen I-V-S0-SP4.....	125
Figure D.7: Finite element model specimen I-V-S0-SP5.....	126
Figure D.8: Finite element model specimen I-VH-SP3	126
Figure D.9: Finite element model specimen I-VH-SP5	126
Figure E.1: Principal strain and crack strain values specimen I-C-SP3.....	127
Figure E.2: Principal strain and crack strain values specimen I-C-SP4.....	127
Figure E.3: Principal strain and crack strain values specimen I-C-SP5.....	128
Figure E.4: Principal strain and crack strain values specimen I-V-SP3	128
Figure E.5: Principal strain and crack strain values specimen I-V-SP4	129
Figure E.6: Principal strain and crack strain values specimen I-V-SP5	129
Figure E.7: Debonding CFRP sheets in re-entrant corner specimen I-V-SP3	130
Figure E.8: Debonding CFRP sheets in re-entrant corner specimen I-V-SP5	130
Figure E.9: Principal strain and crack strain values specimen I-V-S0-SP3	131
Figure E.10: Principal strain and crack strain values specimen I-V-S0-SP4	131
Figure E.11: Principal strain and crack strain values specimen I-V-S0-SP5	132
Figure E.12: Principal strain and crack strain values specimen I-V-L2-SP3	132
Figure E.13: Principal strain and crack strain values specimen I-V-L2-SP4	133
Figure E.14: Principal strain and crack strain values specimen I-V-L2-SP5	133
Figure E.15: Load-deflection curves specimens I-V-PB-SP3, I-V-PB-SP4 and I-V-PB-SP5	134
Figure E.16: Displacement and strain plots specimens I-V-SP5 and I-V-PB-SP5	135
Figure E.17: Principal strain and crack strain values specimen I-VH-SP3.....	136
Figure E.18: Principal strain and crack strain values specimen I-VH-SP4.....	136
Figure E.19: Principal strain and crack strain values specimen I-VH-SP5.....	137
Figure E.20: Principal strain and crack strain values specimen I-VA-SP3.....	137
Figure E.21: Principal strain and crack strain values specimen I-VA-SP4.....	138
Figure E.22: Principal strain and crack strain values specimen I-VA-SP5.....	138
Figure E.23: Principal strain and crack strain values specimen I-VA-S0-SP3.....	139
Figure E.24: Principal strain and crack strain values specimen I-VA-S0-SP4.....	139
Figure E.25: Principal strain and crack strain values specimen I-VA-S0-SP4.....	139
Figure E.26: Local displacements specimen I-VA-S0-SP3 at load step 60.....	140
Figure E.27: Local displacements specimen I-VA-S0-SP4 at load step 148.....	140
Figure F.1: Cross-section control specimen I-girder.....	141
Figure F.2: Geometry control specimen I-girder.....	142
Figure F.3: Crack pattern control specimen I-girder	142
Figure F.4: Load-deflection curve	142
Figure F.5: Finite element model	143
Figure F.6: Load-deflection curve control specimen fixed crack model.....	144
Figure F.7: Principal strain (E1) load step 62	144
Figure F.8: Principal strain (E1) load step 63	144
Figure F.9: Principal strain (E1) load step 64	145
Figure F.10: Crack widths (E _{cr1}) load step 62	145
Figure F.11: Crack widths (E _{cr1}) load step 63	145
Figure F.12: Crack strains (E _{knn}) load step 62.....	146
Figure F.13: Crack strains (E _{knn}) load step 63.....	146
Figure F.14: Crack strains (E _{knn}) load step 64.....	146

LIST OF TABLES

Table 2.1: Assessment procedure structural safety (Rijkswaterstaat, 2013)	12
Table 2.2: Levels of safety for existing bridges in RBK (Rijkswaterstaat, 2013)	13
Table 3.1: Epoxy properties S&P (S&P Clever Reinforcement Company, 2018)	17
Table 3.2: CFRP sheet properties S&P (S&P Clever Reinforcement Company, 2017a, b)	18
Table 3.3: Existing analytical models	23
Table 3.4: Comparison of shear capacities in literature	33
Table 4.1: Variation shear span-to-depth ratio	41
Table 4.2: Variation anchorage	41
Table 4.3: Variation spacing	41
Table 4.4: Variation layers	42
Table 4.5: Variation CFRP-to-concrete interface model	42
Table 4.6: Overview research specimens	44
Table 4.7: Concrete material properties	46
Table 4.8: Prestressing steel material properties	46
Table 4.9: Reinforcement steel material properties	46
Table 4.10: CFRP material properties (S&P Clever Reinforcement Company, 2017b)	46
Table 4.11: CFRP anchor material properties (S&P Clever Reinforcement Company, 2019)	46
Table 4.12: Summary analytical analysis specimen I-C	47
Table 4.13: Analytical prediction increase in shear capacity	47
Table 5.1: Concrete constitutive model	50
Table 5.2: Material properties concrete	50
Table 5.3: Properties prestressing strands	52
Table 5.4: Properties reinforcement	52
Table 5.5: Orthotropic linear elastic properties CFRP	53
Table 5.6: Bond-slip properties	54
Table 5.7: Linear elastic properties CFRP anchor	55
Table 5.8: Linear elastic properties stiff line element	56
Table 5.9: Overview finite element modelling approaches	56
Table 5.10: Properties steel	57
Table 5.11: Load cases specimens	57
Table 5.12: Load cases reference specimens I-C-SP3, I-C-SP4 and I-C-SP5	58
Table 5.13: Results specimens I-C-SP3, I-C-SP4 and I-C-SP5	59
Table 5.14: Load cases reference specimens I-V-SP3, I-V-SP4 and I-V-SP5	61
Table 5.15: Results specimens I-V-SP3, I-V-SP4 and I-V-SP5	63
Table 5.16: Results specimens I-V-S0-SP3, I-V-S0-SP4 and I-V-S0-SP5	65
Table 5.17: Results specimens I-V-L2-SP3, I-V-L2-SP4 and I-V-L2-SP5	66
Table 5.18: Results specimens I-V-PB-SP3, I-V-PB-SP4 and I-V-PB-SP5	67
Table 5.19: Load cases reference specimens I-VH-SP3, I-VH-SP4 and I-VH-SP5	68
Table 5.20: Results specimens I-VH-SP3, I-VH-SP4 and I-VH-SP5	70
Table 5.21: Load cases reference specimens I-VA-SP3, I-VA-SP4 and I-VA-SP5	72
Table 5.22: Results specimens I-VA-ERS-SP3, I-VA-LES-SP3, I-VA-ERL-SP3 and I-VA-LEL-SP3	73
Table 5.23: Results specimens I-VA-SP3, I-VA-SP4 and I-VA-SP5	76
Table 5.24: Results specimens I-VA-S0-SP3, I-VA-S0-SP4 and I-VA-S0-SP5	80
Table 5.25: Summary increase shear force analysed specimens	83
Table 5.26: Summary increase ductility analysed specimens	83
Table 5.27: Comparison numerical results and analytical prediction	87
Table 7.1: Legend trade-off matrix	99
Table 7.2: Trade-off matrix shear strengthening methods	101

Table C.1: Concrete material properties.....	118
Table C.2: Prestressing steel material properties.....	119
Table C.3: Reinforcement material properties.....	119
Table C.4: Ultimate point load specimen I-C.....	121
Table C.5: Calculation bending moment resistance	121
Table C.6: Input shear resistance calculation	122
Table C.7: Shear resistance specimen I-C.....	122
Table E.1: Peak load specimens I-V-PB-SP3, I-V-PB-SP4 and I-V-PB-SP5	134
Table F.1: Experimental results control specimen	141
Table F.2: Constitutive model finite element analysis control specimen	143

LIST OF SYMBOLS

Latin letters

A_c	Cross-sectional area of concrete	[mm ²]
A_{fv}	Cross-sectional area of FRP	[mm ²]
A_{LW}	Cross-sectional area of FRP	[mm ²]
A_{sl}	Cross-sectional area of tensile reinforcement	[mm ²]
A_{sw}	Cross-sectional area of shear reinforcement	[mm ²]
A_v	Area of shear reinforcement within spacing s	[mm ²]
b_f	Width of the FRP strip	[mm]
b_{LW}	Width of the FRP strip	[mm]
b_w	Width of the web on T- or I-girders	[mm]
d	Effective depth of the cross-section	[mm]
d_{fv}	Effective depth of FRP shear reinforcement	[mm]
d_p	Distance from extreme compression fibre to centroid of prestressing steel	[mm]
E_f	Modulus of elasticity of FRP	[MPa]
E_{frp}	Modulus of elasticity of FRP	[MPa]
E_{Lm}	Average modulus of elasticity of FRP	[MPa]
E_s	Modulus of elasticity of reinforcement steel	[MPa]
$f_{blk,max}$	Characteristic bond strength of shear strengthening at the anchor end	[MPa]
f_{bLwd}	Design value bond strength of shear strengthening	[MPa]
f_{bm}	Average axial tensile strength of concrete	[MPa]
f'_c	Specified compressive strength of concrete	[MPa]
f_{cd}	Design value of concrete compressive strength	[MPa]
f_{ck}	Characteristic compressive cylinder strength of concrete at 28 days	[MPa]
f'_{ck}	Characteristic compressive cube strength of concrete	[MPa]
f_{ctd}	Design value of concrete axial tensile strength	[MPa]
f_{ctk}	Characteristic axial tensile strength of concrete	[MPa]
f_d	Stress due to unfactored dead load, at extreme fibre of section where tensile stress is caused by externally applied loads	[MPa]
f_{Ld}	Ultimate tensile strength of FRP	[MPa]
f_{Lwd}	Design value shear strengthening strength	[MPa]
$f_{Lwd,G}$	Design value material strength shear strengthening	
f_{pc}	Compressive stress in concrete at centroid of cross-section	[MPa]
f_{pe}	Compressive stress in concrete due to effective prestress forces only at extreme fibre of section where tensile stress is caused by externally applied loads	[MPa]
f_{yt}	Specified yield strength of transverse reinforcement	[MPa]
f_{ywd}	Design yield strength of shear reinforcement	[MPa]
G_f	Interfacial fracture energy	[N/mm]
h	Height	[mm]

h_f	Height of the top flange	[mm]
$h_{frp,e}$	Effective height of FRP	[mm]
I	Second moment of area of concrete section	[mm ⁴]
$l_{bL,max}$	Effective bond length	[mm]
M_{cre}	Moment causing flexural cracking at section due to externally applied loads	[Nmm]
M_{max}	Maximum factored moment at section due to externally applied loads	[Nmm]
N_{Ed}	Design value of the applied axial force (tension or compression)	[N]
P	Prestressing force	[N]
r_c	Corner radius	[mm]
S	First moment of area of concrete section	[mm ³]
s	Centre-to-centre distance shear reinforcement	[mm]
s_0	Slip corresponding to the peak bond stress	[mm]
s_f	Centre to centre distance of FRP strips	[mm]
s_{frp}	Centre to centre spacing of FRP strips measured along longitudinal axis	[mm]
s_u	Ultimate slip	[mm]
s_{Lok}	Maximum creep of FRP reinforcement	[-]
s_{Lw}	Centre-to-centre distance of FRP strips	[mm]
t_f	Thickness of FRP reinforcement	[mm]
t_{frp}	Thickness of FRP reinforcement	[mm]
t_L	Thickness of externally bonded reinforcement	[mm]
t_{Lw}	Thickness of FRP reinforcement	[mm]
V	Shear force	[N]
V_{ccd}	Shear capacity provided by the concrete	[N]
V_d	Shear force at section due to unfactored dead load	[N]
V_i	Factored shear force at section due to externally applied loads occurring simultaneously with M_{max}	[N]
V_p	Vertical component of effective prestressed force at section	[N]
$V_{Rd,s}$	Shear capacity provided by the reinforcement steel	[N]
w_f	Width of individual FRP strip	[mm]
w_{frp}	Width of individual FRP strip perpendicular to fibre orientation	[mm]
y_t	Distance from centroidal axis of gross section, neglecting reinforcement, to tension face	[mm]
z	Lever arm of internal forces	[mm]

Greek letters

α	Angle	[°]
α_{cc}	Coefficient taking account of long term effects on the compressive strength and of unfavourable effects resulting from the way the load is applied	[-]
α_{ct}	Coefficient taking account of long term effects on the tensile strength and of unfavourable effects resulting from the way the load is applied	[-]
α_{zeit}	Coefficient taking account of long term effects on the strength of the FRP reinforcement	[-]
β	Angle	[°]
γ_{BA}	Partial factor externally bonded reinforcement	[-]
γ_C	Partial factor for concrete	[-]
γ_{frp}	Partial factor for FRP	[-]
γ_G	Partial factor for permanent actions	[-]
γ_P	Partial factor for actions associated with prestressing	[-]
γ_Q	Partial factor for variable actions	[-]

γ_m	Partial factor for FRP strengthening	[-]
ζ	Reduction factor	[-]
ε_{fe}	Effective strain of FRP	[‰]
ε_{fu}	Fracture strain of FRP	[‰]
ε_{feff}	Effective strain of FRP	[‰]
$\varepsilon_{frp,e}$	Effective strain of FRP	[‰]
θ	Angle	[°]
ν	Poisson's ratio	[-]
ρ_f	FRP area fraction	[-]
ρ_{frp}	FRP area fraction	[-]
ρ_l	Reinforcement ratio for longitudinal reinforcement	[-]
σ_{cp}	Compressive stresses in the concrete from axial load or prestressing	[MPa]
τ_f	Peak bond stress of CFRP-to-concrete interface	[MPa]
τ_{L1k}	Maximum bond strength externally bonded reinforcement	[MPa]
τ_{LF}	Residual bond stress	[MPa]

1

INTRODUCTION

1.1. Problem definition

The Netherlands has many bridges because of the dense infrastructure network, rivers and canals. Approximately 60% of the bridges managed by Rijkswaterstaat (responsible department for the design, construction, management and maintenance of the main infrastructure facilities in the Netherlands) were built before 1975. Most of the bridges built between 1950-1975 are reaching the end of their intended service life. Concrete bridges built in this period have been designed according to former design regulations and traffic predictions. The structural safety of the concrete bridges built before 1975 have been assessed by Rijkswaterstaat. From this assessment it is concluded that some of these concrete structures have insufficient bending moment and shear capacity (Rijkswaterstaat, 2007). Rijkswaterstaat started the "Programma Vervanging en Renovatie" (Program Replacement and Renovation) in 2018 to guarantee the structural safety and quality of the infrastructure network.

Measures to guarantee the structural safety of concrete bridges with insufficient moment and shear capacity are load limitations, replacement or renovation and strengthening. Load limitations are not desirable because bridges are important connections in the infrastructure network. Replacement of all the bridges with insufficient structural capacity is not possible because of insufficient economical resources. Renovation of bridges with insufficient structural capacity is the desired choice in most cases.

Shear capacity is an important topic for bridges built before 1975 with prestressed concrete I-, T- or box-girders. Typical cross-sections of I-, T- and box-girders are illustrated in Figure 1.2. These girders are likely to have insufficient shear capacity because these types of girders have thin webs and the shear capacity was checked in a fundamentally different way before 1974 (Rijkswaterstaat, 2007). The I- and T-girders made before 1975 probably have insufficient or no shear reinforcement. Shear failure is considered as the critical failure mode for girders with insufficient or without shear reinforcement. Shear failure should be prevented because almost no warning occurs before the structure fails in shear. Because the cross-sectional shape of I- and T-girders are comparable, the scope of this report is limited to prestressed concrete I-girders.

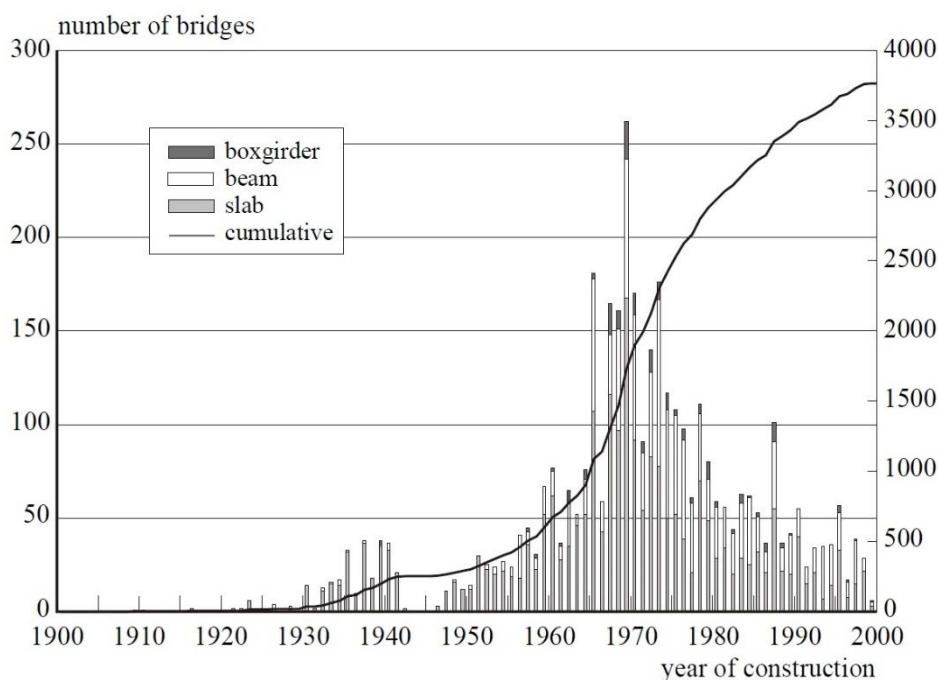


Figure 1.1: History of concrete bridge construction in Dutch highways (Gaal, 2004)

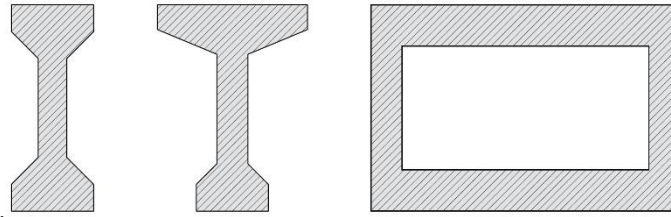


Figure 1.2: Cross-sections I-girder, T-girder and box-girder

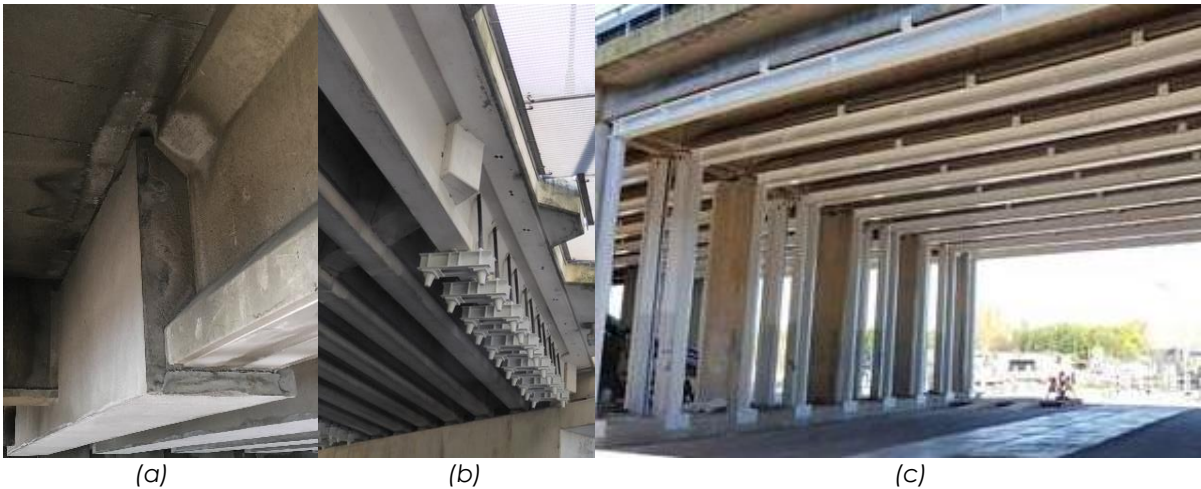
One of the bridges with insufficient shear capacity was the Nijkerker Bridge (see Figure 1.3). The shear capacity of the I-girders was exceeded by 60% due to the increase in traffic load and the absence of shear reinforcement. During the design phase the choice was made to renovate the bridge instead of demolishing and replacing the bridge. During the design phase several shear strengthening methods have been investigated. One of these methods was shear strengthening with CFRP (Carbon Fibre-Reinforced Polymer) reinforcement. Shear strengthening of prestressed I-girders using externally bonded CFRP reinforcement seems promising because of the favourable properties of CFRP. These are the combination of low application costs, negligible increase in weight and minimising the hinderance during installation. However, this method was not applied due to the lack of knowledge and the time constraints.

Rijkswaterstaat is still interested in the shear strengthening method using externally bonded CFRP reinforcement because of the disadvantages of the existing shear strengthening methods. Some existing methods are presented in Figure 1.4. The disadvantages of the existing shear strengthening methods are an increase in self-weight, a decrease of the clear height underneath the bridge deck and hindrance on top of the deck.

Rijkswaterstaat decided together with Mourik, BESIX, Vogel and ABT to continue the research. The aim of the research is to investigate the feasibility of shear strengthening I-girders using externally bonded CFRP reinforcement by experimental testing. Rijkswaterstaat, Mourik, Vogel and ABT are planning to do full-scale experimental testing of I-girders strengthened with externally bonded CFRP reinforcement in the near future. Three prestressed I-girders with a cross-sectional shape similar to the cross-section of the I-girders of the Nijkerker Bridge will be produced and tested in a laboratory. The aim of the experimental test is to increase the shear capacity of the I-girder with 50% compared to the design shear strength.



Figure 1.3: Nijkerker Bridge



(a) Conventional shear reinforcement with concrete cover
 (b) External prestressing braces
 (c) External steel support structure

Figure 1.4: Existing shear strengthening methods

1.2. Research objective

Some bridges built with prestressed concrete I-girders made before 1975 do not satisfy the current regulations. The bending moment and shear capacity of these girders are insufficient according to the current design guidelines. Renovation and strengthening of these girders to increase the service life of the bridges is preferred.

Shear strengthening of prestressed I-girders using externally bonded CFRP reinforcement seems promising because of the favourable properties of this shear strengthening method compared to the existing shear strengthening methods.

While bending moment strengthening using CFRP reinforcement is already applied in practice, experience and knowledge using CFRP to strengthen I-girders in shear is very limited in the Netherlands. The limited amount of research abroad showed the potential of externally bonded CFRP reinforcement to strengthen prestressed I-girders in shear. However, more research is needed before CFRP reinforcement can be used to strengthen these girders in shear.

The aim of this research is to investigate the feasibility of using externally bonded CFRP reinforcement to strengthening prestressed concrete I-girders in shear. The main research question is:

What is the potential for shear strengthening of bridges built with prestressed concrete I-girders using externally bonded CFRP reinforcement?

The potential of externally bonded CFRP reinforcement mainly depends on the increase in shear capacity of the I-girder. Rijkswaterstaat aims at an increase in shear capacity of 50% compared to the design shear capacity. Furthermore the sustainability, durability and the costs determine the feasibility of CFRP shear strengthening.

1.3. Outline

The outline of the report will be explained in this section. The shear strength assessment of concrete structures in literature is described in Chapter 2. The shear behaviour of prestressed concrete elements is also explained in this chapter. The literature study of externally bonded CFRP reinforcement is included in Chapter 3. The material properties of CFRP, design guidelines for externally bonded CFRP reinforcement and the results of experimental tests are described in this chapter. Chapter 4 describes the research methodology of this thesis. Nonlinear finite element analysis (NLFEA) software DIANA has been used to investigate the performance of externally bonded CFRP reinforcement. The research parameters and the specimens are also explained in this chapter. The finite element model of the specimens and the results of the NLFEAs are given in Chapter 5. The chapter also includes the discussion and the comparison of the results of the numerical analyses. The additional design consideration regarding externally bonded CFRP reinforcement are explained in Chapter 6. Several existing shear strengthening methods of prestressed concrete girders are explained in Chapter 7. In this chapter, these methods and shear strengthening with externally bonded CFRP reinforcement are compared in this chapter using a trade-off matrix. The conclusions and recommendations are given in Chapter 8.

2

SHEAR STRENGTH ASSESSMENT IN LITERATURE

2.1. Shear behaviour of prestressed girders

The shear behaviour of prestressed concrete girders is discussed in this section. Good understanding of shear behaviour of prestressed concrete girders is essential to assess the shear strength and to investigate the feasibility of shear strengthening using externally bonded CFRP reinforcement. The shear strength of concrete prestressed girders depends on the resistance against shear failure. The distinction is made between three types of shear failure. These are shear flexural failure, shear tension failure and shear compression failure (Regan, 1993).

2.1.1. Flexural shear failure

Flexural shear failure originates from flexural cracks. The flexural cracks develop in the area where the cracking moment is exceeded. The flexural cracks propagate into the web of the girder (Regan, 1993). The flexural shear failure is illustrated in Figure 2.1.

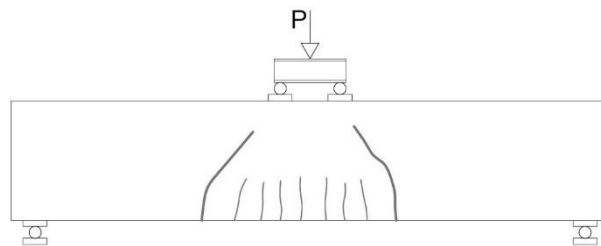


Figure 2.1: Flexural shear failure

2.1.2. Shear tension failure

Shear tension failure starts with the development of diagonal cracks in the web. The diagonal cracks develop in the regions without flexural cracking. The diagonal cracks are perpendicular to the principle tensile stress in the girder. The diagonal crack propagates to the top and the bottom of the web (Nawy, 2009). The shear tension crack formation is shown in Figure 2.2. In case no shear reinforcement is present, the critical diagonal crack develops and brittle failure occurs. In case of a girder with insufficient shear reinforcement, the load can be increased after the propagation of the critical diagonal crack. The failure mode is rupture of the shear reinforcement without crushing of the concrete. Prestressed I-girders are especially sensitive to shear tension failure because of the thin webs.

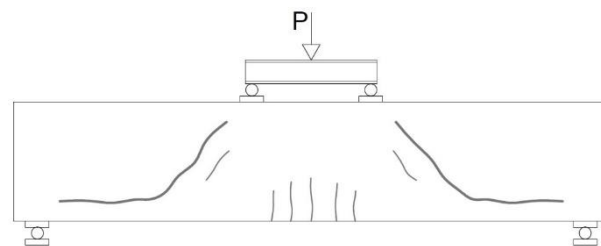


Figure 2.2: Shear tension failure

2.1.3. Shear compression failure

Shear compression failure is also known as crushing of the web. In case of shear compression failure diagonal cracks develop in the web of the girder. The region between the diagonal cracks fail in compression due to principle compressive stresses. When a high shear reinforcement ratio is present, the concrete between the diagonal cracks will crush before the shear reinforcement yields.

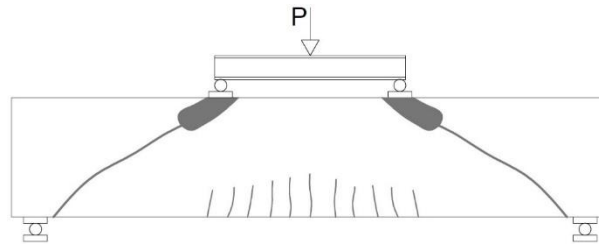


Figure 2.3: Shear compression failure

2.2. Shear strength verification Eurocode

The verification of the shear resistance is included in Eurocode NEN-EN 1992-1-1 (Nederlands Normalisatie-instituut, 2011c):

- The design shear resistance of the girder without shear reinforcement.
- The maximum shear force which can be sustained by the yielding shear reinforcement.
- The maximum shear force which can be sustained by the compression struts in the girder.

2.2.1. Shear resistance without shear reinforcement

The shear resistance of prestressed girders without shear reinforcement depends on the flexural cracks. The regions in a prestressed concrete girder are given in Figure 2.4. Region I is the region without flexural cracks because the principle tensile stress in the concrete does not exceed the tensile capacity of the concrete. The shear resistance in region I is given by (NEN-EN 1992-1-1 eq. (6.4)):

$$V_{Rd,c} = \frac{I \cdot b_w}{S} \sqrt{f_{ctd}^2 + \alpha_l \sigma_{cp} f_{ctd}} \quad (2.1)$$

where

$$\begin{aligned} f_{ctd} &= \alpha_{ct} f_{ctk;0,05} / \gamma_c \\ \alpha_l &= l_x / l_{pt2} \leq 1.0 \\ \sigma_{cp} &= N_{Ed} / A_c \end{aligned}$$

Region II is the region with flexural cracks. The behaviour of the failure in this region is complicated. The shear resistance in region II is given by (NEN-EN 1992-1-1 eq. (6.2)):

$$V_{Rd,c} = (C_{Rd,c} k (100 \rho_l f_{ck})^{1/3} + k_1 \sigma_{cp}) b_w d \quad (2.2)$$

$$V_{Rd,c} \geq (v_{min} + k_1 \sigma_{cp}) b_w d \quad (2.3)$$

where

$$\begin{aligned} C_{Rd,c} &= 0.18 / \gamma_c \\ k &= 1 + \sqrt{200/d} < 2.0 \\ \rho_l &= A_{sl} / (b_w d) \leq 0.02 \\ \sigma_{cp} &= N_{Ed} / A_c < 0.2 f_{cd} \\ v_{min} &= 0.035 k^{3/2} f_{ck}^{1/2} \end{aligned}$$

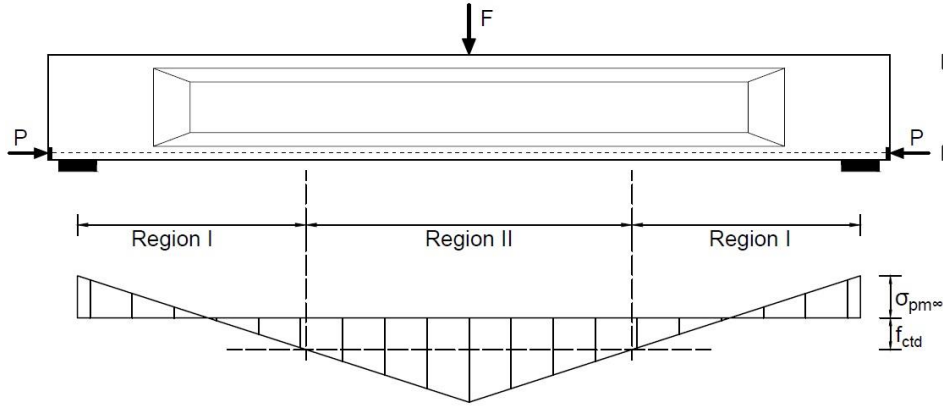


Figure 2.4: Shear failure (Walraven & Braam, 2019)

2.2.2. Shear resistance with shear reinforcement

The shear resistance of girders with shear reinforcement is based on the truss analogy. The truss model of a simple supported beam is illustrated in Figure 2.5. The angle θ is the angle between the compression struts and the angle α is the inclination of the shear reinforcement. The shear resistance of the prestressed girder with shear reinforcement is given by (NEN-EN 1992-1-1 eq. (6.13)):

$$V_{Rd,s} = \frac{A_{sw}}{s} z f_{yd} (\cot(\theta) + \cot(\alpha)) \sin(\alpha) \quad (2.4)$$

The maximum shear resistance is limited by the compressive strength of the compressive struts. The maximum shear resistance of the compressive strut is given by (NEN-EN 1992-1-1 eq. (6.9)):

$$V_{Rd,max} = \frac{\alpha_{cw} b_w z v_1 f_{cd} (\cot(\theta) + \tan(\theta))}{1 + \cot^2(\theta)} \quad (2.5)$$

where

$$\alpha_{cw} = \begin{cases} 1 + \sigma_{cp}/f_{cd} & \text{for } 0 < \sigma_{cp} \leq 0.25 f_{cd} \\ 1.25 & \text{for } 0.25 f_{cd} < \sigma_{cp} \leq 0.5 f_{cd} \\ 2.5(1 + \sigma_{cp}/f_{cd}) & \text{for } 0.5 f_{cd} < \sigma_{cp} < 1.0 f_{cd} \end{cases}$$

$$v_1 = \begin{cases} 0.6 & \text{for } f_{ck} \leq 60 \text{ MPa} \\ 0.9 - f_{ck}/200 > 0.5 & \text{for } f_{ck} > 60 \text{ MPa} \end{cases}$$

The shear resistance of concrete prestressed girders with shear reinforcement is given by:

$$V_{Rd} = \min\{V_{Rd,s}; V_{Rd,max}\} \quad (2.6)$$

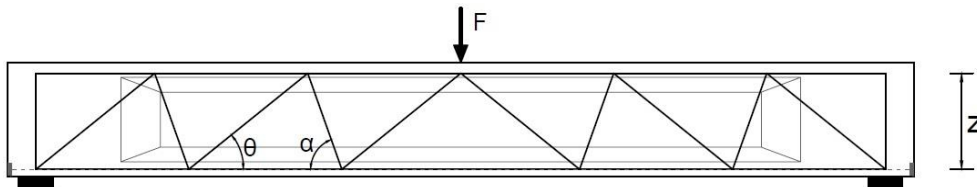


Figure 2.5: Truss model

2.3. Shear strength verification ACI

2.3.1. Shear resistance without shear reinforcement

The shear strength verification in the United States of America is described in the Building Code Requirements for Structural Concrete (ACI 318-11). The shear strength verification of prestressed members and reinforced members is separated (ACI Committee 318, 2011). The shear resistance of prestressed members is given by (ACI 318-11):

$$V_c = \min\{V_{ci}; V_{cw}\} \quad (2.7)$$

$$2\sqrt{f'_c}b_wd_p \leq V_c \leq 5\sqrt{f'_c}b_wd_p \quad (2.8)$$

The shear resistance V_{ci} is the capacity in the flexural shear region and the shear resistance V_{cw} is the capacity in the web shear region. The web shear region is the region without flexural cracks. The flexural shear and web shear region are illustrated in Figure 2.6. The shear force causing flexural shear cracking is given by (ACI 318-11 (11-10)):

$$V_{ci} = 0.6\sqrt{f'_c}b_wd_p + V_d + \frac{V_iM_{cre}}{M_{max}} \quad (2.9)$$

$$M_{cre} = \frac{I}{y_t} (6\sqrt{f'_c} + f_{pe} - f_d) \quad (2.10)$$

The shear force causing web shear cracking is given by (ACI 318-11 (11-12)):

$$V_{cw} = (3.5\sqrt{f'_c} + 0.3f_{pc})b_wd_p + V_p \quad (2.11)$$

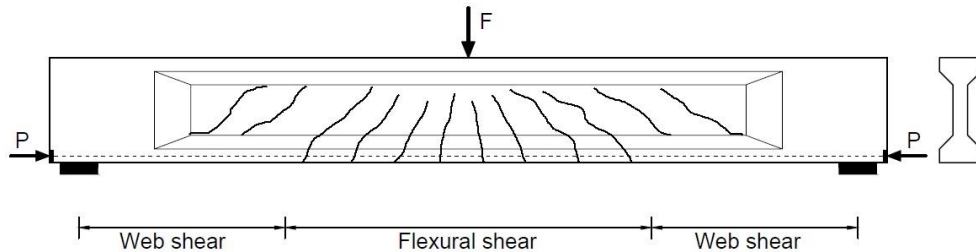


Figure 2.6: Types of shear cracks in prestressed girder (ACI Committee 318, 2011)

2.3.2. Shear resistance with shear reinforcement

The shear resistance of the shear reinforcement is given by (ACI 318-11 (11-16)):

$$V_s = \frac{A_v f_{yt} (\sin(\alpha) + \cos(\alpha)) d}{s} \quad (2.12)$$

The angle α is the inclination of the shear reinforcement.

2.4. Structural safety assessment concrete bridges

The safety of existing structures in the infrastructure network of Rijkswaterstaat is assessed according to the RBK (Rijkswaterstaat, 2013). The RBK describes in which case existing structures should be assessed. Damage to the structure, increase of traffic load and changed design regulations are reasons to assess the structural safety of existing bridges. The assessment procedure is given in Figure 2.7 and Table 2.1.

Table 2.1: Assessment procedure structural safety (Rijkswaterstaat, 2013)

Stage AI	<ul style="list-style-type: none"> ▪ Load factors, remaining lifetime and reference period according to the level of safety in operation ▪ Traffic loads according to the design traffic loads (NEN-EN 1991-2)
Stage AII	<ul style="list-style-type: none"> ▪ Load factors, remaining lifetime and reference period according to the level of safety in operation ▪ Traffic loads according to the actual traffic loads (NEN 8701)
Stage AIII	<ul style="list-style-type: none"> ▪ Load factors, remaining lifetime and reference period according rejection level of safety ▪ Traffic loads according to the actual traffic loads (NEN 8701)

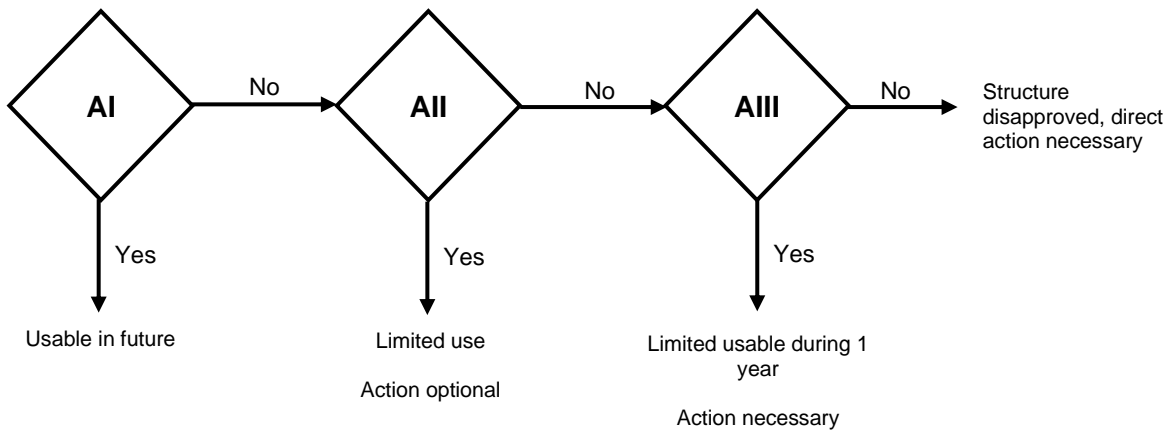


Figure 2.7: Assessment procedure structural safety (Rijkswaterstaat, 2013)

2.4.1. Loads

The assessment procedure of existing bridges is given in the RBK, which states that the loads should be calculated according to NEN 8700 and NEN 8701. NEN 8700 describes the consequence classes and the minimum level of safety (Nederlands Normalisatie-Instituut, 2011a). The NEN 8701 describes the calculation of the traffic loads according to the actual traffic loads (Nederlands Normalisatie-Instituut, 2011b).

Load factors

The reliability index corresponds to the level of safety of structural elements and is related to the failure probability. It depends on the design situation of the structure. The load factors are based on the reliability index and the reference period. The design situations and the corresponding reliability index and load factors are given in Table 2.1.

Table 2.2: Levels of safety for existing bridges in RBK (Rijkswaterstaat, 2013)

	β	Permanent	Permanent	Traffic	Wind	Other
		γ_G	$\xi\gamma_G$	$\gamma_{Q,i}$	$\gamma_{Q,i}$	$\gamma_{Q,i}$
New construction	4.3	1.40	1.25	1.50	1.65	1.65
Renovation	3.6	1.30	1.15	1.30	1.60	1.50
Operation	3.3	1.25	1.15	1.25	1.50	1.30
Rejected	3.1	1.25	1.10	1.25	1.50	1.30

Traffic loads

The traffic loads are based on NEN-EN 1991-2 and NEN 8701. The traffic load on bridges depends on the traffic composition, traffic intensity, circumstances and maximum vehicle weight. Load models (LM) are defined in the Eurocode to design or assess bridges.

- LM1: Concentrated and uniformly distributed loads
- LM2: Single axle load applied on specific tyre contact areas
- LM3: Set of axle loads representing special vehicles
- LM4: Crowd loading

The concentrated and uniformly distributed loads are corrected with adjustment factors α_{Qi} , α_{qi} and α_{qr} . These factors depend on the number of heavy vehicles per year per lane (Nederlands Normalisatie-Instituut, 2015). LM1 and LM2 should be corrected with the adjustment factor α_{trend} according to the NEN 8701. The adjustment factor α_{trend} depends on the span and the trend (Nederlands Normalisatie-Instituut, 2011b).

2.4.2. Assessment structural safety

The ultimate limit state should be verified using the unity check. The unity check is the ratio between the design value of the action effect and the design value of the resistance. The effect of the action should be calculated according to the NEN 8700 and the NEN 8701. The resistance of concrete structures should be calculated according to the NEN-EN 1992-1-1 and the RBK.

Shear strength assessment

The shear resistance of existing prestressed girders is the sum of the shear resistance provided by the shear reinforcement and the concrete according to the RBK:

$$V_{Rd} = V_{Rd,s} + V_{Rd,c} \quad (2.13)$$

The shear resistance provided by the shear reinforcement should be determined using the equation (2.4). The angle of the compression strut is 30° for prestressed concrete girders. The shear resistance of the shear reinforcement should not be used when the detailing of the shear reinforcement is not according to the NEN-EN 1992-1-1 9.2.2. The shear resistance provided by the concrete is given by equation (2.2).

3

EXTERNALLY BONDED CFRP SHEAR STRENGTHENING IN LITERATURE

3.1. Introduction

CFRP (Carbon Fibre Reinforced Polymer) is a commonly used material in the aerospace and car industry. However, CFRP has also become a popular material in the construction industry because of its favourable properties. CFRP reinforcement has been used to increase the flexural and shear strength of concrete elements. Many researchers investigated the material properties of the CFRP reinforcement and the behaviour of concrete elements strengthened with externally bonded CFRP reinforcement. Guidelines have been developed to design externally bonded CFRP reinforcement to strengthen existing concrete elements. However, the research and the guidelines focus mainly at shear strengthening of rectangular reinforced concrete elements. This chapter includes a literature review of the application of CFRP reinforcement, its material properties and the design guidelines to get a better understanding of the structural behaviour of externally bonded CFRP reinforcement. Previous research of prestressed concrete I-girders strengthened with externally bonded CFRP reinforcement is described in Section 3.7. Parameters that possibly affect the performance of the externally bonded CFRP reinforcement are given in Section 0.

3.2. Material characteristics CFRP

Fibre Reinforced Polymer (FRP) materials are polymer composite products made of carbon fibres, glass fibres or carbon fibres. The fibres are embedded in a polymer matrix. FRP materials are suitable to strengthen concrete elements because of the high tensile strength-to-weight ratio of the fibres. The matrix allows for transfer of forces between the fibres (Matthys, 2000). Furthermore the matrix protects the fibres against damage and environmental deterioration. The FRP is bonded to concrete elements by an adhesive. Carbon fibres are the most used fibres for strengthening of concrete elements because they are the stiffest and strongest fibre type.

3.2.1. Constituents materials for CFRP

Carbon fibres

Carbon fibres have a high modulus of elasticity and high tensile strength compared to construction steel. The tensile stress-strain curves of carbon fibres and steel are given in Figure 3.1. Carbon fibres with high modulus of elasticity and tensile strength are produced from polyacrylonitrile. The stress-strain behaviour of the carbon fibres is linear-elastic up to tensile failure. Carbon fibres have a high resistance against creep and fatigue. Furthermore, they have a good chemical, UV light and moisture resistance (Matthys, 2000).



Figure 3.1: Stress-strain curves carbon fibre and construction steel

Polymer matrices

The main component of the polymer matrix is the polymer binder. The polymer binder holds the fibres together, provides lateral support to the fibres and protects the fibres against damage (Matthys, 2000). The polymer binder is made from thermosetting or thermoplastic polymers. Thermosetting resins polyester, vinyl ester and epoxy are often used as polymer binder for structural application. Fillers and additives are used in the polymer matrix to improve certain material properties of the CFRP.

Adhesives

Adhesives are used to connect CFRP materials to the surface of concrete elements. The Adhesive provides a load path between the CFRP and the concrete. Epoxies are often used as adhesive because of their favourable material properties (Matthys, 2000). Typical properties of available epoxy resins are given in Table 3.1.

Table 3.1: Epoxy properties S&P (S&P Clever Reinforcement Company, 2018)

	Modulus of elasticity [MPa]	Compressive strength [MPa]	Tensile strength [MPa]	Creep [%]
Resicem HP	6500	110	14.5	0.01
Resin 55 HP	3200	100	15.9	0.02
Resin 220 HP	7100	83	15.0	0.01

3.2.2. CFRP products

CFRP products are available in various shapes. The CFRP products are provided as 'prefab' or as 'wet lay-up'. The CFRP laminates are pre-cured 'prefab' straight strips. The CFRP sheets are available as 'wet lay-up' unidirectional or multidirectional fabric. The unidirectional sheets are produced by stitching the parallel aligned carbon fibres with glass fibres. 'Prefab' or 'wet lay-up' bundles of carbon fibres are available to make CFRP anchors.

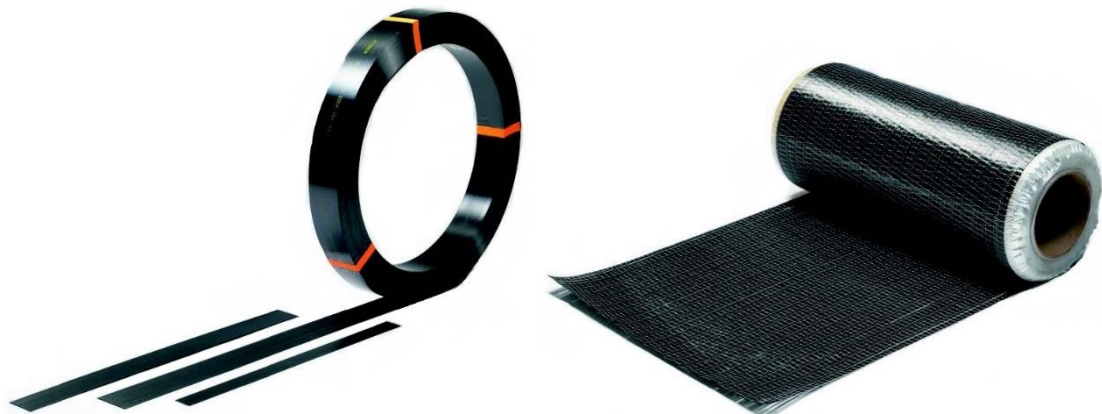


Figure 3.2: CFRP lamellas (left) and CFRP sheet (right) (S&P Clever Reinforcement Company, 2017a)

3.2.3. Mechanical properties of CFRP

Stress-strain behaviour

CFRP is an orthotropic material characterised by the high tensile strength in the direction parallel to the carbon fibres. The tensile strength of the carbon fibres is high compared to the tensile strength of the polymer matrix. The stress-strain behaviour of CFRP loaded in tension is mainly determined by the carbon fibres. The tensile strength and modulus of elasticity of CFRP reinforcement are lower compared to the individual carbon fibres. (Matthys, 2000). Typical

mechanical properties of CFRP sheets are given in Table 3.2. The actual behaviour of CFRP is not perfectly linear elastic. During production the carbon fibres are not fully aligned. The carbon fibres straighten as the load increases and become more effective. Therefore, the stress-strain response stiffens during loading. Close to the ultimate strain of the CFRP the fibres start to fracture and the stiffness decreases.

Table 3.2: CFRP sheet properties S&P (S&P Clever Reinforcement Company, 2017a, b)

	Density [g/cm ³]	Modulus of elasticity [GPa]	Tensile strength [MPa]	Ultimate strain [%]
C-sheet 240	1.78	240	4300	1.8
C-sheet 640	2.12	640	2600	0.4

Durability

The material properties of CFRP are strongly affected when reaching the glass-transition temperature. The glass-transition temperature of epoxy resins is about 50 to 60 °C (S&P Clever Reinforcement Company, 2018). Because of this low glass-transition temperature the fire behaviour is poor. The event of fire will quickly result in a complete loss of adhesive strength (Blontrock, Taerwe & Matthys, 1999). The fire behaviour of CFRP strengthening should be taken into account in the design.

Structures subjected to temperature changes will initiate thermal stresses in the CFRP and the concrete. Thermal bond stresses are generated in the interface between the concrete and the CFRP in case of large temperature changes (Matthys, 2000). Furthermore freeze-thaw action may cause problems by expansion of freezing water. Both effects do not have significant impact on the mechanical properties of CFRP.

Carbon fibres are relatively inert to water in contrast to the polymer matrix and the adhesive. Absorption of moisture results in a reduction of the glass-transition temperature and stiffening of the polymer (Matthys, 2000). Moisture does not have a significant impact on the performance of CFRP reinforcement.

Carbon fibres have a high chemical and UV radiation resistance. The polymer matrix can be affected by UV radiation in a limited way. The degradation due to UV radiation can be avoided by addition of appropriate additives to the polymer binder (Matthys, 2000).

Creep

Carbon fibres have a good resistance to creep deformations. However, the viscoelastic polymer matrix has a low resistance to creep deformations. The creep deformations of the CFRP will be mainly caused by creep of the polymer matrix. The tensile force in the polymer matrix is usually low because the carbon fibres are aligned and the glass transition temperature is well above the service temperature (Hollaway & Leeming, 1999).

The creep behaviour of the adhesive may significantly affect the load transfer between the concrete element and the CFRP. The adhesive exhibits linear viscoelastic or viscoplastic tensile behaviour (Costa & Barros, 2015). Costa & Barros (2015) observed creep deformations larger than the short-term ultimate strain without rupture. They concluded that the adhesive is able to reorganize its internal structure. The externally bonded CFRP reinforcement should be designed to low sustained stresses to prevent excessive creep (Matthys, 2000).

3.3. CFRP reinforcement applications

3.3.1. Externally bonded CFRP reinforcement

The configuration of the CFRP reinforcement determines the performance of the shear strengthening. Three configurations of externally bonded CFRP reinforcement can be distinguished (ACI Committee 440, 2008). The first configuration is full-wrap of the circumference of the girder. The second configuration is U-wrap. The third configuration is the side bonded configuration. The three configurations of externally bonded CFRP reinforcement are illustrated in Figure 3.1.

Full-wrap CFRP strengthening is the most effective configuration (Matthys, 2000). Full-wrap CFRP strengthening can be compared to the closed shear reinforcement as described in the Eurocode. However, from a practical point of view the full-wrap CFRP reinforcement is often not feasible. U-wrap and side bonded CFRP reinforcement are more practical configurations. However, these are less effective. The connection between the CFRP reinforcement and the concrete element is a chemical bond. The full-wrap CFRP reinforcement is not only a chemical connection, but also a mechanical connection because the CFRP forms a closed system.

Two types of externally bonded CFRP reinforcement distribution can be distinguished. The first application are strips with a free space between the strips while the second application is continuous with no spacing between the strips. These two types are presented in Figure 3.4.

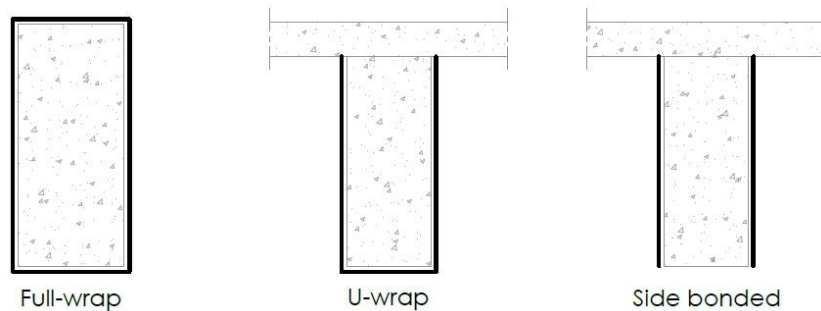


Figure 3.3: Configurations of externally bonded CFRP sheets (Khalifa et al., 1998)

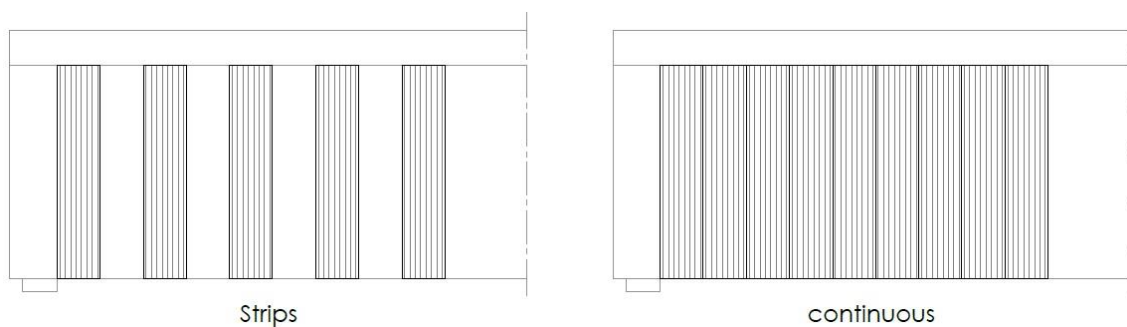


Figure 3.4: Distribution of externally bonded reinforcement (Khalifa et al., 1998)

3.3.2. Anchoring

The performance of U-wrap CFRP reinforcement can be increased by anchoring of the CFRP reinforcement in the compression zone. The externally bonded CFRP reinforcement can be anchored with mechanical anchors or with CFRP anchors (Kalfat, Al-Mahaidi & Smith, 2013). The application of CFRP reinforcement with anchors is illustrated in Figure 3.2. A CFRP anchor is a bundle of carbon fibres which is placed into a predrilled hole in the concrete, where the fibres are connected to the concrete using adhesive, as illustrated in Figure 3.6. An example of a mechanical anchor is presented in Figure 3.7.

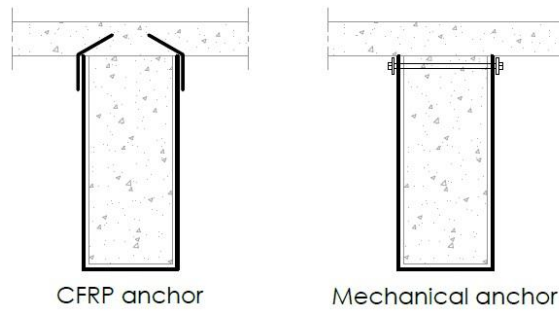


Figure 3.5: Anchoring

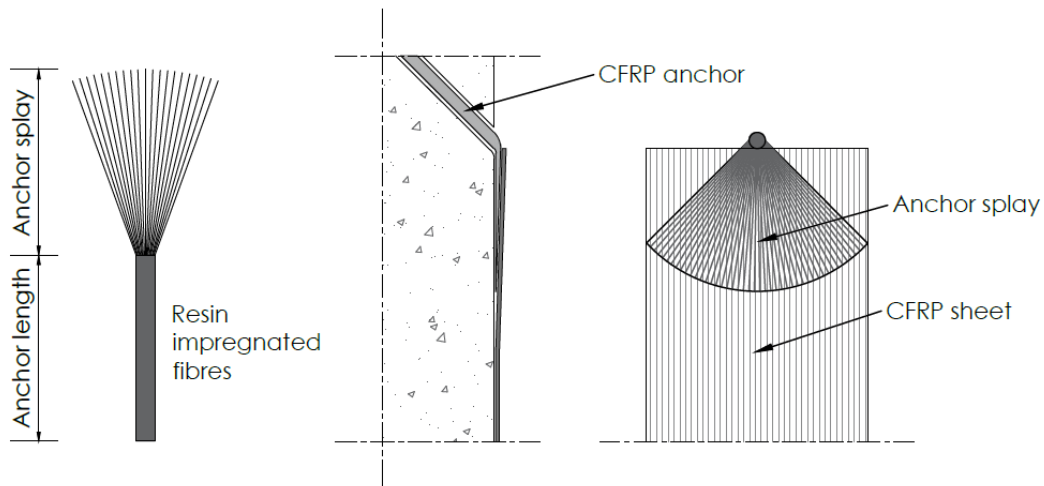


Figure 3.6: CFRP anchor

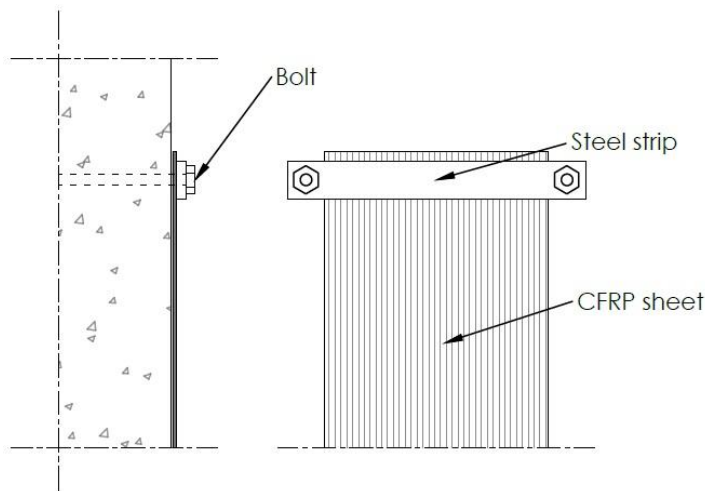


Figure 3.7: Mechanical anchor

3.4. Failure mechanisms of CFRP

3.4.1. Failure mechanisms of externally bonded CFRP reinforcement

The two main failure mechanisms of externally bonded CFRP reinforcement are CFRP rupture and CFRP debonding. The U-wrap and the side-bonded CFRP reinforcement configurations are susceptible to debonding failure, while the failure mechanism of full-wrap CFRP is governed by rupture (Ary & Kang, 2012).

In case of CFRP rupture the carbon fibres achieve their ultimate strain. At ultimate strain the carbon fibres in the reinforcement fracture. The stress at fracture may be lower than the ultimate tensile strength of the CFRP reinforcement, because of stress concentrations (Triantafillou, 1998). The tensile behaviour of CFRP reinforcement is multi-linear elastic (Woo et al., 2013). This is due to the multiple linear behaviour of the CFRP reinforcement is caused by the two main materials of CFRP, the polymer matrix and the carbon fibres. The multi-linear elastic tensile behaviour of CFRP reinforcement is illustrated in Figure 3.8. The first stage is linear elastic until the first cracks appear in the polymer matrix. The second stage describes the material behaviour after cracking. The behaviour of the CFRP is determined by the behaviour of the damaged polymer matrix and the linear elastic behaviour of the carbon fibres. The third stage is linear elastic until fracture of the carbon fibres. However, it is common practice to describe the tensile stress-strain behaviour of CFRP reinforcement using a linear elastic model.

Debonding of externally bonded CFRP reinforcement from the concrete surface occurs before the CFRP achieves its ultimate strain. Debonding almost always occurs in the concrete, near the interface between the concrete and the adhesive (Chen & Teng, 2003a). The interfacial bond strength is affected by the material properties of the concrete, the epoxy matrix and the carbon fibres (Iovinella, Prota & Mazzotti, 2013). The most important material properties are the concrete strength, the roughness of the concrete surface and the stiffness of the CFRP reinforcement. Debonding of CFRP reinforcement usually leads to brittle failure of a concrete element. However, some debonding of the externally bonded reinforcement is required for the CFRP reinforcement to act effectively. Cracks in the concrete cause local debonding of the CFRP reinforcement as illustrated in Figure 3.9.

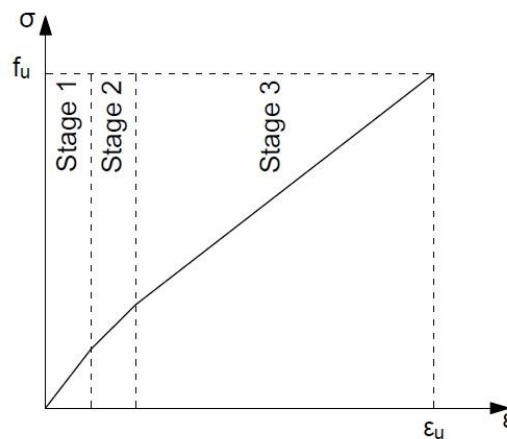


Figure 3.8: Multi-linear elastic CFRP model (Woo et al., 2013)

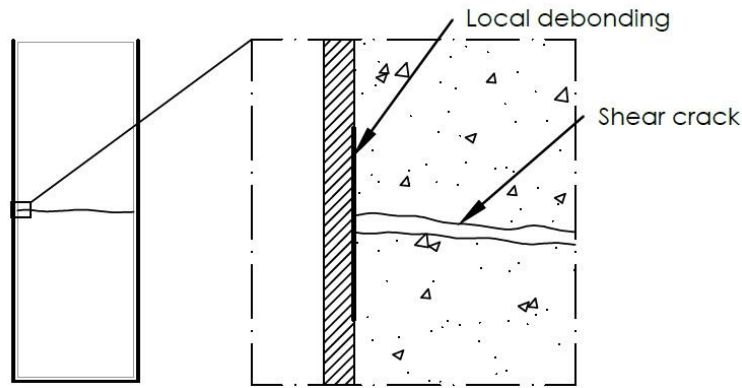


Figure 3.9: Local debonding of CFRP reinforcement (Kim et al, 2012)

3.4.2. Failure mechanisms of CFRP anchors

CFRP anchors have successfully been used to overcome the debonding problems of externally bonded CFRP reinforcement. The observed failure mechanisms of CFRP anchors are concrete cone failure, combined cone-bond failure and anchor rupture (Ozbakkaloglu & Saatcioglu, 2009). These failure mechanisms are illustrated in Figure 3.10. The embedment length of the anchor determines the type of failure. Concrete cone failure is the most common failure mechanism for very shallow embedment lengths and combined cone-bond failure is the most common failure mechanism for larger embedment lengths. Combined cone-bond failure is characterized by pull-out of a small concrete cone with an adhesive core. Anchor rupture is caused by failure of the carbon fibres in the CFRP anchor. The tensile capacity of the CFRP anchor is significantly lower than the ultimate tensile capacity of the carbon fibres in the anchor.

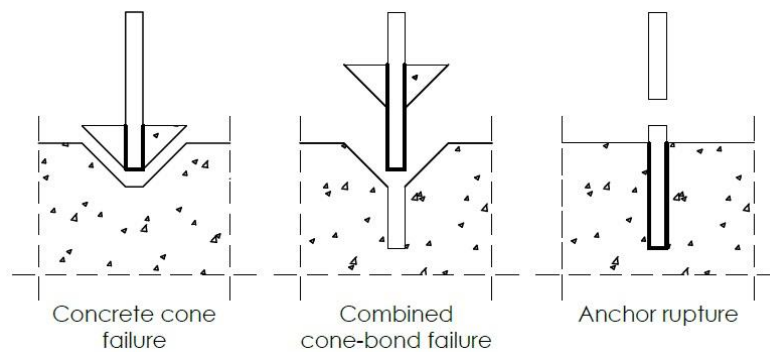


Figure 3.10: CFRP anchor failure mechanisms (Ozbakkaloglu & Saatcioglu, 2009)

3.5. Existing analytical models

3.5.1. Shear capacity of concrete elements strengthened with CFRP

Many analytical models have been developed to calculate the shear capacity of concrete members strengthened with externally bonded CFRP reinforcement. These have been developed for concrete members with rectangular cross-sections. Some of the analytical models are presented in this section, as presented in Table 3.3.

Triantafillou (1998) developed a model for the shear capacity of externally bonded CFRP reinforcement based on the truss analogy and the effective CFRP strain. The shear depends on the strain along the shear crack. The CFRP strain varies along the shear crack. Therefore, Triantafillou proposed to limit the shear capacity of the CFRP reinforcement to the effective strain. The effective strain depends on several aspects, such as crack propagation of the shear

crack, local debonding of the CFRP reinforcement and the force which can be anchored. Modelling these aspects and their interaction is difficult. Triantafillou suggested an empirical approach. He observed that the effective strain is a function of the axial rigidity of the CFRP reinforcement, the bond conditions and the concrete tensile strength. This relationship is derived by exponential curve fitting. The experimental data used for the derivation include rectangular beams and T-shaped beams. Khalifa et al. (1998) proposed the effective strain to be a product of the rupture strain and a reduction factor. Triantafillou and Antonopoulos (2000) developed effective strain models with respect to the type of application.

Chen and Teng (2003) proposed a model based on the non-uniform strain distribution in the CFRP reinforcement along the shear crack.

Deniaud and Cheng (2004) developed an analytical model based on a mechanic-based theoretical approach. They used the strip method and the shear friction method to describe the contribution of the CFRP.

Table 3.3: Existing analytical models

<p>Triantafillou (1998)</p> <p>The shear capacity of a reinforced concrete beam is given by:</p> $V_{Rd} = \min\{V_{cd} + V_{wd} + V_{frp,d}; V_{Rd2}\}$ <p>The shear capacity provided by the externally bonded CFRP reinforcement is:</p> $V_{frp,d} = \frac{0.9}{\gamma_{frp}} \rho_{frp} E_{frp} \varepsilon_{frp,e} b_w d (1 + \cot(\beta)) \sin(\beta)$ <p>The effective strain based on experimental data of full-wrap and side bonded FRP strengthened beams is:</p> $\varepsilon_{frp,e} = \begin{cases} 0.0119 - 0.0205(\rho_{frp} E_{frp}) + 0.0104(\rho_{frp} E_{frp})^2 & \text{if } 0 \leq \rho_{frp} E_{frp} \leq 1 \\ -0.00065(\rho_{frp} E_{frp}) + 0.00245 & \text{if } \rho_{frp} E_{frp} > 1 \end{cases}$
<p>Khalifa et al. (1998)</p> <p>The shear capacity of a reinforced concrete beam is given by:</p> $V_n = V_c + V_s + V_f$ <p>The shear capacity provided by the externally bonded CFRP reinforcement is:</p> $V_f = \rho_f E_f \varepsilon_{fe} b_w 0.9d (1 + \cot(\beta)) \sin(\beta)$ <p>The effective strain is:</p> $\varepsilon_{fe} = R \varepsilon_{fu}$ <p>The reduction factor based on experimental data is:</p> $R = 0.5622(\rho_{frp} E_{frp})^2 - 1.2188(\rho_{frp} E_{frp}) + 0.778 \leq 0.50$

Table 3.3. (continued)**Triantafillou and Antonopoulos (2000)**

The shear capacity of a reinforced concrete beam is given by:

$$V_{Rd} = \min\{V_{cd} + V_{wd} + V_{exp}; V_{Rd2}\}$$

The experimentally derived contribution of CFRP to the shear capacity is:

$$V_{exp} = 0.9\varepsilon_{f,e}E_f\rho_f b_w d(1 + \cot(\beta))\sin(\beta)$$

The effective strain of full-wrap CFRP reinforcement is:

$$\varepsilon_{f,e} = 0.17 \left(\frac{f_c^{2/3}}{E_f \rho_f} \right)^{0.30} \varepsilon_{f,u}$$

The effective strain of U-wrap or side bonded CFRP reinforcement is:

$$\varepsilon_{f,e} = \min \left\{ 0.65 \left(\frac{f_c^{2/3}}{E_f \rho_f} \right)^{0.56} ; 0.17 \left(\frac{f_c^{2/3}}{E_f \rho_f} \right)^{0.30} \varepsilon_{f,u} \right\}$$

Chen and Teng (2003)

The shear capacity of a reinforced concrete beam is given by:

$$V_n = V_c + V_s + V_{frp}$$

The design equation for U-wrap and side-bonded CFRP reinforcement is:

$$V_{frp} = 2 \frac{f_{frp,ed}}{\gamma_b} t_{frp} w_{frp} \frac{h_{frp,e}(\sin(\beta) + \cos(\beta))}{s_{frp}}$$

The design effective FRP stress for debonding:

$$f_{frp,ed} = D_{frp} \sigma_{frp,max,d}$$

$$\sigma_{frp,max,d} = 0.315 \beta_w \beta_L \sqrt{\frac{E_{frp}}{t_{frp}}} \sqrt{f'_c} \leq f_{frp}$$

The design effective FRP stress for FRP rupture:

$$f_{frp,ed} = D_{FRP} \sigma_{FRP,max}$$

$$\sigma_{FRP,max} = \begin{cases} 0.8 f_{FRP} & \text{if } f_{FRP}/E_{FRP} \leq \varepsilon_{max} \\ 0.8 \varepsilon_{max} E_{FRP} & \text{if } f_{FRP}/E_{FRP} > \varepsilon_{max} \end{cases}$$

Deniaud and Cheng (2004)

The shear capacity of a reinforced concrete beam strengthened with CFRP is given by:

$$V_r = k \sqrt{f'_c A_c (T_v + T_{FRP})} \frac{d_s}{s} - T_v$$

The tension force in the stirrup is:

$$T_v = A_v f_{vy}$$

The contribution of the CFRP reinforcement is:

$$T_{FRP} = d_{FRP} t_{FRP} \varepsilon_{max} R_L \left(\frac{W_{FRP}}{S_{FRP}} \right)^2 \left(\frac{s}{d_s} \sin(\alpha) + \cos(\alpha) \right) \sin(\alpha)$$

3.5.2. Bond behaviour of CFRP-to-concrete interface

Many theoretical models to predict the debonding propagation are available in the existing literature. However, these theoretical models are rarely implemented in analytical models to predict the shear capacity provided by the CFRP reinforcement. The bilinear bond-slip model is the most commonly used theoretical model to describe the relationship between the bond shear stress and the slip at the CFRP-to-concrete interface (Lu, Teng & Jiang, 2005). The bilinear bond-slip is a combination of a linear ascending branch and a linear descending branch as shown in Figure 3.11 (Teng, Yuan & Chen, 2006). The bond shear stress increases linear with the interfacial slip until it reaches the peak shear stress. The bond shear stress decreases linear until the shear stress is zero during the interfacial softening stage. The bilinear bond-slip model does not include any residual shear strength after debonding which implies that friction and aggregate interlock are neglected. However, the bilinear bond-slip model is considered a good relationship to describe the CFRP-to-concrete interface in engineering practice (Woo et al., 2013). Sato and Vecchio (2003) developed analytical equations to calculate the peak shear stress, the interfacial fracture energy and the interfacial slip. These equations are a function of the compressive strength of the concrete.

$$\tau_f = (54f'_c)^{0.19} \quad (3.1)$$

$$G_f = \left(\frac{\tau_f}{6.6}\right)^2 \quad (3.2)$$

$$s_0 = 0.057 \sqrt{G_f} \quad (3.3)$$

$$s_u = \frac{2G_f}{\tau_f} \quad (3.4)$$

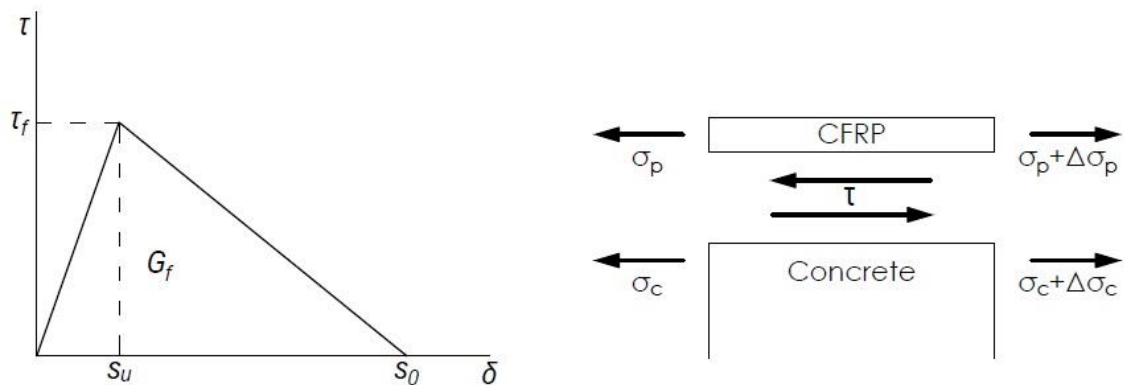


Figure 3.11: Bilinear bond-slip model (Teng, Yuan & Chen, 2006)

3.6. Design guidelines externally bonded CFRP strengthening

Design rules of shear strengthening using externally bonded CFRP reinforcement are included in both national and international guidelines. Most of these are based on limited strain in the carbon fibre. The shear capacity is the sum of the shear capacity provided by the concrete, the present shear reinforcement and the externally bonded CFRP reinforcement in the national and international guidelines.

3.6.1. National design recommendation

Design rules for strengthening of reinforced concrete structures with externally bonded CFRP reinforcement are given in the CUR 91 (CURNET, 2007). The first edition of the CUR 91 was published in 2002 and was revised in 2007.

Verification ultimate limit state

The shear capacity of a member strengthened with CFRP is based on the calculation in the NEN 6720 (CURNET, 2007). The NEN 6720 is the precursor of the Eurocode NEN-EN 1992-1-1. The shear stress capacity of a concrete member strengthened with externally bonded CFRP is given by:

$$\tau_u = \tau_1 + \tau_s + \tau_f \leq \tau_2 \quad (3.5)$$

The shear stress τ_1 is the shear stress capacity provided by the concrete, the shear stress τ_s is the shear stress capacity of the present reinforcement steel and the shear stress τ_f is the shear stress capacity provided by the CFRP reinforcement. The contribution of the internal shear reinforcement should be checked because the stress in the stirrups might be lower than the yield stress. The shear stress capacity of a member strengthened with CFRP is limited by the threshold value of the shear stress with shear reinforcement τ_2 . The shear stress capacity of the CFRP reinforcement is based on the truss analogy:

$$\tau_f = \frac{A_{fv} z E_f \varepsilon_{feff} \sin(\alpha) (\cot(\theta) + \cot(\alpha))}{b_w d} \quad (3.6)$$

where

$$A_{fv} = \begin{cases} 2 t_f & \text{Complete wrap with CFRP sheets} \\ 2 t_f \cdot b_f / s_f & \text{Strips of CFRP lamellas or sheets (c.t.c. distance } s_f) \end{cases}$$

The angle θ is the angle of the compression struts and the angle α is the inclination of the carbon fibres.

The distance between the CFRP lamellas should be limited to:

- $0.9d - 0.5b_f$ for rectangular cross-sections
- $0.9d - h_f - 0.5b_f$ for T-beams

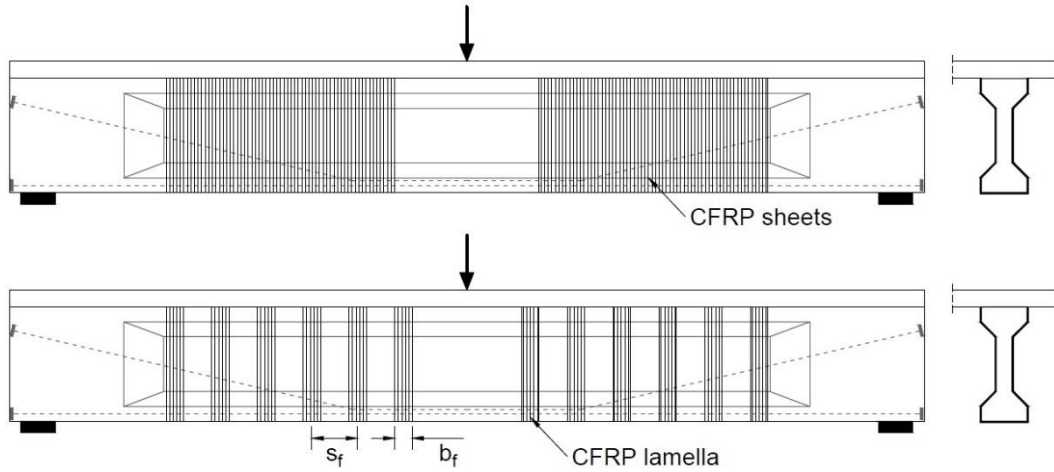


Figure 3.12: CFRP shear strengthening with CFRP sheets and CFRP lamellas

The configuration of the CFRP reinforcement affects the effective strain. The configurations given in the CUR 91 are full-wrap of the circumference, U-wrap with anchors in the compression zone and externally bonded U-wrap. The configurations are illustrated in Figure 3.13. The effective strain of full-wrap and U-wrap with anchors in the compression zone is given by:

$$\epsilon_{feff} = \frac{1.6}{\gamma_m} \left(\frac{f_{bm} b_w}{E_f A_{fv}} \right)^{0.30} \epsilon_{fu} \quad (3.7)$$

where

$$\gamma_m = 1.3$$

The average axial tensile strength of concrete f_{bm} is replaced by f_{ctm} in the Eurocode NEN-EN 1992-1-1.

The calculation of the U-wrap is based on the fictitious compression zone in contrast to the international guidelines. The calculation of the bending moment and shear capacity should be based on the fictitious compression zone. The effective strain of the U-wrap strengthening is given by:

$$\epsilon_{feff} = \frac{0.055}{\gamma_m} \left(\frac{f_{bm} b_w}{E_f A_{fv}} \right)^{0.56} \leq \frac{1.6}{\gamma_m} \left(\frac{f_{bm} b_w}{E_f A_{fv}} \right)^{0.30} \epsilon_{fu} \quad (3.8)$$

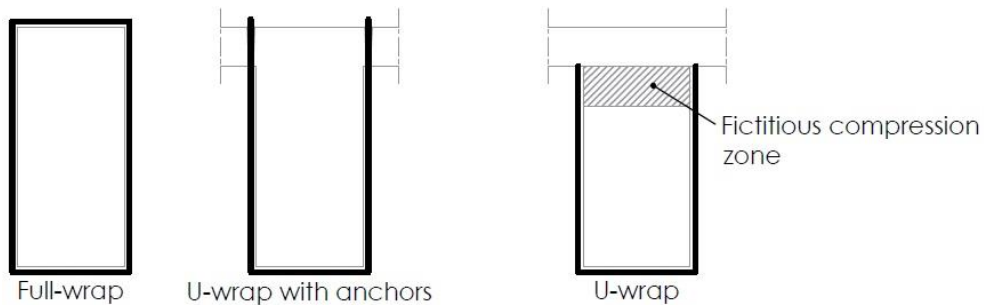


Figure 3.13: Configurations CFRP shear strengthening CUR 91 (CURNET, 2007)

Verification serviceability limit state

The reinforcement in the concrete element may not yield due to bending of the concrete element. The maximum strain of the CFRP reinforcement should be limited to:

$$\varepsilon_{max} \leq \frac{f_s}{E_s} \quad (3.9)$$

Application CFRP reinforcement

The bond strength of the concrete surface should be at least 1.5 MPa according to the CUR 20. The concrete surface should be roughened by removing the outer cement layer. Sandblasting and grinding are the most used surface preparation techniques to increase the bond strength of the concrete surface.

3.6.2. International design guidelines

The dimensioning of shear strengthening with CFRP reinforcement is given in the following international design guidelines:

- Europe: 'Fib bulletin 14 Externally bonded FRP reinforcement for RC structures'
- USA: ACI440.2R-08 'Guide for the Design and Construction of Externally Bonded FRP Systems for Strengthening Concrete Structures'
- Italy: CNR -DT 200/2004 'Guide for the Design and Construction of Externally Bonded FRP Systems for Strengthening Existing Structures'
- Great Britain: TR55 'Design Guidance for strengthening concrete structures using fibre composite materials'
- Germany: DAfStb-heft 595 'Verstärken von Betonbauteilen mit geklebter Bewehrung'

The design guidelines of the Fib bulletin 14, ACI440.2R-08, CNR -DT 200/2004 and TR55 are based on the effective strain, like the national design recommendation CUR 91. The design rules in the DAfStb are based on the available anchoring length of the CFRP reinforcement (DAfStb, 2012).

ACI440.2R-08

The nominal shear capacity of a concrete members strengthened with CFRP is given in the ACI440.2R-08 by:

$$\phi V_n = \phi(V_c + V_s + \psi_f V_f) \quad (3.10)$$

The shear capacity provided by the CFRP reinforcement is given by :

$$V_f = \frac{A_{fv} d_{fv} E_f \varepsilon_{fe} (\sin(\alpha) + \cos(\alpha))}{s_f} \quad (3.11)$$

where:

$$A_{fv} = 2 n \cdot t_f \cdot w_f$$

The effective strain is limited to 4‰ to prevent loss of aggregate interlock of the concrete (ACI Committee 440, 2008). Three application types are distinguished in the ACI440.2R-08. These are full-wrap, U-wrap and side bonded CFRP strengthening. The effective strain for full-wrap CFRP is 75% of the fracture strain:

$$\varepsilon_{fe} = 0.75\varepsilon_{fu} \leq 0.004 \quad (3.12)$$

The effective strain for U-wrap and side bonded CFRP strengthened members depends on the properties of the bond. The effective strain is the product of the fracture strain of the CFRP and the bond reduction coefficient:

$$\varepsilon_{fe} = k_v \varepsilon_{fu} \leq 0.004 \quad (3.13)$$

The properties of the bond taken into account in the bond reduction coefficient are the effective bond length and modification factors that account for the concrete strength and the type of application. The bond reduction coefficient is given by:

$$k_v = \frac{k_1 k_2 L_e}{11900 \varepsilon_{fu}} \quad (3.14)$$

The effective bond length of the CFRP reinforcement is given by:

$$L_e = \frac{23300}{(n_f t_f E_f)^{0.58}} \quad (3.15)$$

The modification factor that accounts for the concrete strength is given by:

$$k_1 = \left(\frac{f'_c}{27} \right)^{2/3} \quad (3.16)$$

The modification factor for the type of application of the CFRP strengthening is given by:

$$k_2 = \begin{cases} \frac{d_{fv} - L_e}{d_{fv}} & \text{for U-wrap} \\ \frac{d_{fv} - 2L_e}{d_{fv}} & \text{for side bonded} \end{cases} \quad (3.17)$$

DAfStb-heft 595

The shear capacity of a concrete structure is the sum of the shear capacity provided by the shear reinforcement and the CFRP reinforcement:

$$V_{Rd} = V_{Rd,s} + V_{Rd,Lw} \quad (3.18)$$

The shear strengthening configurations included in the DAfStb-heft 595 guideline are full-wrap and U-wrap. The U-wrap with anchoring in the top flange of a T-beam is covered by full-wrap. The application of the U-wrap is limited to rectangular beams. The shear strengthening configurations are illustrated in Figure 3.14.

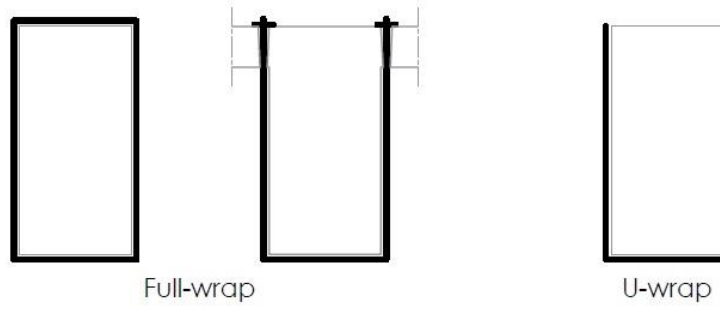


Figure 3.14: Configurations CFRP shear strengthening DAfStb (DAfStb, 2012)

The expression of the shear capacity provided by the CFRP reinforcement is based on the truss analogy. The shear capacity provided by the CFRP reinforcement is given by:

$$V_{Rd,Lw} = \frac{A_{Lw}}{s_{Lw}} \cdot z \cdot f_{Lwd} \cdot \cot(\theta) \quad (3.19)$$

where:

$$\frac{A_{Lw}}{s_{Lw}} = \begin{cases} 2 t_{Lw} & \text{Complete wrap with CFRP sheets} \\ 2 t_{Lw} \cdot b_{Lw} / s_{Lw} & \text{Strips of CFRP lamellas or sheets (spacing } s_{Lw}) \end{cases}$$

The bearing strength of the shear strengthening f_{Lwd} depends on the type of application. Two types of application are distinguished in the DAfStb-heft 595, the full-wrap and the U-wrap shear strengthening. The bearing strength of the full-wrap CFRP reinforcement is given by:

$$f_{Lwd} = k_R \cdot \alpha_{zeit} \cdot f_{Ld} \quad (3.20)$$

where:

$$k_R = \begin{cases} 0.5 \cdot (r_c/60)(2 - r_c/60) & r_c \leq 60 \text{ mm} \\ 0.5 & r_c \geq 60 \text{ mm} \end{cases}$$

$$\alpha_{zeit} = 0.75$$

The factor k_R is a reduction factor for the short-term stress concentration at the corners of the girder. The bearing strength of the full-wrap CFRP reinforcement is reduced by 50% for corners with a radius larger than 60 mm. For corners with a radius smaller than 60 mm the tensile strength of the CFRP is reduced more than 50%. The creep rupture factor α_{zeit} takes into account the time dependent behaviour of the adhesive joint.

The bearing strength of the U-wrap CFRP reinforcement is the minimum of the bearing strength of the full-wrap, given in equation (3.16), and the bond strength of the CFRP shear strengthening:

$$f_{Lwd} = \min\{f_{bLwd}; f_{Lwd,G}\} \quad (3.21)$$

The performance of the U-wrap CFRP reinforcement depends on the position of the CFRP strips or sheets. The shear crack affects the effective bond length of the adhesive joint as illustrated in Figure 3.15. The bond strength f_{bLwd} between the CFRP reinforcement and the concrete is given by:

$$f_{bLwd} = \begin{cases} \frac{f_{bLk,max}}{\gamma_{BA}} & \text{for } d \geq l_{bL,max} \text{ and} \\ \frac{f_{bLk,max}}{\gamma_{BA}} \cdot \left(\left(1 - \frac{m_{LW} - 1}{n_{LW} - 1} \right) + \frac{m_{LW}(m_{LW} - 1)s_{LW}}{2(n_{LW} - 1)l_{bL,max}} \right) & l_{bL,max} \leq s_{LW} \leq d \\ \frac{f_{bLk,max}}{\gamma_{BA}} \frac{n_{LW}s_{LW}}{2l_{bL,max}} & \text{for } d \geq l_{bL,max} \text{ and} \\ & s_{LW} \leq l_{bL,max} \\ & \text{for } d \leq l_{bL,max} \text{ and } s_{LW} \leq d \end{cases} \quad (3.22)$$

where:

$$\begin{aligned} n_{LW} &= d/s_{LW} && \text{(integer)} \\ m_{LW} &= l_{bL,max}/s_{LW} && \text{(integer)} \\ f_{bLk,max} &= \sqrt{(E_{Lm} \cdot s_{L0k} \cdot \tau_{L1k})/t_L} \\ l_{bL,max} &= 1.773 \sqrt{(E_{Lm} \cdot t_L \cdot s_{L0k})/\tau_{L1k}} \\ s_{L0k} &= 0.201 \text{ mm} \\ s_{L1k} &= 2.5(50/E_{cm})\tau_{L1k} \\ \tau_{L1k} &= 0.366 \sqrt{\alpha_{cc} \cdot f_{cm} \cdot \alpha_{ct} \cdot f_{ctm,surf}} \\ \tau_{LF} &= 10.8 \cdot \alpha_{cc} \cdot f_{cm}^{-0.89} \end{aligned}$$

The expressions for the bond strength $f_{bLk,max}$ and the effective bond length $l_{bL,max}$ are mechanics-based (Zilch, Niedermeier & Finckh, 2014). The bond strength and the effective bond length depend on the CFRP-to-concrete interface. This interface is described by the extended bilinear bond stress-slip relationship as given in Figure 3.16. This relationship consists of an elastic stage and a linear softening stage. The shear stress increases with the slip in the elastic stage. The linear softening stage starts after reaching the ultimate strength of the interface. The shear stresses decrease with the slip in the softening stage, resulting in debonding of the CFRP reinforcement. The bond coefficient τ_{L1k} is based on the near-surface tensile strength of the concrete. The near-surface tensile strength should be determined according to measurements on the concrete surface. The pull-off test method, used to measure the near-surface tensile strength, is described in the NEN-EN 1542 (Nederlands Normalisatie-Instituut, 1999). The near-surface tensile strength of the concrete should be at least 1.5 MPa according to the DAfStb-heft 595 (2012).

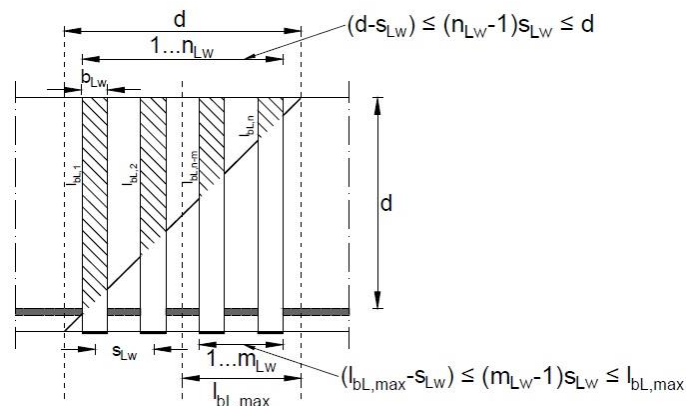


Figure 3.15: Schematic illustration U-wrap strips (DAfStb, 2012)

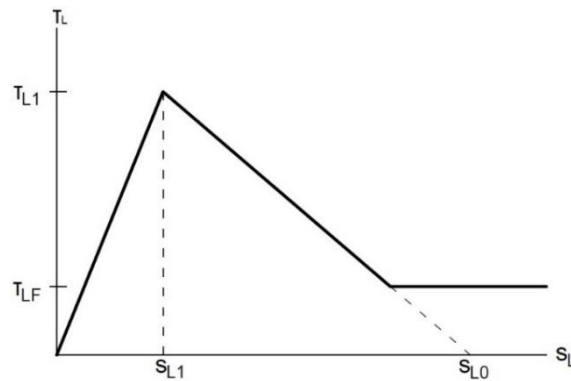


Figure 3.16: Extended bilinear bond stress-slip relationship (DAfStb, 2012)

3.7. Previous studies on CFRP shear strengthening of I-girders

3.7.1. Experimental results

Some researchers investigated the influence of CFRP reinforcement on the shear capacity of prestressed concrete I-girders. The results of three experimental programs are given in Table 3.4. The dimensions of the I-girders used in these programs are illustrated in Figure 3.17.

Ary and Kang (2012) did experimental research in order to observe the behaviour of prestressed concrete I-girders strengthened with vertical CFRP strips. The two specimens that were investigated are specimen IB-10 and specimen IB-5. The spacing of the strips was 254 mm and 127 mm for specimen IB-10 and specimen IB-5, respectively. The shear capacity of specimen IB-5 increased with 38% compared to the control specimens without CFRP. The increase in shear capacity of specimen IB-10 was only 1.5%. The researchers reported rupture of the CFRP strips at failure for both specimens. They concluded that the spacing between the CFRP strips should be smaller than half of the effective depth.

The experimental program of Massa et al. (2018) consisted of prestressed concrete I-girders with internal shear reinforcement. This experimental program included three different configurations of CFRP strips. However, the CFRP strips are only externally bonded and not anchored with CFRP anchors. Massa et al. (2018) concluded that CFRP strips are difficult to anchor at the re-entrant corners. Horizontal CFRP strips helped to improve the anchorage of the vertical CFRP strips. However, the increase in shear capacity was still very limited. Furthermore, they concluded that CFRP strips significantly decrease the shear crack width. The limited increase in shear capacity might be caused by the type of failure. The load-deflection curve of the specimens shows a yield plateau. The yield plateau indicates flexural failure instead of shear failure. The experimental results and NLFEA results show crushing of the concrete in the deck.

Garcia et al. (2018) applied three different configurations of CFRP reinforcement with CFRP anchors to strengthen prestressed concrete I-girders. They applied the CFRP in the re-entrant corners of the I-girder to ensure that the externally bonded CFRP sheets did not pull away from the re-entrant corner. Figure 3.18 shows how the tensile forces in the externally bonded CFRP reinforcement were resisted by the CFRP anchor. They concluded that the application of vertical CFRP strips delay shear cracking, however the shear capacity of the I-girder strengthened with vertical CFRP sheets and CFRP anchors hardly increased. The application of vertical and horizontal strips increased the shear capacity of the strengthened I-girder. Furthermore, they concluded that the CFRP strengthening makes the failure mode of the girder more brittle and explosive.

These three experimental programs show divergent results. Ary and Kang (2012) reported an increase in shear capacity of almost 38% for a small prestressed I-girder strengthened with

CFRP strips with a small spacing and no anchoring in the re-entrant corners. In contrast, Massa et al (2018) did not observe an increase in shear capacity. Garcia et al. (2018) showed an promising increase in shear capacity of almost 38%. The results of these three experimental programs show that more research is needed to understand the shear behaviour of prestressed concrete I-girders strengthened with externally bonded shear reinforcement.

Table 3.4: Comparison of shear capacities in literature

		Configuration	Horizontal strips	CFRP anchors	b_s [mm]	c.i.c. [mm]	Shear load [kN]	Increase in shear capacity
Ary & Kang	Control	-	-	-	-	-	117	-
	IB-10	U-strip	No	No	76	127	119	1.50%
	IB-5	U-strip	No	No	76	254	162	37.85%
Massa et al.	Control(S1)	-	-	-	-	-	660	-
	S2	U-strip	Yes	No	100	150	661	0.15%
	S3	U-strip	No	No	100	200	665	0.76%
Garcia et al.	Control (I-1)	-	-	-	-	-	1819	-
	I-2	U-sheet	No	Yes	254	508	1855	1.98%
	I-3	U-sheet	Yes	Yes	254	254	2504	37.66%
	I-4	U-sheet	Yes	Yes	254	508	2478	36.23%

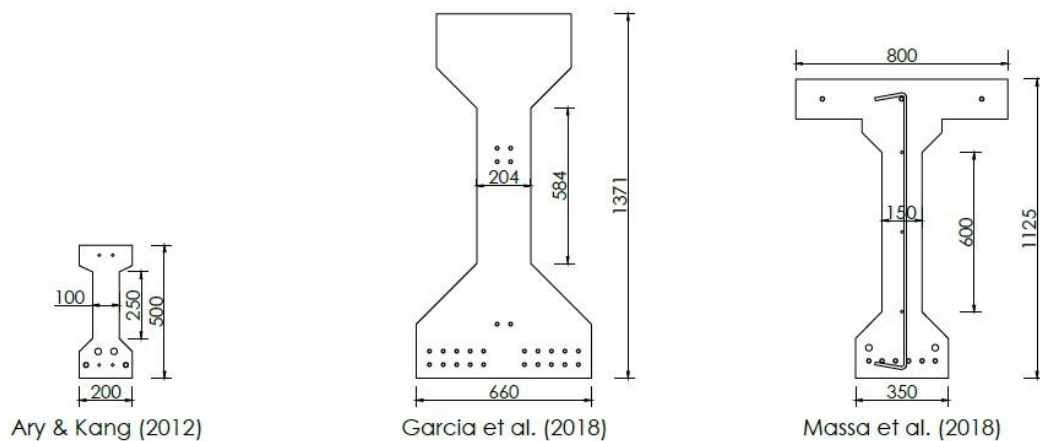


Figure 3.17: I-girders in experimental programs

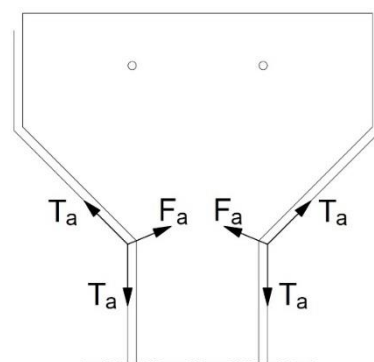


Figure 3.18: CFRP tension forces resisted by CFRP anchor (Garcia et al., 2018)

Ozbakkaloglu and Saatcioglu (2009) did experimental research to determine the pull-out capacity of the CFRP anchor. Pull-out capacities between 20.6 kN and 60.8 kN have been reported for CFRP anchors failing in combined cone-bond failure. They concluded that the pull-out capacity depends on the diameter, embedment length and angle of inclination of the anchor. In contrast to the bond strength of externally bonded CFRP reinforcement, the concrete strength hardly affects the capacity of the CFRP anchor. The average bond strength of the CFRP anchor decreases with increasing diameter or embedment length. Furthermore, they concluded that the pull-out capacity of the CFRP anchors decreases with an increasing angle of inclination. However, the researchers did not investigate the influence of the transition radius. The angle of inclination is the angle between the surface of the concrete and the CFRP anchors. An inclined anchor is illustrated in Figure 3.19. The study of Kobayashi et al. (2001) showed the behaviour of the CFRP anchor by different splay angles of the fan. According to this study the splay angle should be limited to 90° to prevent stress concentrations in the fibres of the CFRP anchor.

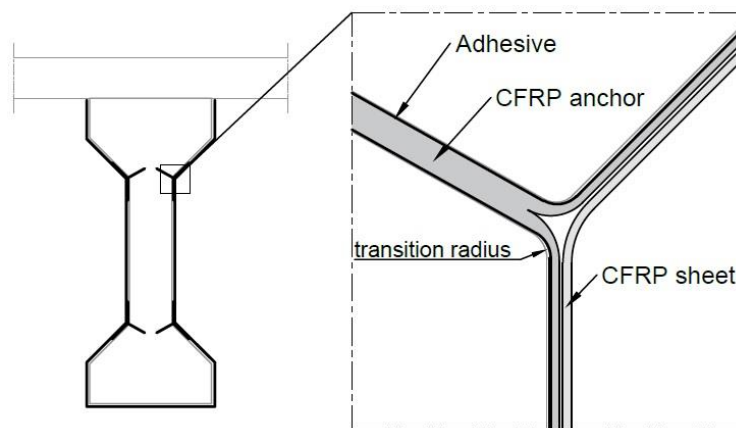


Figure 3.19: Inclined CFRP anchor re-entrant corner

3.7.2. Numerical finite element analysis

Properly calibrated numerical finite element models have been proven to provide decent predictions of the structural behaviour of concrete beams strengthened with CFRP (Kalfat & Al-Mahaidi, 2018a). Numerical finite element models have been used by several researchers to investigate the CFRP-to-concrete interface performance. Kalfat and Al-Mahaidi (2018b) developed a guideline for finite element modelling of concrete structures strengthened with externally bonded CFRP reinforcement. This guideline describes finite element modelling techniques for the CFRP reinforcement.

The researchers suggested two approaches to model the CFRP reinforcement. The CFRP reinforcement can be modelled as an orthotropic material assigned to shell elements or as an isotropic material assigned to three-dimensional solid elements with smeared reinforcement.

The researchers described three approaches to model the behaviour of the CFRP-to-concrete interface using finite element models. The first approach is to model the CFRP-to-concrete interface as a perfect bond. The second approach is using one-dimensional nonlinear spring elements to model the interface between the concrete and the CFRP reinforcement. The third approach is to model the CFRP-to-concrete interface with interface elements. The perfect bond approach is easy to model, however, the accuracy of the perfect bond approach depends heavily on the material model and the mesh size of the concrete underneath the adhesive layer. The most commonly used approach in literature is to model the CFRP-to-concrete interface with interface elements. A constitutive bond-slip model should

be assigned to the interface elements to describe the debonding behaviour of the CFRP reinforcement.

Numerical finite element analysis of prestressed concrete I-girders strengthened with externally bonded FRP reinforcement is very limited in literature. Kalfat and Al-Mahaidi (2018a) used experimental results of a full-scale prestressed concrete I-girder to calibrate their three-dimensional finite element model. They modified the model to add the externally bonded FRP reinforcement. Interface elements were used to model the CFRP-to-concrete interface. A constitutive bond-slip model with an ascending and a descending branch were assigned to this interface elements.

Al-Sammari and Breña (2018) investigated the influence of several parameters on the behaviour and capacity of CFRP anchors using NLFEA. They modelled the CFRP anchors with three-dimensional brick elements. The finite element model was calibrated using experimental data. The strength of the joint between the sheet and the concrete was increased with more than 100% due to the addition of the CFRP anchors. CFRP anchors with shallow embedment lengths are not able to increase the strength of the joint. The splay angle of the anchor should be at 90° for maximum efficiency of the CFRP anchor. The CFRP anchor splays should cover the entire width of the CFRP sheet or strip to obtain the maximum strength of the joint.

3.8. Parameters affecting the performance of CFRP

Several parameters affecting the performance of externally bonded CFRP reinforcement have been investigated. The most important parameters affecting the performance of CFRP reinforcement, according to the literature, are described in this section.

3.8.1. Shear span-to-depth ratio

The shear span is defined as the distance between the load point and the support. The shear failure mode is affected by the shear span-to-depth ratio. The behaviour of a girder with a shear span-to-depth ratio smaller than two will be governed by deep beam behaviour. The typical failure mechanism of a deep beam is crushing of the concrete because of the direct load transfer from the load point to the support (Kim et al., 2012). The CFRP reinforcement has only a minor contribution to the shear capacity of girders with a shear span-to-depth ratio smaller than two (Bousselham and Chaallal, 2006). For shear span-to-depth ratios greater than two, the shear failure mode may be shear tension failure or flexural shear failure. When the shear span-to-depth ratio increases above two, the performance of the CFRP reinforcement will increase. The difference between the contribution of CFRP reinforcement on both failure modes was not investigated.

3.8.2. Concrete strength

The concrete strength affects the shear capacity of the unstrengthened prestressed I-girder. The influence of the concrete strength on the shear capacity is included in the shear strength verification of national and international design guidelines. The concrete strength affects the CFRP-to-concrete bond strength as described in Section 3.5 (Sato & Vecchio, 2003). However, the increase in concrete strength does not significantly increase the bond strength. The contribution of the concrete strength to the percentual increase in shear capacity provided by the concrete is limited.

3.8.3. Internal shear reinforcement

Experimental investigation performed by Bouselham and Chaallal (2006) shows the interaction between the externally bonded CFRP reinforcement and the internal steel stirrups. They concluded that internal steel stirrups resulted in a significant decrease of the CFRP contribution to the shear capacity. On the other hand, the externally bonded CFRP reinforcement reduces the strains in the internal steel stirrups. The internal steel stirrups may not yield because of the reduced strains. The contribution of the internal steel stirrups to the shear capacity is reduced when the stirrups do not yield.

3.8.4. CFRP reinforcement configuration

The CFRP wrapping configurations for concrete elements are full-wrap, U-wrap and side bonded. The full-wrap CFRP configuration is not preferred because the installation would cause hindrance on top of the deck. U-wrap CFRP reinforcement is the most suitable wrapping configuration for I-girders. Side bonded CFRP reinforcement can be applied but this configuration is less efficient than U-wrap CFRP reinforcement.

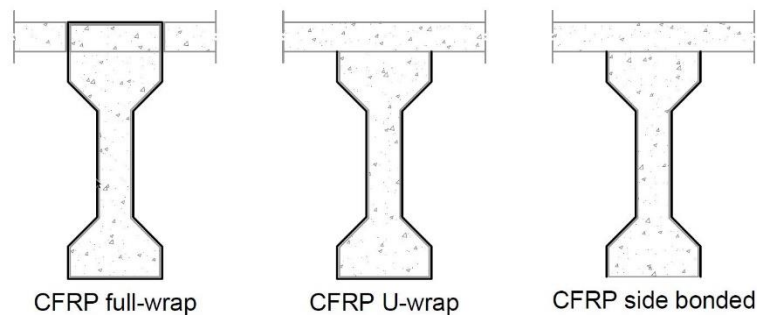


Figure 3.20: CFRP wrapping configurations

3.8.5. Fibre orientation CFRP reinforcement

Literature makes a distinction between vertical, diagonal and horizontal orientated fibres in the CFRP reinforcement. Diagonal orientated fibres results in the most effective shear strengthening according to the experiments of Zhang and Hsu (2005) and Kim et al. (2012). However, the difference in performance between diagonal fibre orientation and vertical fibre orientation is small. Khalifa and Nanni (2000) did not observe a contribution to the shear strength for CFRP reinforcement with horizontal orientated fibres.

Adhikary and Mutsuyoshi (2004) investigated the effect of a combination of vertical and horizontal layers of CFRP reinforcement. The first layer of CFRP reinforcement was vertical orientated and the second layer was horizontal orientated. Compared to only one vertical orientated layer of CFRP reinforcement a small increase in shear capacity was observed. The researchers concluded that the additional horizontal orientated layer of CFRP reinforcement does provide some anchorage to the vertical layer of CFRP reinforcement.

3.8.6. CFRP width-to-spacing ratio

The CFRP width-to-spacing ratio is the ratio between the width of the CFRP sheets or strips and the spacing between the CFRP sheets or strips. The CFRP width-to-spacing ratio determines the performance of the CFRP reinforcement. The spacing should be limited to avoid the development of shear cracks between two CFRP sheets or strips. Kang and Ary (2012) concluded that the shear capacity of the girder hardly increases, when the spacing between the CFRP strips is larger than half the effective depth of the girder. The national and

international guidelines include requirements for the spacing between the CFRP sheets or strips. The CUR 91 includes requirements for rectangular beams and T-beams, while the requirements in the ACI 440 are the same as for the internal shear reinforcement.

3.8.7. Multiple layers of CFRP sheets

Multiple layers of CFRP sheets affect the contribution to the shear capacity of the CFRP reinforcement by an increase in axial rigidity. The effect of multiple layers depends on the debonding of the CFRP reinforcement (Bousselham and Chaallal, 2006). Debonding of CFRP reinforcement is the most common failure mode for I-girders strengthened with CFRP reinforcement without anchoring. The effect of multiple CFRP layers may be very limited due to the debonding of the externally bonded CFRP reinforcement.

3.8.8. Anchoring

Debonding failure is the most common failure mode for U-wrap CFRP reinforcement. The re-entrant corners of I-girders are especially sensitive to debonding (Kang & Ary, 2012; Garcia et al., 2018; Massa et al., 2018). The performance of U-wrap CFRP reinforcement can be increased by anchoring the sheets in the re-entrant corners and underneath the deck. CFRP anchors are able to anchor the U-wrap CFRP reinforcement in the re-entrant corners according to Garcia et al. (2018). The detail of the CFRP anchor in the re-entrant corner is illustrated in Figure 3.21.

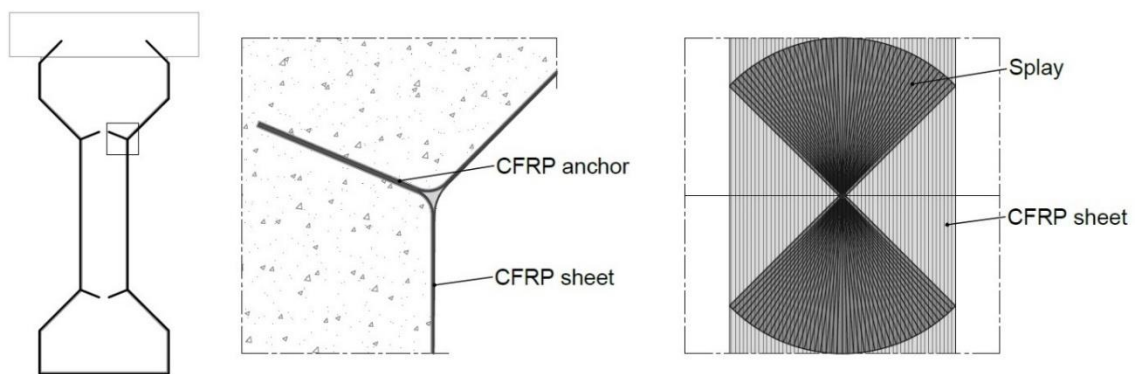


Figure 3.21: Detail CFRP anchor re-entrant corner

4

RESEARCH METHODOLOGY

4.1. Research outline

The feasibility of strengthening I-girders in shear depends on the contribution of the externally bonded CFRP reinforcement to the shear capacity. The analytical formulas in the national and international guidelines describe the contribution of CFRP reinforcement to the shear capacity. However, these design guidelines are developed for beams with rectangular cross-sections. The contribution of externally bonded CFRP reinforcement to the shear capacity of I-girders may be affected by, but is not limited to, the parameters described in Section 0. To investigate the contribution of a selection of these parameters a parametric study with NLFEA is proposed by the author. The selection of the parameters is presented in Section 4.3.

Numerical simulations are suitable to perform a parametric study. NLFEAs have been successfully used to predict the structural behaviour of prestressed concrete I-girders. The knowledge of NLFEA to investigate the structural behaviour of I-girders strengthened with externally bonded CFRP reinforcement is limited. The NLFEA results should be validated by experimental results. However, there are only a few experimental results because full-scale experimental testing is expensive and time-consuming.

The experimental results of three experimental programs are presented and described in Section 3.7.1. These experimental results are not useful to validate numerical finite element results because the shear failure mechanisms were not clearly shear tension or flexural shear failure.

Solution strategies validated in literature for quite similar concrete elements can be used to develop reliable NLFEAs (De Putter, 2020). These solution strategies are mainly based on the RTD2016 guideline provided by Rijkswaterstaat and the fib Model Code 2010. The RTD2016 guideline improves the robustness of NLFEAs without validation with experimental data (Hendriks, de Boer & Belletti, 2017a). This guideline is developed based on scientific research and long-term experience of researchers.

To investigate the feasibility of using externally bonded CFRP reinforcement to strengthen I-girders in shear, a typical prestressed concrete I-girder with insufficient shear capacity was strengthened with externally bonded CFRP reinforcement. The cross-section and dimensions of the I-girder in this research were based on the cross-section and the dimensions of the I-girders of the Nijkerker Bridge. The I-girders of the Nijkerker Bridge are suitable for this research because the I-girders did not have sufficient shear capacity. The design shear resistance of the I-girders was exceeded by 60%. Furthermore, these I-girders did not have shear reinforcement and have a kinked tendon profile. The design of the I-girder was slightly changed to ensure that the specimens failed in shear. The test-setup is a four-point bending test with a variable shear span.

4.2. Finite element method

The numerical software DIANA 10.4 is used for the numerical analysis in this research. The NLFEA makes DIANA useful to analyse shear failure of concrete girders. The NLFEA in this research was executed according to the guidelines proposed by Rijkswaterstaat (Hendriks et al., 2017a). This guideline was developed to improve the robustness of NLFEA of concrete structures such as girders, slabs, culverts, etc. Modelling of the finite element model of the prestressed concrete girder includes two steps. The first step is the abstraction from the prestressed concrete girder to the mechanical model. The geometry, material properties, boundary conditions and the loads are modelled in this step. The second step is dividing the mechanical model in a finite number of elements.

4.3. Parametric study

The investigated parameters are presented in this section. One of these parameter is the shear span-to-depth ratio. The parameters of the I-girder such as the concrete strength, tendon profile and internal shear reinforcement are not taken into account in the numerical research. The I-girder in the research setup has a typical tendon profile and concrete strength. The I-girder has no shear reinforcement because this is the most extreme case. The parameter of the CFRP reinforcement that have been investigated are given in Section 4.3.2.

4.3.1. Shear span-to-depth ratio

The shear span to-depth ratio affects the failure mechanism of the I-girder. The I-girder should fail in shear tension or flexural shear failure because this research aims at strengthening of I-girders in shear tension and flexural shear. The shear span-to-depth ratio should be larger than 2 to prevent direct load transfer from the loading point to the support. The effect of the shear span-to-depth ratio is investigated by increasing the shear span with steps of 1.0 m. The variation of the shear span-to-depth ratio is presented in Table 4.1.

Table 4.1: Variation shear span-to-depth ratio

Set	Shear span	Shear span-to-depth ratio
SP3	3.0 [m]	3.40
SP4	4.0 [m]	4.40
SP5	5.0 [m]	5.35

4.3.2. Externally bonded CFRP reinforcement parameters

The three possible configurations for the CFRP reinforcement are discussed in Section 3.8.4. The CFRP U-wrap configuration is the most effective configuration for I-girders. The CFRP sheets had a width of 300 mm and a thickness of 0.19 mm. The material properties of the CFRP sheets are given in Section 4.4.2. Debonding of the CFRP sheets is expected at the re-entrant corners of the I-girder. To prevent the debonding of the CFRP sheets two types of anchorage are investigated, the horizontal CFRP sheets and the CFRP anchors.

The effect of the CFRP width-to-spacing ratio and the number of layers are investigated. The variation of the spacing and the number of layers are presented in Table 4.3 and Table 4.4.

Table 4.2: Variation anchorage

Set	Anchorage
V	No
VH	Horizontal CFRP anchorage sheets
VA	CFRP anchors

Table 4.3: Variation spacing

Set	Spacing	Width-to-spacing ratio
	600 [mm]	0.5
S0	300 [mm]	1.0

Table 4.4: Variation layers

Set	Layers	Thickness
	1	0.19 [mm]
L2	2	0.38 [mm]

4.3.3. Finite element modelling parameters

The RTD 2016 guideline and the fib Model Code 2010 provide guidelines for NLFEA of concrete structures. However, these documents do not provide guidelines for NLFEA of concrete structures strengthened with externally bonded CFRP reinforcement. Kalfat and Al-Mahaidi (2018b) developed a guideline for finite element modelling of concrete structures strengthened with externally bonded CFRP reinforcement. The externally bonded CFRP reinforcement is modelled as an orthotropic linear elastic material according to the guideline. The CFRP-to-concrete interface can be modelled as a bond-slip model or as a perfect bond model. According to Kalfat and Al-Mahaidi (2018b) the perfect bond model is very sensitive to the mesh size which affect the results of the numerical analysis. The variation of the CFRP-to-concrete interface model is presented in Table 4.5. The CFRP-to-concrete interface model is a bond-slip interface model in this research. However, the affect of the perfect bond model will also be investigated.

Table 4.5: Variation CFRP-to-concrete interface model

Set	CFRP-to-concrete interface model
	Bond-slip interface model
PB	Perfect bond model

4.4. Research setup

4.4.1. Geometry prestressed I-girder

The geometry of the I-girder used for the numerical finite element analysis is based on the geometry of the I-girder applied at the Nijkerker Bridge. The geometry of this I-girder is suitable for the research because the I-girder did not have shear reinforcement and the I-girder has a typical shape for Dutch prestressed I-girders made between 1960 and 1975. The technical drawings of the prestressed I-girder of the Nijkerker Bridge are given in Appendix A. The geometry of the I-girder was adjusted to make the model appropriate for the research setup. The end block of the I-girder was removed because the research focuses at the shear capacity of the I-shaped cross-section. The I-girder specimen used for the research had a length of 20 m, a height of 1000 mm and a width of 400 mm. The web had a width of 140 mm. A concrete deck with a thickness of 140 mm was applied on top of the I-girder. The geometry and the dimensions of the I-girder are illustrated in Figure 4.2 and Figure 4.1. The I-girder was prestressed with 30 seven-wire low relaxation strands with a diameter of 9.3 mm and a cross-sectional area of 52 mm². Ten additional longitudinal reinforcement bars were added to ensure shear failure instead of flexural failure. The reinforcement bars had a diameter of 30 mm. The analytical calculation of the shear tension, flexural shear and flexural resistance are given in Section 4.4.4.

The test-setup is a four-point bending test. This test-setup is presented in Figure 4.3. The four-point bending setup is suitable for the finite element analysis, because the test-setup is symmetrical.

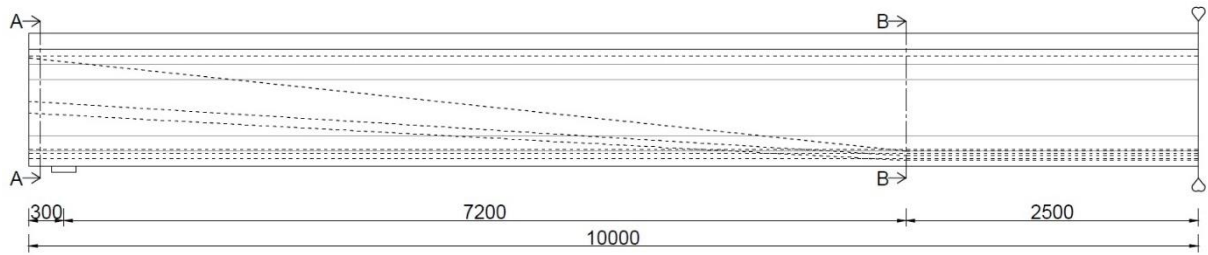


Figure 4.1: Side view I-girder

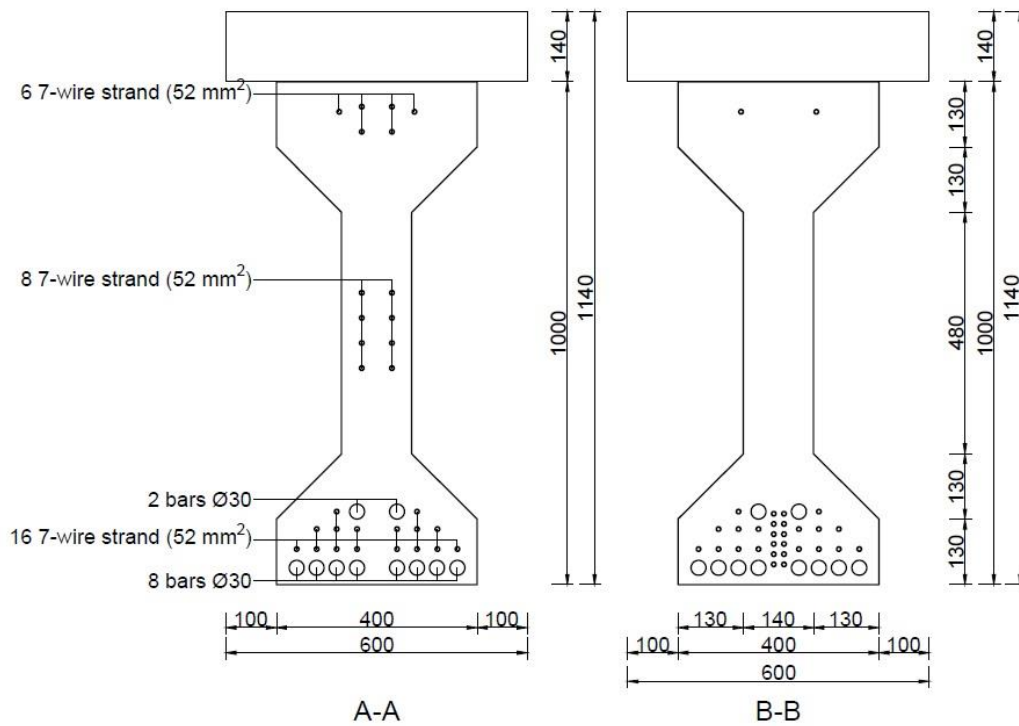


Figure 4.2: Cross-sections I-girder

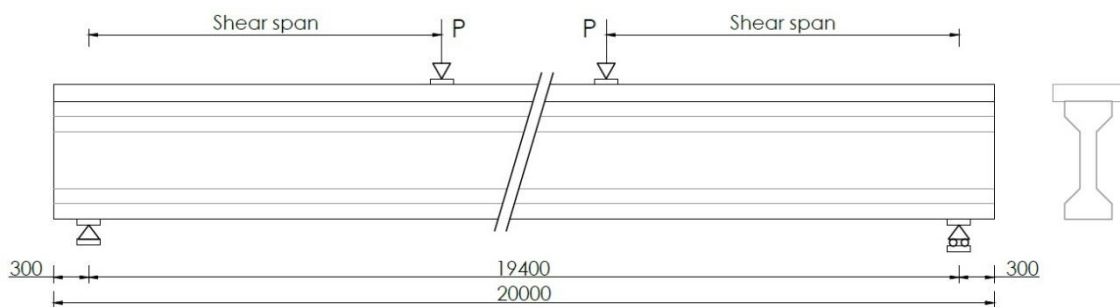


Figure 4.3: Test-setup I-girder

4.4.2. Geometry I-girders strengthened in shear using CFRP

Table 4.6 gives an overview of the research specimens. The geometry and the dimensions of the I-girder are given in Section 4.4.1. All specimens except the reference specimens were strengthened with vertical CFRP sheets. One of the suppliers of CFRP reinforcement, S&P, provides C-sheet 640 CFRP sheets with a width of 300 mm and a thickness of 0.19 mm. The material properties of the C-sheet 640 are given in Section 4.4.3.

The geometry of the specimens I-V and I-V-L2 is illustrated in Figure 4.4. The CFRP width-to-spacing ratio was 0.5. The number of CFRP sheets depends on the shear span. The detailed geometry of all the specimens can be found in Appendix B. The CFRP width-to-spacing ratio of

specimen I-V-S0 was 1.0 instead of 0.5. The cross-sectional area of CFRP was equal for the specimen I-V-S0 and I-V-L2.

The geometry of the specimen I-VH is given in Figure 4.6. The vertical CFRP sheets were anchored with horizontal CFRP sheets in the re-entrant corners. The horizontal sheets had a width of 100 mm and a thickness of 0.19 mm. The material properties of the horizontal CFRP sheets were equal to the material properties of the vertical CFRP sheets.

Figure 4.7 shows the geometry of the specimen I-VA. The vertical CFRP sheets were anchored with CFRP anchors in the re-entrant corners and underneath the deck. The CFRP anchors had a diameter of 12 mm. The CFRP anchors in the re-entrant corners were placed at an angle of 22.5°. The material properties of the CFRP anchors are given in Section 4.4.3. Two rows of anchors were applied to anchor every sheet. The centre-to-centre distance between the two anchors was 150 mm. The geometry of all the specimens I-VA and I-VA-S0 can be found in Appendix B.

Table 4.6: Overview research specimens

Specimen	Shear span [m]	Width-to-spacing ratio	Layers	Anchorage
I-C-SP3	3.0	-	-	-
I-V-SP3	3.0	0.5	1	No
I-V-PB-SP3	3.0	0.5	1	No
I-V-L2-SP3	3.0	0.5	2	No
I-V-S0-SP3	3.0	1.0	1	No
I-VH-SP3	3.0	0.5	1	Horizontal CFRP sheet
I-VA-SP3	3.0	0.5	1	CFRP anchors
I-VA-S0-SP3	3.0	1.0	1	CFRP anchors
I-C-SP4	4.0	-	-	-
I-V-SP4	4.0	0.5	1	No
I-V-PB-SP4	4.0	0.5	1	No
I-V-L2-SP4	4.0	0.5	2	No
I-V-S0-SP4	4.0	1.0	1	No
I-VH-SP4	4.0	0.5	1	Horizontal CFRP sheet
I-VA-SP4	4.0	0.5	1	CFRP anchors
I-VA-S0-SP4	4.0	1.0	1	CFRP anchors
I-C-SP5	5.0	-	-	-
I-V-SP5	5.0	0.5	1	No
I-V-PB-SP5	5.0	0.5	1	No
I-V-L2-SP5	5.0	0.5	2	No
I-V-S0-SP5	5.0	1.0	1	No
I-VH-SP5	5.0	0.5	1	Horizontal CFRP sheet
I-VA-SP5	5.0	0.5	1	CFRP anchors
I-VA-S0-SP5	5.0	1.0	1	CFRP anchors

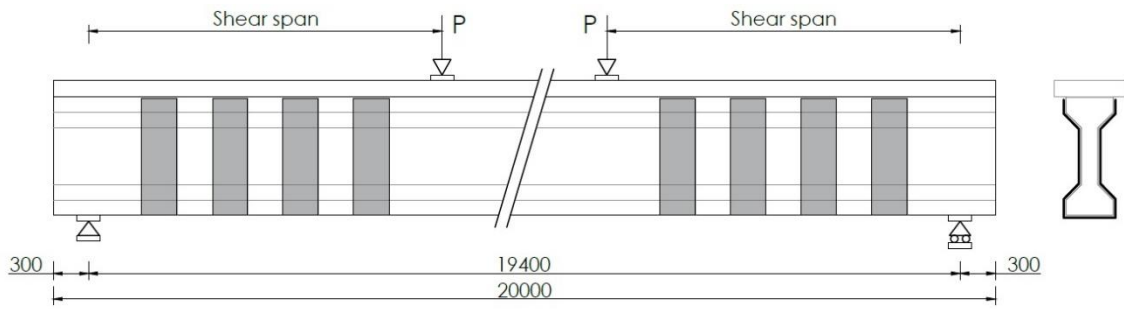


Figure 4.4: Specimens I-V and I-V-L2

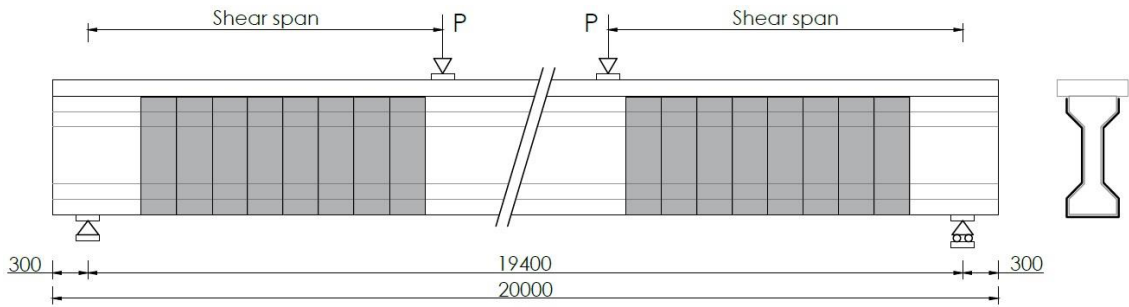


Figure 4.5: Specimen I-V-S0

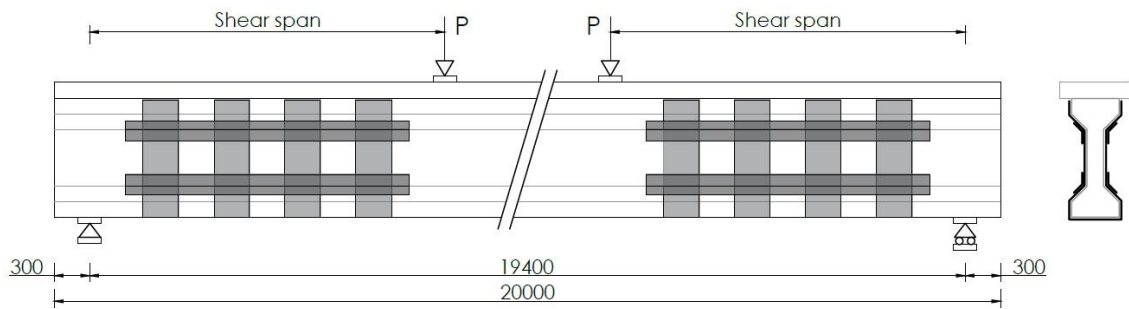


Figure 4.6: Specimen I-VH

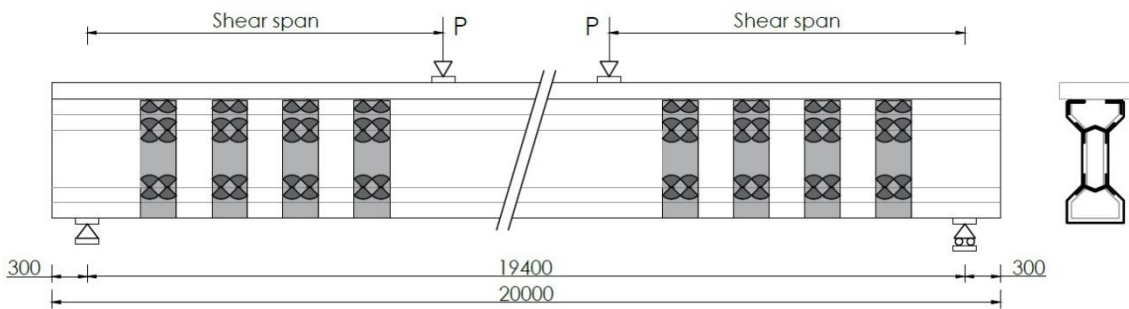


Figure 4.7: Specimen I-VA

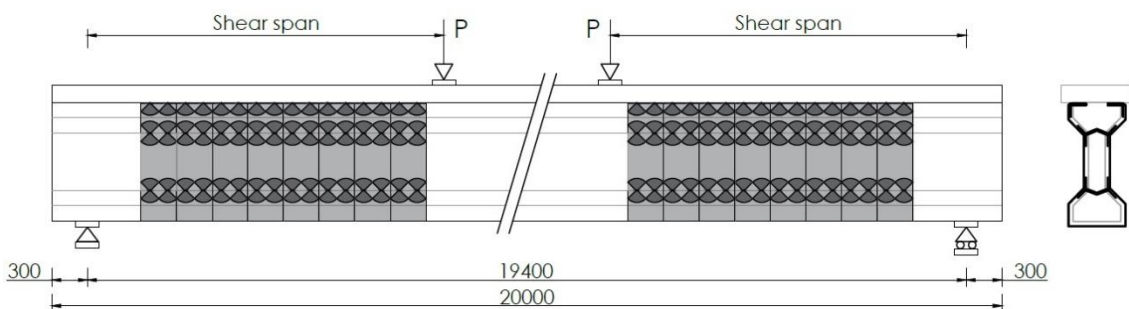


Figure 4.8: Specimen I-VA-S0

4.4.3. Material properties

The concrete, prestressing steel and reinforcement properties are given in Table 4.7, Table 4.8 and Table 4.9, respectively. The properties of the CFRP sheets used to strengthen the I-girder are presented in Table 4.10 (S&P Clever Reinforcement Company, 2017b). C-sheet 640 from S&P Clever Reinforcement Company has a standard width of 300 mm.

Table 4.7: Concrete material properties

		I-girder	Deck	Units
Young's modulus	E_{cm}	39	35	[GPa]
Characteristic compressive strength	f_{ck}	60	40	[MPa]
Mean compressive strength	f_{cm}	68	48	[MPa]
Mean tensile strength	f_{ctm}	4.4	3.5	[MPa]

Table 4.8: Prestressing steel material properties

		QP190/Y1860	Units
Young's modulus	E_p	195	[GPa]
Yield stress	$f_{p,0.1k}$	1674	[MPa]
Yield strain	ϵ_p	0.86	[%]
Ultimate stress	f_{pk}	1860	[MPa]
Ultimate strain	ϵ_{uk}	3.5	[%]

Table 4.9: Reinforcement steel material properties

		B500B	Units
Young's modulus	E_s	200	[GPa]
Yield stress	f_{yk}	500	[MPa]
Yield strain	ϵ_y	0.25	[%]
Ultimate stress	f_{uk}	540	[MPa]
Ultimate strain	ϵ_u	5.0	[%]

Table 4.10: CFRP material properties (S&P Clever Reinforcement Company, 2017b)

		C-sheet 640	Units
Young's modulus	E_f	640	[GPa]
Thickness	t_f	0.19	[mm]
Tensile strength	f_{fu}	2600	[Mpa]
Ultimate strain	ϵ_{fu}	0.4	[%]

Table 4.11: CFRP anchor material properties (S&P Clever Reinforcement Company, 2019)

		C-anchor 240	Units
Young's modulus	E_f	240	[GPa]
Tensile strength	f_{fu}	4400	[Mpa]
Ultimate strain	ϵ_{fu}	0.4	[%]

4.4.4. Analytical analysis reference specimen

The shear resistance and the bending moment resistance of the reference specimen I-C was calculated according the Eurocode NEN-EN 1992-1-1. The analytical analysis of the reference specimen I-C can be found in Appendix C. The partial safety factors for concrete, reinforcement and prestressing steel are included in the analytical analysis. The summary of the analytical analysis is presented in Table 4.12. The design shear resistance in the region without flexural cracks is 470.6 kN and in the region with flexural crack 213.8 kN. The resistance in the region with flexural cracks is not constant, because the effective depth increases towards the

middle of the specimen. The location of the transition between the region with and without flexural cracks depends on the applied load. The region without flexural cracks is quite limited. For a shear span-to-depth ratio smaller than 2.0 the I-girder will most likely fail in shear compression failure due to direct load transfer from the loading point to the support. For a shear span larger than 2.0 the I-girder will most likely fail in flexural shear failure according to the analytical analysis.

Table 4.12: Summary analytical analysis specimen I-C

	Capacity	
Shear tension resistance	470.6	[kN]
Flexural shear resistance	213.8	[kN]
Cracking moment	704.3	[kNm]
Bending moment resistance	4089.6	[kNm]

4.4.5. Prediction increase in shear capacity using CFRP reinforcement

The increase in shear capacity of concrete elements using externally bonded CFRP reinforcement were calculated according to the design guidelines and the design recommendations. The Dutch design recommendation CUR 91, the American design guideline ACI440.2R-08 and the German design guideline DAfStb heft 595 are used to predict the increase in shear capacity of the specimens. These guidelines have been developed to calculate the increase in shear capacity of rectangular cross-sections instead of I-shaped cross-sections. The prediction of the increase in shear capacity is calculated according to the expressions given in Section 3.6. Table 4.13 presents the prediction of the increase in shear capacity using externally bonded CFRP reinforcement.

Table 4.13: Analytical prediction increase in shear capacity

	Shear span [m]	Layers	Spacing [mm]	$V_{f,CUR 91}$ [kN]	$V_{f,ACI440}$ [kN]	$V_{f,DAfStb}$ [kN]
I-V-SP3	3.0	1	300	85.0	81.0	160.6
I-V-L2-SP3	3.0	2	300	138.0	108.6	252.8
I-V-S0-SP3	3.0	1	0	138.0	162.0	321.3
I-VH-SP3	3.0	1	300	85.0	81.0	160.6
I-VA-SP3	3.0	1	300	85.0	81.0	160.6
I-VA-S0-SP3	3.0	1	0	138.0	162.0	321.3
I-V-SP4	4.0	1	300	85.0	81.0	160.6
I-V-L2-SP4	4.0	2	300	138.0	108.6	252.8
I-V-S0-SP4	4.0	1	0	138.0	162.0	321.3
I-VH-SP4	4.0	1	300	85.0	81.0	160.6
I-VA-SP4	4.0	1	300	85.0	81.0	160.6
I-VA-S0-SP4	4.0	1	0	138.0	162.0	321.3
I-V-SP5	5.0	1	300	85.0	81.0	160.6
I-V-L2-SP5	5.0	2	300	138.0	108.6	252.8
I-V-S0-SP5	5.0	1	0	138.0	162.0	321.3
I-VH-SP5	5.0	1	300	85.0	81.0	160.6
I-VA-SP5	5.0	1	300	85.0	81.0	160.6
I-VA-S0-SP5	5.0	1	0	138.0	162.0	321.3

5

SHEAR BEHAVIOUR OF I-GIRDER STRENGTHENED WITH CFRP REINFORCEMENT

5.1. Finite element modelling

5.1.1. Concrete

The three-dimensional mechanical model of the girder was modelled according to the dimensions of the test setup as given in Section 4.4.1. A quarter of the test-setup was modelled, because the test-setup is symmetrical in two directions as illustrated in Figure 5.1. The mechanical model of the I-girder was divided in three-dimensional 20-node hexahedral brick elements. The 20-node hexahedral element is based on quadratic interpolation of the displacement field. The 3 x 3 x 3-point Gauss integration scheme was used for the 20-nodes hexahedral elements. The mesh sizes of the undistorted elements were 100 x 100 x 100 mm. The finite element mesh was generated by the algorithm of DIANA. Figure 5.2 illustrates an example of the finite element mesh.

The mesh of the specimens strengthened with CFRP were adjusted because the size of the three-dimensional brick element layer underneath the CFRP should be limited to improve the results of the NLFEA (Kalfat & Al-Mahaidi, 2018b). A thick layer of three-dimensional brick elements underneath the CFRP could cause inconsistencies in the NLFEA. Therefore, the first layer of three-dimensional brick element underneath the CFRP had a thickness of 5 mm in the finite element models.

The constitutive concrete model was derived from the provisions of the fib Model Code 2010 as prescribed by the RTD2016 guideline (Hendriks et al., 2017a). The concrete constitutive model is presented in Table 5.1. The concrete material properties of the I-girder and the deck are given in Table 5.2. A total strain based rotating crack model or a total strain based fixed crack model with an adequate shear retention model should be used according to the RTD2016 guideline. Results from recent research reveal that concrete beams without shear reinforcement are robustly modelled using a total strain based fixed crack model with a damage based shear retention model (De Putter, 2020). The total strain based fixed crack model with a damage based shear retention model was assigned to the three-dimensional concrete elements in this research.

Table 5.1: Concrete constitutive model

	Constitutive model
Crack model	Total strain based fixed crack model
Tensile curve	Hordijk curve
Compression curve	Parabolic curve
Crack bandwidth estimator	Govindjee
Compressive strength reduction	Vecchio & Collins 1993
Poisson reduction	Damage based

Table 5.2: Material properties concrete

		I-girder	Deck	Units
Young's modulus	E_{cm}	39	35	[GPa]
Poisson ratio	N	0.15	0.15	[-]
Density	ρ	2400	2400	[kg/m ³]
Tensile strength	f_{ctm}	4.4	3.5	[MPa]
Mode-I tensile fracture energy	G_{FI}	0.156	0.147	[N/mm]
Mean compressive strength	f_{cm}	68	48	[MPa]
Compressive fracture energy	G_C	39.004	36.634	[N/mm]
Lower bound reduction curve	β_σ	0.4	0.4	[-]

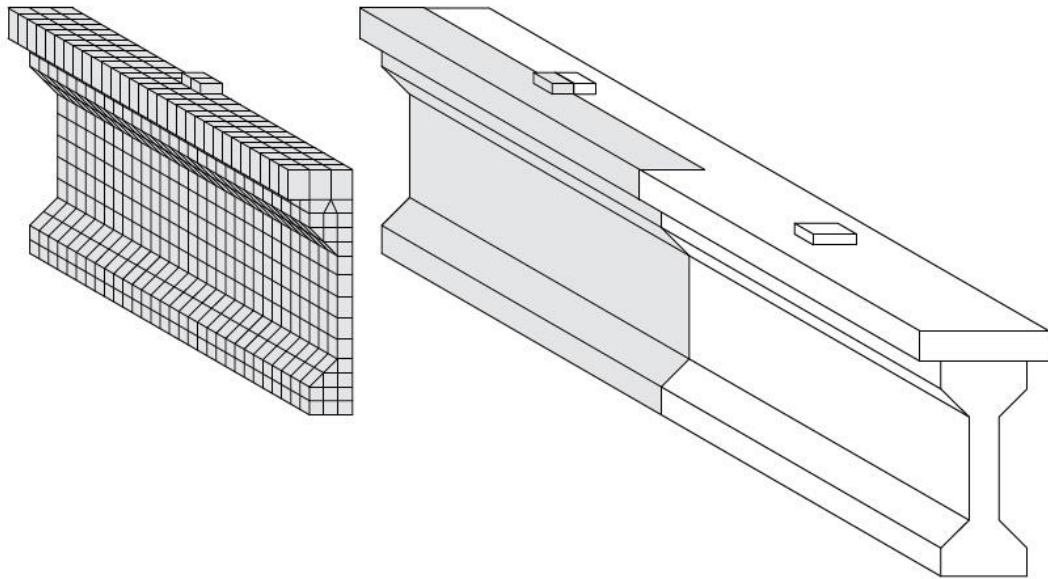


Figure 5.1: Finite element model prestressed concrete I-girder

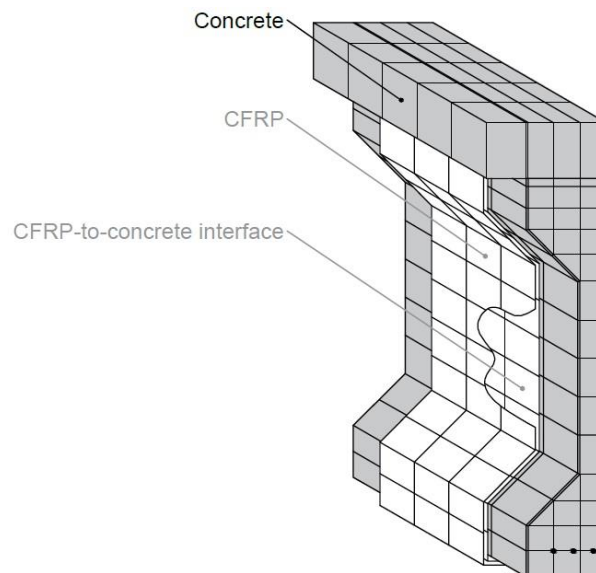


Figure 5.2: Overview finite element model concrete

5.1.2. Prestressing strands and reinforcement bars

The seven-wire low-relaxation prestressing strands and reinforcement bars were modelled as lines. The lines were divided into embedded reinforcement elements. Their shape and interpolation were based on those of the concrete model in which the reinforcement is embedded.

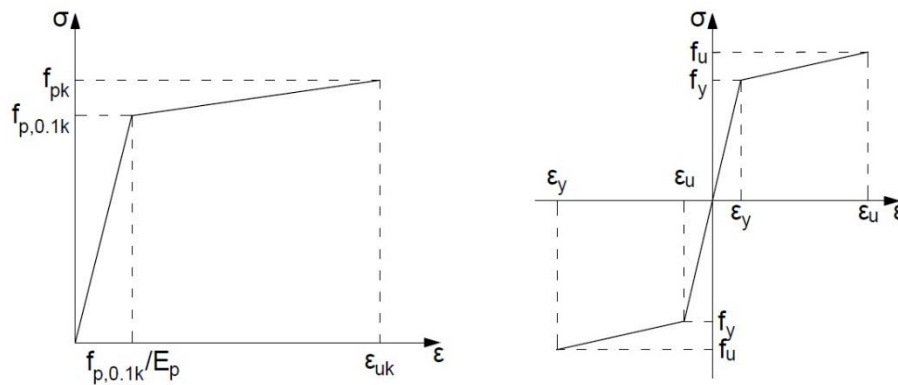
The material properties of prestressing strands and reinforcement bars were derived from the original specification as prescribed in the fib Model Code 2010. The constitutive model for prestressing strands and reinforcement bars is an elastoplastic model with hardening. The hardening is described by a bilinear stress-strain relationship. The stress-strain relationships of the prestressing strands and the reinforcement bars are illustrated in Figure 5.3. The material properties of the prestressing strands and the reinforcement bars are given in Table 5.3 and Table 5.4

Table 5.3: Properties prestressing strands

		Value	Units
Young's modulus	E_p	195	[GPa]
Yield stress	$f_{p,0.1k}$	1674	[MPa]
Yield strain	ϵ_p	0.86	[%]
Ultimate stress	f_{pk}	1860	[MPa]
Ultimate strain	ϵ_{uk}	3.5	[%]

Table 5.4: Properties reinforcement

		Value	Units
Young's modulus	E_s	200	[GPa]
Yield stress	f_y	500	[MPa]
Yield strain	ϵ_y	0.25	[%]
Ultimate stress	f_u	540	[MPa]
Ultimate strain	ϵ_u	5	[%]

**Figure 5.3: Stress-strain diagrams prestress strands and reinforcement bars**

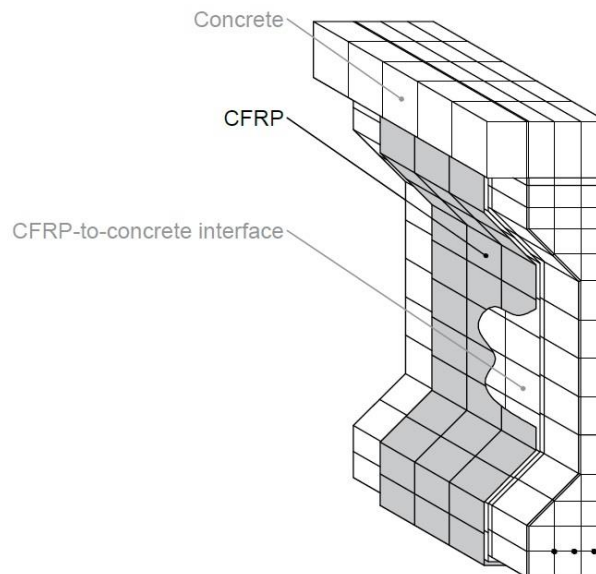
5.1.3. CFRP reinforcement

Kalfat and Al-Mahaidi (2018b) defined two approaches to model the externally bonded CFRP reinforcement. The CFRP reinforcement can be modelled as an orthotropic material assigned to two-dimensional shell elements or as three-dimensional brick elements with smeared reinforcement. Modelling the CFRP reinforcement with three-dimensional brick element was not suitable for this research because of the large amount of elements in the model. The CFRP reinforcement was therefore modelled with two-dimensional regular curved shell elements. The size of the regular curved shell elements was 100 x 100 mm. An overview of the finite element model of the CFRP is illustrated in Figure 5.4.

The externally bonded CFRP reinforcement was modelled as a linear elastic orthotropic material as proposed by Kalfat and Al-Mahaidi (2018b) because unidirectional CFRP sheets have different material properties in the three principal directions. The difference in material properties in these directions is significant. The Young's modulus parallel to the direction of the carbon fibres depends on the Young's modulus of the carbon fibres. While the Young's modulus perpendicular to the direction of the carbon fibres depends on the Young's modulus of the polymer matrix. The orthotropic linear elastic material properties of the CFRP reinforcement are given Table 5.5.

Table 5.5: Orthotropic linear elastic properties CFRP

		Value	Units
Young's modulus	E_x	640	[GPa]
	E_y	7.1	[GPa]
	E_z	7.1	[GPa]
Poisson ratio	ν	0.3	[-]
	ν	0.3	[-]
	ν	0.3	[-]
Shear modulus	G_x	2731	[MPa]
	G_y	2731	[MPa]
	G_z	2731	[MPa]

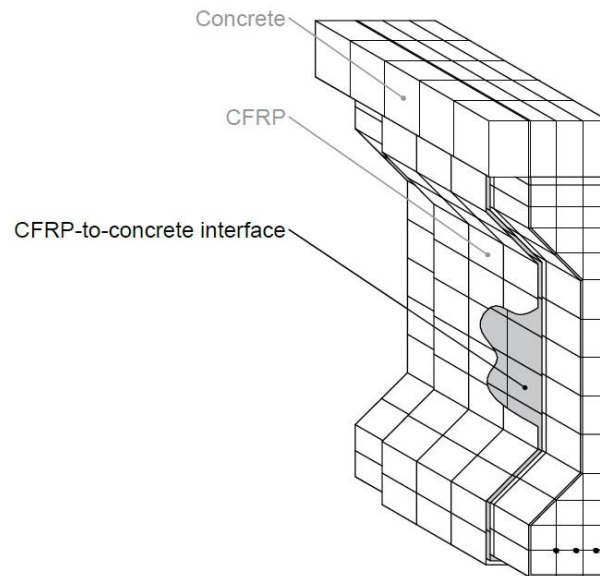
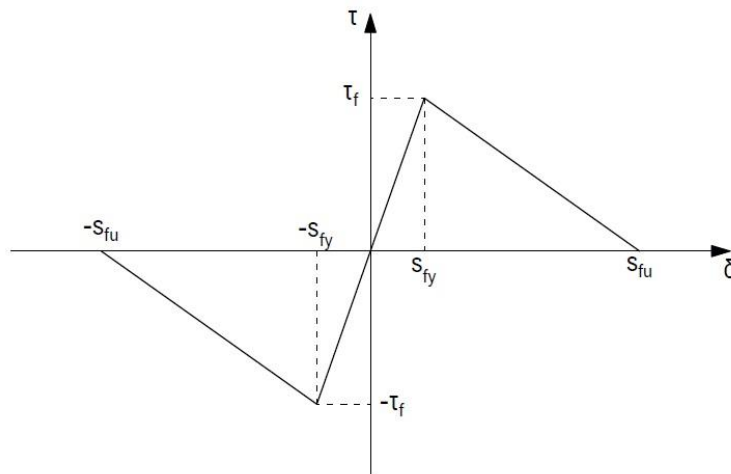
**Figure 5.4: Overview finite element model CFRP**

5.1.4. CFRP-to-concrete interface

Kalfat and Al-Mahaidi (2018b) described three approaches for modelling the interface between the externally bonded CFRP reinforcement and the concrete. A perfect bond at the interface or a layer of interface elements are commonly used in practice as mentioned in Section 3.7.2. However, the results of the NLFEA of models with a perfect bond show that such an interface model is mesh size dependent. The CFRP-to-concrete interface was therefore modelled with nonlinear elastic interface elements in this research. The CFRP-to-concrete interface was modelled as a layer of two-dimensional interface elements between the CFRP and the concrete with a thickness of 0 mm. Figure 5.5 shows an illustration of the interface elements. The behaviour of the nonlinear elastic interface was described by the bond-slip model proposed by Sato and Vecchio (2003) as illustrated in Figure 5.6. The values in the bond-slip diagram were calculated according to the expressions given in Section 3.4. The bond-slip diagram is based on the mean compressive concrete strength of the concrete. The material properties of the bond-slip model are given in Table 5.6.

Table 5.6: Bond-slip properties

		Value	Units
Mean compressive strength	f_{cm}	60	[MPa]
Peak bond shear stress	τ_f	4.645	[MPa]
Slip at peak bond shear stress	s_{fy}	0.040	[mm]
Maximum slip	s_{fu}	0.213	[mm]
Interfacial fracture energy	G_f	0.495	[N/mm]

**Figure 5.5: Finite element model****Figure 5.6: Bond-slip diagram**

5.1.5. CFRP anchors

In contrast to the finite element modelling approaches of the externally bonded CFRP reinforcement and the CFRP-to-concrete interface no guidelines to model CFRP anchors can be found in literature. Al-Sammari and Breña (2018) modelled CFRP anchors using finite element modelling to investigate the effect of key parameters such as diameter, embedment length and splay angle. They used small three-dimensional brick elements to model the CFRP anchors as illustrated in Figure 5.7. This approach is not useful to investigate the behaviour of externally bonded CFRP reinforcement anchored with CFRP anchors due to the large amount of very small elements.

To investigate the performance of CFRP anchors, finite element modelling approaches are proposed. Some of these were modelled and analysed using NLFEA. The CFRP anchor consists of two parts: the bundle of impregnated carbon fibres in the predrilled hole in the concrete, and the carbon fibre splay. The bundle of impregnated carbon fibres is a straight element with a circular cross-section. The material properties of this bundle is uniform, and therefore suitable to be modelled with beam elements or embedded reinforcement. The drawback of the embedded reinforcement elements is that these elements could not be connected to the two-dimensional CFRP elements and the drawback of the beam elements is that these element could not be embedded into the concrete. The diameter of the CFRP anchors in this research is 12 mm. The linear elastic material properties of the CFRP anchors are given in Table 5.7.

The carbon fibre splay allows for a more uniform load transfer between the CFRP anchor and the CFRP sheet. The behaviour of the splay should be modelled in the finite element model to prevent stress concentrations in the connection between the CFRP anchor and the CFRP sheet. Two approaches to model the effect of the splay were investigated. These are illustrated in Figure 5.8. The first approach is the accurate geometry approach while the second is more simplistic. The geometry of the splay was modelled as a triangular two-dimensional plane using shell elements. These were connected to the two-dimensional CFRP shell elements. The second approach focussed on the behaviour of the anchor to prevent the CFRP sheets from pulling away from the re-entrant corner. To introduce a more uniform load transfer between the anchor and the CFRP sheet a stiff element was added in the re-entrant corners of the I-girder. The material properties of the splays in specimen I-VA-ERS and I-VA-LES are equal to the material properties of the anchors. The properties of the stiff line element used in specimen I-VA-ERL and I-VA-LEL are based on the properties of the CFRP sheet in the re-entrant corner. The CFRP sheet in the corner has a stiffness due to the angle in the CFRP sheet. The material properties of the stiff line element are given in Table 5.8. The second moment of inertia of the stiff line element is based on the angle profile of the CFRP sheet in the re-entrant corner. The assumed value for the moment of inertia is 9.3 cm^4 was based on an angle profile with a height of 100 mm.

Another approach to model the CFRP anchor is to apply one-dimensional springs in the re-entrant corners. However, this approach is not suitable for CFRP anchors placed at an angle. The one-dimensional springs can only be applied horizontally and not diagonally. This approach is not modelled and analysed because this approach is not suitable to model the behaviour of the anchors in the re-entrant corners.

An overview of the proposed approaches and the corresponding element types are presented in Table 5.9.

Table 5.7: Linear elastic properties CFRP anchor

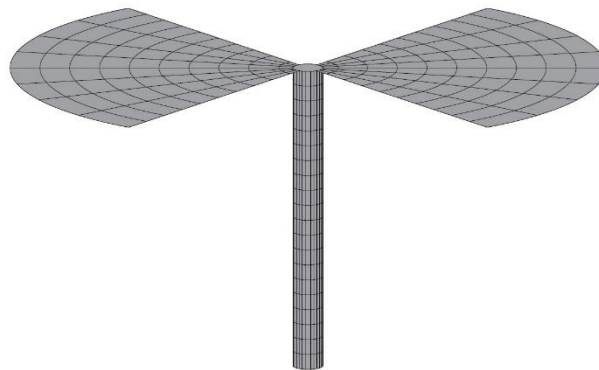
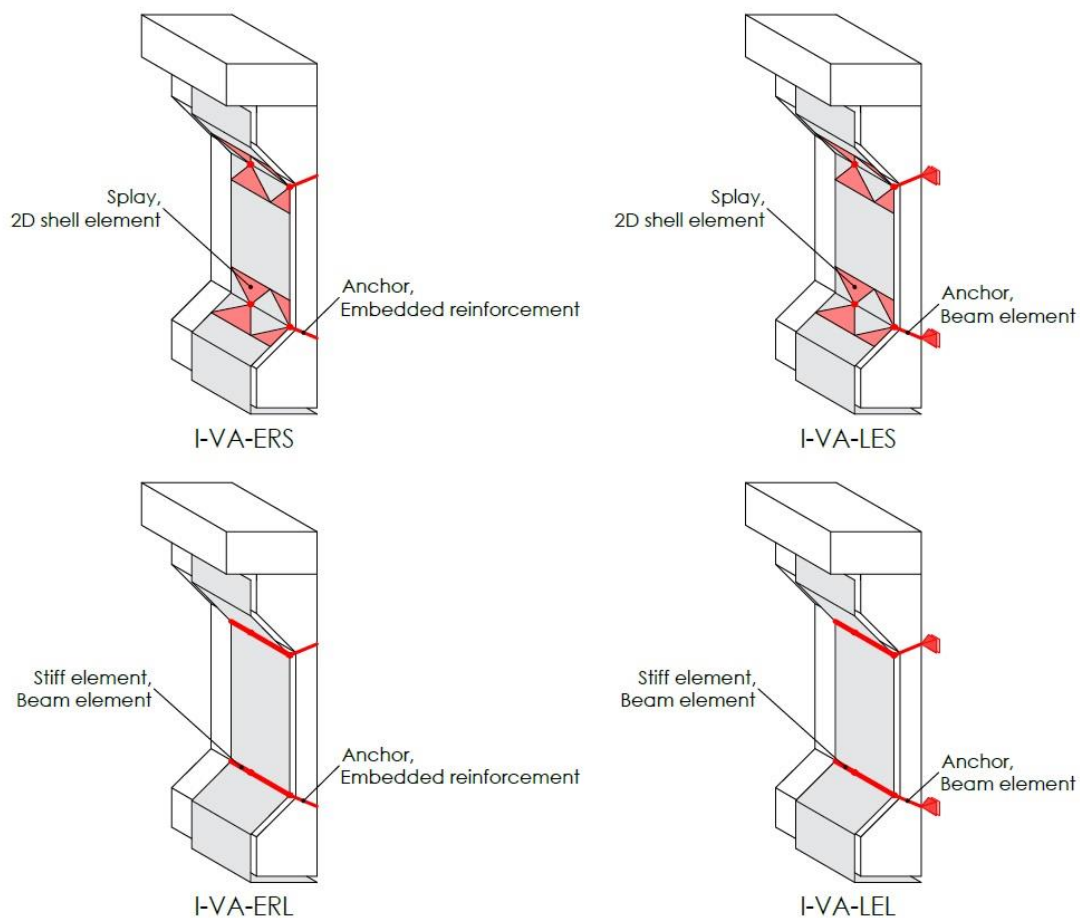
		Value	Units
Young's modulus	E	240	[GPa]
Poisson ratio	ν	0.3	[-]

Table 5.8: Linear elastic properties stiff line element

		Value	Units
Young's modulus	E	640	[GPa]
Poisson ratio	ν	0.3	[-]

Table 5.9: Overview finite element modelling approaches

Specimen	Anchor	Splay/stiff line element
I-VA-ERS	Embedded reinforcement	2D shell elements
I-VA-LES	Class-III beam element	2D shell elements
I-VA-ERL	Embedded reinforcement	Class-III beam element
I-VA-LEL	Class-III beam element	Class-III beam element

**Figure 5.7: Finite element model CFRP anchor with three-dimensional elements****Figure 5.8: Finite element modelling approaches for CFRP anchors**

5.1.6. Support plate and load plate

Support and loading points were applied using support and load plates. The aim of the support and load plates is to reduce local stress concentrations in the concrete. The support and load plates were modelled as steel plates with linear elastic material properties in this finite element models. The material properties of the steel plates are given in Table 5.10.

Table 5.10: Properties steel

		Value	Units
Young's modulus	E	210	[GPa]
Poisson ratio	ν	0.3	[-]

5.1.7. Boundary conditions and loading

The boundary conditions were implemented to simulate the conditions of the experimental test. The support line was restrained against movement in the Z-direction. The support was also restrained against rotation around the X-axis because the support is a line support. The line support allows rotation around the Y-axis. The first plane of symmetry was restrained against movement in the X-direction and the second plane of symmetry was restrained against movement in the y-direction. The boundary conditions are illustrated in Figure 5.9.

In the numerical model two load cases were considered. A prestressing force and the self-weight of the specimen were applied in the first load case. The first load case was applied in 1 step with a load factor of 1.0. A prescribed deformation of 1 mm in the Z-direction was applied in the second load case. The second load case was applied in two parts. The first part had a load factor of 2.0 and the second part had a load factor of 0.2. The load steps of both parts depended on the deflection at the peak load. The load steps just before and after the peak load were applied with a load factor of 0.2. The convergence tolerances of both load cases are presented in Table 5.11. The analysis is set to continue even when the convergence criteria for the force and energy norm were not satisfied.

Table 5.11: Load cases specimens

Load case	Load	Load factor	Load steps	Force norm	Energy norm
LC1	Prestressing	1.0	1	0.01	0.001
	Self weight	1.0	1	0.01	0.001
LC2	Point load	2.0	-	0.01	0.001
		0.2	-	0.01	0.001

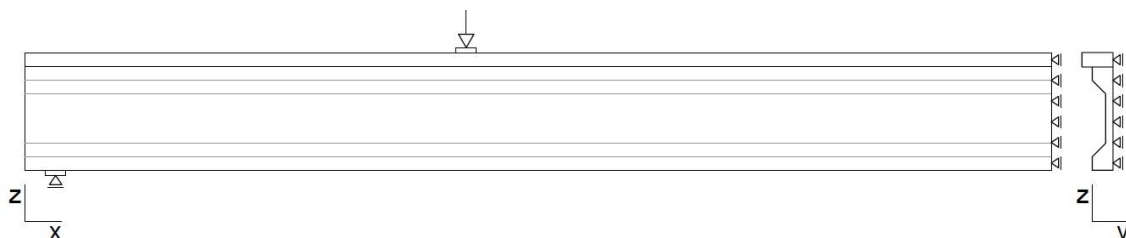


Figure 5.9: Boundary conditions

5.2. Shear behaviour reference specimen I-C

5.2.1. Finite element model specimen I-C

The finite element model of specimen I-C-SP4 is shown in Figure 5.10. The finite element model of the specimens I-C-SP3 and I-C-SP5 are presented in Appendix D. The material properties of the concrete, reinforcement bars, prestressing tendons and the steel plates are given in Section 5.1. The boundary conditions and the convergence criteria are given in Section 5.1.7. The load cases and the load steps of the specimens are presented in Table 5.12.

Table 5.12: Load cases reference specimens I-C-SP3, I-C-SP4 and I-C-SP5

Load case	Load	Load factor	Load steps		
			I-C-SP3	I-C-SP4	I-C-SP5
LC1	Prestressing & self weight	1.0	1	1	1
LC2	Point load	2.0	10	12	16
		0.2	100	200	200

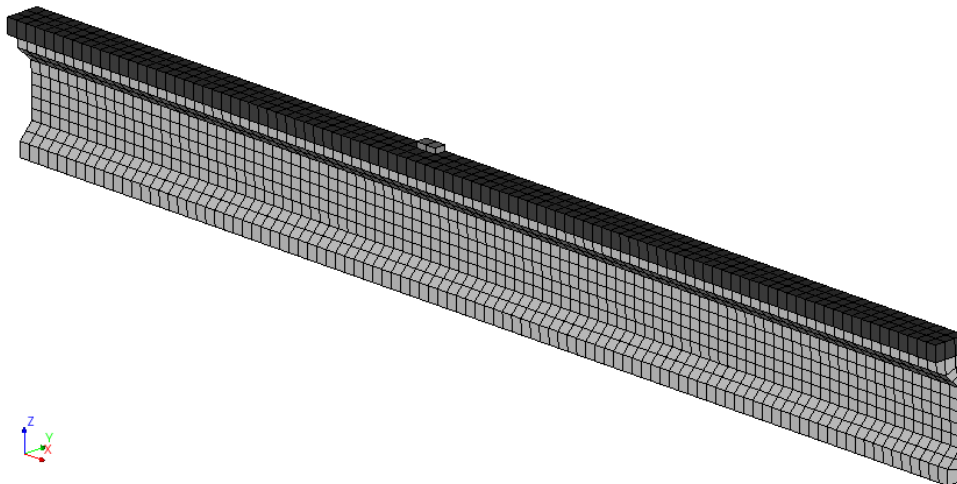


Figure 5.10: Finite element model specimen I-C-SP4

5.2.2. Results reference specimen I-C

The load-deformation curves of specimens I-C-SP3, I-C-SP4, and I-C-SP5 are given in Figure 5.11. The deformation is the prescribed deformation at the loading point. The deflection due to the prestressing and the self-weight of the I-girder are not included in the load-deformation curves. However, the self-weight and the effect of the kinked tendons are included in the calculation of the shear force of the specimens, as presented in Table 5.13. The maximum mid-span deflection is also given in Table 5.13.

Specimen I-C-SP3

The crack pattern of specimen I-C-SP3 is presented in Figure 5.12. The development of the crack pattern can be found in the principal strain and crack strain plots as given in Appendix E.1. The first flexural cracks started in the span between the loading point and the middle of the I-girder at load step 7 (382 kN). The flexural crack propagated into the web of the I-girder towards the loading point. At load step 10 (512 kN) a horizontal crack started in the corner between the web and the bottom flange. The horizontal crack developed into the shear crack at load step 25 (517 kN). The principal strain plot and the crack pattern at load step 25 is presented in Figure 5.12. The crack propagated into the web, towards the loading plate and along the bottom of the web towards the support. The propagation of the shear crack was

extremely brittle. The brittle failure behaviour of this specimen is also visible in the load-deformation curve as shown in Figure 5.11. The peak load of 559.8 kN was reached at load step 24 just before the brittle propagation of the critical crack and failure of the specimen. The equilibrium iteration in the load steps after the peak load did not converge anymore. The failure mode of this specimen was shear tension failure, however the starting location of the shear tension crack at the bottom of the web is not common for I-girders.

Specimen I-C-SP4

The crack pattern in Figure 5.13 shows the propagation of flexural cracks into diagonal cracks in the web of specimen I-C-SP4. The principal strain and the crack strain plots of this specimen are given in Appendix E.1. The flexural cracks in the region between the support and the loading point started to develop into the web towards the loading point at load step 24 (416 kN). The diagonal cracks propagated towards the loading point between load step 24 and load step 30 (427 kN). The diagonal crack started to open at load step 31 (426 kN). The crack propagated horizontally towards the support at the load steps after load step 31. The propagation of the horizontal crack is visible in the principal strain plot presented in Figure 5.13. The peak load of 426.6 kN was reached at load step 30 just before the flexural crack developed towards the support. The failure mode of this specimen was flexural shear failure. The specimen failed due to the propagation of the dowel crack at the bottom of the web. The dowel crack propagated from the diagonal crack towards the support.

Specimen I-C-SP5

The flexural cracks in the shear span of specimen I-C-SP5 developed into diagonal cracks in the web of the I-girder. The crack pattern at the last load step before the analysis aborted is indicated in Figure 5.14. The flexural cracks developed into diagonal cracks in the web of the I-girder at load step 23 (356 kN). The diagonal crack propagated further towards the loading point between load step 23 and load step 34 (361 kN). The dowel crack propagated towards the support between load step 34 and load step 43 (308 kN). The equilibrium iteration at the load steps between load step 34 and load step 43 did not converge. The energy and force convergence tolerances were not satisfied anymore within the maximum number of iterations. These load steps are plotted in the load-deformation curve with red symbols. The load-deformation curve started to ascend after load step 43 and the convergence tolerances were satisfied within the maximum number of iterations. These loads steps converged because the kinked tendons prevented further propagation of the dowel crack. The load-deformation curve started to descend after load step 89 (350 kN) and the equilibrium iteration diverged at load step 91.

Table 5.13: Results specimens I-C-SP3, I-C-SP4 and I-C-SP5

Specimen	Shear span [m]	Peak load [kN]	Deflection [mm]	Shear force [kN]
I-C-SP3	3.0	559.8	43.65	574.2
I-C-SP4	4.0	426.6	42.97	433.2
I-C-SP5	5.0	361.0	47.23	359.8

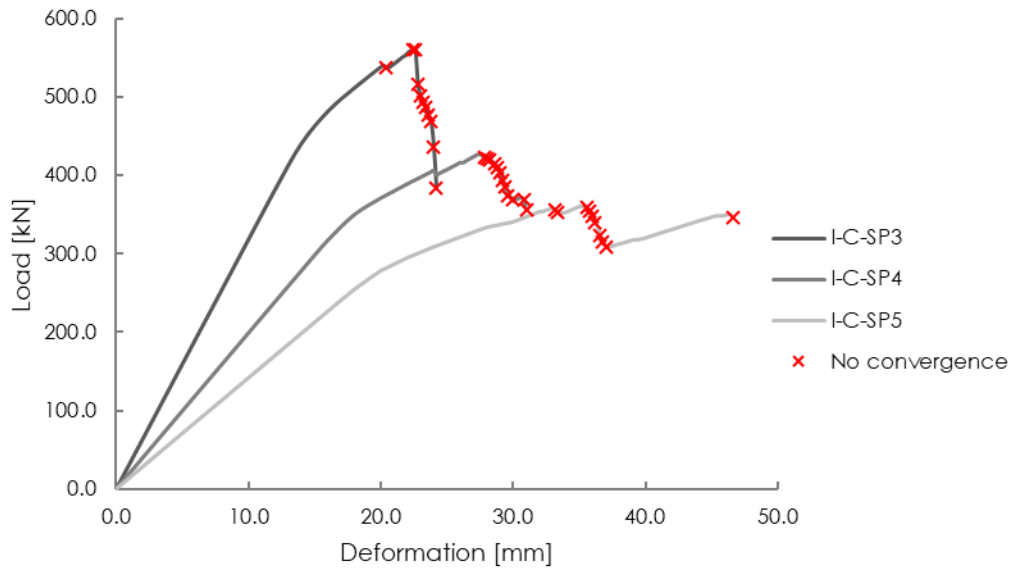


Figure 5.11: Load-deformation curves reference specimens I-C-SP3, I-C-SP4 and I-C-SP5

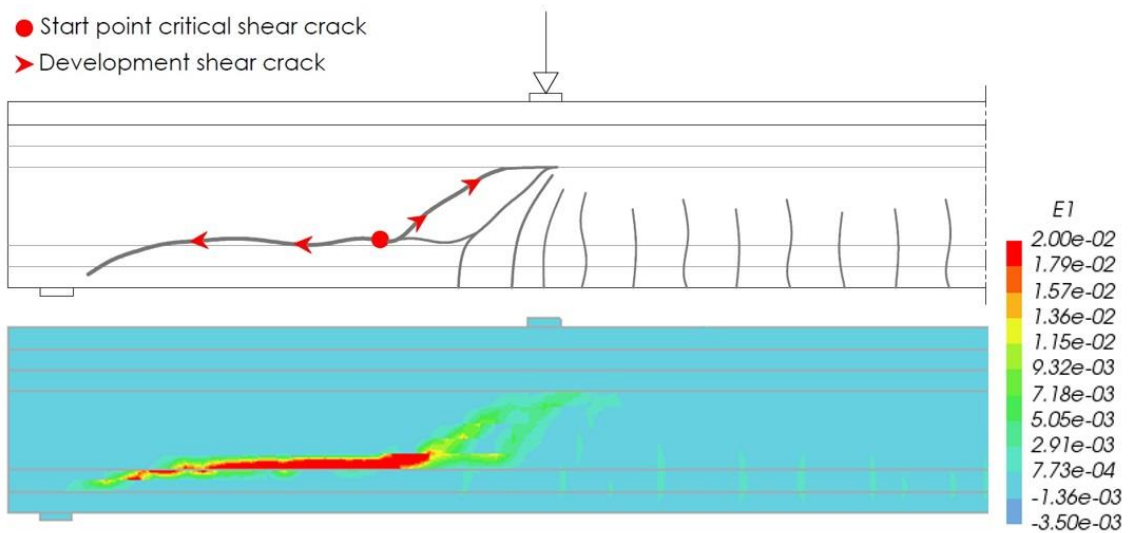


Figure 5.12: Crack pattern and principal strain plot specimen I-C-SP3 at load step 25

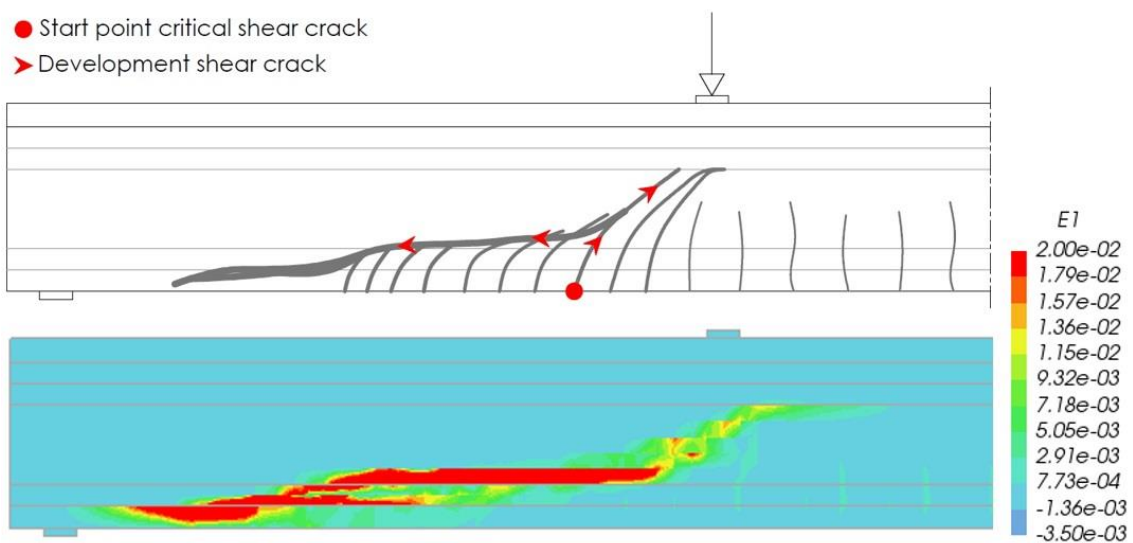


Figure 5.13: Crack pattern and principal strain plot specimen I-C-SP4 at load step 40

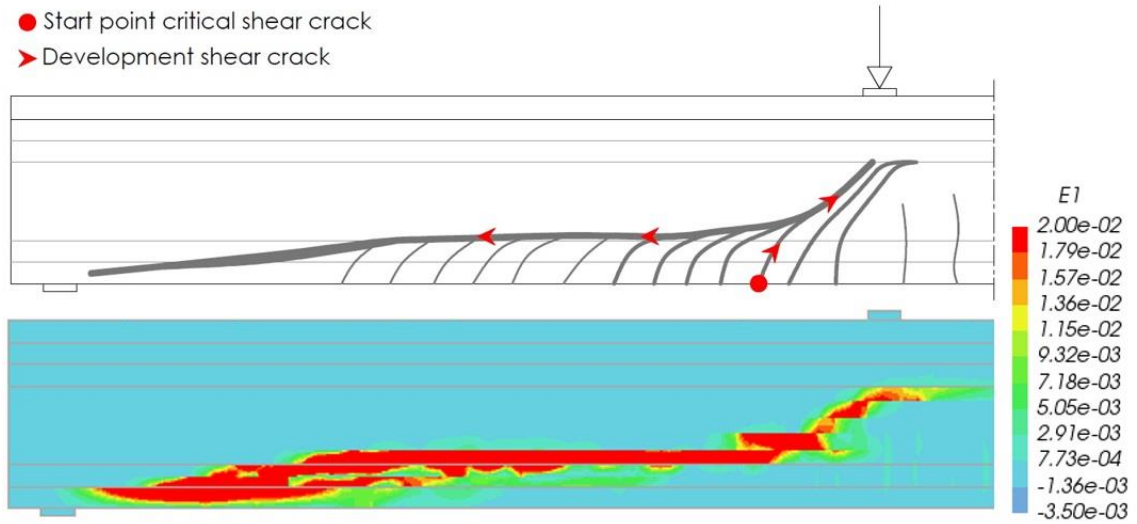


Figure 5.14: Crack pattern and principal strain plot specimen I-C-SP5 at load step 42

5.3. Shear behaviour specimen I-V

5.3.1. Finite element model specimen I-V

Figure 5.15 shows the finite element model of specimen I-V-SP4 strengthened with vertical CFRP sheets. The geometry and dimensions of the CFRP strengthening of specimens I-V-SP3, I-V-SP4 and I-V-SP5 are presented in Appendix B. The finite element model of specimen I-V-SP3 and I-V-SP5 are given in Appendix D. The material properties of the prestressed concrete I-girder are given in Section 5.1. The orthotropic material model as described in Section 5.1.3 was assigned to the CFRP regular curved shell elements. The bond-slip model as described in Section 5.1.4 was assigned to the interface elements between the CFRP and the concrete. The load cases and the load steps for the specimens are given in Table 5.14.

Table 5.14: Load cases reference specimens I-V-SP3, I-V-SP4 and I-V-SP5

Load case	Load	Load factor	Load steps		
			I-V-SP3	I-V-SP4	I-V-SP5
LC1	Prestressing & self weight	1.0	1	1	1
LC2	Point load	2.0	10	12	16
		0.2	100	200	200

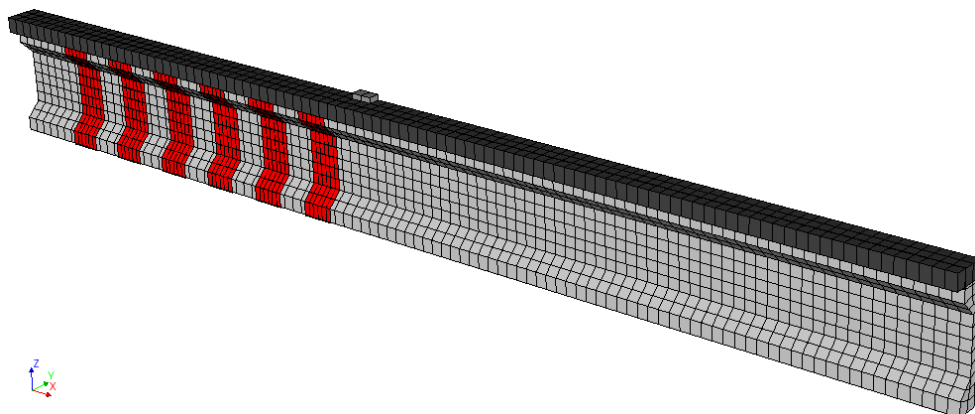


Figure 5.15: Finite element model specimen I-V-SP4

5.3.2. Results specimen I-V

The load-deformation curves of the specimens I-V-SP3, I-V-SP4 and I-V-SP5 are presented in Figure 5.16 and the maximum shear force and the maximum mid-span deflection of the specimens is given in Table 5.15.

Specimen I-V-SP3

The critical shear crack started in the web of the I-girder as a horizontal crack between the third and the fourth CFRP sheet at load step 10 (513 kN). At load step 25 (570 kN) the crack developed diagonally towards the loading point and horizontally towards the support. The development of the crack was very similar to the development of the crack of the reference specimen as presented in Figure 5.12. The peak load of 572.6 kN was reached just after the brittle propagation of the shear crack, while the peak load of specimen I-C-SP3 was reached just before the brittle propagation of the shear crack. The local debonding of the CFRP sheets started around the critical shear crack and developed towards the bottom flange. The opening of the critical crack directly led to debonding of the CFRP sheet in the corner between the web and the bottom flange of the I-girder. The plot of the CFRP sheets pulling away from the corner between the web and the bottom flange at load step 27 (563 kN) is given in Appendix E.2. The debonding of the CFRP sheets is presented in Figure 5.17. The NLFEA of specimen I-V-SP3 aborted just after the peak load because load step 28 diverged. However, the load increased at load step 26 (573 kN) due to the addition of the CFRP sheets. The maximum axial stress in the CFRP sheets was 1082 MPa. The highest axial stresses in the CFRP sheets were reached around the shear crack. The axial stress values at load step 27 are given in Figure 5.20. The stress concentrations around the shear cracks are visible in the axial stress plot. The shear force of the specimen increased with 2.2% compared to the reference specimen. The limited increase in shear capacity is mainly caused by the increase in stiffness of the I-girder instead of the closure of the critical shear crack.

Specimen I-V-SP4

The maximum shear force of specimen I-V-SP4 increased with 6.4%. The flexural cracks in the bottom flange of the specimen developed into the web towards the loading point. The diagonal crack propagated into the web at load step 48 (453 kN). The diagonal crack caused local debonding of the CFRP sheets around the crack. The debonding of the CFRP sheets propagated towards the corner between the web and the bottom flange. The load increased after appearance of the first diagonal cracks in the web of the I-girder. The NLFEA of the specimen aborted at load step 51 because the equilibrium iteration diverged. The load-deformation curve was still ascending in load step 50 (454 kN). The peak load in Table 5.15 is the load at load step 50. The shear force of this specimen increased compared to the reference specimen. The debonding of the CFRP sheets started before the analysis aborted and the CFRP sheet started to pull away from the re-entrant corner. Stress concentrations appeared around the diagonal cracks due to the propagation of the shear cracks. The stress concentrations disappeared due to the debonding of the CFRP sheets.

Specimen I-V-SP5

The flexural cracks in the shear span propagated into the web at load step 18 (356 kN). The diagonal cracks developed towards the loading point. The diagonal cracks in the web of the I-girder caused local debonding of the CFRP sheets. The debonding of the CFRP sheets propagated towards the corner between the web and the bottom flange due to the opening of the shear cracks. After the peak load of 395.7 kN at load step 52 the crack started to propagate horizontally towards the support. The propagation of the flexural shear crack

caused the CFRP sheet to pull away from the corner. The propagation of the shear crack and the debonding of the CFRP sheets in the corner between the web and the bottom flange is illustrated in Figure 5.19 and Figure 5.21. The plot of the CFRP sheets pulling away from the re-entrant corner is presented in Appendix E.2. The flexural shear crack did not develop horizontally towards the support, but the new flexural cracks in the shear span propagated into the web towards the loading point. The load-deformation curve started to ascend after the peak load was reached. However, the load was almost constant in the load steps after the peak load. The analysis aborted after load step 61 (393 kN). Due to the propagation of the diagonal cracks the CFRP sheets were loaded in tension. The maximum axial stress at load step 18 was only 156 MPa. The axial stresses in the CFRP sheets increased till a maximum axial stress of 1653 MPa at load step 61. The maximum axial stresses were reached around the critical shear crack. The axial stress values at load step 61 are presented in Figure 5.20. The stress distribution became more uniform due to the debonding of the CFRP sheets around the diagonal cracks. The maximum shear force of the specimen increased with 9.7% compared to the reference specimen.

Table 5.15: Results specimens I-V-SP3, I-V-SP4 and I-V-SP5

	Shear span [m]	Peak load [kN]	Deflection [mm]	Shear force [kN]	Increase shear force
I-C-SP3	3.0	559.8	43.65	574.2	-
I-V-SP3	3.0	572.6	44.72	587.1	2.2%
I-C-SP4	4.0	426.6	42.97	433.2	-
I-V-SP4	4.0	454.2*	48.78	460.9	6.4%
I-C-SP5	5.0	361.0	47.23	359.8	-
I-V-SP5	5.0	395.7	52.29	394.5	9.7%

* Peak load is the load in the last step before the analysis of specimen aborted.

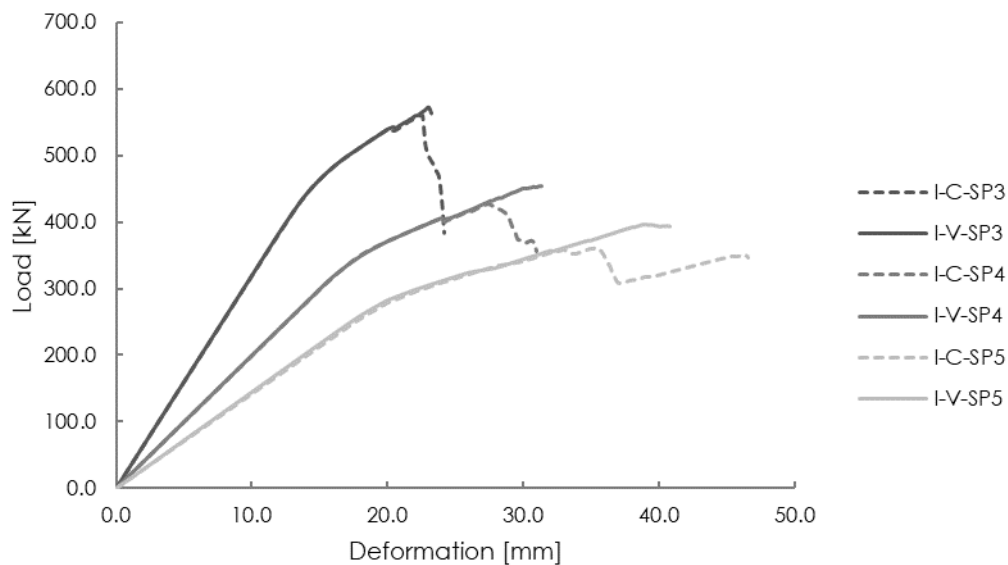


Figure 5.16: Load-deformation curves specimens I-V-SP3, I-V-SP4 and I-V-SP5

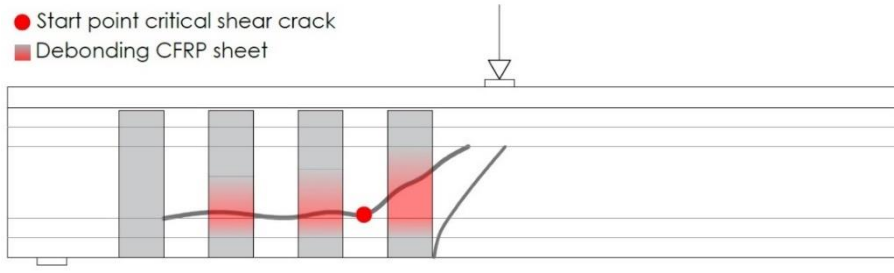


Figure 5.17: Debonding CFRP sheets specimen I-V-SP3 at load step 27

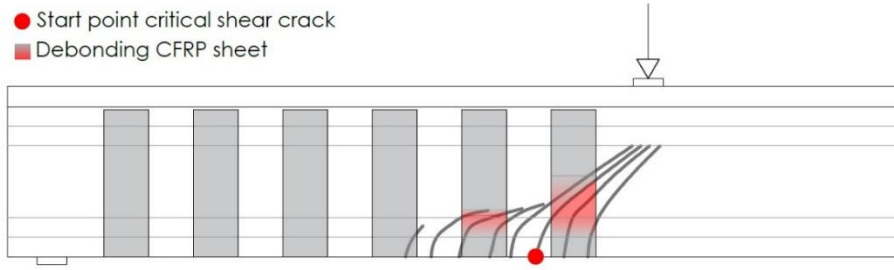


Figure 5.18: Debonding CFRP sheets specimen I-V-SP4 at load step 50

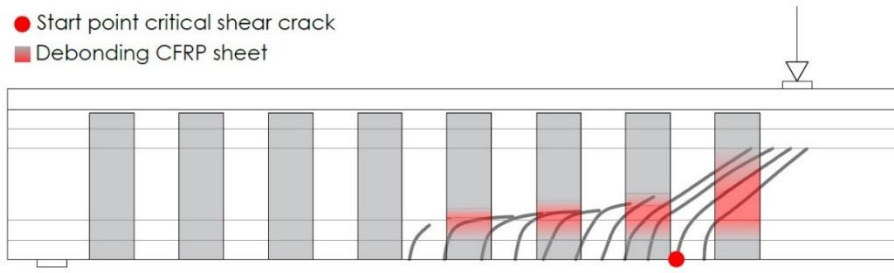


Figure 5.19: Debonding CFRP sheets specimen I-V-SP5 at load step 51

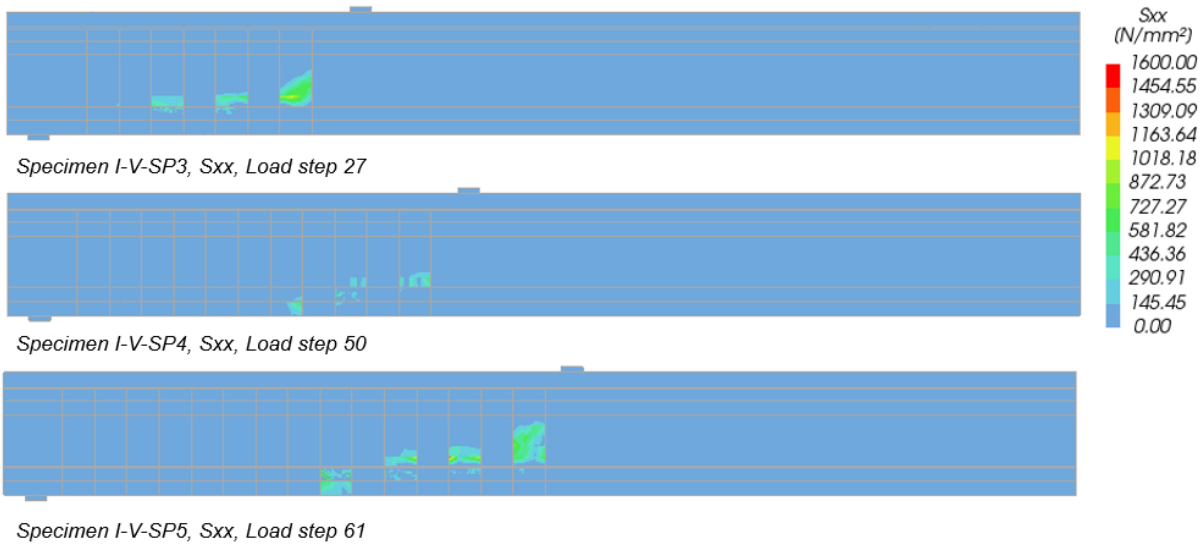


Figure 5.20: Axial stress values specimens I-V-SP3, I-V-SP4 and I-V-SP5

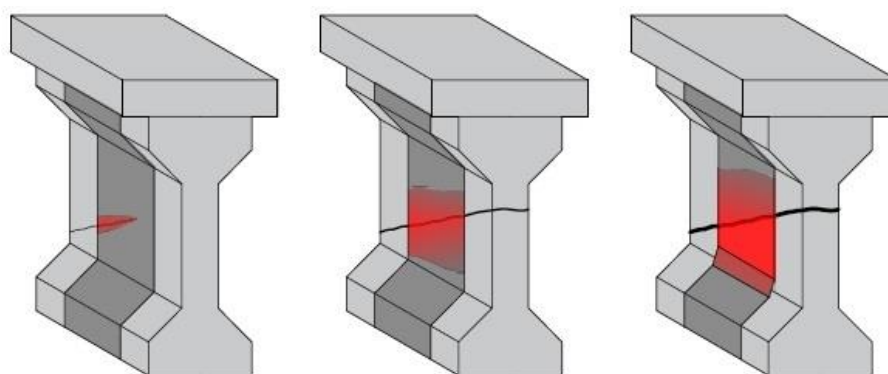


Figure 5.21: Debonding propagation CFRP sheets

5.3.3. Results specimen I-V-S0

The results of the specimens strengthened with vertical CFRP sheets and no spacing between the sheets are briefly described in this section. The load-deformation curves from the specimens I-V-S0-SP3, I-V-S0-SP4 and I-V-S0-SP5 are presented in Figure 5.22. The peak load of the specimens at failure is given in Table 5.16. Appendix E.3 includes the principal strain plots and crack strain plots at some load steps of these specimens.

The crack pattern of the three specimens was comparable to the crack pattern of the specimens with vertical CFRP sheets and a spacing of 300 mm. However, the propagation of the shear cracks of the specimens with a shear span of 4.0 and 5.0 m was less brittle due to the decreased spacing. The development of the flexural shear cracks caused local debonding of the CFRP sheets. The debonding of the CFRP sheets propagated towards the corner between the web and the bottom flange. The CFRP sheets started to pull away from this corner. The NLFEA of both specimens aborted after the CFRP sheets started to pull away from the re-entrant corners. The shear force of the specimens I-V-S0-SP4 and I-V-S0-SP5 increased compared to the specimens I-V-SP4 and I-V-SP5. The load-deformation curve of the specimen I-V-S0-SP4 does not have a post peak branch. The NLFEA of the specimen aborted before failure of the I-girder. The failure load is probably slightly higher than the maximum load in the load-deformation curve. The NLFEA showed that the I-girder was close to failure because the flexural shear cracks were already developed into the web at the last load steps before the analysis aborted. The failure load of the specimen I-V-S0-SP3 did not increase compared to the specimen I-V-SP3 due to the brittle propagation of the shear tension crack. The CFRP sheets started to pull away directly after the propagation of the shear tension crack.

Table 5.16: Results specimens I-V-S0-SP3, I-V-S0-SP4 and I-V-S0-SP5

	Shear span [m]	Peak load [kN]	Deflection [mm]	Shear force [kN]	Increase shear force
I-C-SP3	3.0	559.8	43.65	574.2	-
I-V-SP3	3.0	572.6	44.72	587.1	2.2%
I-V-S0-SP3	3.0	569.4	44.59	583.9	1.7%
I-C-SP4	4.0	426.6	42.97	433.2	-
I-V-SP4	4.0	454.2*	48.78	460.9	6.4%
I-V-S0-SP4	4.0	458.4*	49.20	465.0	7.4%
I-C-SP5	5.0	361.0	47.23	359.8	-
I-V-SP5	5.0	395.7	52.29	394.5	9.7%
I-V-S0-SP5	5.0	416.4	56.92	415.2	15.4%

* Peak load is the load in the last step before the analysis of specimen aborted.

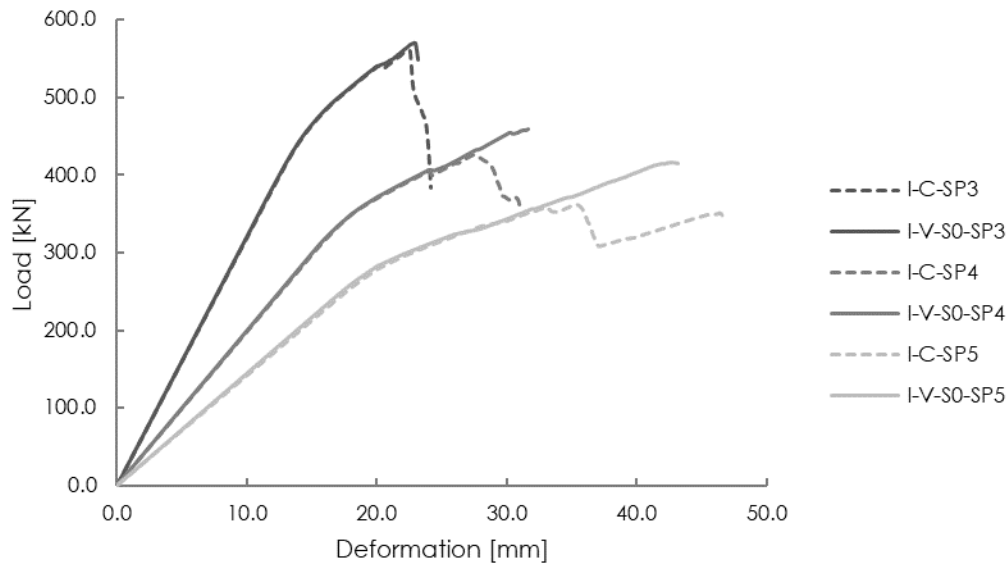


Figure 5.22: Load-deformation curves specimens I-V-S0-SP3, I-V-S0-SP4 and I-V-S0-SP5

5.3.4. Results specimen I-V-L2

The results of the specimens I-V-L2-SP3, I-V-L2-SP4 and I-V-L2-SP5 are briefly discussed in this section. The load-deformation curves of these specimens are given in Figure 5.23. The maximum shear force of the specimens is presented in Table 5.17. The principal strain plots and crack strain plots at some load steps are given in Appendix E.4.

The increase in peak load and maximum shear force of the specimens strengthened with two layers of CFRP sheets was not significant compared to the specimens with one layer. The addition of one additional layer of CFRP sheets did not affect the crack pattern and propagation of the shear cracks. The propagation of the shear tension and the flexural shear cracks caused debonding of the CFRP sheets. The debonding propagated towards the re-entrant corner due to the opening of the shear cracks. The load-deformation curves of the specimens ascended till the CFRP sheets started to pull away from the re-entrant corners. The axial stiffness of the CFRP reinforcement doubled due to the additional CFRP sheet. The increase in axial stiffness hardly affected the debonding of the CFRP sheets.

Table 5.17: Results specimens I-V-L2-SP3, I-V-L2-SP4 and I-V-L2-SP5

	Shear span [m]	Peak load [kN]	Deflection [mm]	Shear force [kN]	Increase shear force
I-C-SP3	3.0	559.8	43.65	574.2	-
I-V-SP3	3.0	572.6	44.72	587.1	2.2%
I-V-L2-SP3	3.0	572.7	44.73	587.1	2.3%
I-C-SP4	4.0	426.6	42.97	433.2	-
I-V-SP4	4.0	454.2*	48.78	460.9	6.4%
I-V-L2-SP4	4.0	466.9	50.03	473.6	9.3%
I-C-SP5	5.0	361.0	47.23	359.8	-
I-V-SP5	5.0	395.7	52.29	394.5	9.7%
I-V-L2-SP5	5.0	399.7	54.87	398.5	10.8%

* Peak load is the load in the last step before the analysis of specimen aborted.

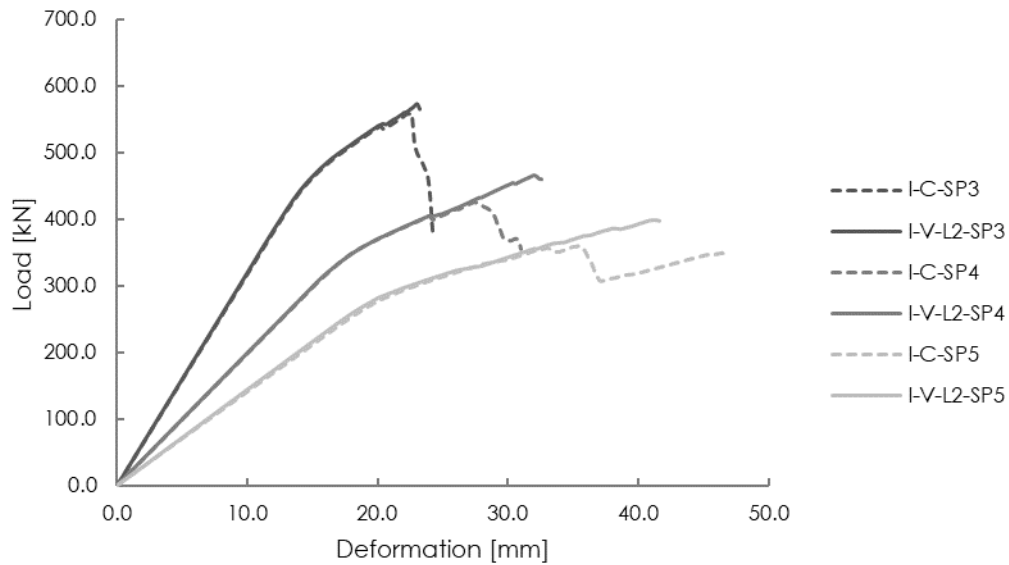


Figure 5.23: Load-deformation curves specimens I-V-L2-SP3, I-V-L2-SP4 and I-V-L2-SP5

5.3.5. Results specimen I-V-PB

The bond-slip interface and the perfect bond model are the most commonly used interface models for the CFRP-to-concrete interface. Both approaches were analysed for the specimens with a shear span of 3.0 m, 4.0 m and 5.0 m. The shear capacity of the specimens is presented in Table 5.18. The results of the specimens with a bond-slip interface and the perfect bond model were comparable. The perfect bond between the two-dimensional shell elements of the CFRP and the three-dimensional brick elements of the concrete caused debonding of the concrete in the outer layer. The disadvantage of the perfect bond are inconsistencies in the outer layer. The analysis of the specimens with a perfect bond were aborted due to large local displacement of the three-dimensional brick elements in the outer layer. However, the analyses of the three specimens with a perfect bond between the CFRP and the concrete aborted after the load-deformation curve started to descend. The crack pattern and the critical crack of the specimens with the bond-slip interface and the perfect bond were comparable, but the crack pattern of the specimens with a perfect bond was difficult to analyse because of the cracks in the outer layer due to debonding of the concrete.

Table 5.18: Results specimens I-V-PB-SP3, I-V-PB-SP4 and I-V-PB-SP5

	Shear span [m]	Peak load [kN]	Shear force [kN]
I-V-SP3	3.0	572.6	587.1
I-V-PB-SP3	3.0	568.8	583.3
I-V-SP4	4.0	454.2*	460.9
I-V-PB-SP4	4.0	459.9	466.5
I-V-SP5	5.0	395.7	394.5
I-V-PB-SP5	5.0	397.2	396.1

* Peak load is the load in the last step before the analysis of specimen aborted.

5.4. Shear behaviour specimen I-VH

5.4.1. Finite element model specimen I-VH

The finite element model of the specimen I-VH-SP4 strengthened with horizontal and vertical orientated CFRP sheets is shown in Figure 5.24. The finite element model of the specimens I-VH-SP3 and I-VH-SP5 can be found in Appendix D. The CFRP layout and the dimensions of the specimens are presented in Appendix B. The material properties of the prestressed concrete I-girder are given in Section 5.1. The orthotropic material model described in Section 5.1.3 and the bond-slip model described in Section 5.1.4 were assigned to the CFRP elements and the interface elements, respectively. The load cases and the load factors of the specimens are given in Table 5.19.

Table 5.19: Load cases reference specimens I-VH-SP3, I-VH-SP4 and I-VH-SP5

Load case	Load	Load factor	Load steps		
			I-VH-SP3	I-VH-SP4	I-VH-SP5
LC1	Prestressing & self weight	1.0	1	1	1
LC2	Point load	2.0	10	12	16
		0.2	100	200	200

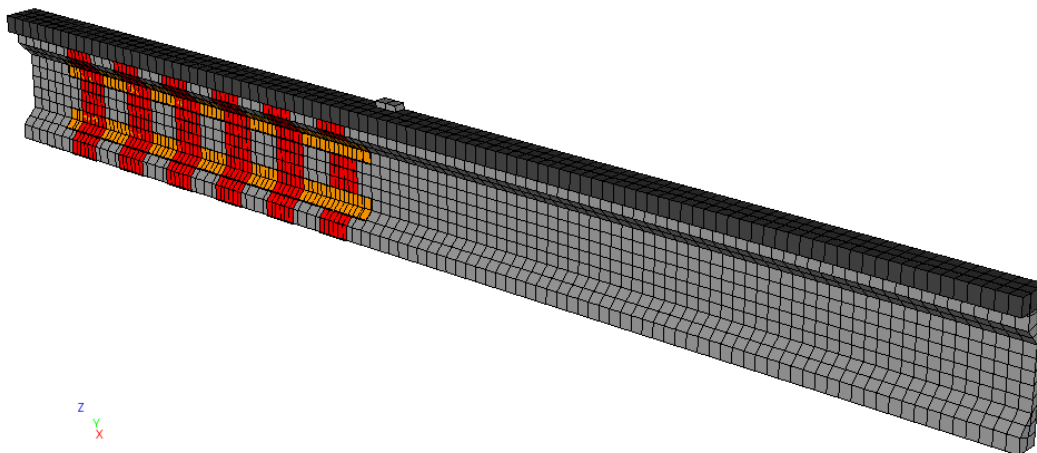


Figure 5.24: Finite element model specimen I-VH-SP4

5.4.2. Results specimen I-VH

Figure 5.25 shows the load-deformation curves of the specimens I-VH-SP3, I-VH-SP4 and I-VH-SP5. The maximum shear force and the maximum mid-span deflection of the specimens is presented in Table 5.20.

Specimen I-VH-SP3

The shear force of the specimen I-VH-SP3 hardly increased compared to the reference specimen. The crack pattern and the debonding of the CFRP sheets of specimen I-VH-SP3 is given in Figure 5.26. The first horizontal crack in the web appeared at load step 11 (533 kN). At the same time a flexural crack developed into the web of the I-girder towards the loading point. The propagation of this crack was not prevented by the CFRP reinforcement because the flexural crack appeared outside the region with CFRP reinforcement. The horizontal crack propagated towards the loading point and the support at load step 25 (563 kN). The peak load of 566.5 kN was reached just before the horizontal crack propagated at load step 24. The brittle development of the crack caused the debonding of the CFRP sheets in the region around the

crack. The CFRP sheets immediately started to pull away in the corner between the web and the bottom flange due to the propagation of the horizontal crack towards the support. The crack pattern and crack propagation was similar to the crack pattern and crack propagation of specimen I-V-SP3. The NLFEA aborted at step 26 just after the peak load was reached. The maximum axial stress in the CFRP sheets appeared around the shear crack. The axial stress plot of the specimen at load step 25 is given in Figure 5.29. The axial stress was limited because the analysis of the specimen aborted just after the appearance of the shear tension crack. The increase in maximum shear force was limited compared to the maximum shear force of the reference specimen because the development of the shear tension crack immediately caused debonding of the CFRP sheets.

Specimen I-VH-SP4

The shear cracks of the specimen I-VH-SP4 started as flexural cracks at the bottom flange of the I-girder. The flexural cracks started to develop into the web of the I-girder towards the loading point at load step 37 (441 kN). The principal strain and crack strain plot of the load step is presented in Appendix E.6. Appearing flexural cracks developed into the web of the I-girder between load step 37 and load step 60. The CFRP sheet started to debond around the shear crack. The debonding of the CFRP sheet propagated towards the corner between the web and the bottom flange. The development of the diagonal shear cracks was less brittle due to the CFRP reinforcement. The analysis of the specimen aborted at load step 61 because the analysis diverged. The load-deformation curve was still ascending at load step 60 (464 kN). The peak load given in Table 5.20 is the load at load step 60. However, the load-deformation curve of the specimen I-VH-SP4 was still ascending in the last step before the analysis aborted. The axial stress values at the last load step before the analysis aborted is given in Figure 5.29. The axial stress plot shows stress concentrations around the diagonal crack. The shear force at load step 60 of this specimen increased with 8.7% compared to the shear force of the reference specimen.

Specimen I-VH-SP5

The crack pattern of the specimen I-VH-SP5 is presented in Figure 5.28. The shear cracks of the specimen started as flexural cracks at the bottom flange of the I-girder at load step 18 (259 kN). The flexural cracks propagated into the web diagonally towards the loading point. The propagation of the flexural cracks into the web is visible in the principal strain and the crack strain plots given in Appendix E.6. The appearing flexural cracks in the region between the loading point and the support developed into the web of the I-girder towards the other diagonal cracks. The opening of the diagonal crack caused local debonding of the CFRP sheets. The debonding of the CFRP sheets developed towards the bottom flange. The first CFRP sheet started to pull away from the re-entrant corner at load step 47 (390 kN). The effect of the horizontal CFRP anchoring sheets is visible when the load-deformation curves of specimens I-V-SP5 and I-VH-SP5 are compared. The ductility of the specimen increased due to the addition of the horizontal CFRP sheets. The peak load of specimen I-V-SP5 was reached at load step 52 (396 kN) while the peak load of specimen I-VH-SP5 was reached at load step 64 (401 kN). Load step 52 corresponds to a 39 mm displacement of the loading point and load step 64 corresponds to a 41.4 mm displacement of the loading point. The load did not descend but stayed constant in the load steps after the peak load. The CFRP sheets started to pull away from the corner in the last steps before the analysis aborted. The first CFRP sheet was loaded in tension at load step 18 due to the progression of the diagonal crack in the web of the I-girder. The axial stresses in the CFRP sheets increased due to the opening of the diagonal cracks. The axial stress values at load step 74 are given in Figure 5.29. The maximum axial stresses of 1426

MPa appeared around the critical shear crack. The maximum shear force of the specimen increased with 11.2% compared to the reference specimen.

Table 5.20: Results specimens I-VH-SP3, I-VH-SP4 and I-VH-SP5

	Shear span [m]	Peak load [kN]	Deflection [mm]	Shear force [kN]	Increase shear force
I-C-SP3	3.0	559.8	43.65	574.2	-
I-V-SP3	3.0	572.6	44.72	587.1	2.2%
I-VH-SP3	3.0	566.5	43.92	580.9	1.2%
I-C-SP4	4.0	426.6	42.97	433.2	-
I-V-SP4	4.0	454.2*	48.78	460.9	6.4%
I-VH-SP4	4.0	464.3*	51.53	471.0	8.7%
I-C-SP5	5.0	361.0	47.23	359.8	-
I-V-SP5	5.0	395.7	52.29	394.5	9.7%
I-VH-SP5	5.0	401.1	55.09	399.9	11.2%

* Peak load is the load in the last step before the analysis of specimen aborted.

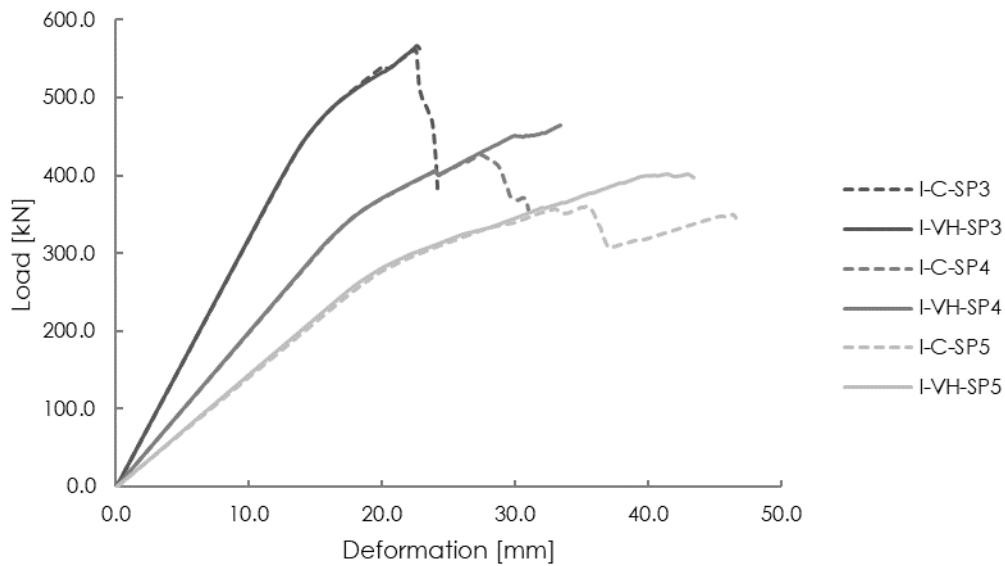


Figure 5.25: Load-deformation curves specimens I-VH-SP3, I-VH-SP4 and I-VH-SP5

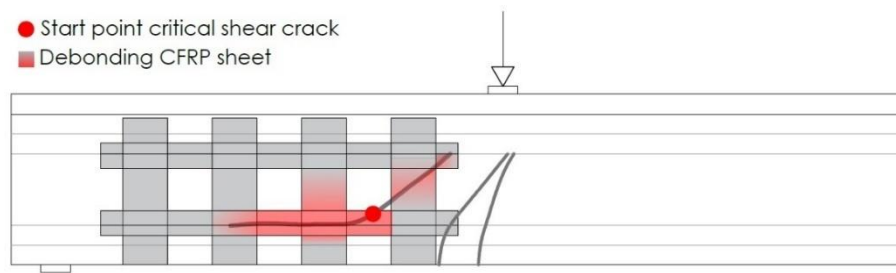


Figure 5.26: Debonding CFRP sheets specimen I-VH-SP3 at load step 25

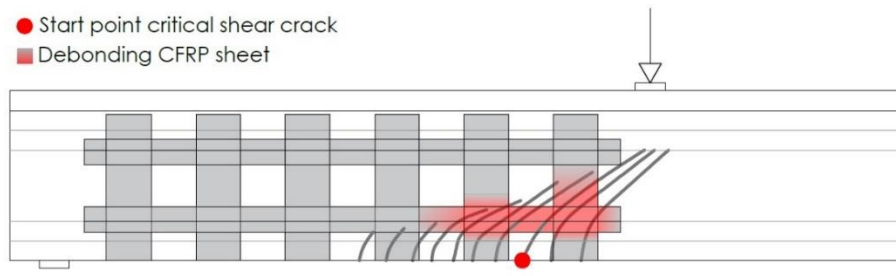


Figure 5.27: Debonding CFRP sheets specimen I-VH-SP4 at load step 60

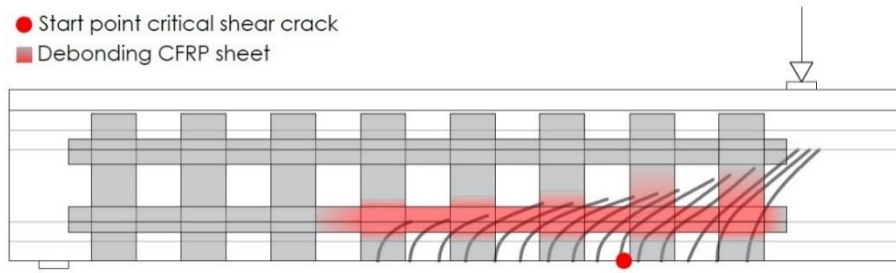


Figure 5.28: Debonding CFRP sheets specimen I-VH-SP5 at load step 74

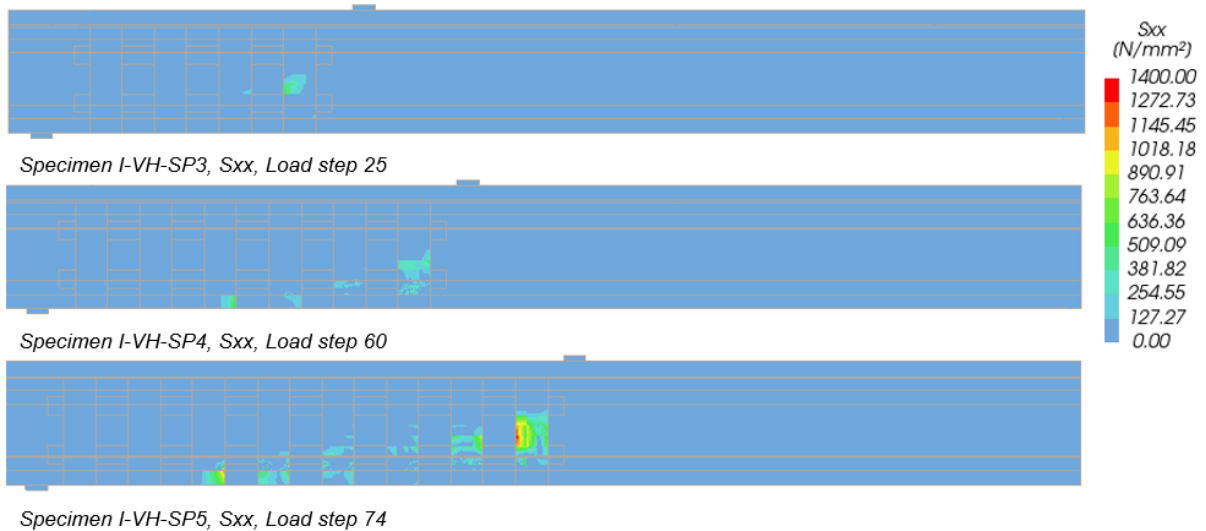


Figure 5.29: Axial stress values specimens I-VH-SP3, I-VH-SP4 and I-VH-SP5

5.5. Shear behaviour specimen I-VA

5.5.1. Finite element model specimen I-VA

Four approaches to model the CFRP anchors are proposed in Section 5.1.5. The four approaches were analysed using specimen I-VA-SP3. The anchors of specimen I-VA-ERS-SP3 were modelled as an embedded reinforcement anchor and a two-dimensional shell element splay. The anchor of specimen I-VA-LES-SP3 was modelled using a class-III beam element. The anchors of specimen I-VA-ERL-SP3 were modelled as an embedded reinforcement anchor and a class-III beam element stiff line. The anchor of specimen I-VA-LEL was modelled as a class-III beam element. The finite element model of specimen I-VA-ERS-SP3 is given in Figure 5.30. The best approach was used to strengthen the specimens I-VA-SP4 and I-VA-SP5. The CFRP layout and the dimensions of the specimens I-VA-SP3, I-VA-SP4 and I-VA-SP5 are presented in Appendix B. The finite element model of the specimens I-VA-SP3, I-VA-SP4 and I-VA-SP5 can be found in Appendix D. The specimens with the shear span fully wrapped in CFRP sheets were

also analysed. The CFRP layout and the dimensions of the specimens I-VA-S0-SP3, I-VA-S0-SP4 and I-VA-S0-SP5 are given in Appendix B. The material properties of the prestressed concrete I-girder are given in Section 5.1. The orthotropic material model described in Section 5.1.3 and the bond-slip model described in Section 5.1.4 are assigned to the CFRP elements and the interface elements, respectively. The material properties of the CFRP anchors are described in Section 5.1.5. The load cases and the load factors of the specimens are presented in Table 5.21.

Table 5.21: Load cases reference specimens I-VA-SP3, I-VA-SP4 and I-VA-SP5

Load case	Load	Load factor	Load steps		
			I-VA-SP3	I-VA-SP4	I-VA-SP5
LC1	Prestressing & self weight	1.0	1	1	1
LC2	Point load	2.0	10	12	16
		0.2	100	200	200

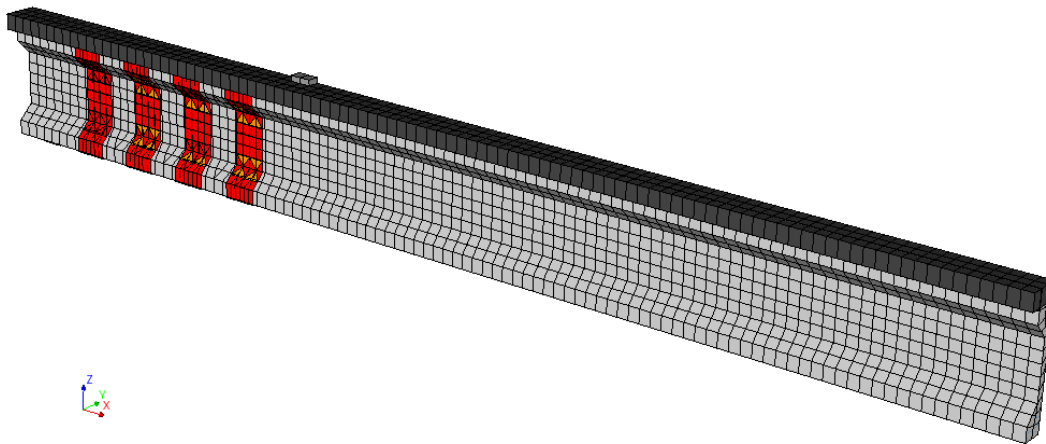


Figure 5.30: Finite element model specimen I-VA-ERS-SP3

5.5.2. Results finite element analysis CFRP anchor modelling approaches

The peak loads of the four specimens and the corresponding maximum shear forces are presented in Table 5.22. The increase in shear force of the specimens is limited due to the brittle propagation of the shear crack. The maximum shear force of specimen I-VA-ERS-SP3 and I-VA-LES-SP3 increased the most compared to the other two specimens. However, the structural behaviour of the specimens was more important than the increase in maximum shear force.

The embedded reinforcement element is the most accurate element to model the anchor. However, the embedded reinforcement could not be connected to the two-dimensional shell elements or the beam elements. The two-dimensional shell elements of the CFRP splays in specimen I-VA-ERS-SP3 and the beam elements of the stiff lines in specimen I-VA-ERL-SP3 were connected to the three-dimensional concrete brick elements with a perfect bond. The embedded reinforcement elements were connected to the CFRP elements due to the perfect bond between the concrete elements and the CFRP elements. However, this bond depends on the properties of the concrete and not on the properties of the CFRP. The numerical analyses of the specimens I-VA-ERS-SP3 and I-VA-ERL-SP3 showed problems with the connection between the embedded reinforcement and the concrete elements. The concrete elements started to debond from the embedded reinforcement elements.

Crack formation started in the re-entrant corner at load step due to the perfect bond between the stiff line elements in specimen I-VA-ERL-SP3. The crack formation in the re-entrant corners weakened the web of the I-girder. The crack strain plot is presented in Figure 5.31. The

propagation of the shear crack started at load step 22 (559 kN) while the propagation of the shear crack of specimen I-V-SP3 started at load step 25 (570 kN). The approach with embedded reinforcement and a stiff line element in the re-entrant corner was not suitable to model the CFRP anchor.

The outer layer of the concrete started to debond around the embedded reinforcement of specimen I-VA-ERS-SP3. The behaviour of the concrete in the re-entrant corner was very similar to the behaviour of the concrete in the re-entrant corner of specimen I-V-PB-SP3 with a perfect bond between the CFRP sheets and the concrete. The connection between the embedded reinforcement and the two-dimensional shell elements in the re-entrant corner completely relied on the connection between the outer layer of the concrete and the embedded reinforcement. This connection was able to transfer a limited load from the elements in the re-entrant corner to the embedded reinforcement. The debonding of the outer layer of the concrete was caused by stress concentrations in the splays and the CFRP sheets. The axial stress values of specimen I-VA-ERS-SP3 are given in Figure 5.32. The purpose of the splay is to avoid stress concentrations, however, its finite element model did not achieve this.

The results of specimen I-VA-LES-SP3 were comparable to the results of specimen I-VA-ERS-SP3. Unlike specimen I-VA-ERS-SP3 the anchors were connected to the splays in specimen I-VA-LES-SP3 and the splay was no longer connected to the concrete. Nevertheless, stress concentrations were present around the connection between the splay and the anchor. Figure 5.33 shows the axial stress values of the specimen I-VA-LES-SP3. The axial stress in the CFRP sheet exceeded the maximum tensile strength of the CFRP sheet. The triangular splay was not able to prevent local stress concentrations in CFRP sheets around the connection between the anchor and the CFRP.

The stiff line element of specimen I-VA-LEL-SP3 is not connected to the concrete. The connection between the anchor and the stiff line element is a point connection. The stiff line elements did not introduce crack formation in the re-entrant corners in contrast to specimen I-VA-ERL-SP3. The axial stress plot at load step 29 is given in Figure 5.34. There were some stress concentrations in the CFRP sheets, but these are smaller than the stress concentrations in the CFRP sheets of specimens I-VA-ERS-SP3 and I-VA-LES-SP3. The stiff line element is suitable to create a more uniform load transfer between the anchors and the CFRP sheets. Modelling the CFRP anchors with beam elements and stiff line elements is therefore the best approach to investigate the effect of the CFRP anchors on the overall shear capacity of the I-girder.

Table 5.22: Results specimens I-VA-ERS-SP3, I-VA-LES-SP3, I-VA-ERL-SP3 and I-VA-LEL-SP3

	Shear span [m]	Peak load [kN]	Shear force [kN]
I-C-SP3	3.0	559.8	574.2
I-VA-ERS-SP3	3.0	573.4	587.8
I-VA-LES-SP3	3.0	574.1	588.6
I-VA-ERL-SP3	3.0	559.4	573.8
I-VA-LEL-SP3	3.0	569.9	584.4

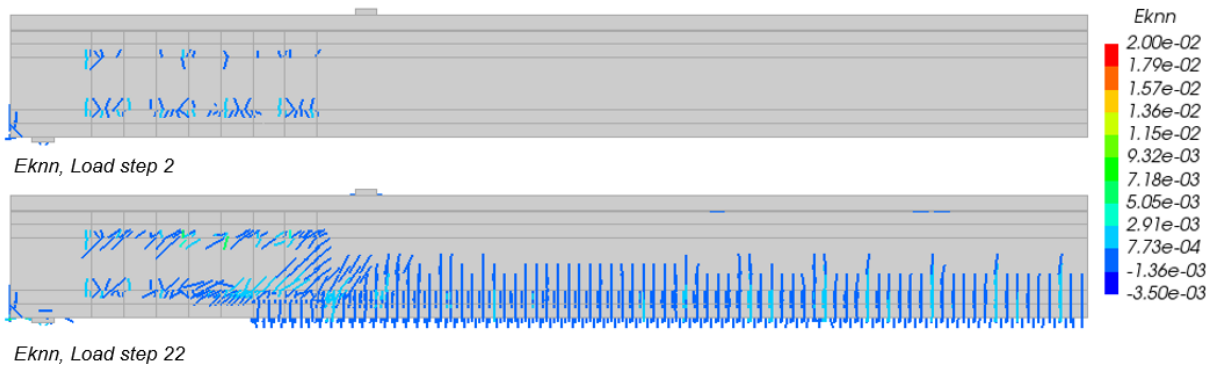


Figure 5.31: Crack strain values specimen I-VA-ERL-SP3

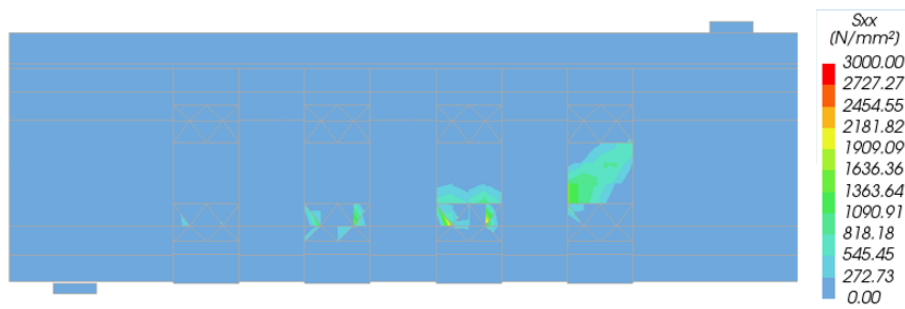


Figure 5.32: Axial stress values specimen I-VA-ERS-SP3

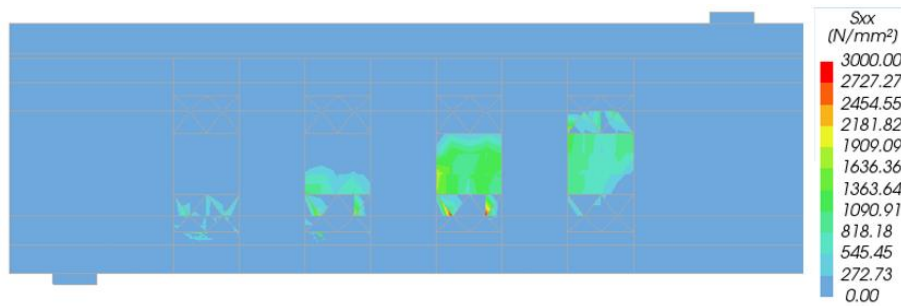


Figure 5.33: Axial stress values specimen I-VA-LES-SP3

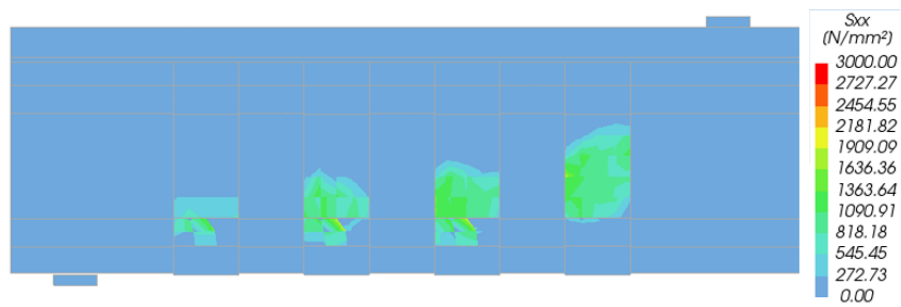


Figure 5.34: Axial stress values specimen I-VA-LEL-SP3

5.5.3. Results specimen I-VA

The load-deformation curves of specimens I-VA-SP3, I-VA-SP4 and I-VA-SP5 are presented in Figure 5.35. The maximum shear force and the maximum mid-span deflection of the three specimens are given in Table 5.23. Figure 5.36 gives the contribution of the concrete and the CFRP to the shear force. The contribution of the CFRP was estimated based on the axial stresses close to the critical shear crack. This location is given in Figure 5.37, Figure 5.38 and Figure 5.39

Specimen I-VA-SP3

The maximum shear force of specimen I-VA-SP3 hardly increased due to the brittle failure behaviour. The principal strain and the crack strain plots are given in Appendix E.7. The crack pattern and the debonding of the CFRP sheets is presented in Figure 5.37. The critical crack started in the web of the I-girder at load step 23 (564 kN). The peak load of 569.9 kN was reached at load step 26 when the crack started to develop towards the loading point. The crack propagated horizontally towards the support at load step 27 (558 kN). The opening of the horizontal crack in the corner of the web and the bottom flange was prevented by the CFRP sheets. The load was constant in the three steps after the peak load. The analysis of the specimen aborted in load step 30. The shear crack developed in the load steps between the peak load and the last load step. The crack pattern of this specimen was similar to the crack pattern of the reference specimen. The debonding of the CFRP sheets started around the diagonal crack at load step 23. The debonding of the CFRP sheets propagated upwards and downwards to the re-entrant corners. The CFRP anchors avoided the CFRP sheets pulling away from the corner between the web and the bottom flange at load step 27. The maximum tensile stress in the CFRP anchors was 469 MPa. The tensile stress of 469 MPa corresponds to a tensile force of 53.0 kN. The maximum shear force of the specimen increased with only 1.8% compared to the reference specimen. The brittle propagation of the shear tension crack was not prevented by the applied externally bonded CFRP reinforcement because of their unfavourable position. This is because the shear tension crack started between two CFRP sheets.

Specimen I-VA-SP4

The first flexural crack propagated into the web towards the loading point at load step 37 (440 kN). The flexural cracks appearing in the shear span propagated into the web between load step 37 and load step 69. The principal strain and the crack strain plot is presented in Appendix E.7. The peak load of 494.5 kN was reached at load step 69. The diagonal crack opened in load step 70 (493 kN) and developed towards the support. The analysis of the specimen aborted at load step 73. The load very slowly decreased between load step 69 and load step 72 (491 kN). The CFRP sheets prevented the opening of the shear cracks between load step 37 and load step 69. The CFRP sheets started to debond after load step 37. The debonding of the CFRP sheets propagated towards the re-entrant corners. The debonding of the CFRP sheets and the crack pattern is illustrated in Figure 5.38. The CFRP sheets did not pull away from the corner between the web and the bottom flange because of the CFRP anchors. The connection between the anchors and the CFRP reinforcement caused stress concentrations in the CFRP sheets around the CFRP anchors. The maximum axial stress in the CFRP sheets was 1613 MPa and appeared in the re-entrant corner. The axial stress plot of the specimen at load step 29 is given in Figure 5.40. The maximum tensile stress in the CFRP anchors was 176 MPa which corresponds to a tensile force of 19.9 kN. The maximum shear force of specimen I-VA-SP4 increased with 15.7% compared to the reference specimen.

Specimen I-VA-SP5

The crack pattern of specimen I-VA-SP5 is presented in Figure 5.39. The first flexural crack started to propagate into the web of the I-girder at load step 18 (259 kN). The brittle development of the crack towards the loading point was prevented by the CFRP sheets. The diagonal cracks propagated slowly towards the loading point and caused local debonding of the CFRP sheets. The development of the cracks is visible in the principal strain and crack strain plots given in Appendix E.7. New flexural cracks started in the shear span in the load steps after load step 18. These flexural cracks propagated into the web towards the loading point between load step 18 and the last load step before the analysis aborted. The peak load of 508.3 kN was reached in load step 157 and the analysis aborted in load step 159. The load slightly decreased in load step 158. The analysis aborted because load step 159 diverged. Unlike the crack pattern of the reference specimen not one diagonal crack is visible but multiple diagonal crack parallel to each other. The debonding of the CFRP sheets propagated towards the re-entrant corners. The CFRP anchors prevented the CFRP sheets pulling away from the re-entrant corners. The CFRP anchors were loaded in tension due to the debonding of the CFRP sheets. The maximum tensile stress in the CFRP anchors was 301 MPa. This tensile stress corresponds to a tensile force in the CFRP anchor of 34.0 kN. The maximum axial stress (1957 MPa) in the CFRP sheets was reached around the diagonal cracks. The axial stress plot at load step 158 is presented in Figure 5.40. The axial stress in the CFRP sheets is uniform, because the sheets were completely debonded from the web of the I-girder. The maximum shear force of the specimen increased with 41,0% compared to the reference specimen because brittle propagation of the dowel crack was prevented.

Table 5.23: Results specimens I-VA-SP3, I-VA-SP4 and I-VA-SP5

	Shear span [m]	Peak load [kN]	Deflection [mm]	Shear force [kN]	Increase shear force
I-C-SP3	3.0	559.8	43.65	574.2	-
I-V-SP3	3.0	572.6	44.72	587.1	2.2%
I-VA-SP3	3.0	569.9	44.63	584.4	1.8%
I-C-SP4	4.0	426.6	42.97	433.2	-
I-V-SP4	4.0	454.2*	48.78	460.9	6.4%
I-VA-SP4	4.0	494.5	54.93	501.2	15.7%
I-C-SP5	5.0	361.0	47.23	359.8	-
I-V-SP5	5.0	395.7	52.29	394.5	9.7%
I-VA-SP5	5.0	508.3*	79.27	507.1	41.0%

* Peak load is the load in the last step before the analysis of specimen aborted.

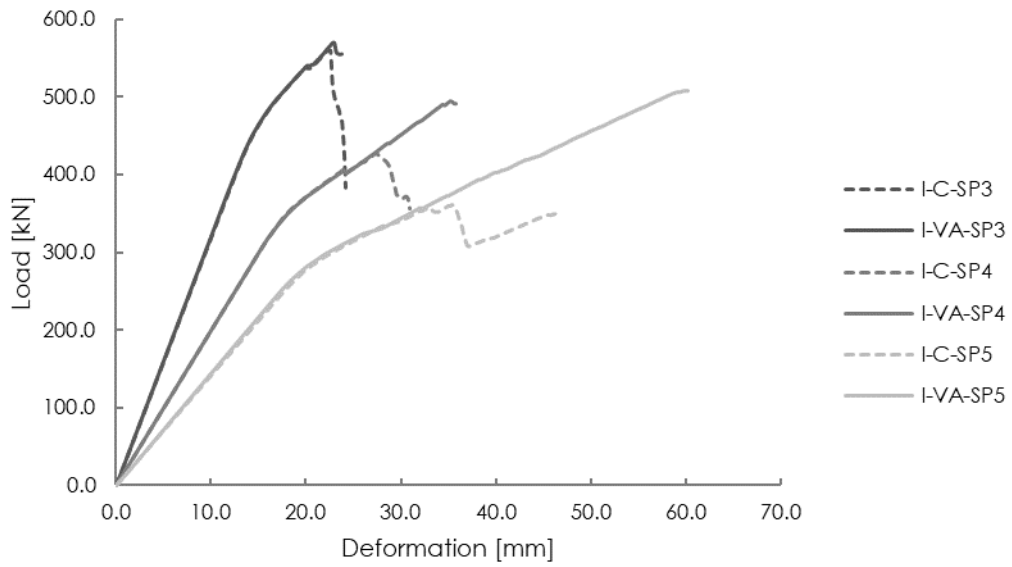


Figure 5.35: Load-deformation curves specimens I-VA-SP3, I-VA-SP4 and I-VA-SP5

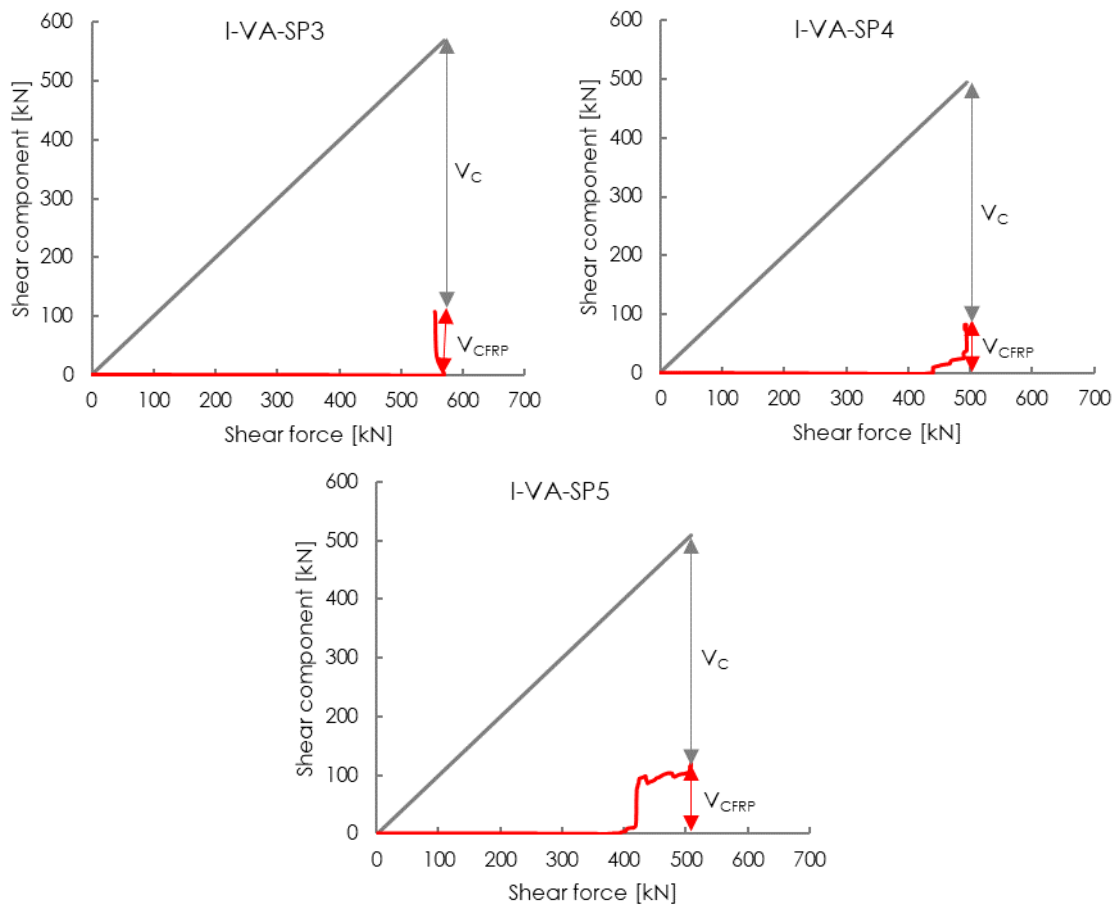


Figure 5.36: Components of shear force specimens I-VA-SP3, I-VA-SP4 and I-VA-SP5

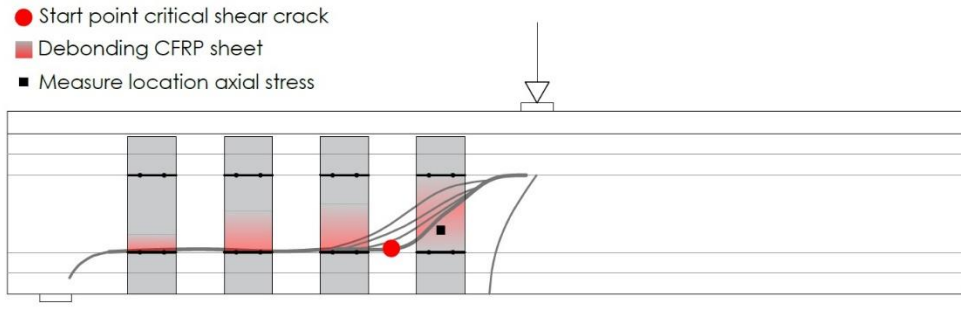


Figure 5.37: Crack pattern and CFRP debonding specimen I-VA-SP3 at load step 29

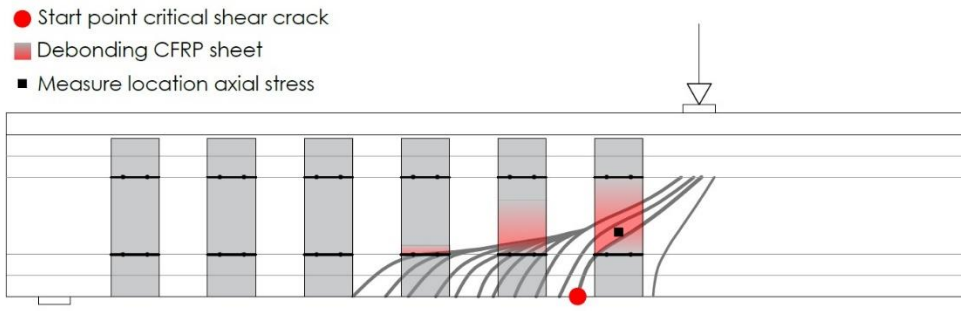


Figure 5.38: Crack pattern and CFRP debonding specimen I-VA-SP4 at load step 72

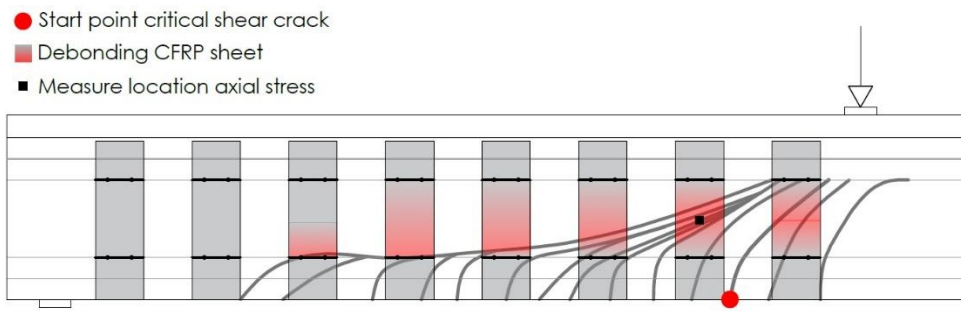


Figure 5.39: Crack pattern and CFRP debonding specimen I-VA-SP5 at load step 158

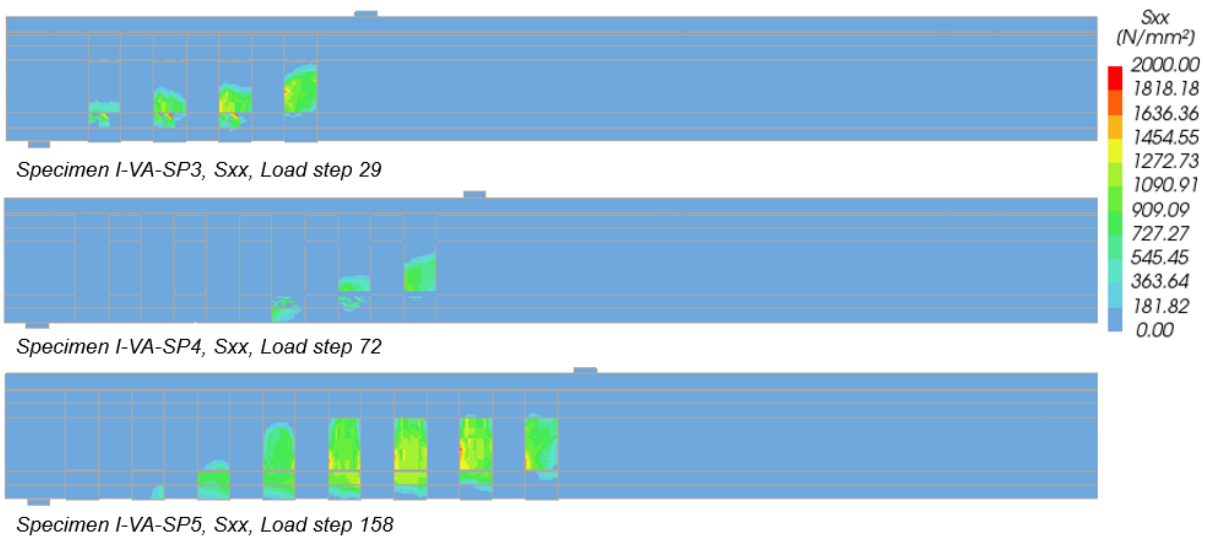


Figure 5.40: Axial stress values specimens I-VA-SP3, I-VA-SP4 and I-VA-SP5

5.5.4. Results specimen I-VA-S0

Figure 5.41 shows the load-deformation curves of specimens I-VA-S0-SP3, I-VA-S0-SP4 and I-VA-S0-SP5. The maximum shear force and the maximum mid-span deflection of the specimens is given in Table 5.24. The contribution of the CFRP reinforcement to the shear force of the specimens is presented in Figure 5.42. The axial stresses in the CFRP close to the critical crack have been used to estimate the contribution of the CFRP. These locations are given in Figure 5.43, Figure 5.44 and Figure 5.45.

Specimen I-VA-S0-SP3

The crack pattern of specimen I-VA-S0-SP3 is presented in Figure 5.43. The first crack in the shear span started in the web as a horizontal crack. The crack propagated into the web towards the loading point and the support at load step 29 (579 kN). Meanwhile, a flexural crack developed into the web. More diagonal cracks appeared in the web between load step 29 and load step 59 (643 kN). The principal strain and crack strain plot of the specimen is presented in Appendix E.8. Due to the development of the shear crack, the CFRP sheets started to debond around the cracks. The CFRP sheets prevented the opening of the dowel. The analysis of the specimen aborted at load step 60 while the load was still increasing. The NLFEA aborted due to large local displacements in the outer layer of the concrete. The plot of the large local displacements is presented in Appendix E.8. The peak load of 642.9 kN is defined as the load in the last step, before the analysis aborted. The CFRP anchors prevented the CFRP sheets to pull away from the re-entrant corners. The CFRP anchors were loaded in tension. The maximum tensile stress in the CFRP anchors was 333 MPa which corresponds to a tensile force of 37.6 kN. Stress concentrations in the CFRP sheets appeared around the appearing shear cracks in the web of the I-girder. However, after the debonding of the CFRP sheets the stress concentrations around the shear cracks disappeared. The maximum stresses appeared in the CFRP sheets around the CFRP anchors. The axial stress plot at load step 59 is given in Figure 5.46. The maximum shear force increased with 14.5% compared to the reference specimen.

Specimen I-VA-S0-SP4

Figure 5.44 shows the crack pattern and the CFRP debonding of specimen I-VA-S0-SP4. The first flexural crack propagated into the web at load step 28 (435 kN). The crack caused local debonding of the CFRP sheets around the diagonal crack. The appearing flexural cracks developed into the web towards the loading point between load step 28 and 119 (570 kN). The CFRP anchors prevented the CFRP sheets from pulling away from the re-entrant corners. At load step 119 a new diagonal crack started in the web of the I-girder. The crack started as a small horizontal crack at the bottom of the web in the middle of the shear span and developed diagonally towards the top flange. The dowel crack developed simultaneously towards the loading point in the corner between the web and the top flange. This crack is not a flexural shear crack because the crack did not propagate from a flexural crack. The crack can be described as a shear tension crack. The development of the crack is visible in the principal strain and crack strain plot given in Appendix E.8. The opening of the crack was prevented by the CFRP sheets between load step 119 and 147 (609 kN). The analysis of the specimen aborted at load step 148. The load was still increasing at load step 147. The equilibrium iteration diverged due to inconsistencies caused by local displacements in the outer layer of the concrete. The plot of the local displacements at load step 148 is given in Appendix E.8. The maximum tensile stress in the anchors was 389 MPa, which corresponds to a tensile force of 44.0 kN. The maximum axial stresses in the CFRP sheets appeared around the connection between the CFRP anchors and the CFRP sheets. The maximum stress in the CFRP sheets was 1987 MPa. This stress concentration appeared around the connection between

CFRP anchors and the CFRP sheets. Due to the debonding of the CFRP sheets from the web of the I-girder the axial stress distribution in the CFRP reinforcement became more uniform. The axial stress plot at load step 147 is given in Figure 5.46. The maximum shear force increased with 42.1% compared to the reference specimen.

Specimen I-VA-S0-SP5

The crack pattern of the specimen I-VA-S0-SP5 is given in Figure 5.45 and the principal strain plot is presented in Appendix E.8. The first flexural crack propagated into the web of the I-girder at load step 17 (355 kN). The diagonal crack propagated towards the loading point which caused local debonding of the CFRP reinforcement. More flexural cracks appeared in the shear span between load step 17 and load step 199. These cracks developed into the web and propagated towards the loading point. The debonding of the CFRP reinforcement propagated towards the re-entrant corners. The CFRP sheets did not pull away from the re-entrant corners because of the CFRP anchors. The analysis of the specimen aborted at load step 200 (568 kN) due to very large local displacements in the concrete. The load-deformation curve was still ascending at the last load step before the analysis aborted. The load at load step 199 is given in Table 5.24. The increase in shear force was 57.6% at load step 199 compared to the peak load of the reference specimen. The CFRP anchors were loaded in tension due to the debonding of the CFRP sheets. The maximum tensile stress in the anchors was 288 MPa at load step 199 which corresponds to a tensile force of 32.5 kN. The maximum axial stress in the CFRP sheets was 1518 MPa at load step 199. The maximum axial stress appeared around the CFRP anchors. The axial stress plot at load step 199 is given in Figure 5.46.

Table 5.24: Results specimens I-VA-S0-SP3, I-VA-S0-SP4 and I-VA-S0-SP5

	Shear span [m]	Peak load [kN]	Deflection [mm]	Shear force [kN]	Increase shear force
I-C-SP3	3.0	559.8	43.65	574.2	-
I-V-SP3	3.0	572.6	44.72	587.1	2.2%
I-VA-S0-SP3	3.0	642.9*	55.96	657.4	14.5%
I-C-SP4	4.0	426.6	42.97	433.2	-
I-V-SP4	4.0	454.2*	48.78	460.9	6.4%
I-VA-S0-SP4	4.0	608.7*	77.54	615.4	42.1%
I-C-SP5	5.0	361.0	47.23	359.8	-
I-V-SP5	5.0	395.7	52.29	394.5	9.7%
I-VA-S0-SP5	5.0	568.4*	90.91	567.2	57.7%

* Peak load is the load in the last step before the analysis of specimen aborted

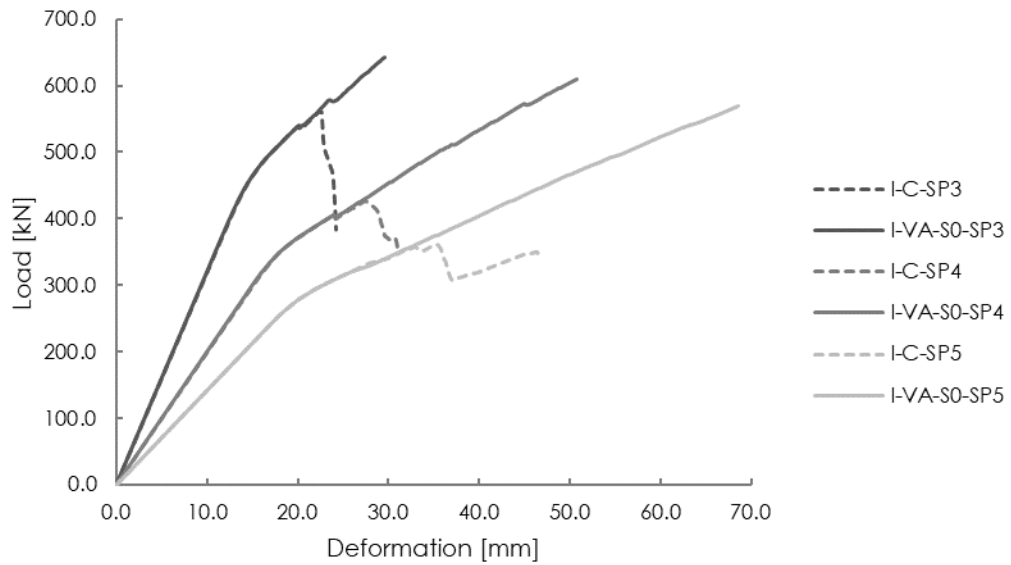


Figure 5.41: Load-deformation curves specimens I-VA-S0-SP3, I-VA-S0-SP4 and I-VA-S0-SP5

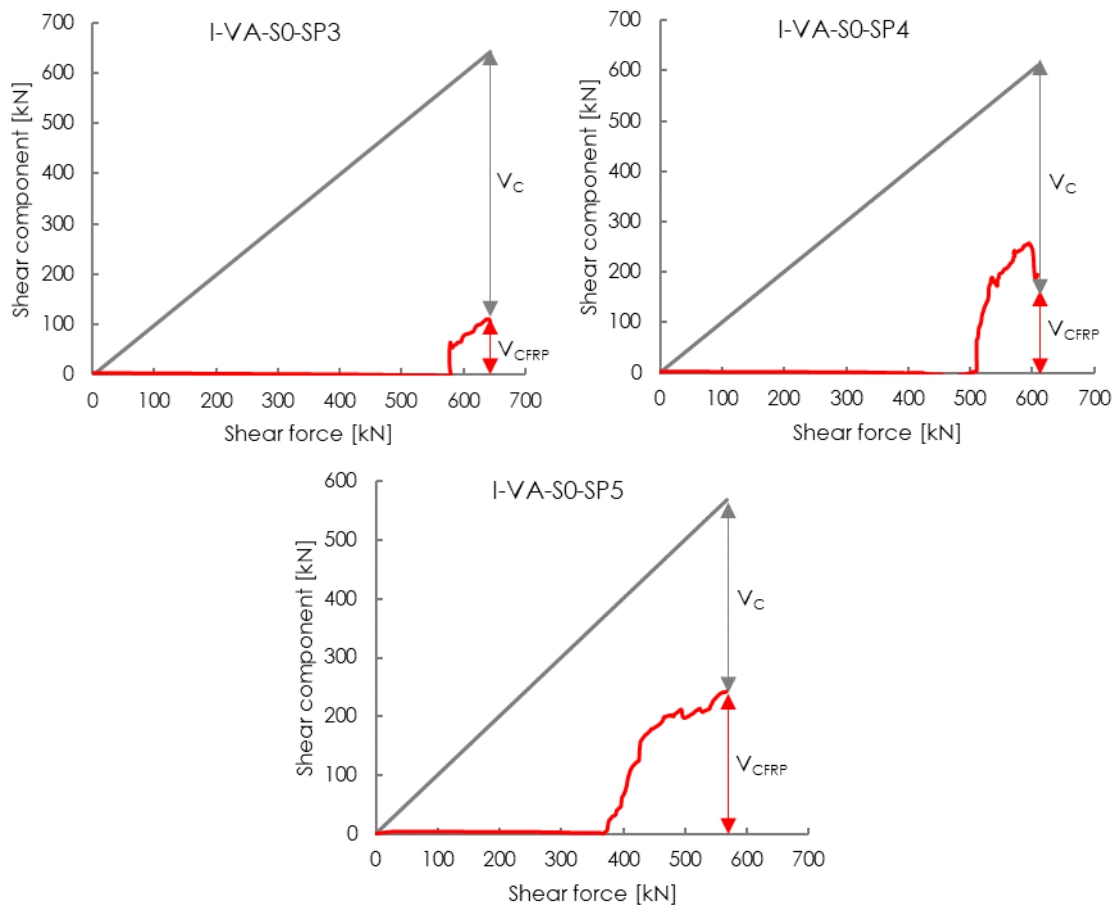


Figure 5.42: Components of shear force specimens I-VA-S0-SP3, I-VA-S0-SP4 and I-VA-S0-SP5

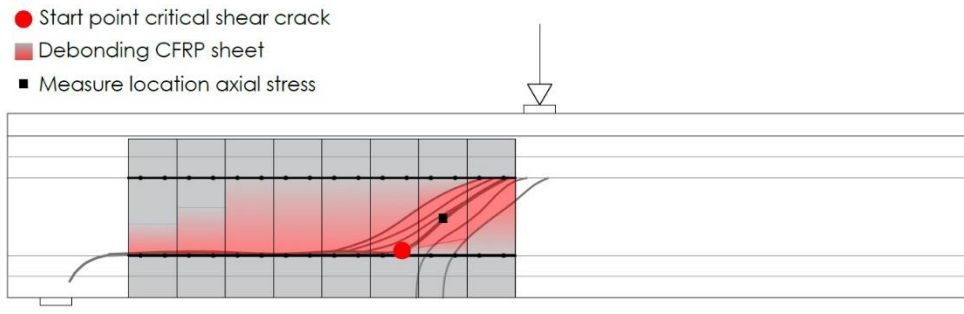


Figure 5.43: Crack pattern and CFRP debonding specimen I-VA-S0-SP3 at load step 59

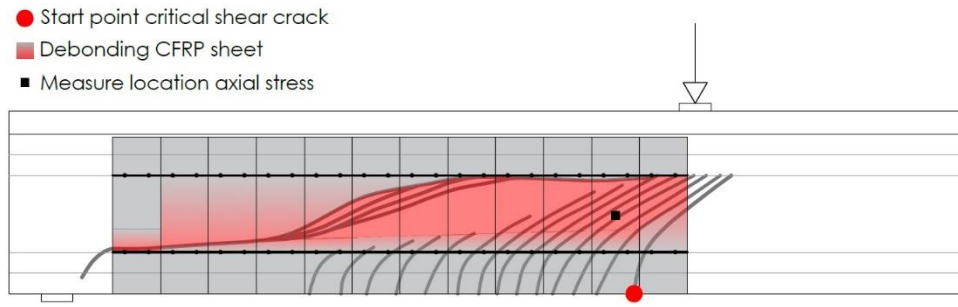


Figure 5.44: Crack pattern and CFRP debonding specimen I-VA-S0-SP4 at load step 147

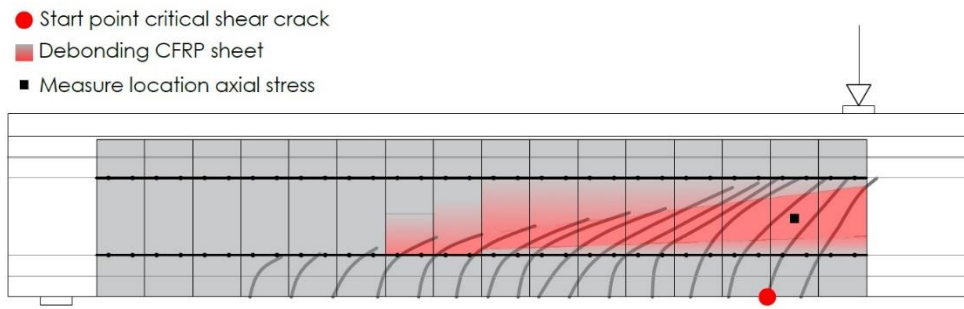


Figure 5.45: Crack pattern and CFRP debonding specimen I-VA-S0-SP5 at load step 199



Figure 5.46: Axial stress values specimens I-VA-S0-SP3, I-VA-S0-SP4 and I-VA-S0-SP5

5.6. Discussion results of finite element analysis

In Table 5.25 the maximum shear force and the increase in shear force are compared to the reference specimen. The increase in ductility of the specimens is presented in Table 5.26. The effect of the parameters on the performance of the CFRP strengthening is discussed in this section. Furthermore, the robustness of the NLFEA is discussed.

Table 5.25: Summary increase shear force analysed specimens

	Shear span [m]	Shear force [kN]	increase shear force [kN]	Increase
I-C-SP3	3.0	574.2	-	-
I-V-SP3	3.0	587.1	12.8	2.2%
I-V-L2-SP3	3.0	587.1	12.9	2.3%
I-V-S0-SP3	3.0	583.9	9.7	1.7%
I-VH-SP3	3.0	580.9	6.7	1.2%
I-VA-SP3	3.0	584.4	10.1	1.8%
I-VA-S0-SP3	3.0	657.4*	83.2	14.5%
I-C-SP4	4.0	433.2	-	-
I-V-SP4	4.0	460.9*	27.7	6.4%
I-V-L2-SP4	4.0	473.6	40.4	9.3%
I-V-S0-SP4	4.0	465.0*	31.8	7.4%
I-VH-SP4	4.0	471.0	37.8	8.7%
I-VA-SP4	4.0	501.2	68.0	15.7%
I-VA-S0-SP4	4.0	615.4*	182.2	42.1%
I-C-SP5	5.0	359.8	-	-
I-V-SP5	5.0	394.5	34.8	9.7%
I-V-L2-SP5	5.0	398.5	38.8	10.8%
I-V-S0-SP5	5.0	398.1	55.4	10.7%
I-VH-SP5	5.0	399.9	40.1	11.2%
I-VA-SP5	5.0	507.1*	147.3	41.0%
I-VA-S0-SP5	5.0	567.2*	207.4	57.7%

* The shear force is based on the load in the last load step before the analysis aborted.

Table 5.26: Summary increase ductility analysed specimens

	Shear span [m]	Deflection [mm]	Increase ductility
I-C-SP3	3.0	43.65	-
I-V-SP3	3.0	44.72	2.5%
I-V-L2-SP3	3.0	44.73	2.5%
I-V-S0-SP3	3.0	44.59	2.2%
I-VH-SP3	3.0	43.92	0.6%
I-VA-SP3	3.0	44.63	2.2%
I-VA-S0-SP3	3.0	55.96	28.2%
I-C-SP4	4.0	42.97	-
I-V-SP4	4.0	48.78	13.5%
I-V-L2-SP4	4.0	50.03	16.4%
I-V-S0-SP4	4.0	49.20	14.5%
I-VH-SP4	4.0	51.53	19.9%
I-VA-SP4	4.0	54.93	27.8%
I-VA-S0-SP4	4.0	77.54	80.5%
I-C-SP5	5.0	47.23	-
I-V-SP5	5.0	52.29	10.7%
I-V-L2-SP5	5.0	54.87	16.2%
I-V-S0-SP5	5.0	56.92	20.5%
I-VH-SP5	5.0	55.09	16.6%
I-VA-SP5	5.0	79.27	67.8%
I-VA-S0-SP5	5.0	90.91	92.5%

5.6.1. Shear span-to-depth ratio

The shear span affected the shear capacity of the prestressed I-girder. The maximum shear force decreased with an increasing shear span. The reference specimen with a shear span of 3.0 m failed in shear tension failure, while the reference specimens with a shear span of 4.0 m and 5.0 m failed in flexural shear failure. The type of shear failure and the shear span affected the contribution of the CFRP reinforcement to the shear capacity.

The crack pattern of both shear failure mechanisms played an important role in the contribution to the shear capacity of the CFRP reinforcement. The shear tension cracks started at the bottom of the web. The shear tension cracks developed diagonal towards the loading point and horizontal along the re-entrant corner towards the support. The horizontal cracks along the corner between the web and the bottom flange caused the CFRP sheets pulling away from the corner. Unlike the shear tension cracks the flexural shear cracks started with flexural cracks at the bottom flange of the I-girder. These cracks propagated diagonal through the web towards the loading point. The diagonal cracks caused local debonding of the CFRP sheets. The debonding of the CFRP sheets propagated towards the re-entrant corners. Finally, the CFRP sheets started to debond in the re-entrant corner. The contribution to the shear capacity of CFRP reinforcement on the specimens failing in flexural shear is better because the debonding started in the middle of the web and not at the re-entrant corner.

5.6.2. Anchoring

The increase in maximum shear force of the specimens strengthened with vertical CFRP sheets was limited, especially for specimen failing in shear tension failure. The maximum shear force of specimen failing in shear tension failure increased by 2% while the specimens failing in flexural shear failure increased by approximately 10%. The ductility of the specimens failing in flexural shear failure increased by more than 10%.

The horizontal CFRP sheets improved the behaviour of the CFRP strengthening in the re-entrant corners of the specimens failing in flexural shear. The maximum shear force increased by approximately 2 percentage points compared to the specimens without horizontal anchoring sheets. The ductility increased due to the addition of the horizontal CFRP sheets from 10% to 15%. The addition of the horizontal CFRP sheets did not improve the maximum shear force of the specimen failing in shear tension failure due to the brittle propagation of the crack.

The addition of the CFRP anchors improved the behaviour of the specimens failing in flexural shear failure. The maximum shear force and the ductility of these specimens increased significantly. The propagation of the shear cracks caused local debonding of the vertical CFRP sheets. The debonding propagated towards the re-entrant corners. However, the CFRP anchors prevented the vertical CFRP sheets pulling away from the re-entrant corners. The ductility of the specimens failing in flexural shear failure increased up to 68%. The maximum shear force of the specimen failing in shear tension failure hardly increased. The addition of CFRP anchors in the re-entrant corners caused a significant improvement of the shear capacity and the ductility of the prestressed I-girder.

5.6.3. Multiple layers of CFRP sheets

The additional layer of CFRP sheets did not change the performance of the specimens strengthened with only vertical CFRP sheets. The tensile stresses in the CFRP sheets did not exceed the maximum tensile strength of the CFRP sheets. Stress concentrations appeared around the shear cracks due to the opening of the cracks. However, the tensile strength of the CFRP sheets was not fully utilized due to the debonding of the CFRP sheets. The increase in axial rigidity did not affect the debonding of the CFRP sheets. The stresses in the CFRP sheets were

lower due to the additional layer of CFRP sheets. The maximum shear force of the specimens strengthened with multiple layers of the CFRP sheets did not increase compared to the specimens with only one layer of CFRP sheets.

5.6.4. CFRP width-to-spacing ratio

The effect of the width-to-spacing ratio was limited for the specimens with only U-wrap CFRP sheets. Increasing the width-to-spacing ratio from 0.5 to 1.0 did not increase the maximum shear force of the specimen failing in shear tension failure, while the maximum shear force of the specimens failing in flexural shear failure increased with approximately 2 percentage points. Increasing the CFRP width-to-spacing ratio was not effective due to the debonding of the vertical CFRP sheets.

Increasing the CFRP width-to-spacing ratio of the specimens with CFRP anchors from 0.5 to 1.0 improved the shear behaviour of the specimens. The brittle propagation of the shear tension crack was prevented. Brittle propagation of the dowel crack at the bottom of the web was prevented by the CFRP sheets. The CFRP anchors prevented the vertical CFRP sheets pulling away from the re-entrant corners. Increasing the CFRP width-to-spacing ratio from 0.5 to 1.0 improved the ductility of the I-girder especially for the specimens with CFRP sheets anchored in the re-entrant corners. The ductility of the specimen I-VA-S0 increased up to 93% for the specimens failing in flexural shear.

5.6.5. Robustness nonlinear finite element analysis

NLFEA was used to investigate the contribution of the externally bonded CFRP reinforcement to the shear capacity of the prestressed I-girder. The finite element model of the reference specimens was not validated because of the lack of good experimental data. A solution strategy validated in literature for similar concrete beams, but without CFRP reinforcement have been used to make the finite element model of the prestressed I-girder. The solution strategy is prescribed in the RTD1016 guideline and has been validated for a prestressed concrete T-girder with shear reinforcement failing in flexural shear (Hendriks et al., 2017a; Hendriks, de Boer & Belletti, 2017b). This guideline has been developed to improve the robustness of nonlinear finite element analyses of prestressed girders. Recent research showed that the solution strategy should be adjusted for concrete elements without shear reinforcement (De Putter, 2020). This solution strategy using a total strain based fixed crack model with a damage based shear retention factor has been applied in this research.

The modelling uncertainty of the solution strategy was investigated using the experimental research of Ary and Kang (2012). The finite element model and the results of the NLFEA of this I-girder are presented in Appendix F. The failure mechanism of the I-girder was predicted correctly by the numerical analysis, however the numerical failure load was more than 50% higher than the experimental failure load.

The solution strategy has been extended for the finite element model with externally bonded CFRP reinforcement. The CFRP sheets were modelled with two-dimensional shell elements. An orthotropic linear elastic material was assigned to the shell elements. The CFRP-to-concrete interface was modelled with two-dimensional nonlinear elastic interface elements. A normal traction and two shear traction diagrams were assigned to the interface elements. The bilinear bond-slip behaviour proposed by Sato and Vecchio (2003) was assigned to the shear traction diagrams. The results of the specimens with a nonlinear elastic interface and a perfect bond were comparable. The perfect bond is not preferable because the cracks in the concrete layer underneath the CFRP elements make it difficult to analyse the crack pattern. Furthermore, the perfect bond between the CFRP elements caused stress concentrations and large local displacements in the outer layer of concrete elements.

There were no guidelines available which describe how to model CFRP anchors. Some proposed modelling approaches were investigated using numerical analyses. From the numerical analyses of these approaches can be concluded that the embedded elements in DIANA are not suitable to model the CFRP anchors, because these elements cannot be connected to the shell elements. Beam elements have been used to model the anchors because these elements can be connected to the shell elements.

No failure criteria was assigned to the linear elastic orthotropic material of the CFRP reinforcement in this research. Postprocessing was performed to verify the maximum stresses in the CFRP reinforcement. The ultimate strength of the CFRP was not reached.

The nonlinear finite element analyses of the reference specimens aborted because the equilibrium iterations diverged. The equilibrium iterations diverged because the reference specimens failed and no equilibrium could be found anymore.

The NLFEA of the specimens I-V and I-VH aborted because equilibrium iterations diverged. The shear cracks propagated due to the debonding of the vertical CFRP sheets. The equilibrium iterations diverged because the CFRP shell elements pulled away from the re-entrant corner.

The NLFEA of some specimens aborted without a post peak branch in the load-deformation curve. The equilibrium iteration of the last load step diverged, but no brittle development the shear cracks was visible at the last load steps. Brittle failure of these specimens is expected in the aborted load step or in the first load steps afterwards, due to the debonding of the vertical CFRP sheets.

The NLFEA of the specimens I-VA and I-VA-S0 aborted because the equilibrium iteration in the last load step diverged. However, no brittle development of the shear cracks was visible. The vertical CFRP sheets prevented the brittle propagation of the shear cracks in these specimens. The NLFEA of the specimens aborted because of singularities in some of the concrete elements in the finite element models. Based on the results of the numerical analyses of these specimens it is not possible to determine the exact failure mechanism. However, the NLFEA provides insight into the increase in shear capacity and the increase in ductility of these specimens.

5.6.6. Comparison numerical and analytical prediction

The results of the NLFEA and the analytical predictions according to the CUR 91, ACI440.2R-08 and the DAfStb heft 595 are given in Table 5.27. The CUR 91 and ACI440.2R-08 use the effective strain method to calculate the contribution of the externally bonded CFRP reinforcement while the DAfStb heft 595 is based on the effective bond length of the CFRP reinforcement. The design recommendation and guidelines have been developed to calculate the contribution of the CFRP reinforcement to the shear capacity of concrete elements with rectangular cross-sections as mentioned in Section 4.4.5.

The comparison of the numerical and analytical predictions shows they do not correspond for the I-girders strengthened with only vertical CFRP sheets. The contribution of the CFRP sheets to the shear capacity of the I-girder was very limited according to the numerical analyses because of the debonding of the vertical CFRP sheets.

According to the analytical predictions the contribution of the externally bonded CFRP reinforcement is equal for shear tension failure and flexural shear failure while the results of the numerical research showed that the contribution of the vertical CFRP sheets was not equal for both shear failure mechanisms. The effect of the type of shear failure to the contribution of the CFRP reinforcement is not included in these analytical predictions.

The CUR91 and ACI440.2R-08 provided a conservative prediction of the contribution of the CFRP reinforcement to the prestressed I-girder failing in flexural shear failure compared to the numerical prediction. The shear capacity of the prestressed concrete I-girder with a shear

span of 4.0 and 5.0 m increased with 182.2 and 207.4 kN according to the numerical analyses. The CUR 91 predicted a contribution of 138.0 kN and the ACI440.2R-08 predicted a contribution of 162.0 kN to the shear capacity. However, the accuracy of the prediction of the numerical analyses is uncertain.

The analytical predictions according to the CUR 91, ACI440.2R-08 and the DAfStb heft 595 are not usable to calculate the contribution of the externally bonded CFRP reinforcement without proper anchoring in the re-entrant corners based on the numerical results.

Table 5.27: Comparison numerical results and analytical prediction

	Shear span [m]	$V_{CFRP,NLFEA}$ [kN]	$V_{f,CUR 91}$ [kN]	$V_{f,ACI440}$ [kN]	$V_{f,DAfStb}$ [kN]
I-V-SP3	3.0	12.8	85.0	81.0	109.0
I-V-L2-SP3	3.0	12.9	138.0	108.6	218.0
I-V-S0-SP3	3.0	9.7	138.0	162.0	218.0
I-VH-SP3	3.0	6.7	85.0	81.0	109.0
I-VA-SP3	3.0	10.1	85.0	81.0	109.0
I-VA-S0-SP3	3.0	83.2	138.0	162.0	218.0
I-V-SP4	4.0	27.7	85.0	81.0	109.0
I-V-L2-SP4	4.0	40.4	138.0	108.6	218.0
I-V-S0-SP4	4.0	31.8	138.0	162.0	218.0
I-VH-SP4	4.0	37.8	85.0	81.0	109.0
I-VA-SP4	4.0	68.0	85.0	81.0	109.0
I-VA-S0-SP4	4.0	182.2	138.0	162.0	218.0
I-V-SP5	5.0	34.8	85.0	81.0	109.0
I-V-L2-SP5	5.0	38.8	138.0	108.6	218.0
I-V-S0-SP5	5.0	55.4	138.0	162.0	218.0
I-VH-SP5	5.0	40.1	85.0	81.0	109.0
I-VA-SP5	5.0	147.3	85.0	81.0	109.0
I-VA-S0-SP5	5.0	207.4	138.0	162.0	218.0

6

ADDITIONAL DESIGN CONSIDERATIONS

6.1. Execution

6.1.1. Surface preparation

The surface roughness of the concrete has a direct influence on the bond between CFRP and concrete (Iovinella, Prota & Mazzotti, 2013). Therefore, surface preparation is an essential factor for the performance of the strengthening. The concrete surface should satisfy the six requirements given in the Dutch design recommendation CUR 91 (CURNET, 2007). First of all, the concrete surface should be free of defects. Existing defects should be repaired according to the recommendation guideline. Secondly, the crack width should be limited to 0.2 mm. Crack widths exceeding 0.2 mm should be injected according to the guideline. Third, the unevenness of the surface should be limited. Fourth, the surface of the concrete should be suitably roughened. The top layer of mortar should be removed completely. Fifth, the concrete cover should be at least 10 mm. Finally, the surface should be clean and dry before the externally bonded CFRP reinforcement is applied. The moisture content of the concrete should be smaller than 4% before application of CFRP reinforcement.

Commonly applied surface treatment methods are brushing, grinding, bush-hammering and sandblasting. Bush-hammering should be avoided according to the Dutch design recommendation CUR 91 because the impact reduces the near-surface tensile strength of the concrete (CURNET, 2007). Iovinella, Prota and Mazzotti (2013) did an experimental investigation on the effects of different surface treatments on the bond between CFRP and concrete. They concluded that sandblasting is the most effective surface treatment method. Sandblasting is the only method which increases the shear strength according to this experimental investigation. The effect of grinding is limited to a small reduction of the initial stiffness. They also concluded that the performance of the surface treatment decreases with increasing concrete strength.

The bond strength of the concrete surface should be at least 1.5 MPa according to the Dutch design recommendation CUR 91 (CURNET, 2007). The pull-off test method should be used to measure the bond strength of the concrete surface after surface preparation (Nederlands Normalisatie-Instituut, 1999).

The corners of the I-girders should have a minimum radius to prevent stress concentrations in the externally bonded CFRP reinforcement. The corners of concrete elements should be rounded according to the Dutch design recommendation CUR 91 (CURNET, 2007). However, the CUR 91 does not prescribe a minimum corner radius. The minimum corner radius should be at least 13 mm according to the ACI440.2R-08 while the DAfStb heft 595 prescribes a minimum corner radius of 25 mm (ACI Committee 440, 2008; DAfStb-heft 595, 2012).

6.1.2. Application CFRP reinforcement

Before application of the CFRP reinforcement the surface of the CFRP should be prepared. The surface of the CFRP reinforcement must be free from dust and grease. The quality of the CFRP reinforcement should be checked before application, the carbon fibres may be damaged during transport.

The process of application depends on the CFRP product (Matthys, 2000). The CFRP products provided by manufacturers are 'prefab' pre-cured CFRP strips and 'wet lay-up' CFRP fabrics, as defined in Section 3.2.2. The CFRP fabric is the most suitable CFRP product to strengthen I-girders because the fabric is flexible and easy to apply around the circumference. The process of application of pre-cured CFRP strips consists of two steps. The first step is application of the adhesive on the concrete surface and at the CFRP strip surface. The second

step is application of the CFRP strip itself. The strip should be pressed against the concrete to squeeze out excessive adhesive and air bubbles.

The application of CFRP fabric consists of three steps. First the adhesive is applied on the concrete surface. The second step is the application of the CFRP fabric. Lastly a second adhesive layer is applied to impregnate the CFRP fabric.

6.1.3. Quality control

Quality control during the surface preparation and the installation of CFRP reinforcement is important to guarantee the performance. The design and execution should be performed by skilled people (Matthys, 2000). The quality of the surface preparation and the application of the CFRP has a considerable impact on the bond strength between the CFRP reinforcement and the concrete. The re-entrant corners of the I-girder deserve special attention during installation and quality control. Figure 6.1 shows problems with the debonding of a CFRP sheet during the installation.



Figure 6.1: CFRP sheet in re-entrant corner (S&P clever reinforcement company)

6.2. Environmental conditions

6.2.1. Temperature effects

The maximum service temperature of a structure strengthened with CFRP reinforcement should be limited. The service temperature should be significantly lower than the glass-transition temperature of the adhesives because the mechanical properties of adhesives degrade close to and above their glass-transition temperature (Matthys, 2000). Adhesives with a glass-transition temperature of at least 45°C or the maximum air temperature in the shadow plus 20°C should be selected according to the Dutch design recommendation CUR 91 (CURNET, 2007).

Thermal stresses may become critical for high temperature changes because the thermal expansion coefficient of concrete and CFRP are not equal. The thermal expansion coefficient of CFRP is at least a factor 10 smaller than the thermal expansion coefficient of concrete (ACI Committee 440, 2008). Decreasing temperatures lead to compression in the CFRP reinforcement (Matthys, 2000). Compression in the CFRP reinforcement should be avoided because the compressive strength of CFRP reinforcement is low.

6.2.2. Moisture

Entrapment of moisture underneath the CFRP reinforcement may cause damage in the outer layer of the concrete. Freezing water causes micro cracks in the concrete. The moisture content of the concrete during application of the CFRP reinforcement should be limited as indicated in Section 6.1.1. Furthermore, permeable adhesives and partial application of the CFRP reinforcement can prevent de accumulation of moisture during the life time of the structure (Matthys, 2000).

Externally bonded CFRP reinforcement is a passive shear strengthening method. The reinforcement becomes active after appearance of the shear crack. Moisture can easily penetrate in these cracks. The crack width should be limited according to the Eurocode to prevent durability issues. The maximum crack width depends on the exposure class of the concrete element. The crack width should be taken into account during the design of shear strengthening using CFRP reinforcement.

6.2.3. Sunlight

The CFRP reinforcement should be protected from direct sunlight according to the Dutch design recommendation CUR 91 (CURNET, 2007). Direct sunlight may increase the temperature of the black coloured CFRP reinforcement rapidly. The temperature may exceed the glass-transition temperature of the adhesive. Furthermore, direct sunlight should be avoided because UV-light affects the mechanical properties of the polymer matrix in the CFRP reinforcement. Direct sunlight is not a problem for the most bridge girders. However, CFRP reinforcement at the outer bridge girders should be protected because direct sunlight is a problem for the CFRP reinforcement at these girders.

6.3. Fire protection

The fire safety of I-girders strengthened with externally bonded CFRP reinforcement should be taken into account because a burning vehicle underneath a bridge could heavily damage the CFRP reinforcement.

The polymer binder and adhesive will lost its strength at high temperatures and results in debonding of the CFRP reinforcement. The critical temperature of the shear strengthening method using externally bonded CFRP reinforcement should be taken as the lowest glass-transition temperature of the adhesive or the polymer matrix (ACI Committee 440, 2008). The strength of the externally bonded CFRP reinforcement is assumed to be lost in a fire according to the ACI440.2R-08. The I-girder without CFRP reinforcement should be able to resist the accidental load combinations during a fire. Fire protection should be applied when the I-girder without CFRP reinforcement is not able to resist the accidental load combinations during a fire. The externally bonded CFRP reinforcement can be protected through the use of protection coating or insulation systems.

The externally bonded CFRP reinforcement should be replaced after a fire. Due to the high temperatures, the structural safety of the CFRP can no longer be guaranteed. The structural condition of the I-girder should also be investigated after a fire. The high temperatures could cause degradation of the concrete skin, which might result in a lower bond strength. The bond strength of the concrete surface should be measured again before applying new CFRP reinforcement.

6.4. Long-term behaviour

The long-term behaviour of externally bonded CFRP reinforcement is applied in the international design guidelines. However, further investigation of the long-term behaviour is recommended by the design guideline ACI440.2R-08. Long-term loading and cyclic loading affect the long-term behaviour of the CFRP reinforcement and the bond between the CFRP reinforcement and the concrete. Stress limitations are prescribed in the ACI440.2R-08 to take in account the effect of fatigue and creep. Sustained stresses in the CFRP reinforcement should be limited because these will cause creep deformations in the adhesive layer between the concrete and the CFRP reinforcement (Matthys, 2000). Sustained stresses in the CFRP should be limited to 55% of the ultimate strength of the CFRP reinforcement to prevent creep-rupture. Fatigue stresses should also be limited to 55% of the ultimate strength according to the ACI440.2R-08. The knowledge of long-term loading and cyclic loading of CFRP anchors and prestressed concrete I-girders strengthened with CFRP reinforcement is limited. The limitation of sustained and fatigue stresses in the CFRP reinforcement should be validated for prestressed I-girders strengthened with CFRP reinforcement.

6.5. Management and maintenance

Concrete structures are generally strengthened for a period of 30 years. Strengthening of concrete structures with CFRP reinforcement require minimum maintenance during this period. However, periodic visual inspection of the CFRP strengthening is advisable. These inspections should focus on colour changes in the CFRP reinforcement, debonding of CFRP reinforcement, blistering of carbon fibres, cracking of the concrete, etc. (ACI Committee 440, 2008). The condition of the CFRP reinforcement at the re-entrant corners and around CFRP anchors deserves extra attention.

Damages or deficiencies should be repaired to prevent further degradation of the CFRP reinforcement. The repairs should be performed by skilled people. Local debonding of CFRP reinforcement can be repaired by injection of an adhesive. Small damages can be repaired by bonding CFRP sheets over the damaged area while large damages require replacement of the CFRP reinforcement (ACI Committee 440, 2008).

7

COMPARISON SHEAR STRENGTHENING METHODS

7.1. Alternative shear strengthening methods

To date, Shear strengthening of bridge girders with externally bonded CFRP material is not applied in the Netherlands. Prestressed bridge girders have been strengthened with other shear strengthening methods. The shear strengthening methods can be divided in active and passive shear strengthening methods. Examples of active shear strengthening methods are external prestressing braces and external prestressing. External support structures can be both active or passive shear strengthening methods. Externally bonded CFRP reinforcement and concrete cover with conventional shear reinforcement are passive shear strengthening methods. The existing shear strengthening systems are briefly described in this section and the shear strengthening methods are compared in Section 7.2.

7.1.1. Concrete cover with conventional shear reinforcement

According to the Eurocode NEN-EN 1992-1-1 shear reinforcement should be provided in regions with insufficient shear capacity. Prestressed girders with insufficient shear capacity can be strengthened with shear reinforcement. However, adding shear reinforcement in the cross-section of existing girders is not possible. The girder can be strengthened with external shear reinforcement. The stirrups should be anchored in the compression zone of the girder and the stirrup should be closed at the bottom of the girder. Finally, the stirrups should be covered in concrete (Ter Maten, Verbaten & Groeneweg, 2018). The concrete cover provide the load transfer between the stirrups and the girder. Furthermore, the concrete cover protects the stirrups against corrosion. The design of the shear reinforcement with concrete cover is illustrated by Figure 3.3. The I-girders of the Nijkerker Bridge are strengthened using this shear strengthening method. Figure 7.2 shows an I-girder of the bridge during construction and after construction.

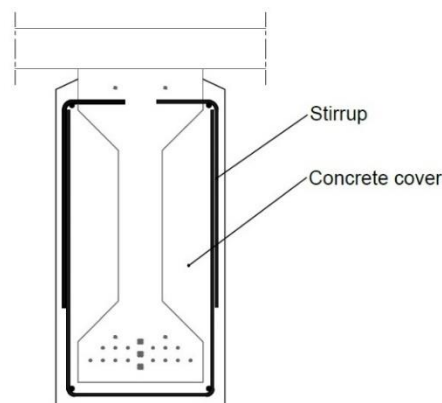


Figure 7.1: Shear strengthening with stirrups



Figure 7.2: Conventional shear reinforcement and concrete cover Nijkerker Bridge

7.1.2. External prestressing brace

Vertical prestressing of I-girders has been applied in the Netherlands. Some of the girders of the Oude Rijn Bridge are strengthened with vertical prestressing braces. This method is illustrated in Figure 7.3. This shear strengthening method is a fully closed system. A steel plate is placed in the deck of the bridge. The prestressing bars are connected to the steel plate through the top flange of the I-girder and the deck. The brace is closed with a steel beam at the bottom of the I-girder. The prestressing bars are prestressed to create a compression stress in the I-girder.

An innovative method to create prestress in a concrete element is SMA (Smart Memory Alloy) steel. SMA steel is able to return to its initial shape when the material is heated. The SMA steel is able to revert to its initial state after being pseudo-plastically deformed (Czaderski et al., 2014). Prestressing forces are introduced in the concrete cross-section by preventing the deformation by embedding the SMA steel in the concrete. The SMA steel is available as reinforcement bars. The SMA reinforcement bars should be applied in the same way as conventional shear reinforcement with concrete cover, as illustrated in Figure 7.1. The concrete cover is needed to embed the SMA reinforcement and to provide the load transfer between the SMA bars and the I-girder. SMA bars have never been used to strengthen I-girders of this size. Several concrete beams of the Kurtheater Baden are strengthened in shear with SMA bars (Re-fer AG, 2019). Figure 7.4 shows the U-shaped SMA reinforcement bars around the concrete beams. The SMA reinforcement bars were covered with concrete before the bars were activated. Prestressed shear reinforcement with SMA steel seems promising to strengthen I-girders in shear.

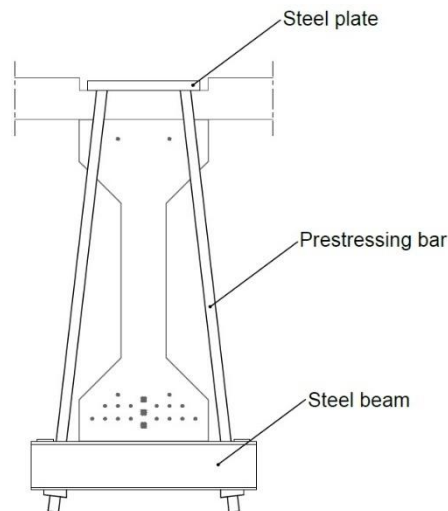


Figure 7.3: Shear strengthening with vertical external prestressing brace



Figure 7.4: Prestressed shear reinforcement Kurtheater baden (Re-fer AG, 2019)

7.1.3. External prestressing

External prestressing is commonly used to prestress box-girders composed of multiple segments. The bending strength and the shear strength of I-girders can be increased with external prestressing (Siwowski, 2015). The prestressing cables of the external prestressing system are anchored at both ends of the girder. The external support force is introduced by steel deviators (Meijer, 2012). The principle of this shear strengthening method is illustrated in Figure 3.5.

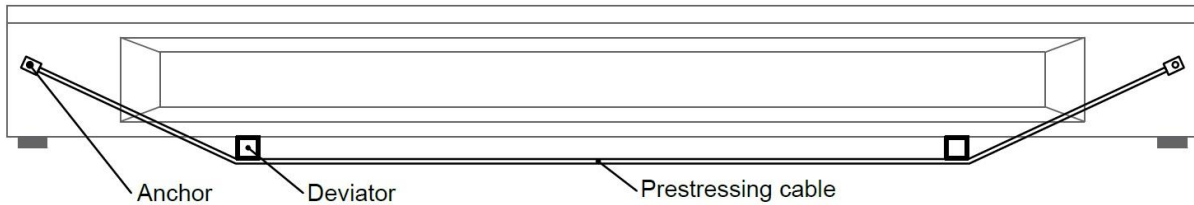


Figure 7.5: Shear strengthening with horizontal external prestressing

7.1.4. External support structure

Prestressed girders with insufficient shear capacity and bending capacity can be strengthened with external support forces. The external support forces are introduced by an external support structure. Two variants of the support structures are illustrated in Figure 3.6. The external support structure is a steel structure underneath the girder. The support force is realised by pre-cambered steel beam and steel columns. The external support structure is used to strengthen the girders of the A4 Ringvaartviaduct. The external support structure consists of steel tube columns and steel pre-cambered HEA400 beams (Mourik, 2019). Figure 7.7 shows the external support structure after completion.

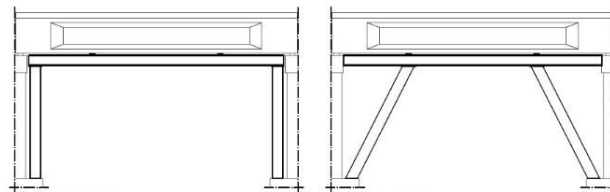


Figure 7.6: External support structure



Figure 7.7: External steel support structure A4 Ringvaartviaduct (Mourik, 2019)

7.2. Comparison shear strengthening methods

The shear strengthening methods described in this chapter and shear strengthening using externally bonded CFRP reinforcement are compared in the trade-off matrix given in Table 7.2. The shear strengthening methods are compared using multiple criteria. The shear strengthening methods are awarded with a score for every criterion. Important criteria get a higher weight in the trade-off matrix. Table 7.1 shows the overview of the scores.

The shear strengthening methods with the externally bonded CFRP reinforcement and the external prestressing get the best scores in the trade-off matrix. The shear strengthening using externally bonded CFRP reinforcement gets high scores for the clear height underneath the bridge and the additional self-weight compared to other shear strengthening methods because the self-weight does not increase and the clear height does not decrease. The shear strengthening method with external prestressing gets a high score because of the limited hindrance and the experience with installation. The shear strengthening method using external prestressing braces is an interesting strengthening method but this method gets a high penalty for the hindrance on top of the deck. Minimizing the hindrance on top of bridge is very important for Rijkswaterstaat. The scores for the most criteria depend mainly on the location of the bridge.

The limited knowledge of the structural performance of I-girders strengthened with externally bonded CFRP reinforcement is still a problem. According to the numerical investigation presented in this report and experimental tests in literature an increase in shear capacity of 10-50% compared to the shear capacity of an unstrengthened I-girder should be possible using externally bonded CFRP reinforcement. Shear strengthening of prestressed I-girders using CFRP reinforcement is an interesting and promising shear strengthening method compared to the other shear strengthening methods.

Table 7.1: Legend trade-off matrix

Symbol		Score
++	Very favourable	2
+	Favourable	1
+/-	Neutral	0
-	Unfavourable	-1
--	Very unfavourable	-2

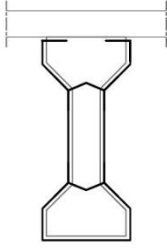
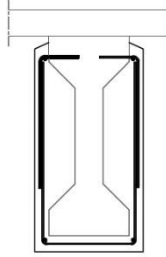
Criteria	Weight factor	Externally bonded CFRP	Shear reinforcement
			
Structure			
▪ Clear height underneath bridge	2	+	+/-
▪ Additional self-weight	1	++	--
▪ (Expected) shear strengthening	3	+	+
▪ Aesthetics	1	+	+
Durability/sustainability			
▪ Durability	2	+	+
▪ Sustainability	2	+/-	-
▪ Fire safety	1	--	+
Execution			
▪ Installation time	2	+	--
▪ Hindrance on deck	2	++	++
▪ Experience	1	-	+
▪ Complexity	1	+	-
Costs			
▪ Material costs	1	+	-
▪ Installation costs	1	+	-
▪ Maintenance costs	1	+	+
Total		17	2

Table 7.2: Trade-off matrix shear strengthening methods

External prestressing brace	External prestressing	External support structure
<p>- - ++ -</p>	<p>- +/- + -</p>	<p>-- - + -</p>
<p>+ - +/-</p>	<p>+ - +/-</p>	<p>+ - +/-</p>
<p>- -- + -</p>	<p>+/- ++ + +/-</p>	<p>- ++ + +/-</p>
<p>- -- -</p>	<p>+/- +/- -</p>	<p>-- - -</p>
<p>-8</p>	<p>4</p>	<p>-4</p>

8

CONCLUSIONS AND RECOMMENDATIONS

8.1. Conclusions

The aim of this thesis was to investigate the feasibility of using externally bonded CFRP reinforcement to strengthen I-girders in shear. The shear behaviour was investigated by analysing several types of externally bonded CFRP reinforcement using the NLFEA software DIANA. The finite element models of the I-girder without shear reinforcement were based on the I-girders of the Nijkerker Bridge.

8.1.1. Feasibility externally bonded CFRP reinforcement

The following conclusions are derived from the results obtained from the NLFEA of the I-girders.

- The presented I-girder with a shear span of 3.0 m failed in shear tension failure while the I-girder with a shear span of 4.0 and 5.0 m failed in flexural shear failure. The shear capacity of the I-girder decreased with an increasing shear span-to-depth ratio.
- The contribution of the vertical CFRP sheets to the shear capacity was limited to approximately 10% for the I-girder failing in flexural shear and 2% for the I-girder failing in shear tension because of the debonding of the CFRP sheets in the re-entrant corner of the I-girder. The ductility of the I-girder failing in flexural shear increased with more than 10%.
- The addition of horizontal CFRP sheets to improve the anchorage of the vertical CFRP sheets in the re-entrant corners did not significantly improve the shear capacity of the I-girder. The increase in the failure load was limited to a maximum of 2% compared to the I-girder strengthened with only vertical CFRP sheets. The ductility of the specimens failing in flexural shear increased with approximately 5% compared to the specimen without horizontal CFRP sheets.
- Anchoring the vertical CFRP sheets in the re-entrant corners significantly improved the shear capacity of the I-girder failing in flexural shear failure when CFRP anchors are modelled. The ultimate load increased up to 42% compared to the reference I-girder. The debonding of the vertical CFRP sheets was prevented which increased the utilisation of the CFRP reinforcement and the ductility of the I-girder. The ductility of the I-girder increased up to 70% compared to the I-girder without CFRP reinforcement. The brittle propagation of the dowel crack at the bottom of the web was prevented by the vertical CFRP sheets.
- increasing the CFRP width-to-spacing ratio from 0.5 to 1.0 increased the shear capacity of the I-girder failing in shear tension and flexural shear failure. The ultimate load of the I-girder failing in flexural shear failure increased up to 58% compared to the I-girder without CFRP reinforcement while the ultimate load of the I-girder failing in shear tension failure increased with 15% compared to the I-girder without CFRP reinforcement. The ductility of the I-girder failing in flexural shear failure increased between 80-90%
- The predictions of the design guidelines (CUR 91, ACI440.2R-08 and the DAfStb heft 595) did not correspond to the predictions of the numerical simulations. A possible explanation could be that these design guidelines do not take the brittle debonding of CFRP reinforcement in the re-entrant corners of the I-girder or the capacity of the CFRP anchors into account. However, numerical simulations include a modelling uncertainty because the finite element models could not be validated.

Based on the results of the NLFEA and the other non-structural advantages it is concluded that shear strengthening of prestressed concrete I-girders without shear reinforcement using externally bonded CFRP sheets and CFRP anchors is a promising shear strengthening method.

Flexural shear failure is often considered to be the most critical shear failure mechanism for precast members without shear reinforcement such as prestressed I-girders. The numerical analyses showed a promising increase in flexural shear capacity between 40-55% and an increase in ductility of more than 80%.

8.1.2. Use of nonlinear finite element analysis

The following conclusions can be drawn about the robustness of the NLFEA.

- The finite element model of the reference specimens was not validated in this research because of the lack of good experimental data. A solution strategy validated in literature for quite similar concrete beams without shear reinforcement was used to make the finite element model of the reference specimens. The solution strategy is able to predict the shear failure mode and the brittle propagation of shear cracks but the shear capacity is overpredicted according to the validation of the solution strategy in literature.
- The numerical analyses of the reference specimens showed that the I-girder with a shear span of 3.0 m failed in shear tension failure and the I-girder with a shear span of 4.0 m and 5.0 m failed in flexural shear failure as expected by analytical verification. The brittle propagation of the shear cracks corresponded to the peak load in the load-deformation curves of the reference specimens.
- The debonding of CFRP sheets can be modelled by a nonlinear elastic interface layer between the CFRP elements and the concrete elements. The debonding started after opening of the crack and propagated towards the re-entrant corners. The CFRP elements started to pull away from the re-entrant corner which was visible in the NLFEA of the specimens strengthened with vertical CFRP sheets.
- The numerical analyses showed that beam elements prevented the debonding of the vertical CFRP sheets in the re-entrant corners of the I-girder and increase the utilisation of the vertical CFRP sheets. However, the load transfer between the CFRP anchor and the concrete is not realistic because the beam element is not embedded into the concrete.
- The numerical analyses of the specimens with vertical CFRP sheets and a combination of horizontal and vertical CFRP sheets showed brittle propagation of the shear cracks before the analyses aborted which corresponded to failure of the specimens. However, the specimens with a combinations of vertical CFRP sheets and CFRP anchors did not show brittle propagation of the shear cracks before the analyses aborted. The numerical analyses of these specimens did not result in a distinct failure mechanism.

The NLFEA has the potential to predict the shear behaviour of prestressed concrete I-girders with externally bonded CFRP reinforcement. However, accurately predicting the increase in shear capacity is not possible without validation of the finite element model of the I-girder. Nevertheless, the nonlinear finite element analyses in this research showed that numerical analysis can be helpful to understand the failure mechanism of I-girders strengthened with externally bonded CFRP reinforcement. Furthermore, the numerical simulations showed that finite element modelling is helpful to perform a parametric study of the application of CFRP reinforcement at prestressed concrete girders.

8.2. Recommendations

Recommendations for further development and research into the topic of this thesis are proposed in this section. Further development and research are needed before CFRP reinforcement can be applied on prestressed concrete girders with insufficient shear capacity.

- More experimental data of prestressed concrete I- and T-girders strengthened with externally bonded CFRP reinforcement and CFRP anchors is needed to get a better understanding of her shear behaviour. Experimental research should focus on both shear tension failure and flexural shear failure of prestressed girders.
- Further research into the effect of concrete strength, internal shear reinforcement and the tendon profile of prestressed concrete girders on the contribution of the externally bonded CFRP reinforcement is recommended.
- The solution strategy used in this research was not validated because of the lack of good experimental data. New experimental data should be used to develop and validate solution strategies for I- and T-girders with and without internal shear reinforcement. Validated finite element models for I- and T-girders with and without internal shear reinforcement can be helpful to investigate the performance of externally bonded CFRP reinforcement using parametric studies in combination with numerical simulations.
- Further research into the failure mechanism of CFRP anchors in the re-entrant corners and the load transfer between the splay and the CFRP sheets is recommended. The capacity of the CFRP anchors mainly determine the contribution of the externally bonded CFRP reinforcement to the shear capacity of prestressed concrete girders.
- Further development of the finite element model of the CFRP anchor is recommended to make finite element analysis useful to design externally bonded CFRP reinforcement. The finite element model of the CFRP anchor should also incorporate the failure mechanisms of the CFRP anchor.
- The CFRP anchors are placed into predrilled holes in the re-entrant corners of the I-girder. The effect of the drilled holes in the re-entrant corners on the shear capacity and the shear crack propagation needs further investigation.
- The effect of crack propagation around the CFRP anchor needs further investigation because the crack might affect the performance of the CFRP anchor because the bond between the anchor and the concrete is lost.

REFERENCES

- ACI Committee 318 (2011). *Building Code Requirements for Structural Concrete*. Farmington Hills, American Concrete Institute.
- ACI Committee 440 (2008). *Guide for the Design and Construction of Externally Bonded FRP Systems for Strengthening Concrete Structures*. Farmington Hills, American Concrete Institute.
- Al-Sammari, A. T. & Breña, S. F. (2018). Finite Element Simulation and Parametric Study of Anchored Fiber-Reinforced Polymer Sheets. *ACI Structural Journal*, 115(2), 365-377.
- Ary, M. I. & Kang, T. H. K. (2012). Shear-Strengthening of Reinforced & Prestressed Concrete Beams Using FRP: Part I – Review of Previous Research. *International Journal of Concrete Structures and Materials*, 6(1), 41-47.
- Blontrock, H., Taerwe, L. & Matthys, S. (1999). Properties of Fibre Reinforced Plastics at Elevated Temperatures with Regard to Fire Resistance of Reinforced Concrete Members. *ACI Symposium*. Michigan: 43-54.
- Bousselham, A. & Chaallal, O. (2004). Shear Strengthening Reinforced Concrete Beams with Fiber-Reinforced Polymer: Assessment of Influencing Parameters and Required Research. *Structural Journal*, 101(2), 219-227.
- Bousselham, A. & Chaallal, O. (2006). Effect of transverse steel and shear span on the performance of RC beams strengthened in shear with CFRP. *Composites Part B: engineering*, 37(1), 37-46.
- Chen, J. F. & Teng, J. G. (2003a). Shear capacity of FRP-strengthened RC beams: FRP debonding. *Construction and Building Materials*, 17(2003), 27-41.
- Chen, J. F. & Teng, J. G. (2003b). Shear capacity of Fiber-Reinforced Polymer-strengthened Reinforced Concrete beams: Fiber Reinforced Polymer rupture. *Journal of Structural Engineering*, 129(5), 615-625.
- CNR (2004). *Guide for the Design and Construction of Externally Bonded FRP Systems for Strengthening Existing Structures*. Rome, CNR.
- Costa, I. & Barros, J. (2015). Tensile creep of a structural epoxy adhesive: Experimental and analytical characterization. *International Journal of Adhesion & Adhesives*, 59(2015), 115-124.
- CURNET (2007). *CUR aanbeveling 91: Versterken van gewapend betonconstructies met uitwendig gelijmde koolstofwapening*. Gouda, Stichting CURNET.
- Czaderski, Z., Shahverdi, W., Brönnimann, R., Leinenbach, C. & Motavalli, M. (2014). Feasibility of iron-based shape memory alloy strips for prestressed strengthening of concrete structures. *Construction and building materials*, 56(2014), 94-105.
- DAfStb (2012). *Verstärken von Betonbauteilen mit geklebter Bewehrung*. Berlin-Tiergarten, Deutscher Ausschuss für Stahlbeton e. V.
- Deniaud, C. & Cheng, J. J. R. (2004). Simplified Shear Design Method for Concrete Beams Strengthened with Fiber Reinforced Polymer Sheets. *Journal of Composites for Construction*, 8(5), 425-433.

- Gaal, G.C.M. (2004). *Prediction of Deterioration of Concrete Bridges – Corrosion of Reinforcement due to Chloride Ingress and Carbonation*. Delft, University of Technology Delft.
- Hendriks, M.A.N., de Boer, A. & Belletti, B. (2017a). *Guidelines for Nonlinear Finite Element Analysis of Concrete Structures*. Rijkswaterstaat Centre for Infrastructure.
- Hendriks, M.A.N., de Boer, A. & Belletti, B. (2017b). *Guidelines for Nonlinear Finite Element Analysis of Concrete Structures – Part: Overview of results*. Rijkswaterstaat Centre for Infrastructure.
- Hollaway, L.C. & Leeming, M.B. (1999). *Strengthening of reinforced concrete structures using externally-bonded FRP composites in structural and civil engineering*. Abington Cambridge, Woodhead Publishing Limited.
- Iovinella, I., Prota, A. & Mazzotti, C. (2013). Influence of surface roughness on the bond of FRP laminates to concrete. *Construction and building materials*, 40(2013), 533-542.
- Kalfat, R. & Al-Mahaidi, R. (2014). Numerical and Experimental Validation of FRP Patch Anchors Used to Improve the Performance of FRP Laminates Bonded to Concrete. *Journal of Composites for Construction*, 18(3), 1-10.
- Kalfat, R. & Al-Mahaidi, R. (2018a). Numerical Simulation of Large-Scale Concrete Beam Strengthened in Shear with FRP Composites and Bidirectional Fiber Patch Anchors. *Symposium Paper*, 322, 19.1-19.12.
- Kalfat, R. & Al-Mahaidi, R. (2018b). *A guideline and review on the modelling techniques used in finite element simulations of concrete structures strengthened using FRP*. Swinburne University of Technology, Melbourne, Australia.
- Kalfat, R., Al-Mahaidi, R. & Smith, S. T. (2013). Anchorage Devices Used to Improve the Performance of Reinforced Concrete Beams Retrofitted with FRP Composites: State-of-the-Art Review. *Journal of Composites for Construction*, 17(1), 14-33.
- Khalifa, A., Gold, W. J., Nanni, A. & Abdel Aziz, M.I. (1998). Contribution of Externally Bonded FRP to Shear Capacity of Flexural Members. *Journal of Composites for Construction*, 2(4), 195-203.
- Khalifa, A. & Nanni, A. (2000). Improving shear capacity of existing RC T-section beams using CFRP composites. *Cement & concrete Composites*, 22(2000), 165-174.
- Kim, Y., Quinn, K., Satrom, N., Garcia, J., Sun, W., Ghannoum, W. M. & Jirsa, J. O. (2012). *Shear Strengthening of Reinforced and Prestressed Concrete Beams Using Carbon Fiber Reinforced Polymer (CFRP) Sheets and Anchors*. Austin, Centre for Transportation Research.
- Kobayashi, K., Fujii, S., Yabe, Y., Tsukugoshi, H., & Sugiyama, T. (2001). Advanced wrapping system with CF-anchor-Stress transfer mechanism of CF-anchor. Proceedings, 5th International Conference on Fibre Reinforced Plastics for Reinforced Concrete Structures, FRPRCS-5, Thomas Telford Publishing, London, 379-388.
- Lu, X. Z., Teng, J. G. & Jiang, J. J. (2005). Bond-slip models for FRP sheets/plates bonded to concrete. *Engineering structures*, 27(2005), 920-937.
- Massa, R. J., Cook, W. D. & Mitchell, D. (2018). Reinforced bridge I-girders using CFRP shear strips. *ACI Symposium Publication*, 328(1), 1.1-1.20.
- Matthys, S. (2000). *Structural behaviour and design of concrete members strengthened with externally bonded FRP reinforcement*. Ghent, Ghent University.
- Meijer, R. (2012). Opwaarderen met externe voorspanning. *Cement*, 2012(3), 30-34.
- Mourik (2019, April 26). Versterking Ringvaartviaduct Badhoevedorp. Retrieved October 8, 2020, from <https://www.mourik.com/nieuws/570/versterking-ringvaartviaduct-badhoevedorp.html>.
- Nawy, E.G. (2009). *Reinforced concrete: a fundamental approach*. New Jersey, Pearson Education, Inc.

- Nederlands Normalisatie-Instituut (1995). *NEN 6720 Regulations for concrete – Structural requirements and calculation methods*. Delft, Nederlands Normalisatie-instituut.
- Nederlands Normalisatie-Instituut (1999). *NEN 1542 Products and systems for the protection and repair of concrete structures – Test Methods – Measurement of bond strength by pull-off*. Delft, Nederlands Normalisatie Instituut.
- Nederlands Normalisatie-Instituut (2011a). *NEN 8700 Assessment of existing structures in case of reconstruction and disapproval – Basic rules*. Delft, Nederlands Normalisatie-instituut.
- Nederlands Normalisatie-Instituut (2011b). *NEN 8701 Assessment of existing structures in case of reconstruction and disapproval – Actions*. Delft, Nederlands Normalisatie-instituut.
- Nederlands Normalisatie-Instituut (2011c). *NEN-EN 1992-1-1+C2 Eurocode 2: Design of concrete structures – Part 1-1: General rules and rules for buildings*. Delft, Nederlands Normalisatie-instituut.
- Nederlands normalisatie-Instituut (2015). *NEN-EN 1991-2+C1 Eurocode 2: Design of concrete structures – Concrete bridges – Design and detailing rules*. Delft, Nederlands Normalisatie-instituut.
- Niu, H. & Wu, Z. (2006). Effects of FRP-Concrete Interface Bond Properties on the Performance of RC Beams Strengthened in Flexure with Externally Bonded FRP sheets. *Journal of Materials in Civil Engineering*, 18(5), 723-731.
- Ozbakkaloglu, T. & Saatcioglu, M. (2009). Tensile Behavior of FRP Anchors in Concrete. *Journal of Composites for Construction*, 13(2), 82-92.
- Refer AG (2019). *Kurtheater Baden*. Retrieved September 30, 2020, from <https://www.refer.eu/en/referenz/kurtheater-baden/>.
- Regan, P.E. (1993). Research on shear: a benefit to humanity or a waste of time? *The Structural Engineer*, 71(19/5), 337-347.
- Rijkswaterstaat (2013). *Richtlijn Beoordeling kunstwerken*. Utrecht, Rijkswaterstaat.
- Rijkswaterstaat (2007). *Inventarisatie Kunstwerken*. Utrecht, Rijkswaterstaat.
- S&P Clever Reinforcement Company (2017a). *S&P C-sheet 240*. Aalsmeer, S&P Clever Reinforcement Company.
- S&P Clever Reinforcement Company (2017b). *S&P C-sheet 640*. Aalsmeer, S&P Clever Reinforcement Company.
- S&P Clever Reinforcement Company (2018). *S&P Resin 220 HP*. Aalsmeer, S&P Clever Reinforcement Company.
- S&P Clever Reinforcement Company (2019). *Test report – Pull-out tests Carbon Anchors*. Aalsmeer, S&P Clever Reinforcement Company.
- Sato, Y. & Vecchio, F. J. (2003). Tension Stiffening and Crack Formation in Reinforced Concrete Members with Fiber-Reinforced Polymer Sheets. *Journal of Structural Engineering*, 129(6), 717-724.
- Siwowski, T. (2015). *Bridge Engineering – selected issues*. Oficyna Wydawnicza Politechniki Rzeszowskiej, Rzeszow, Poland.
- Teng, J.G., Yuan, H. & Chen, J.F. (2006). FRP-to-concrete interfaces between two adjacent cracks: Theoretical model for debonding failure. *International Journal of Solids and Structures*, 43(2006), 5750-5778.
- Ter Maten, R., Verbaten, M. & Groeneweg, T. (2018). Minimale hinder dankzij samenwerking. *Cement*, 2018(5), 18-25.
- Triantafillou, T. C. (1998). Shear Strengthening of Reinforced Concrete Beams Using Epoxy-Bonded FRP Composites. *ACI Structural Journal*, 95(2), 107-115.

- Walraven, J.C. & Braam, C.R. (2019). *Prestressed concrete*. Delft, TU Delft.
- Woo, S.K., Kim, J.H.J., Byun, K.J. & Song, Y.C. (2013). Bond-slip parameter determination procedure of RC flexure member strengthened with prestressed CFRP plates. *KSCE Journal of Civil Engineering*, 17(1), 179-191.
- Zhang, Z. & Hsu, C. T. (2005). Shear Strengthening of Reinforced Concrete Beams Using Carbon-Fiber-Reinforced Polymer Laminates. *Journal of Composites for Construction*, 9(2), 158-169.
- Zilch, K., Niedermeier, R. & Finckh, W. (2014). *Strengthening of Concrete Structures with Adhesively Bonded Reinforcement – Design and Dimensioning of CFRP Laminates and Steel Plates*. Berlin, Wilhelm Ernst & Sohn.

APPENDICES

A. Drawings I-girders Nijkerker Bridge

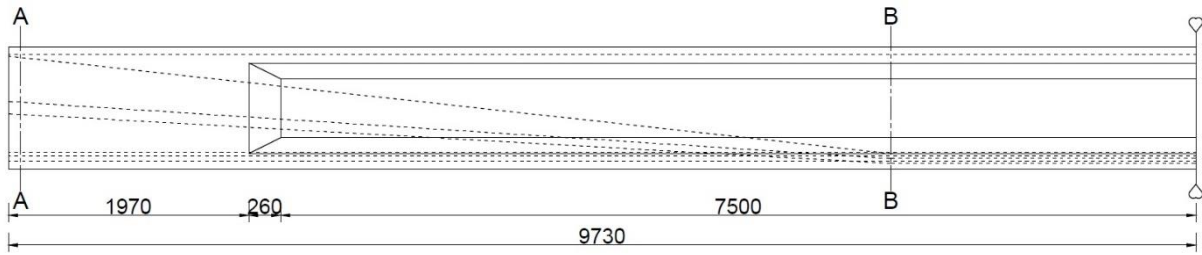


Figure A.1: Side view I-girder Nijkerker Bridge

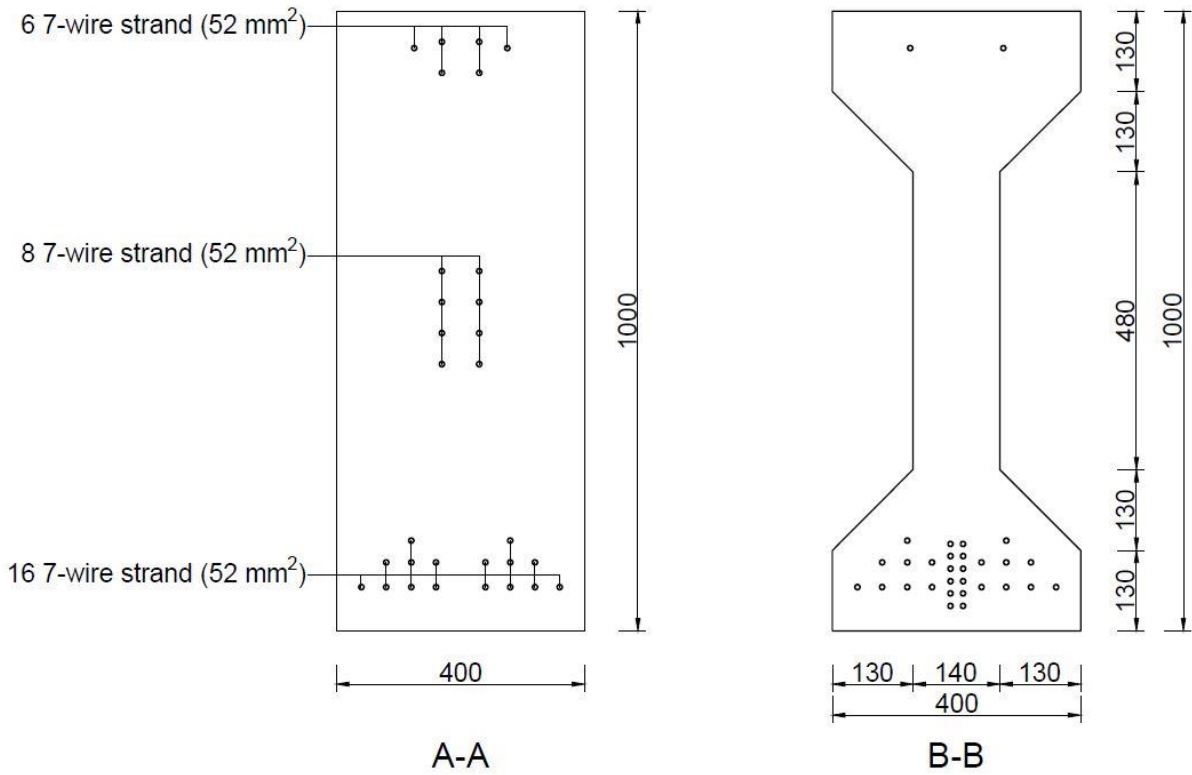


Figure A.2: Cross-sections I-girder Nijkerker Bridge

B. Geometry research specimens

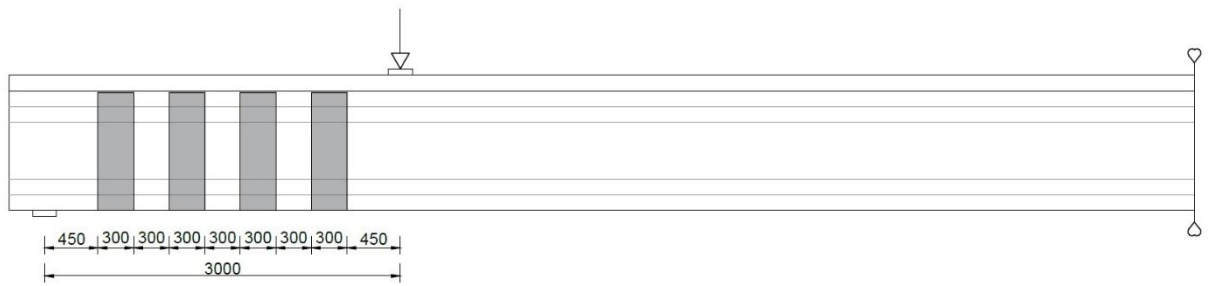


Figure B.1: Specimen I-V-SP3 and specimen I-V-L2-SP3

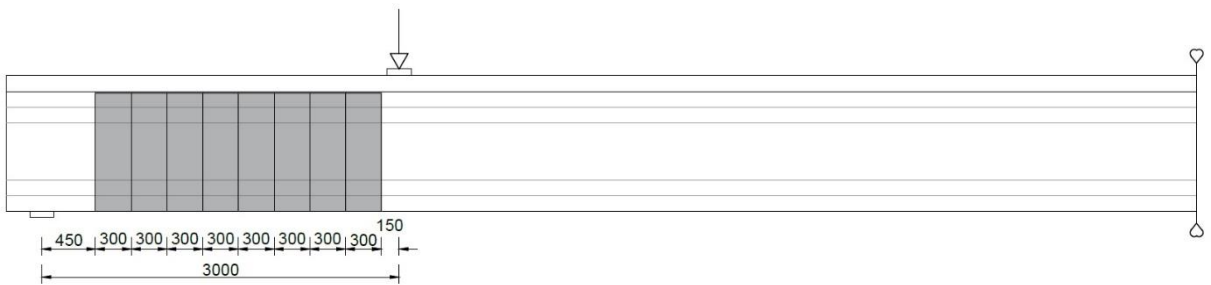


Figure B.2: Specimen I-V-S0-SP3



Figure B.3: Specimen I-VH-SP3

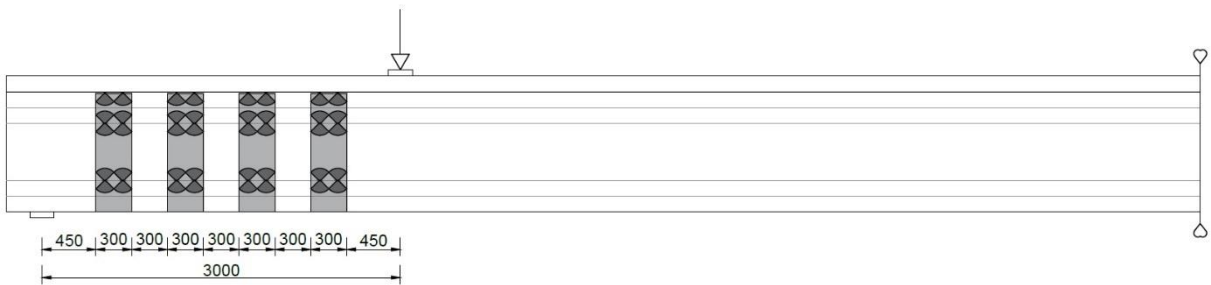


Figure B.4: Specimen I-VA-SP3



Figure B.5: Specimen I-VA-S0-SP3

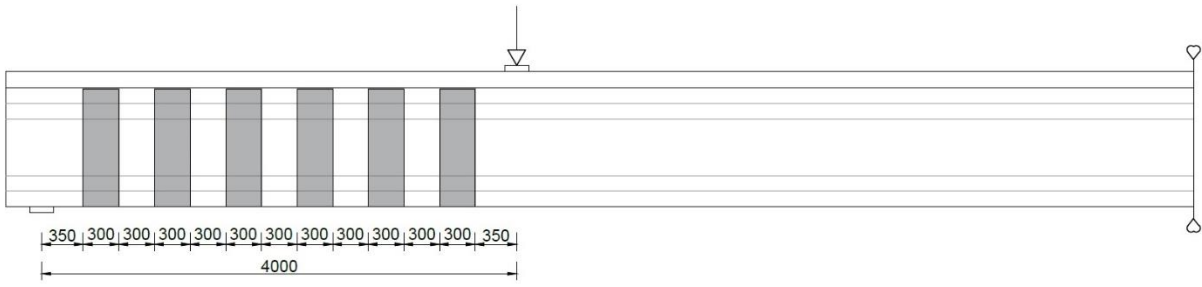


Figure B.6: Specimen I-V-SP4 and I-V-L2-SP4

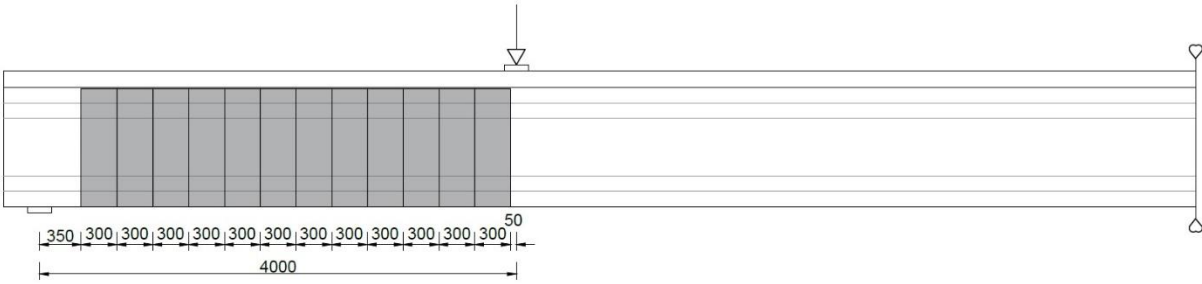


Figure B.7: Specimen I-V-S0-SP4

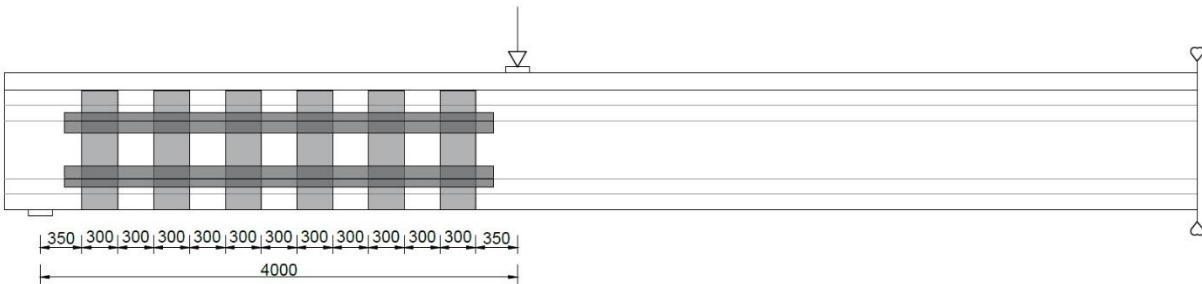


Figure B.8: Specimen I-VH-SP4

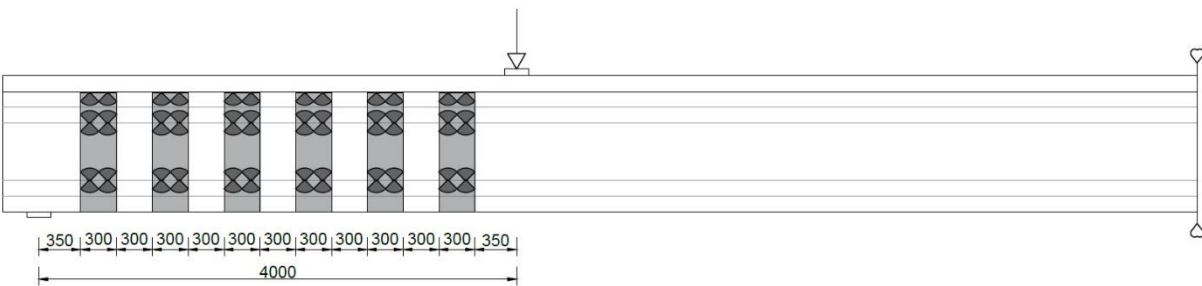


Figure B.9: Specimen I-VA-SP4

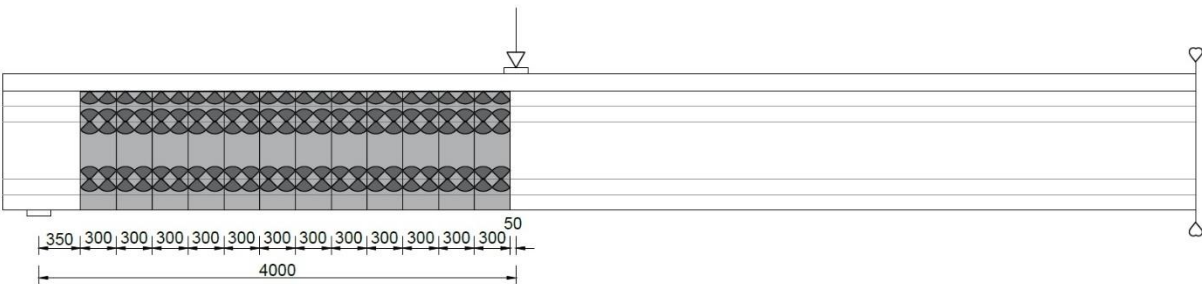


Figure B.10: Specimen I-VA-S0-SP4

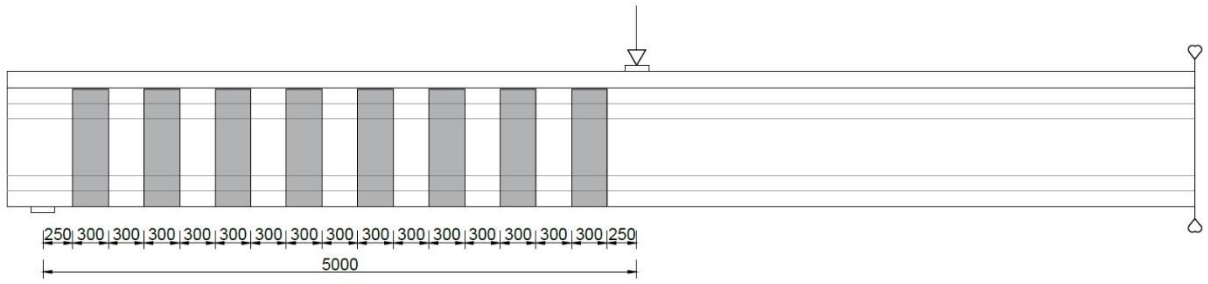


Figure B.11: Specimen I-V-SP5 and I-V-L2-SP5

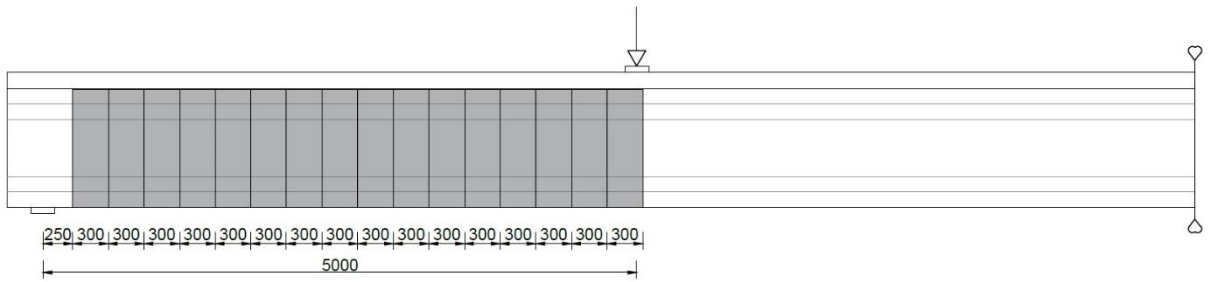


Figure B.12: Specimen I-V-S0-SP5

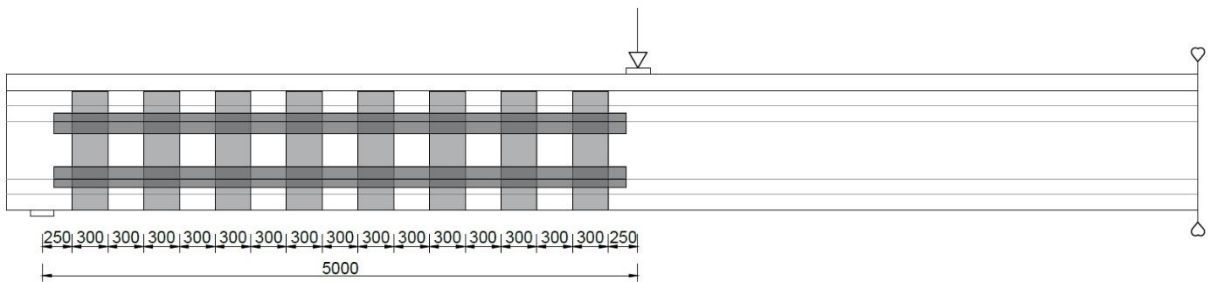


Figure B.13: Specimen I-VH-SP5

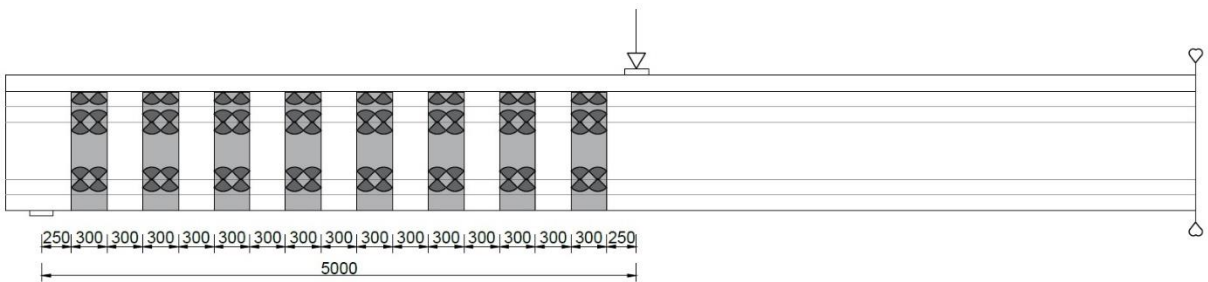


Figure B.14: Specimen I-VA-SP5

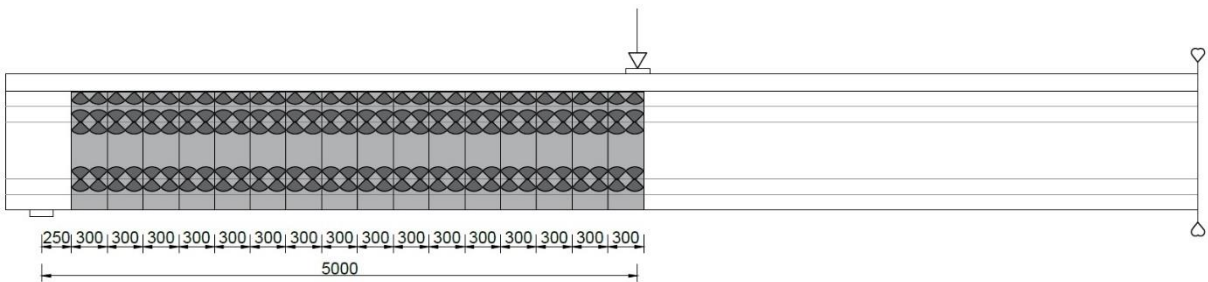


Figure B.15: Specimen I-VA-S0-SP5

C. Analytical analysis reference specimen I-C

Geometry

The test setup and the geometry of reference specimen I-C is given in the figures below.

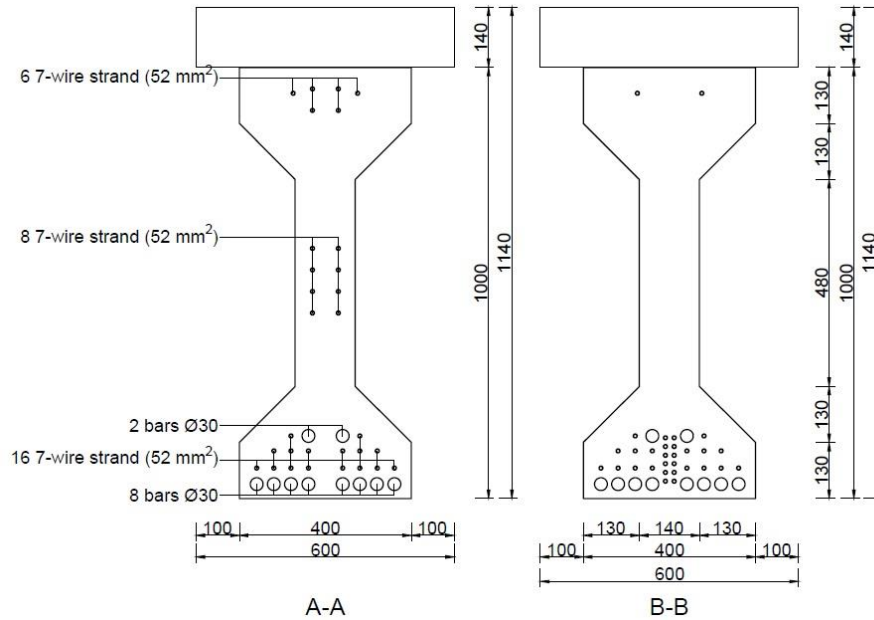


Figure C.1: Cross-section specimen I-C

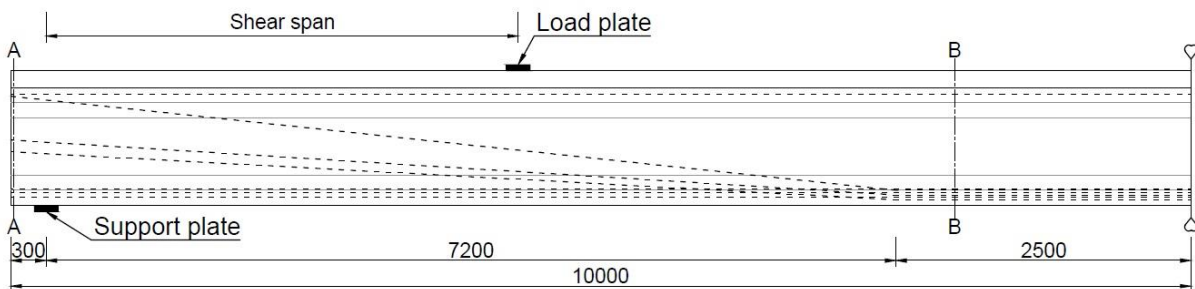


Figure C.2: Geometry specimen I-C

Material properties

The material properties of the concrete, prestressing steel and reinforcement are given in the tables below.

Table C.1: Concrete material properties

		I-girder	Deck	Units
Young's modulus	E_{cm}	39	35	[GPa]
Characteristic compressive strength	f_{ck}	60	40	[MPa]
Design value compressive strength	f_{cd}	40	26.7	[MPa]
Mean compressive strength	f_{cm}	68	48	[MPa]
Characteristic tensile strength	$f_{ctk,0.05}$	3.1	2.5	[MPa]
Design value tensile strength	f_{ctd}	2.1	1.7	[MPa]
Mean tensile strength	f_{ctm}	4.4	3.5	[MPa]

Table C.2: Prestressing steel material properties

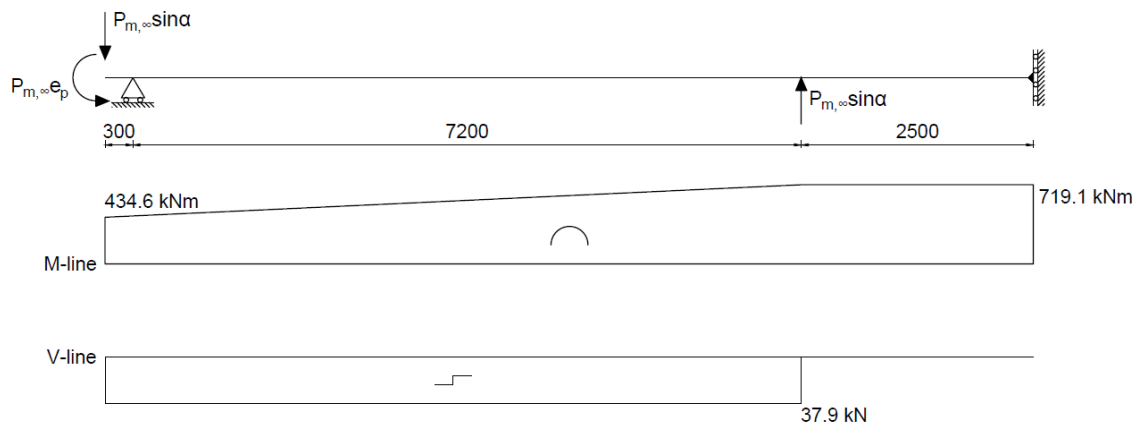
		QP190/Y1860	Units
Young's modulus	E_p	195	[GPa]
Yield stress	$f_{p,0.1k}$	1674	[MPa]
Ultimate stress	f_{pk}	1860	[MPa]
Yield strain	ϵ_p	0.86	[%]
Design value 0.1% proof-stress	f_{pd}	1522	[MPa]
Design value tensile strength	f_{pk}/γ_p	1691	[MPa]
Ultimate strain	ϵ_{uk}	3.5	[%]

Table C.3: Reinforcement material properties

		B500B	Units
Young's modulus	E_s	200	[GPa]
Yield stress	f_{yk}	500	[MPa]
Design yield stress	f_{yd}	435	[MPa]
Yield strain	ϵ_y	0.25	[%]
Ultimate stress	f_{uk}	540	[MPa]
Ultimate strain	ϵ_u	5.0	[%]

Load configuration

The loads are divided in two load cases. The first load case includes the prestressing and the self-weight of the specimens. The weight of the CFRP reinforcement is not taken into account because the weight is negligible compared to the weight of the concrete. The second load case is four-point bending load till failure. The load cases are illustrated in the figures below.

**Figure C.3: Prestressing**

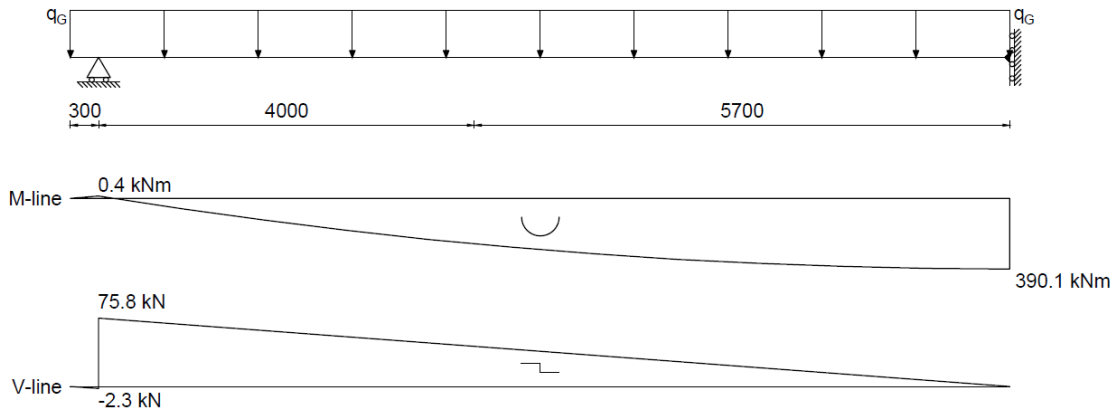


Figure C.4: Self-weight

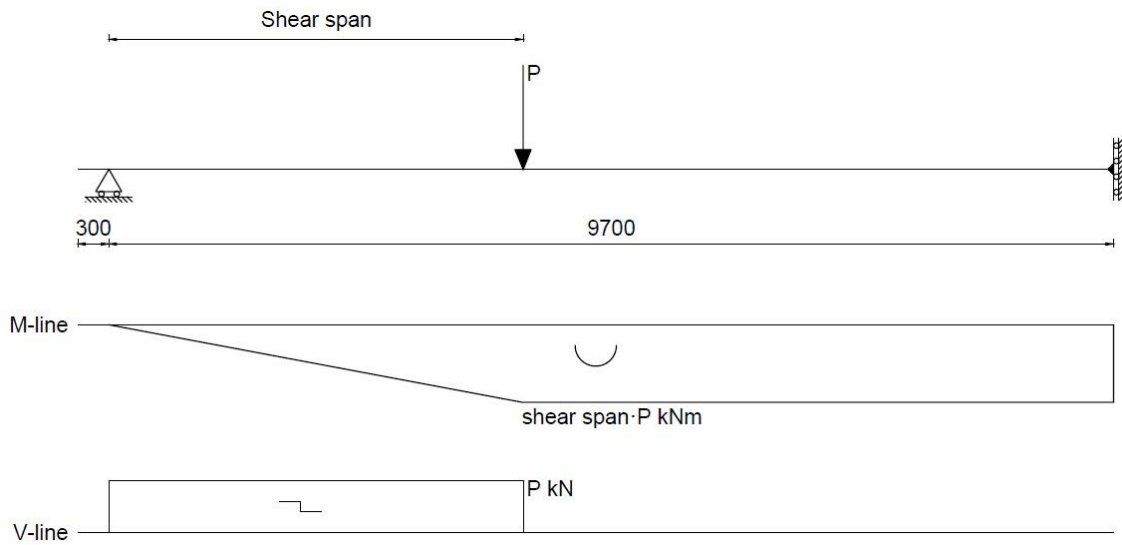


Figure C.5: Point load

Cracking moment

The cracking moment is calculated according to the Eurocode NEN-EN 1992-1-1. The cracking moment is given by:

$$M_{cr} = \left(f_{ctm,fl} + \frac{P_{m,\infty}}{A_c} \right) W_{cb} = \left(4.35 + \frac{1482 \cdot 10^3}{325400} \right) \frac{501 \cdot 10^8}{634.2} = 704.3 \text{ kNm}$$

$$f_{ctm,fl} = \max \left\{ \left(1.6 - \frac{h}{1000} \right) f_{ctm}; f_{ctm} \right\} = \max \left\{ \left(1.6 - \frac{1140}{1000} \right) \cdot 4.4; 4.4 \right\} = 4.35 \text{ MPa}$$

Bending moment resistance

The bending moment resistance is calculated according to the Eurocode NEN-EN 1992-1-1. The Eurocode assumes a bilinear concrete stress block and an elastic-plastic stress-strain relation without hardening.

The height of the compression zone is determined by horizontal force equilibrium.

$$N_c = A_s f_{yd} + 28A_p (f_{pd} - \sigma_{p,\infty,1}) + 2A_p (f_{pd} - \sigma_{p,\infty,2}) + P_{m,\infty} = 5579.2 \text{ kN}$$

The bending moment resistance of the I-girder is:

$$M_{Rd} = N_s e_s + N_p e_s + N_c e_c = 4089.6 \text{ kNm}$$

The maximum point load that can be applied is:

$$P = \frac{4089.6 + 719.1 - 390.1}{\text{shear span}}$$

Table C.4: Ultimate point load specimen I-C

Shear span	Point load
3.0 m	1472.9 [kN]
4.0 m	1104.6 [kN]
5.0 m	883.7 [kN]
6.0 m	736.4 [kN]

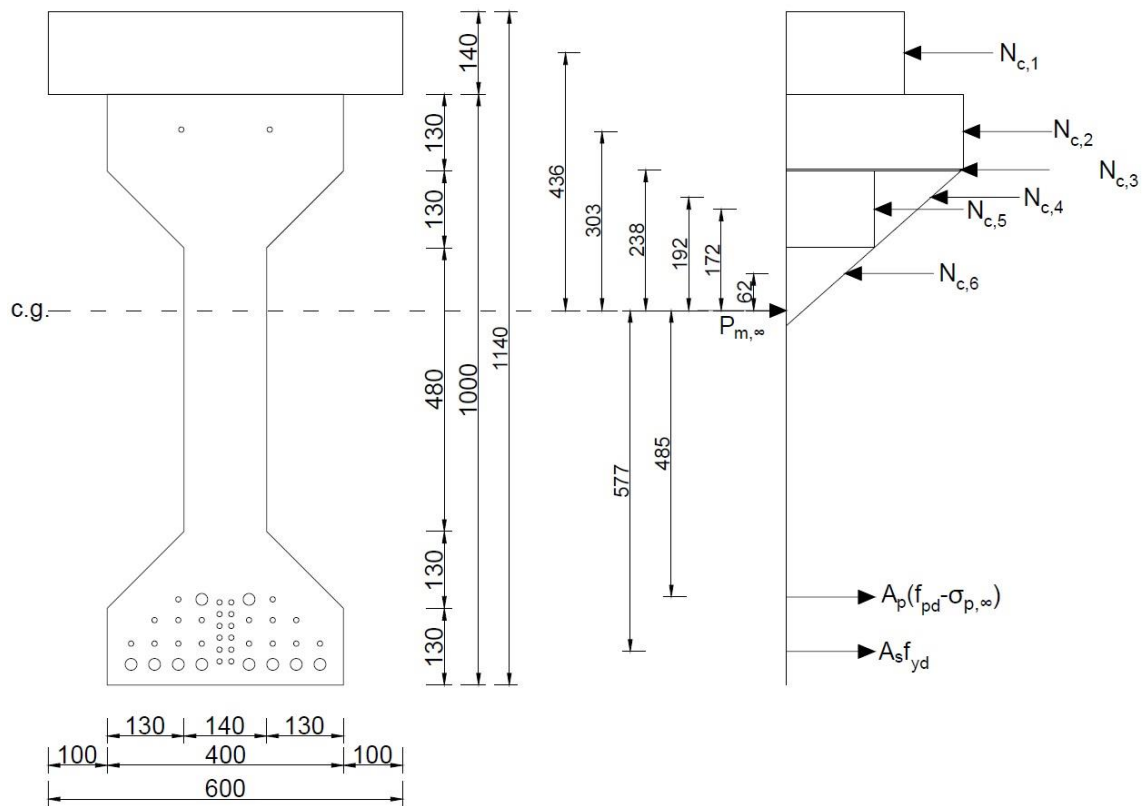


Figure C.6: Stress distribution

Table C.5: Calculation bending moment resistance

$N_{c,1}$	2240.0 [kN]	436 [mm]
$N_{c,2}$	2013.3 [kN]	303 [mm]
$N_{c,3,1}$	65.7 [kN]	238 [mm]
$N_{c,3,2}$	0.5 [kN]	238.7 [mm]
$N_{c,4,1}$	360.6 [kN]	171 [mm]
$N_{c,4,2}$	178.0 [kN]	192.7 [mm]
$N_{c,5,1}$	360.6 [kN]	192.7 [mm]
$N_{c,5,2}$	178.0 [kN]	221.6 [mm]
$N_{c,6}$	182.6 [kN]	62 [mm]
N_c	5579.2 [kN]	

Shear capacity

The shear resistance is calculated according to the Eurocode NEN-EN 1992-1-1.

Table C.6: Input shear resistance calculation

		Value	Units
Prestressing force	$P_{m,\infty}$	1482	[kN]
Compressive stress concrete	σ_{cp}	4.6	[MPa]
Reinforcement ratio	ρ_l	0.011	[-]

The shear resistance in the region without flexural cracks (shear tension failure) is:

$$V_{Rd,c} = \frac{I \cdot b_w}{S} \sqrt{f_{ctd}^2 + \alpha_l \sigma_{cp} f_{ctd}} = \frac{501 \cdot 10^8 \cdot 140}{55.2 \cdot 10^6} \sqrt{2.1^2 + 1.0 \cdot 4.6 \cdot 2.1} = 470.6 \text{ kN}$$

The shear resistance in the region with flexural cracks (flexural shear failure) is:

$$V_{Rd,c,mid} = (C_{Rd,c} k (100 \rho_l f_{ck})^{1/3} + k_1 \sigma_{cp}) b_w d = (0.12 \cdot 1.50 \cdot (100 \cdot 0.020 \cdot 60)^{1/3} + 0.15 \cdot 4.6) \cdot 140 \cdot 799 = 175.8 \text{ kN}$$

$$k = 1 + \sqrt{\frac{200}{d}} = 1 + \sqrt{\frac{200}{799}} = 1.50$$

$$V_{Rd,c,end} = (C_{Rd,c} k (100 \rho_l f_{ck})^{1/3} + k_1 \sigma_{cp}) b_w d = (0.12 \cdot 1.45 \cdot (100 \cdot 0.020 \cdot 60)^{1/3} + 0.15 \cdot 4.6) \cdot 140 \cdot 991 = 213.8 \text{ kN}$$

$$k = 1 + \sqrt{\frac{200}{d}} = 1 + \sqrt{\frac{200}{991}} = 1.45$$

The maximum shear resistance is:

$$V_{Rd,max} = \frac{\alpha_{cw} b_w z v_1 f_{cd} (\cot(\theta) + \tan(\theta))}{1 + \cot^2(\theta)} = \frac{1.11 \cdot 140 \cdot 0.9 \cdot 911 \cdot 0.6 \cdot 26.7 \cdot (\cot(21) + \tan(21))}{1 + \cot^2(21)} = 890.1 \text{ kN}$$

The maximum point load that can be applied is:

$$P = V_{Rd,c} + 37.9 - 75.8$$

Table C.7: Shear resistance specimen I-C

	Point load	
Region I	432.7	[kN]
Region II	137.9	[kN]

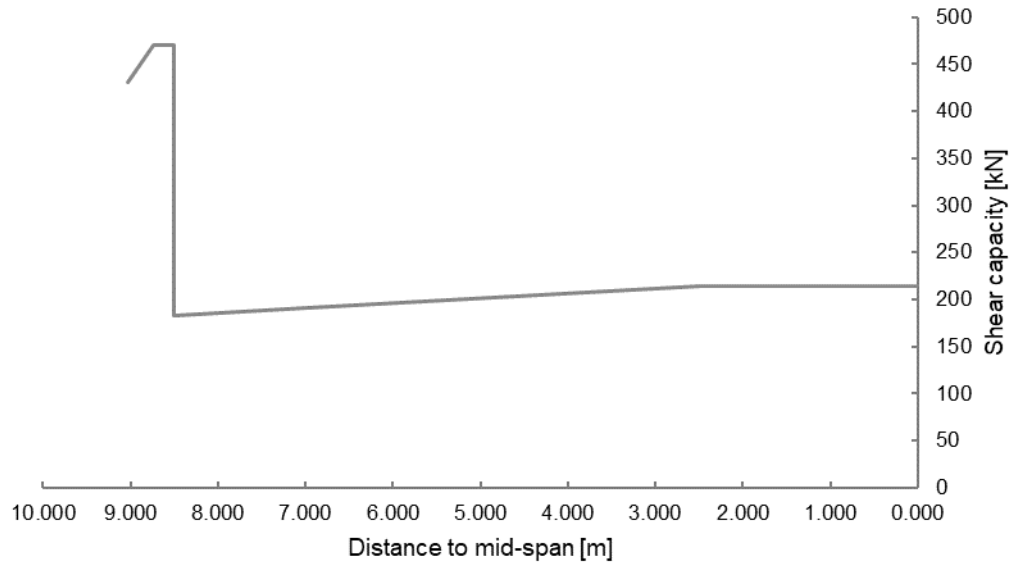


Figure C.7: Shear resistance specimen I-C

D. Finite element model specimens

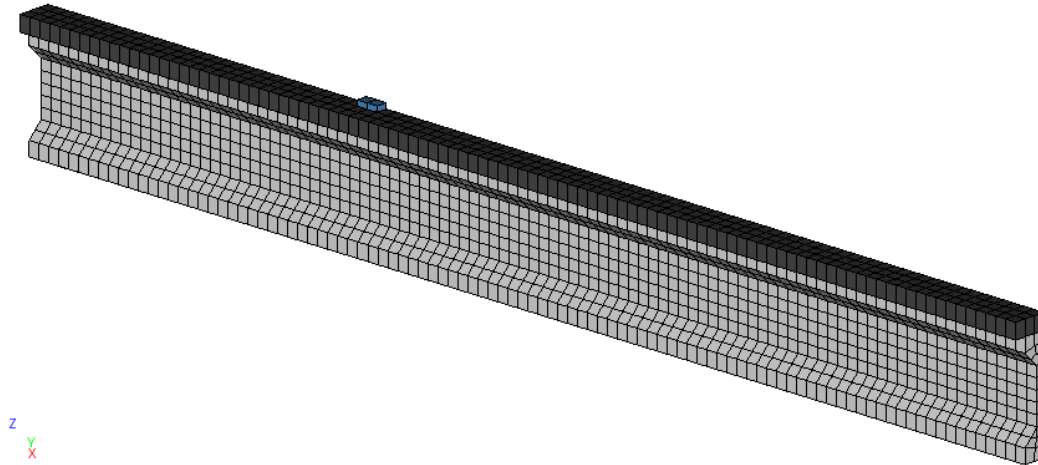


Figure D.1: Finite element model reference specimen I-C-SP3

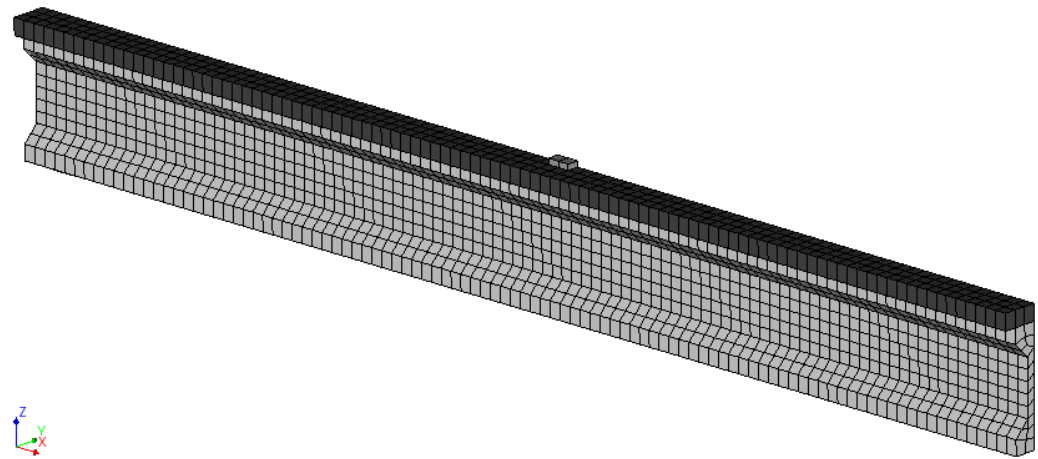


Figure D.2: Finite element model reference specimen I-C-SP5

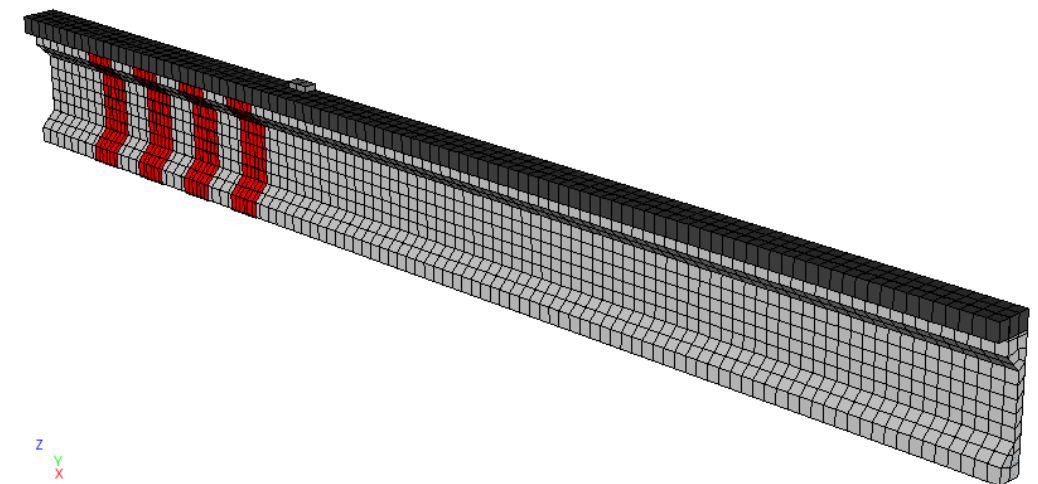


Figure D.3: Finite element model specimen I-V-SP3

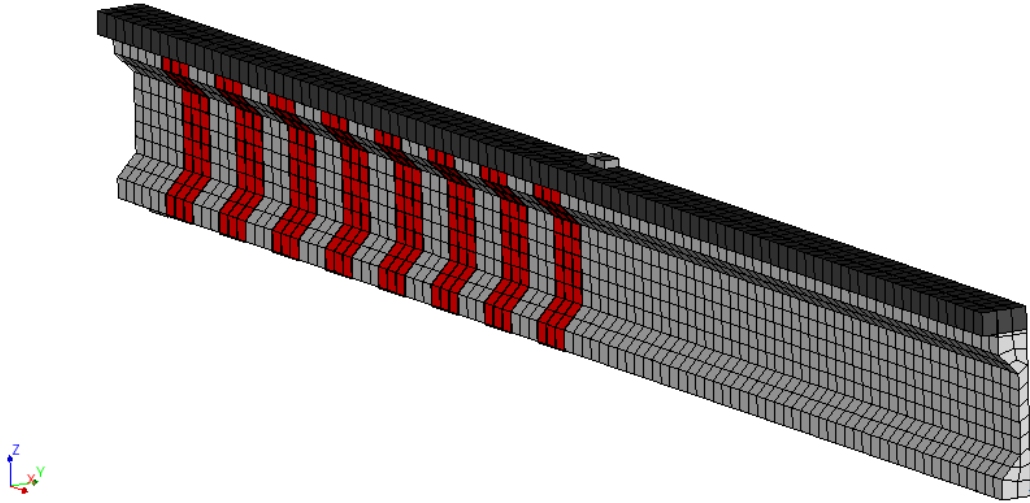


Figure D.4: Finite element model specimen I-V-SP5

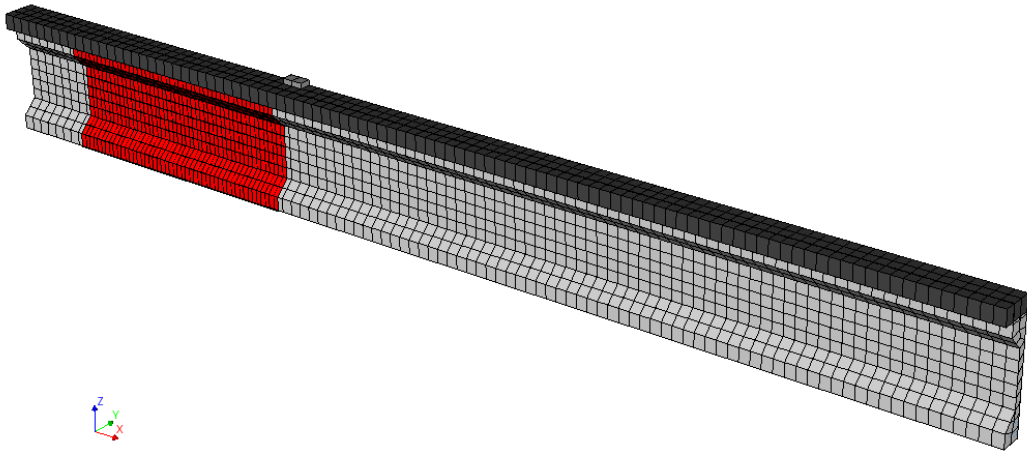


Figure D.5: Finite element model specimen I-V-S0-SP3

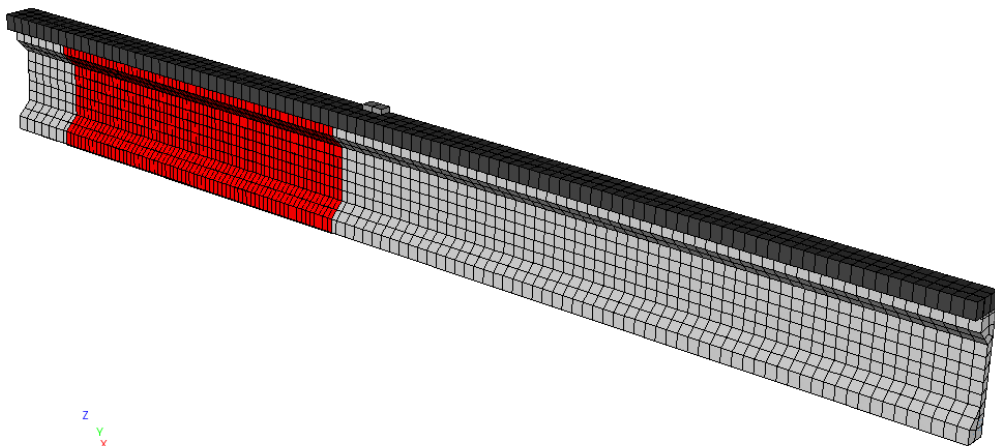


Figure D.6: Finite element model specimen I-V-S0-SP4

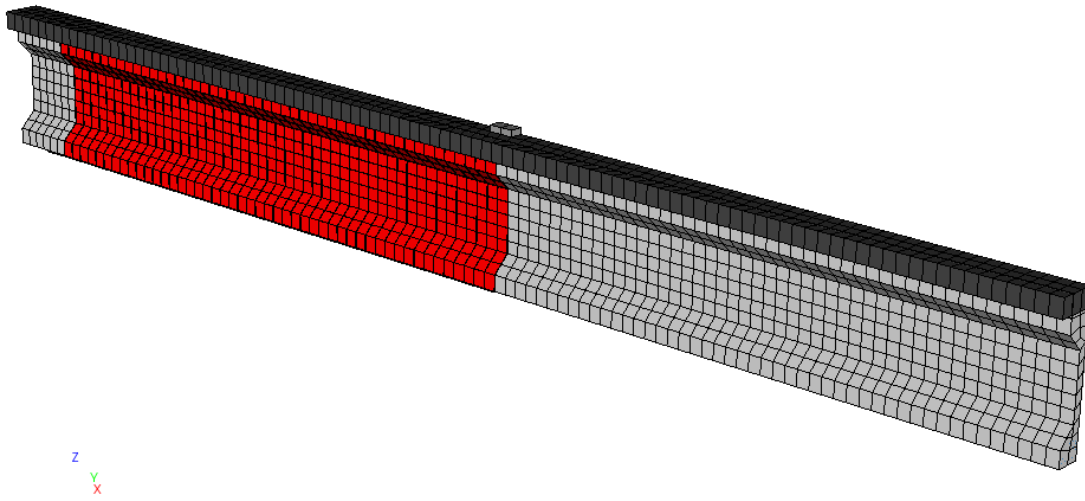


Figure D.7: Finite element model specimen I-V-S0-SP5

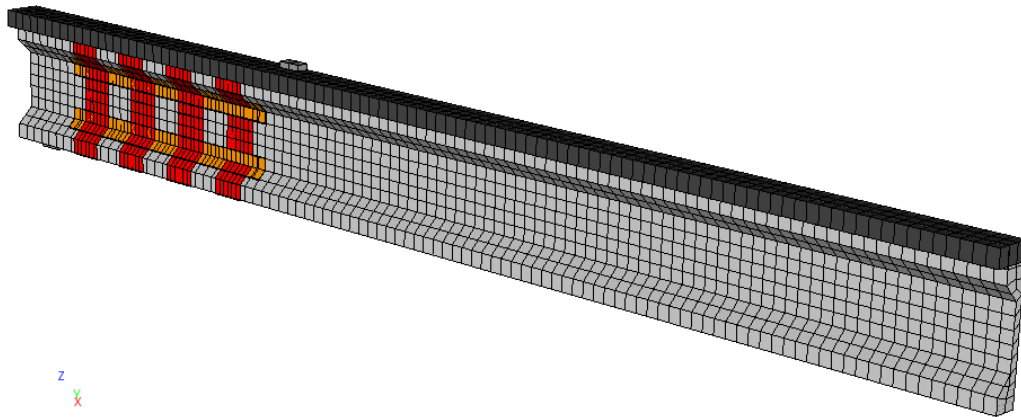


Figure D.8: Finite element model specimen I-VH-SP3

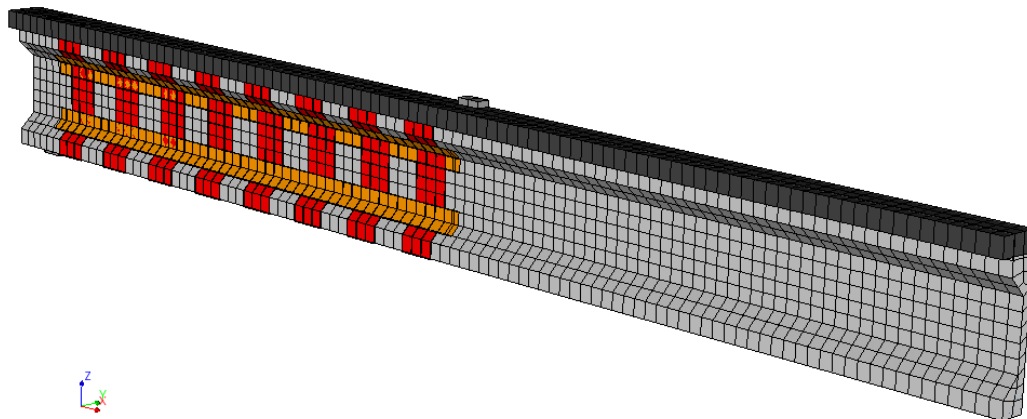


Figure D.9: Finite element model specimen I-VH-SP5

E. Nonlinear finite element analyses results

E.1. NLFEA results specimen I-C

The principal strain and crack strain plots of specimens I-C-SP3, I-C-SP4 and I-C-SP5 are given in Figure E.1, Figure E.2 and Figure E.3.

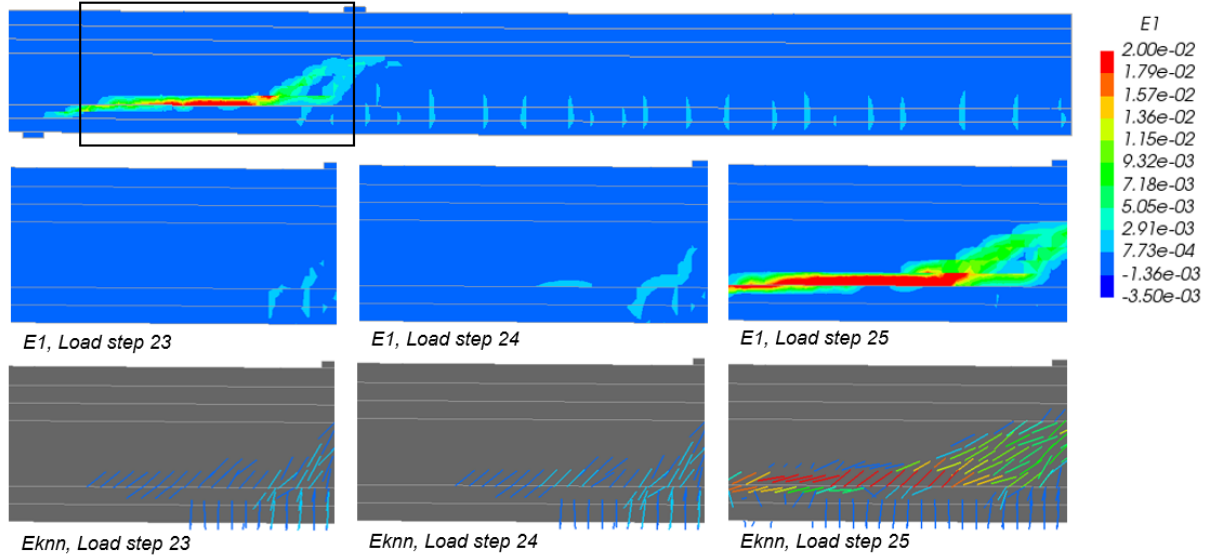


Figure E.1: Principal strain and crack strain values specimen I-C-SP3

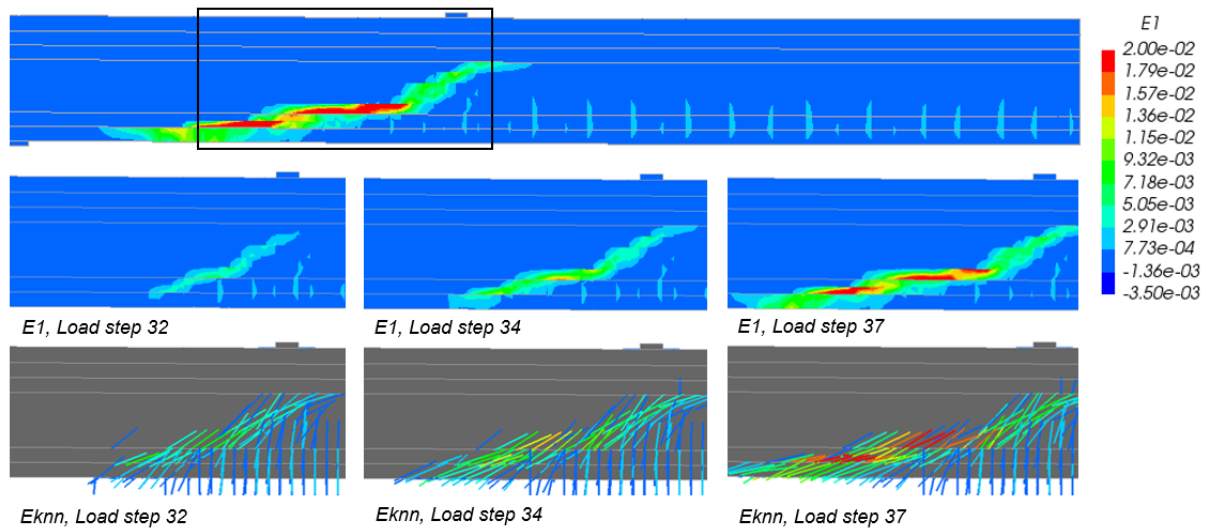


Figure E.2: Principal strain and crack strain values specimen I-C-SP4

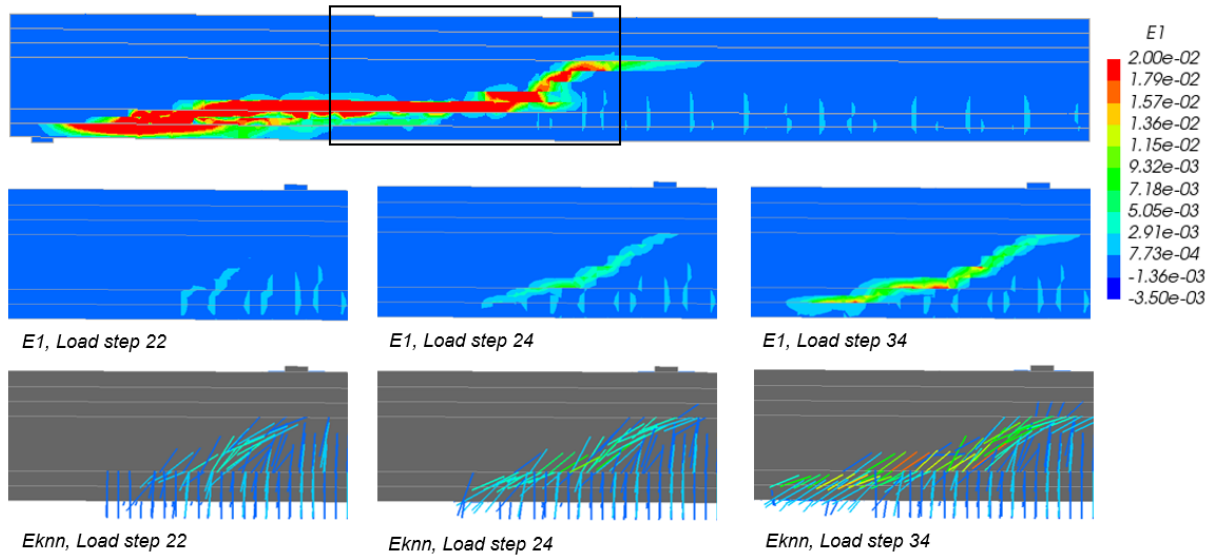


Figure E.3: Principal strain and crack strain values specimen I-C-SP5

E.2. NLFEA results specimen I-V

The principal strain and crack strain plots of the specimens I-V-SP3, I-V-SP4 and I-V-SP5 are presented in Figure E.4, Figure E.5 and Figure E.6. The CFRP sheets pulling away from the re-entrant corner between the web and the bottom flange of the specimens I-V-SP3 and I-V-SP5 is given in Figure E.7 and Figure E.8.

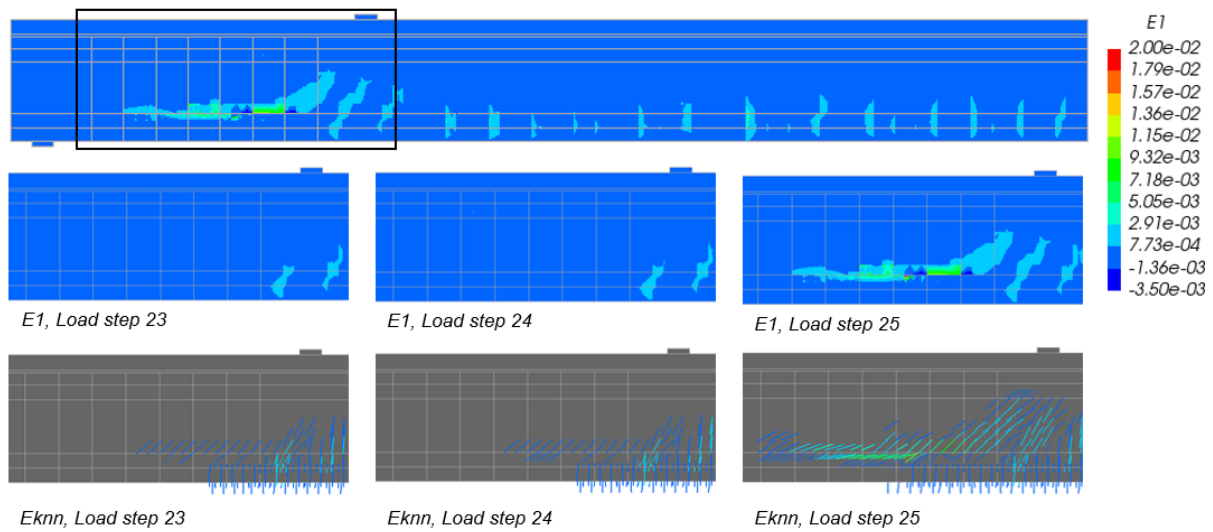


Figure E.4: Principal strain and crack strain values specimen I-V-SP3

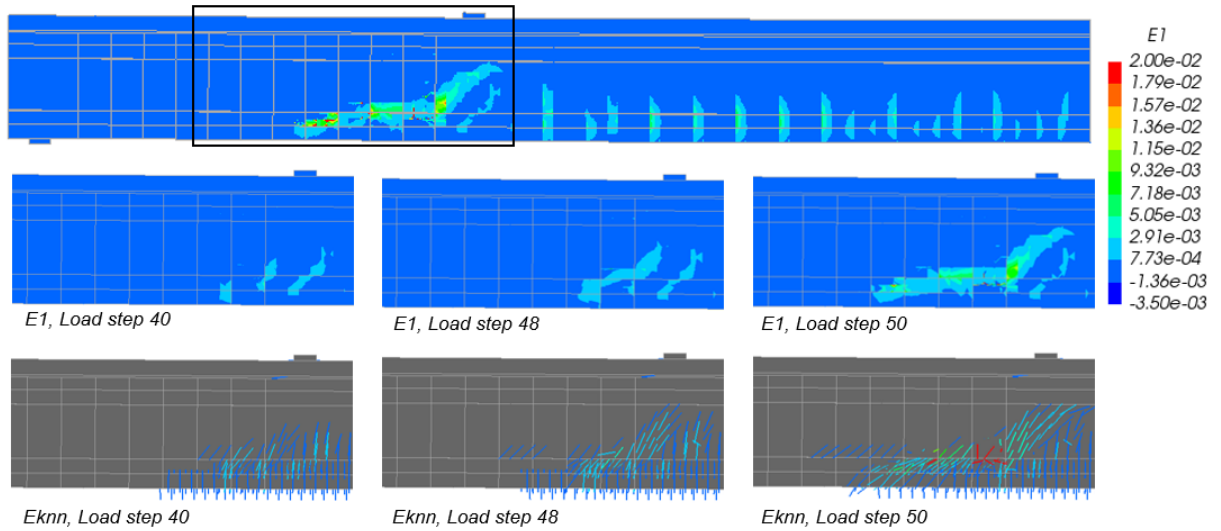


Figure E.5: Principal strain and crack strain values specimen I-V-SP4

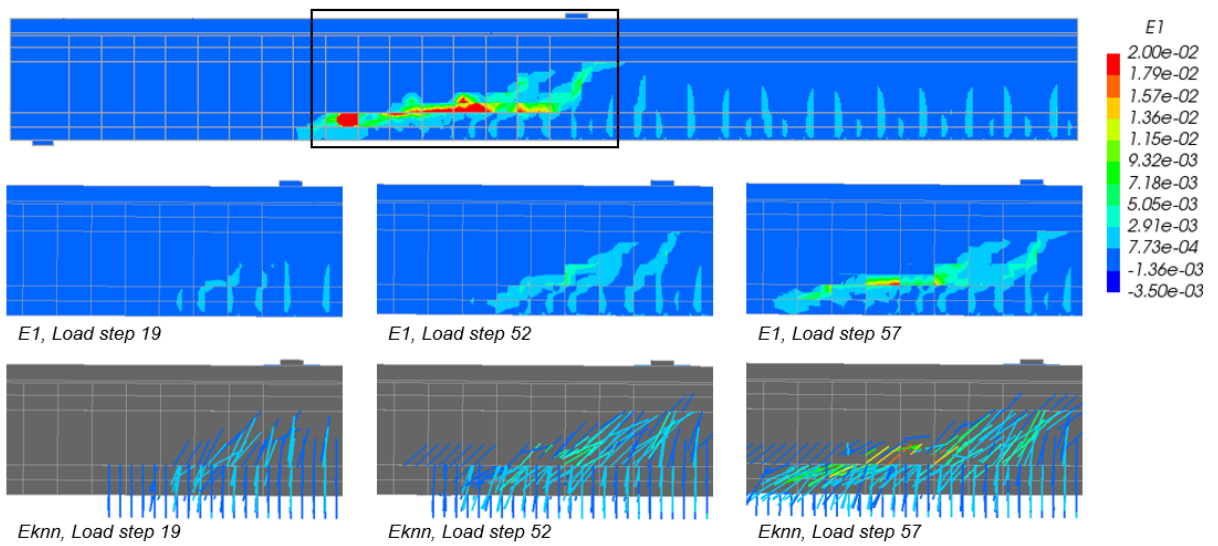


Figure E.6: Principal strain and crack strain values specimen I-V-SP5

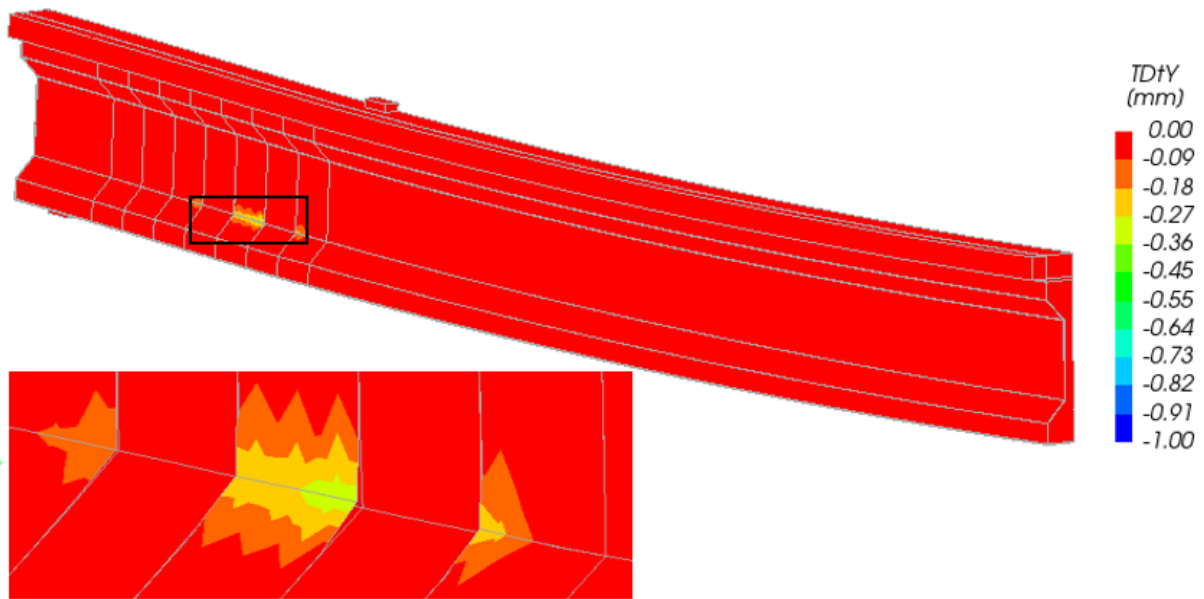


Figure E.7: Debonding CFRP sheets in re-entrant corner specimen I-V-SP3

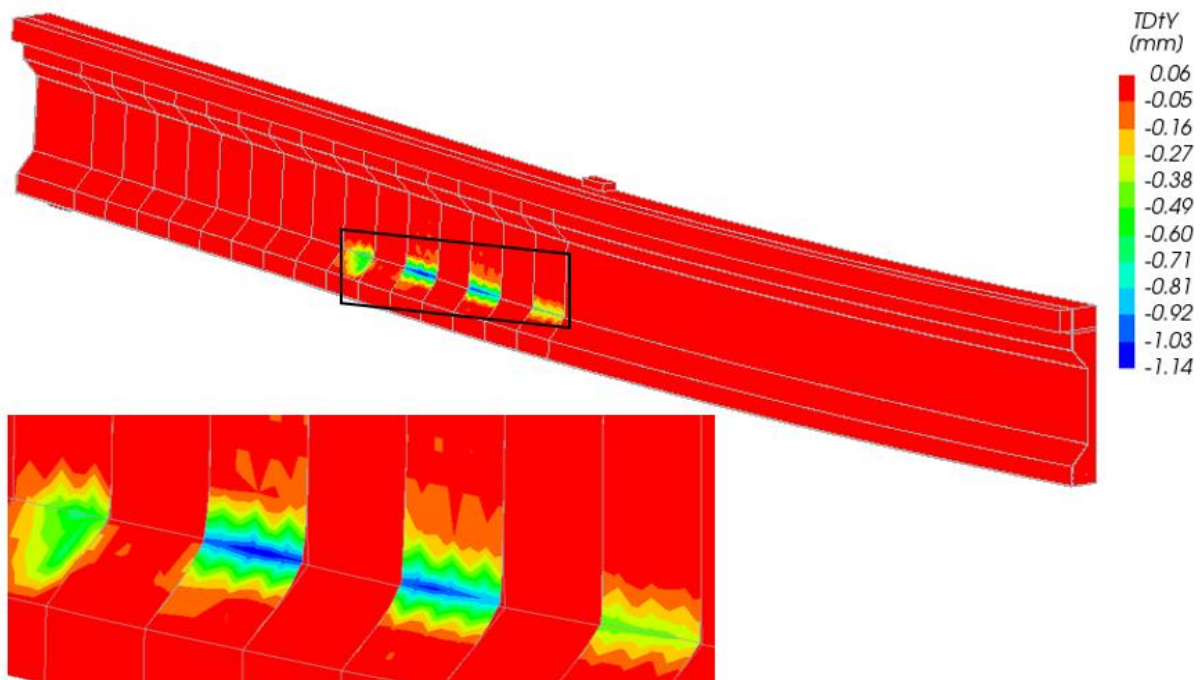


Figure E.8: Debonding CFRP sheets in re-entrant corner specimen I-V-SP5

E.3. NLFEA results specimen I-V-S0

The principal strain plots and crack strain plots of the specimens I-V-S0-SP3, I-V-S0-SP4 and I-V-S0-SP5 are presented in Figure E.9, Figure E.10 and Figure E.11.

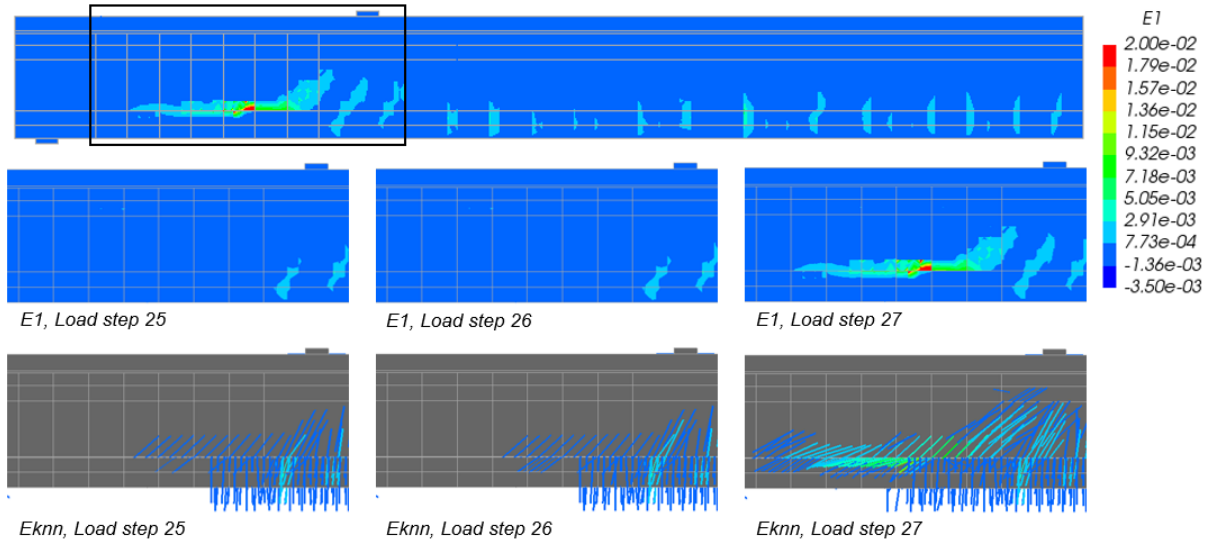


Figure E.9: Principal strain and crack strain values specimen I-V-S0-SP3

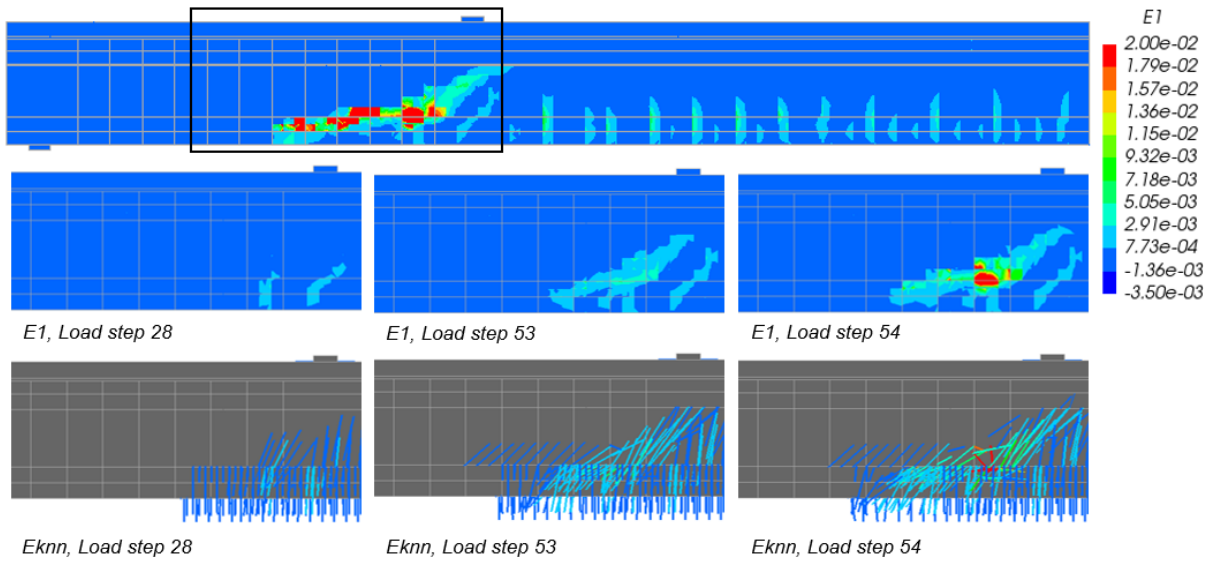


Figure E.10: Principal strain and crack strain values specimen I-V-S0-SP4

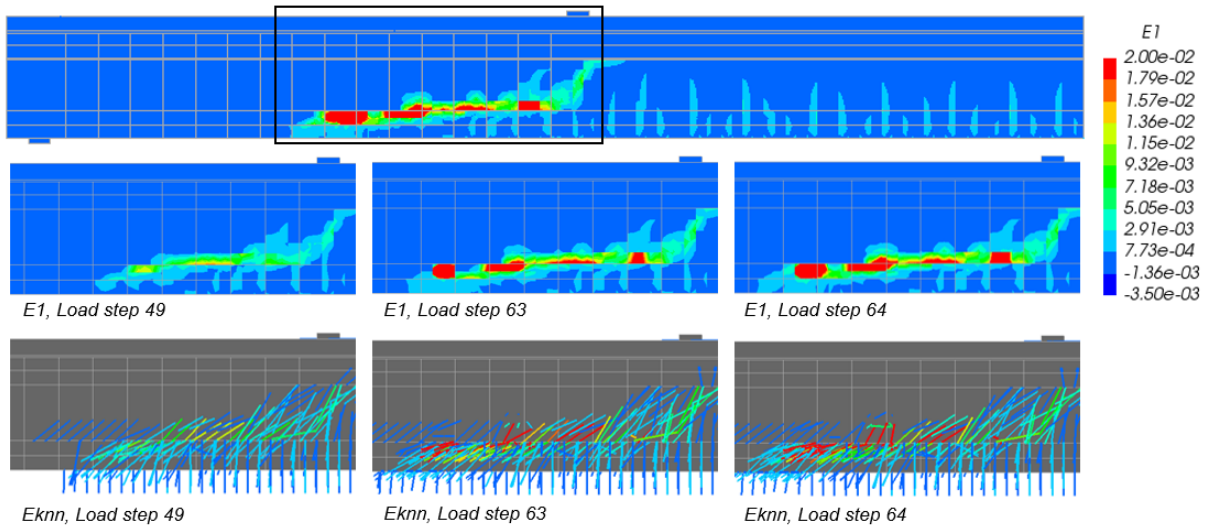


Figure E.11: Principal strain and crack strain values specimen I-V-S0-SP5

E.4. NLFEA results specimen I-V-L2

The principal strain plots and crack strain plots of the specimen I-V-L2-SP3, I-V-L2-SP4 and I-V-L2-SP5 are given in Figure E.12, Figure E.13 and Figure E.14.

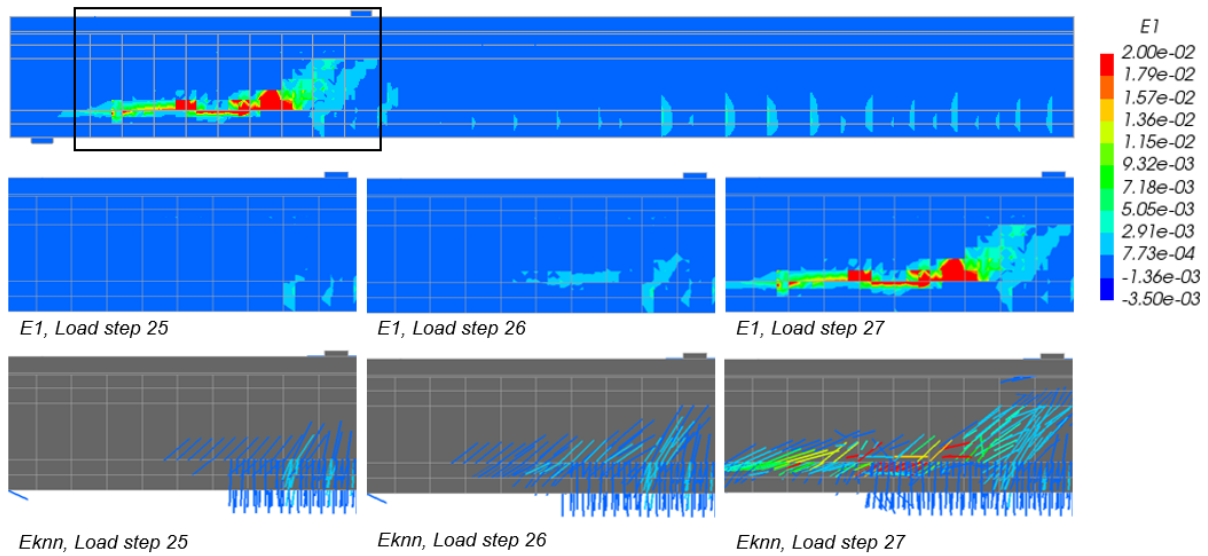


Figure E.12: Principal strain and crack strain values specimen I-V-L2-SP3

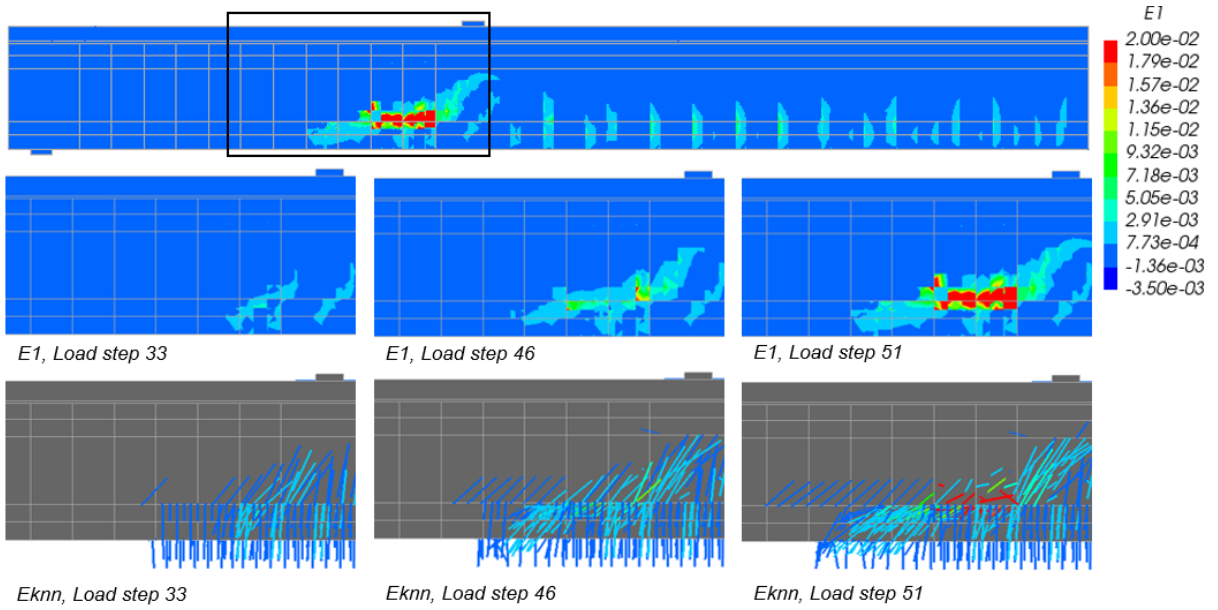


Figure E.13: Principal strain and crack strain values specimen I-V-L2-SP4

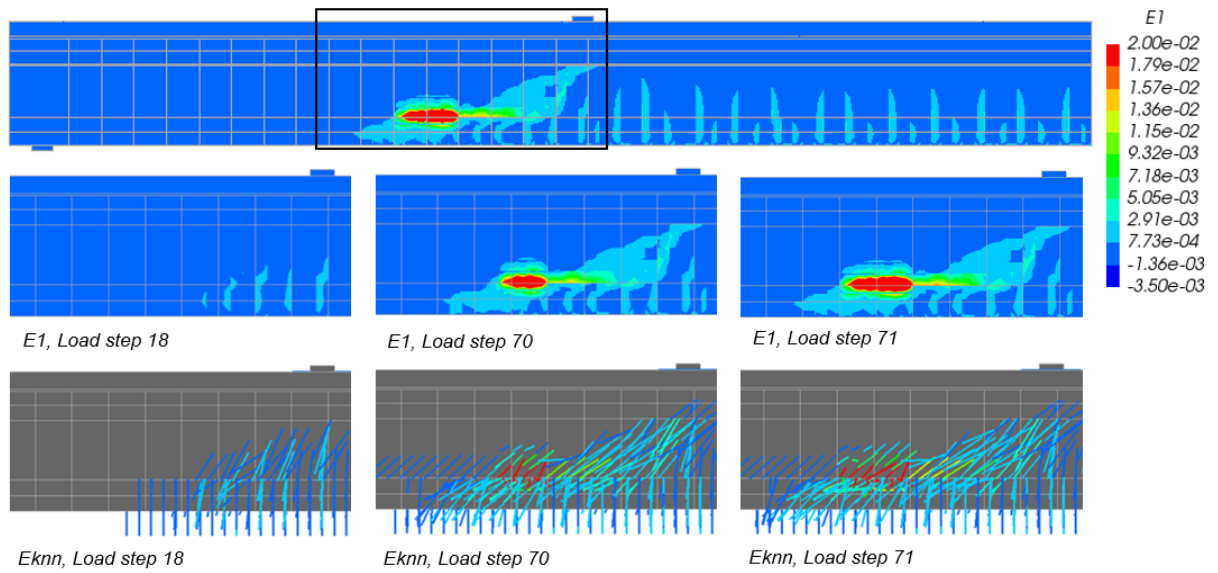


Figure E.14: Principal strain and crack strain values specimen I-V-L2-SP5

E.5. NLFEA results specimen I-V-PB

The peak loads of the specimens I-V-PB-SP3, I-V-PB-SP4 and I-V-PB-SP5 are given Table E.1 and the load-deformation curves are presented in Figure E.15. The local displacement in y-direction, principal strain and crack strain plot of the specimens I-V-SP5 and I-V-PB-SP5 are given in Figure E.16. The perfect bond between the CFRP elements and the concrete elements caused crack formation and local displacements of the concrete elements.

Table E.1: Peak load specimens I-V-PB-SP3, I-V-PB-SP4 and I-V-PB-SP5

	Shear span [m]	Peak load [kN]
I-C-SP3	3.0	559.8
I-V-SP3	3.0	572.6
I-V-PB-SP3	3.0	568.8
I-C-SP4	4.0	426.6
I-V-SP4	4.0	454.2*
I-V-PB-SP4	4.0	459.9
I-C-SP5	5.0	361.0
I-V-SP5	5.0	395.7
I-V-PB-SP5	5.0	397.2

* Peak load is the load in the last step before the analysis of specimen aborted.

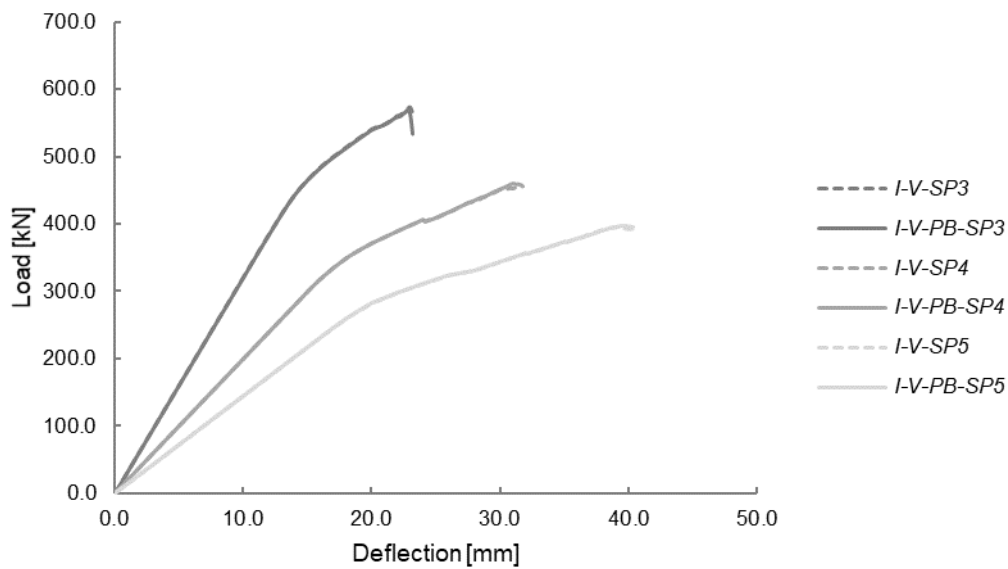


Figure E.15: Load-deflection curves specimens I-V-PB-SP3, I-V-PB-SP4 and I-V-PB-SP5

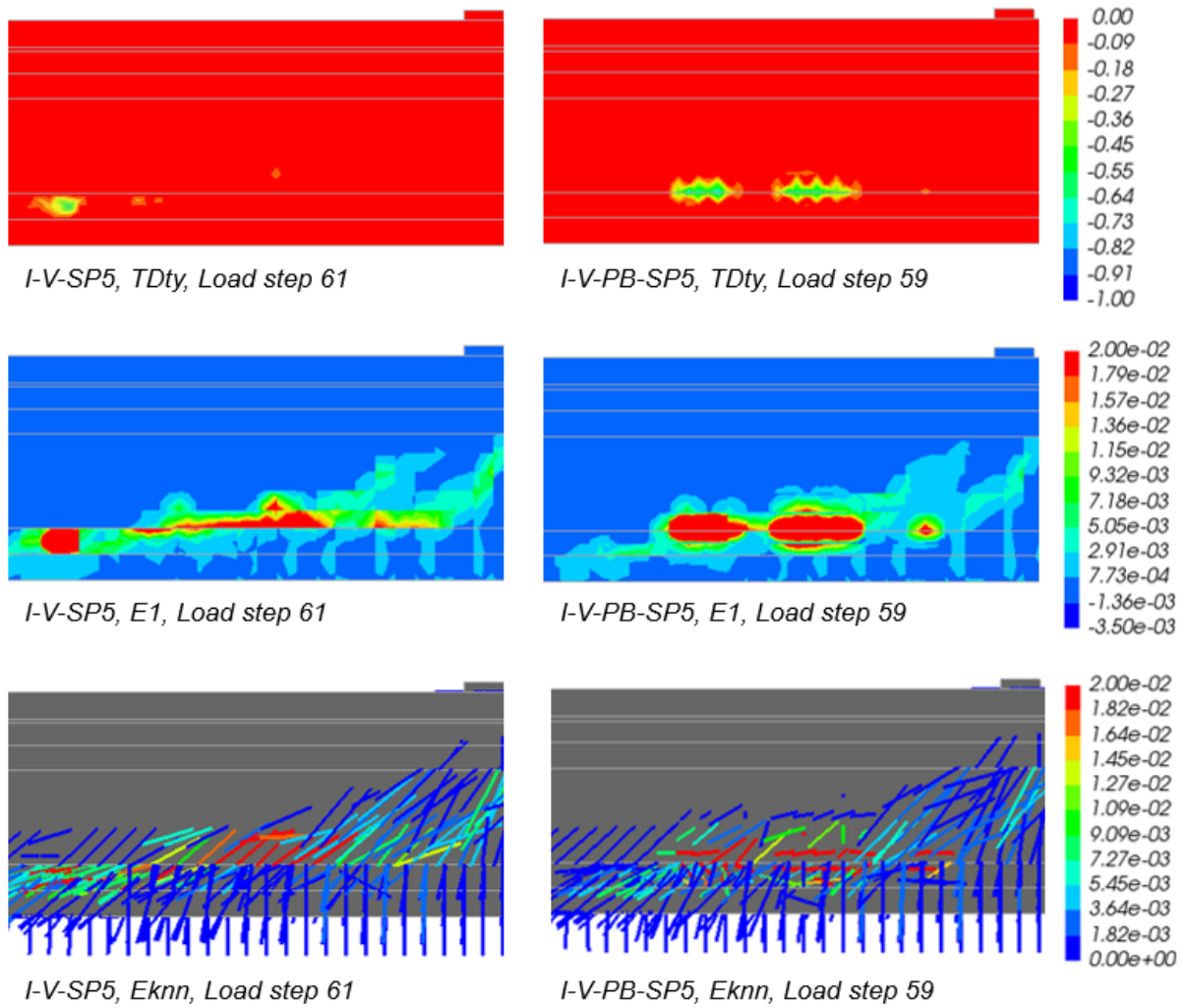


Figure E.16: Displacement and strain plots specimens I-V-SP5 and I-V-PB-SP5

E.6. NLFEA results specimen I-VH

The principal strain and crack strain plots of the specimens I-VH-SP3, I-VH-SP4 and I-VH-SP5 are given in Figure E.17, Figure E.18 and Figure E.19.

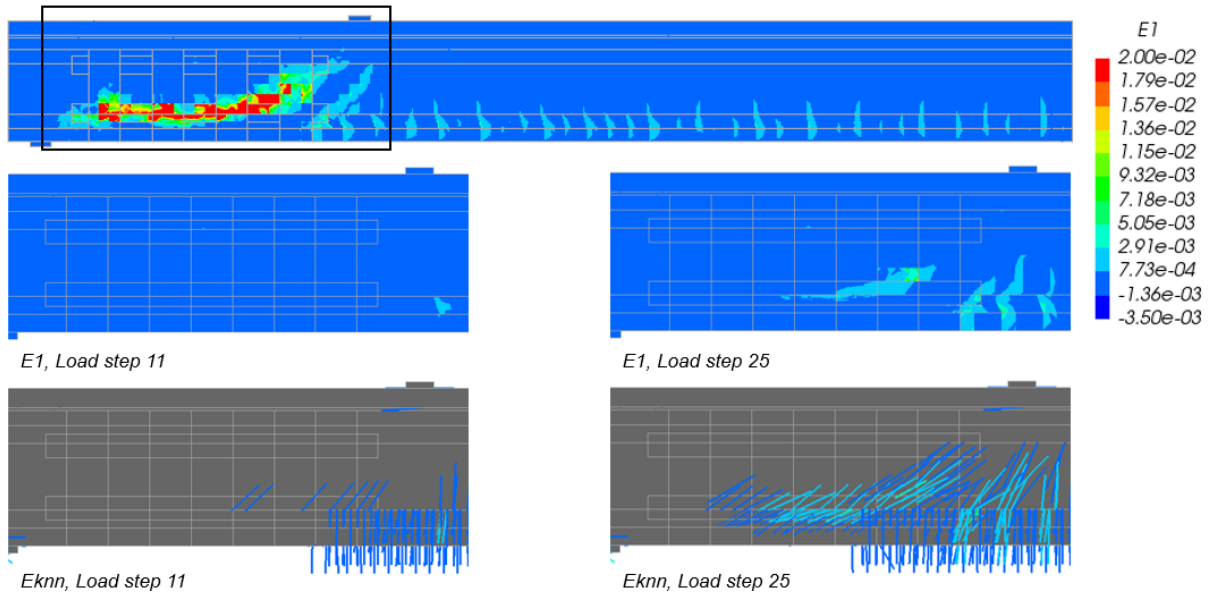


Figure E.17: Principal strain and crack strain values specimen I-VH-SP3

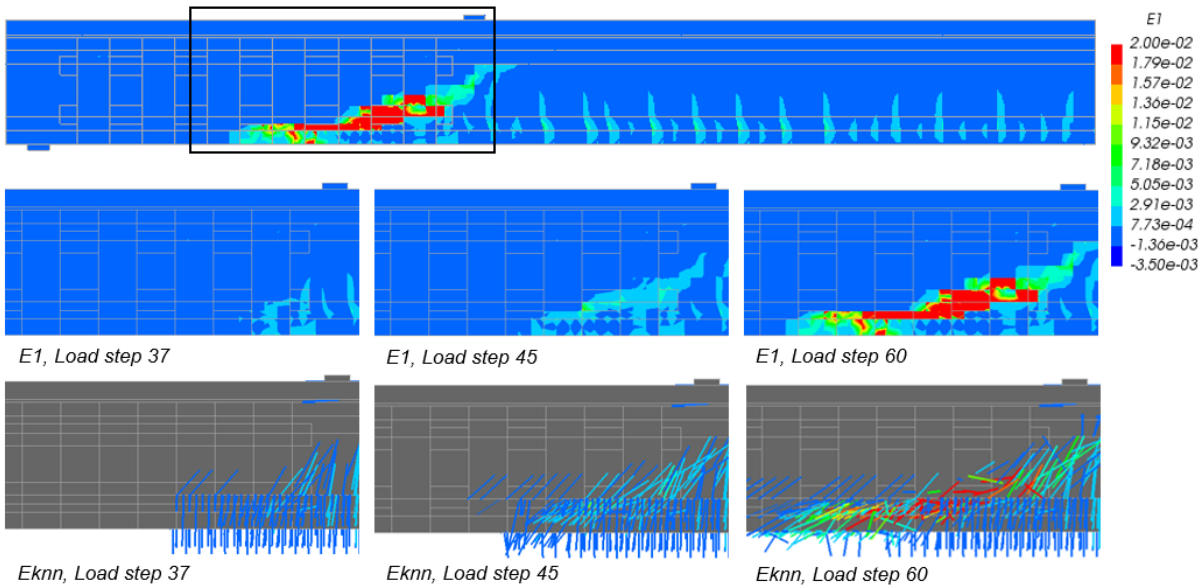


Figure E.18: Principal strain and crack strain values specimen I-VH-SP4

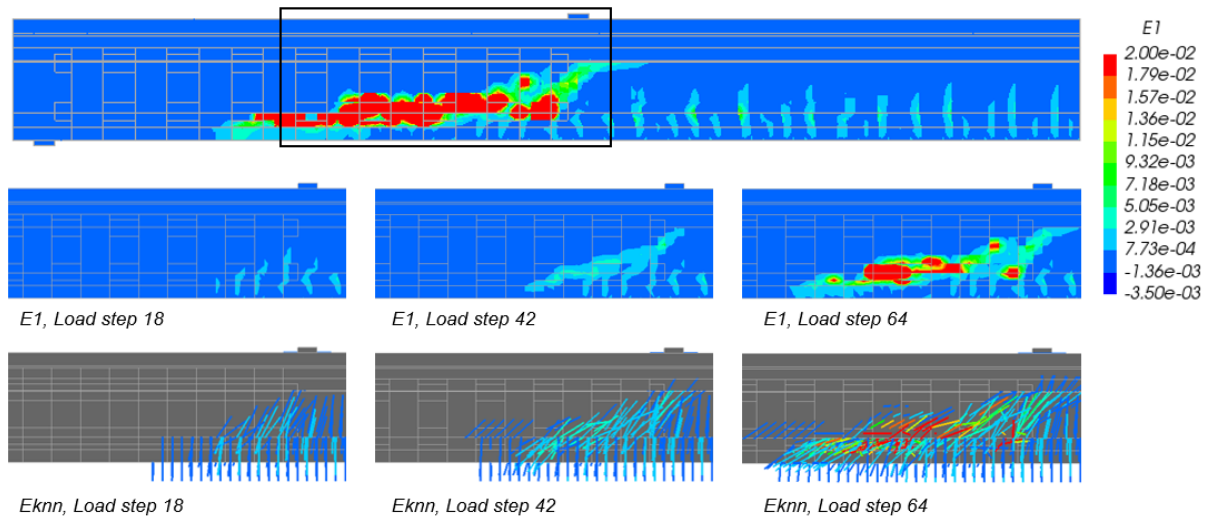


Figure E.19: Principal strain and crack strain values specimen I-VH-SP5

E.7. NLFEA results specimen I-VA

The principal strain and crack strain plots of the specimens I-VH-SP3, I-VH-SP4 and I-VH-SP5 are presented in Figure E.20, Figure E.21 and Figure E.22.

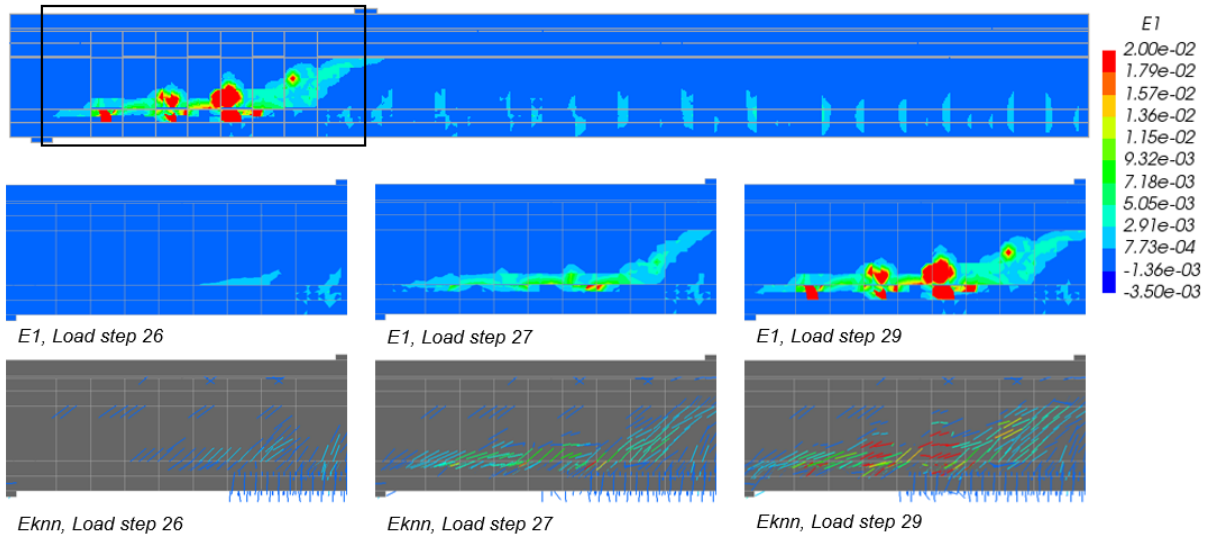


Figure E.20: Principal strain and crack strain values specimen I-VA-SP3

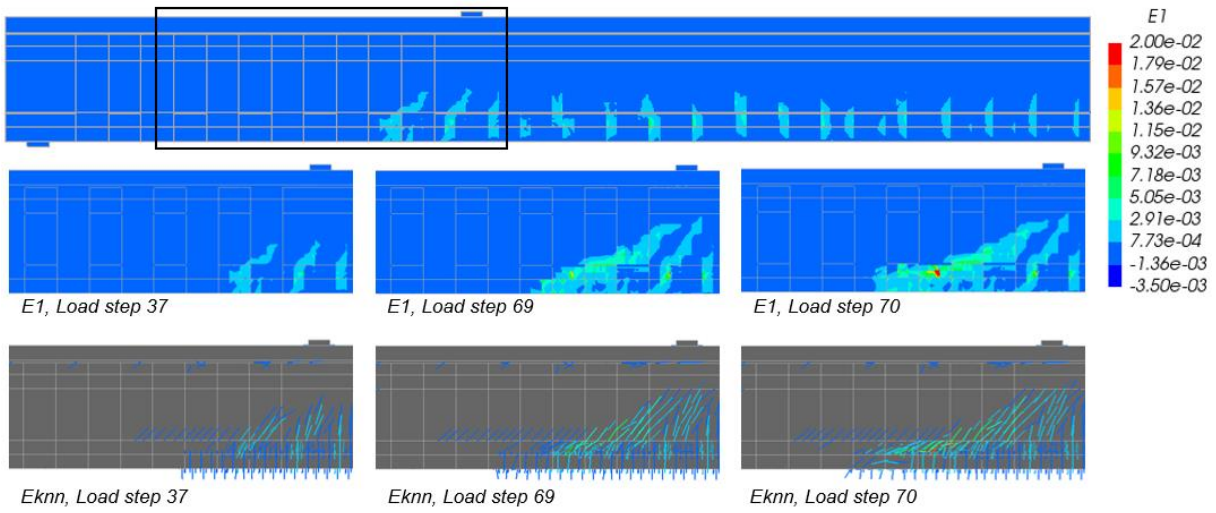


Figure E.21: Principal strain and crack strain values specimen I-VA-SP4

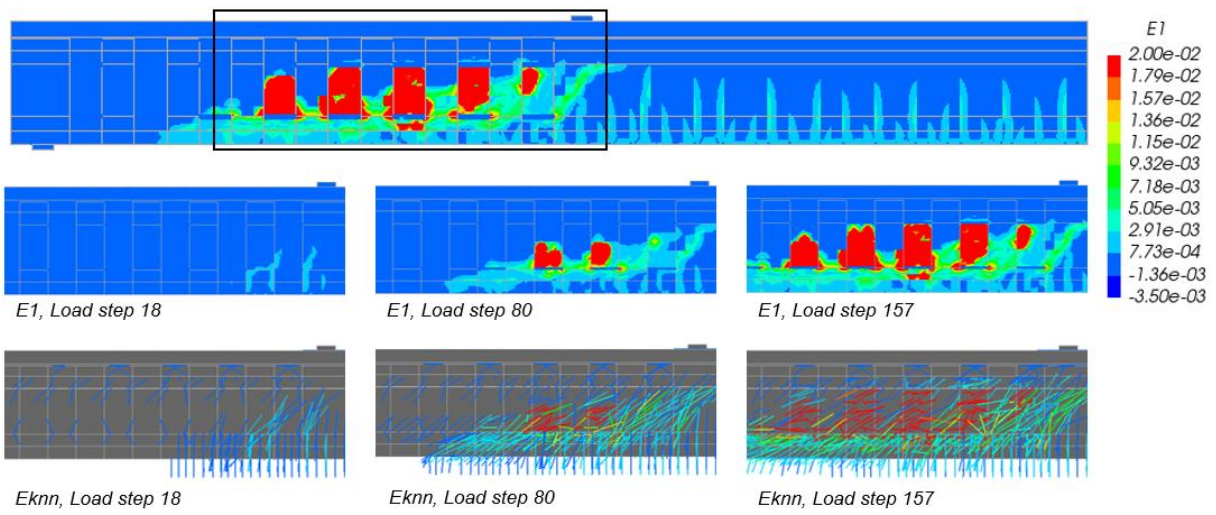


Figure E.22: Principal strain and crack strain values specimen I-VA-SP5

E.8. NLFEA results specimen I-VA-S0

Figure E.23, Figure E.24 and Figure E.25 show the principal strain and crack strain plots of the specimens I-VA-S0-SP3, I-VA-S0-SP4 and I-VA-S0-SP5.

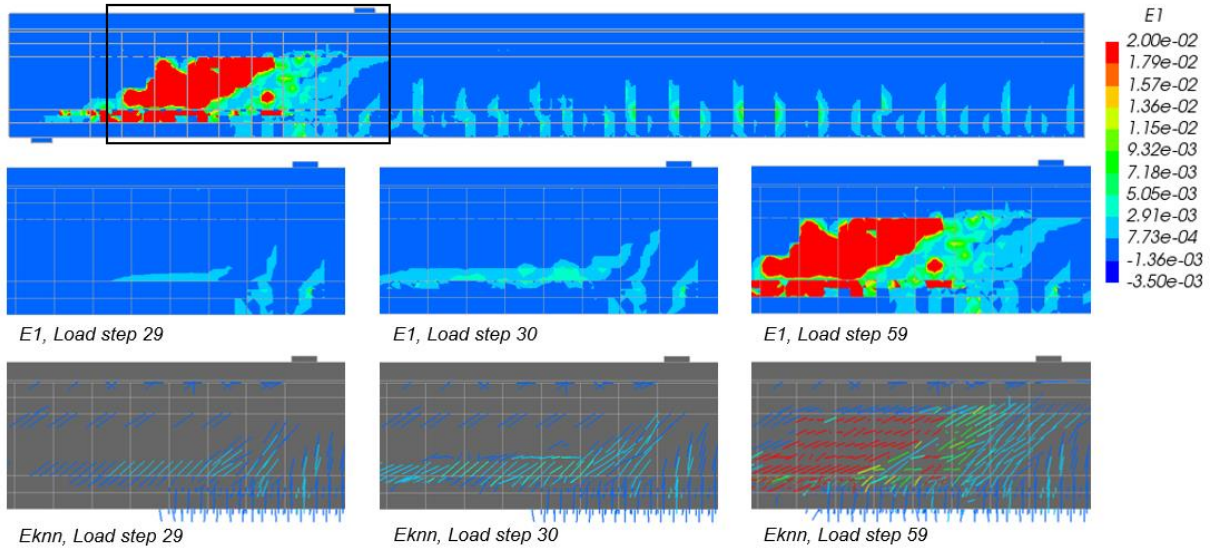


Figure E.23: Principal strain and crack strain values specimen I-VA-S0-SP3

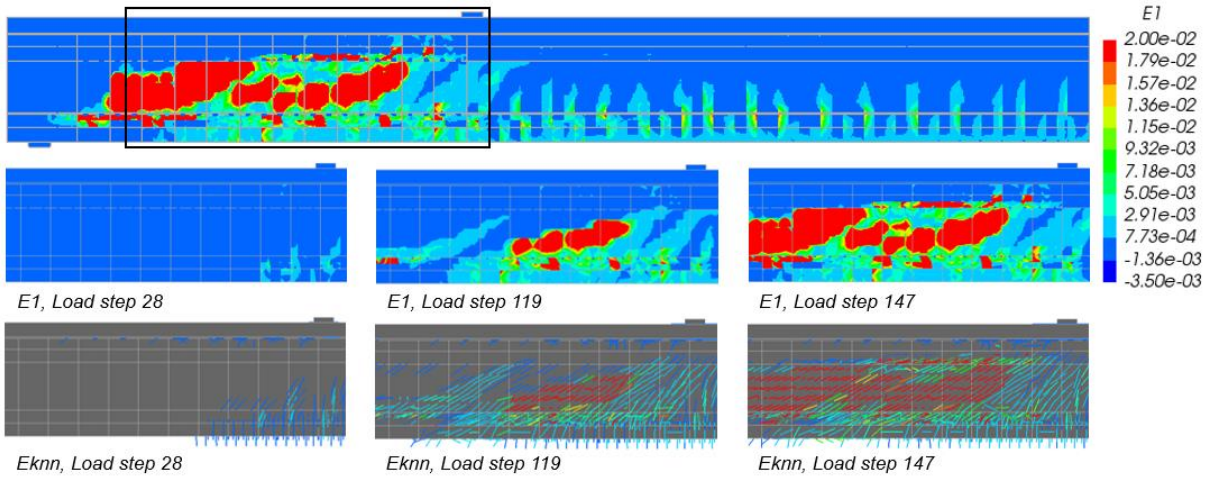


Figure E.24: Principal strain and crack strain values specimen I-VA-S0-SP4

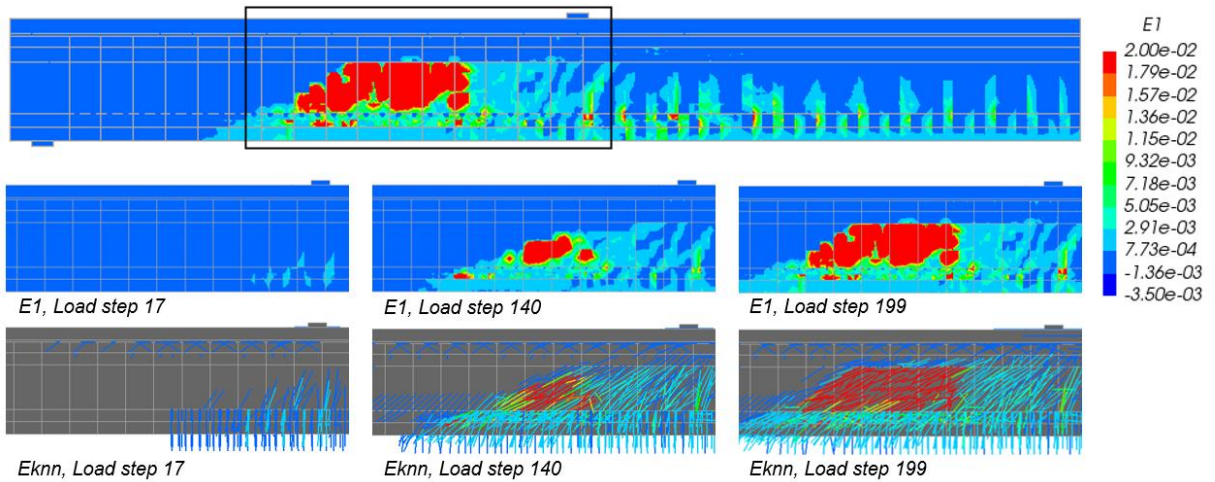


Figure E.25: Principal strain and crack strain values specimen I-VA-S0-SP4

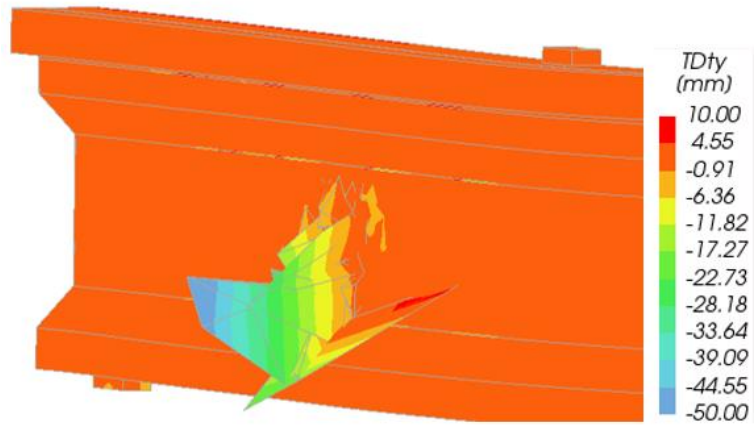


Figure E.26: Local displacements specimen I-VA-S0-SP3 at load step 60



Figure E.27: Local displacements specimen I-VA-S0-SP4 at load step 148

F. Nonlinear finite element analysis I-girder Ary and Kang

F.1. Experimental results Ary and Kang

Experimental test setup

Ary and Kang (2012) did investigate the shear behaviour of prestressed concrete I-girders strengthened with externally bonded CFRP reinforcement. Three prestressed concrete I-girders were designed to investigate the effect of the CFRP reinforcement. The three specimens were designed to fail in shear. The cross-section of the specimens is illustrated in Figure F.1. The test specimens did not have shear reinforcement in the shear span. The test specimens are prestressed with 2 seven-wire strands. The specimens were simply supported and were tested with a four-point bending test. The setup of the experimental test is given in Figure F.2.

Experimental results

According to Ary and Kang (2012) the control beam failed in shear failure with shear cracks propagating from the support to the loading point. They did not mention a specific type of shear failure. The failure pattern of the control specimen is given in Figure F.3. The experimental results of the control specimen are presented in Table F.1 and the load-deflection curve of the control specimen is presented in Figure F.4.

Table F.1: Experimental results control specimen

	Failure load [kN]	Shear load [kN]	Cracking load [kN]
Control specimen	234.9	117.4	176.3

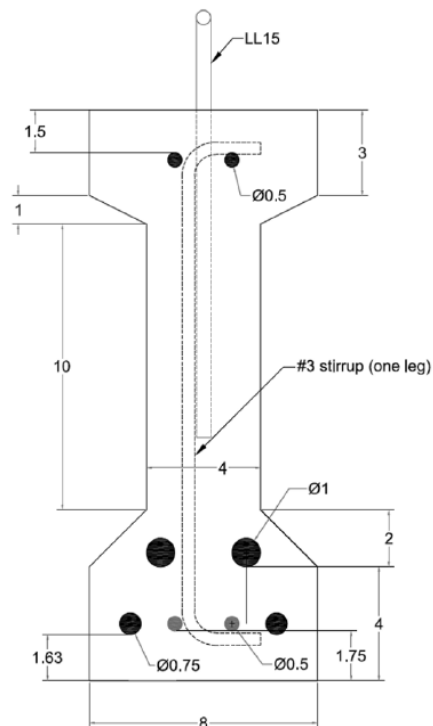


Figure F.1: Cross-section control specimen I-girder

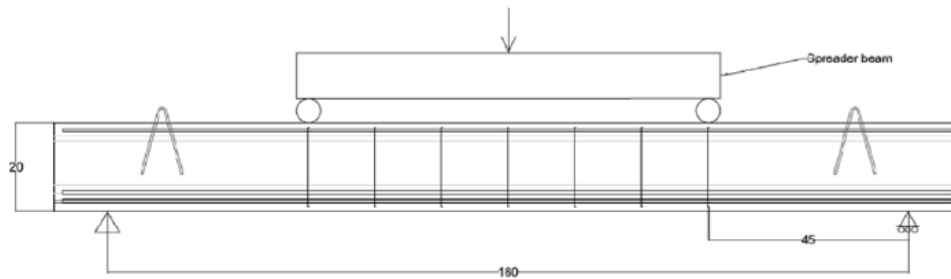


Figure F.2: Geometry control specimen I-girder

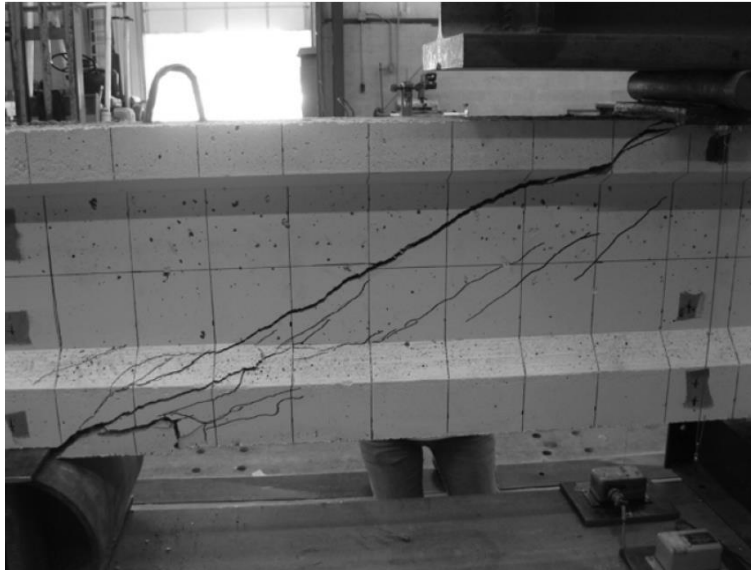


Figure F.3: Crack pattern control specimen I-girder

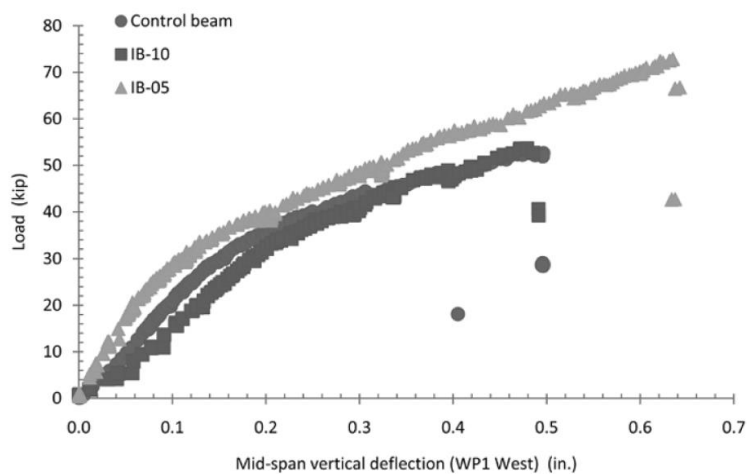


Figure F.4: Load-deflection curve

F.2. Nonlinear finite element model

Geometry

The mechanical model of control specimen was divided in a finite number of three-dimensional brick elements with a typical element size of 50x50x50 mm. The reinforcement bars and the prestressing strands were modelled as line elements. The support and loading plate were modelled as three-dimensional brick elements.

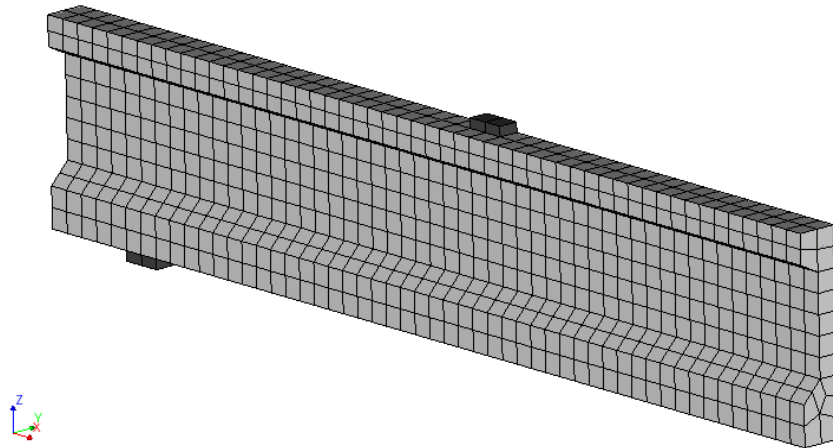


Figure F.5: Finite element model

Material properties

The material properties are given in Table F.2. The effect of the fixed and rotating crack have been investigated.

Table F.2: Constitutive model finite element analysis control specimen

Constitutive concrete model		
Density	2400	kg/m ³
Crack model	Total strain crack	
Tensile curve	Hordijk	
Compression curve	Parabolic	
Crack bandwidth estimator	Govindjee	
Tensile strength	4.2	MPa
Compressive strength reduction	Vecchio & Collins (1993)	
Minimal reduction factor	0.4	
Confinement	Vecchio & Selby	
Poisson reduction	Damage based	
Compressive strength	61	MPa
Steel constitutive model		
Density	7850	kg/m ³
Plasticity model	Von Mises	
Von Mises type	Isotropic linear hardening	
Equilibrium conditions		
Load step size	0.1	
Type	Deformation controlled	
Iteration scheme	Regular Newton-Raphson	

F.3. Nonlinear finite element analysis

Fixed crack, embedded reinforcement

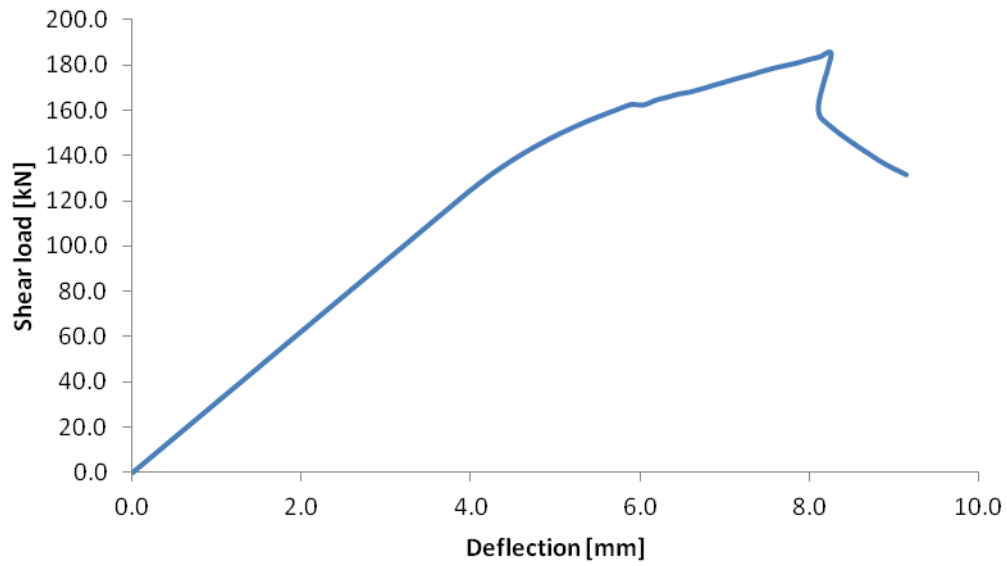


Figure F.6: Load-deflection curve control specimen fixed crack model

Control_beam_analysis_V0.5
 Load-step 02, Load-factor 0.1000, LC 2
 Total Strains E1
 min: -2.79e-05 max: 5.01e-03

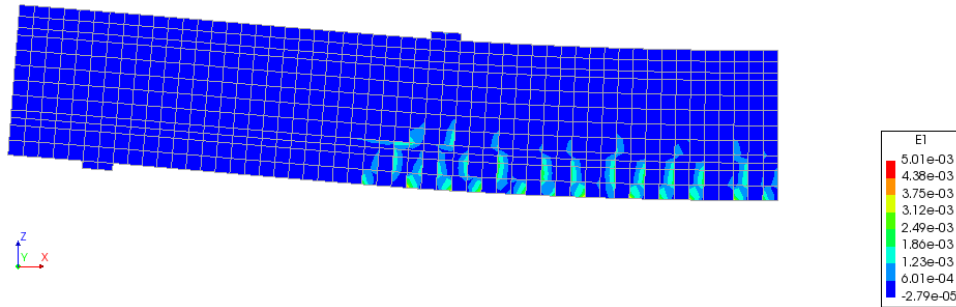


Figure F.7: Principal strain (E1) load step 62

Control_beam_analysis_V0.5
 Load-step 03, Load-factor 0.2000, LC 2
 Total Strains E1
 min: -4.33e-05 max: 4.58e-02

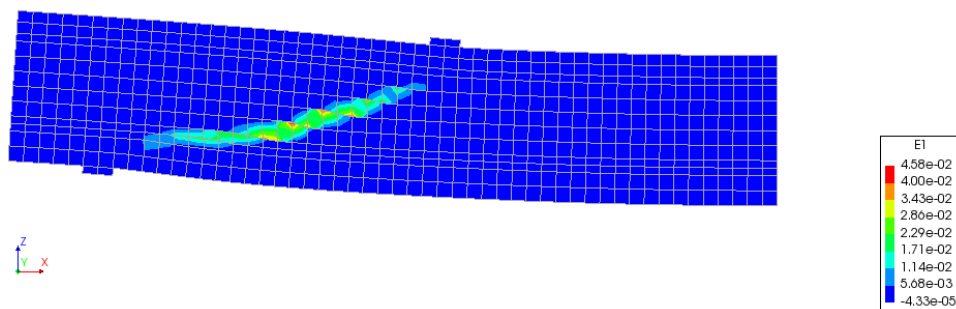


Figure F.8: Principal strain (E1) load step 63

Control_beam_analysis_V0.5
 Load-step 64, Load-factor 0.3000, LC 2
 Total Strains E1
 min: -8.89e-05 max: 6.49e-02

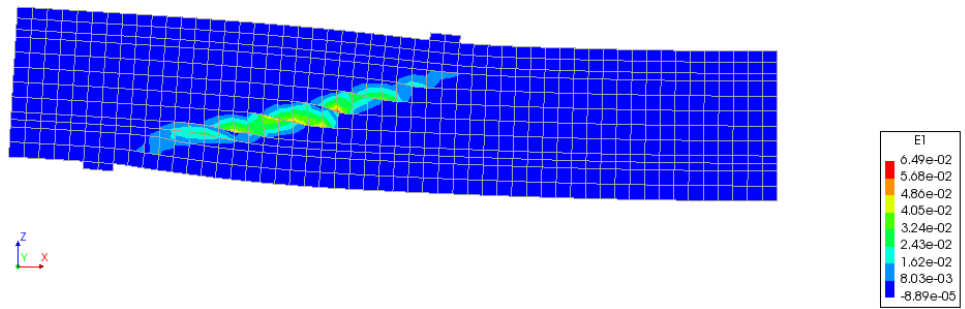


Figure F.9: Principal strain (E1) load step 64

Control_beam_analysis_V0.5
 Load-step 62, Load-factor 0.1000, LC 2
 Crack-widths Ecw1
 min: -0.00mm max: 0.26mm

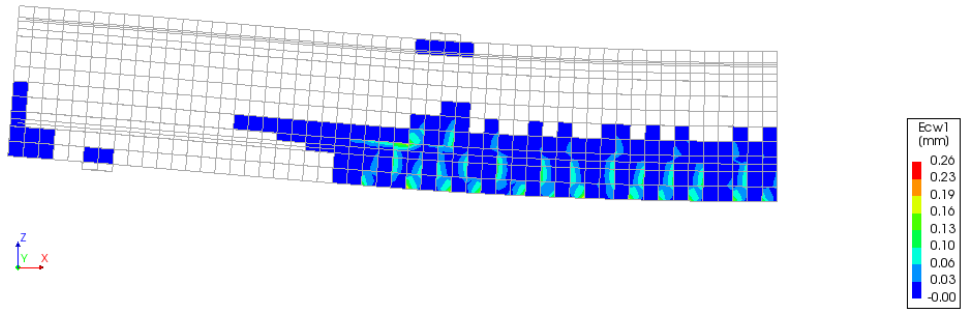


Figure F.10: Crack widths (Ecw1) load step 62

Control_beam_analysis_V0.5
 Load-step 63, Load-factor 0.2000, LC 2
 Crack-widths Ecw1
 min: -0.00mm max: 3.18mm

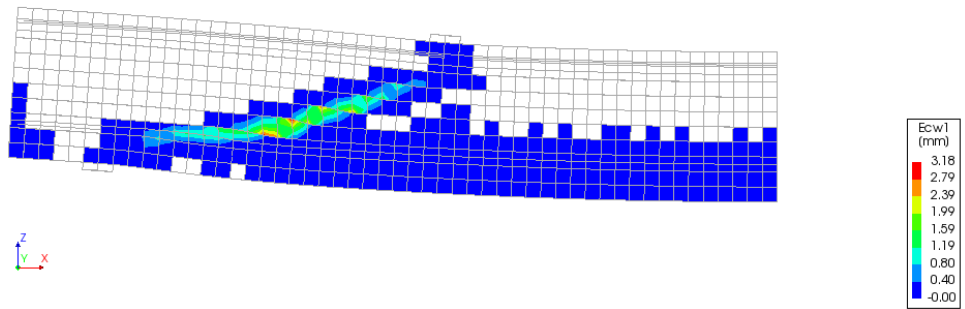


Figure F.11: Crack widths (Ecw1) load step 63

Control_beam_analysis_V0.5
 Load-step 02, Load-factor 0.1000, LC 2
 Crack Strains Eknn
 min: 0.00e+00 max: 3.81e-03

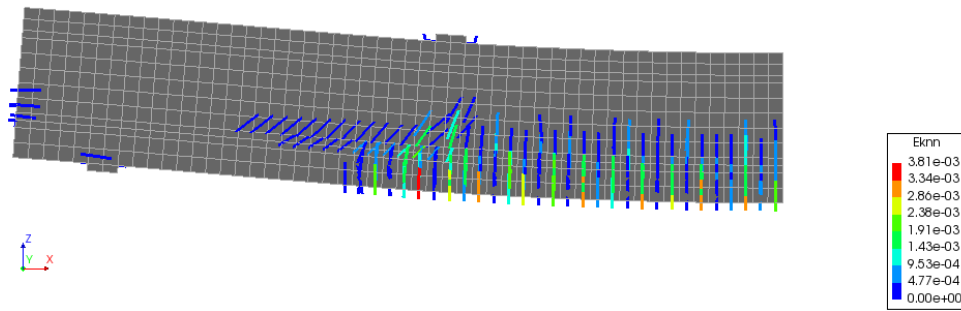


Figure F.12: Crack strains (Eknn) load step 62

Control_beam_analysis_V0.5
 Load-step 03, Load-factor 0.2000, LC 2
 Crack Strains Eknn
 min: 0.00e+00 max: 3.68e-02

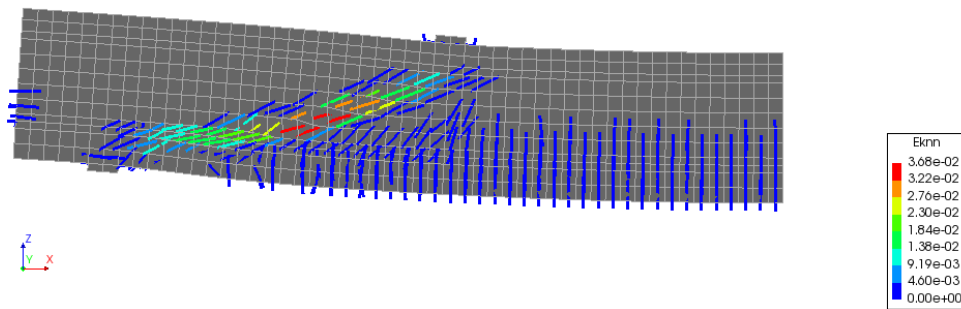


Figure F.13: Crack strains (Eknn) load step 63

Control_beam_analysis_V0.5
 Load-step 04, Load-factor 0.3000, LC 2
 Crack Strains Eknn
 min: 0.00e+00 max: 5.28e-02

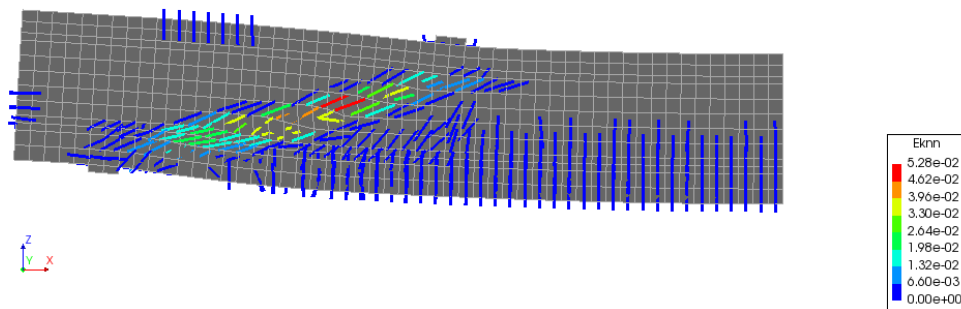


Figure F.14: Crack strains (Eknn) load step 64

